

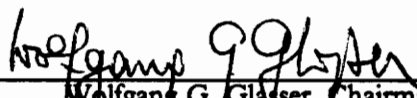
Multiphase Star-Like Copolymers Containing Lignin: Synthesis, Properties and Applications.

by

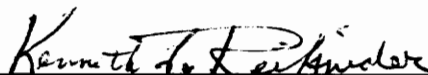
Willer de Oliveira

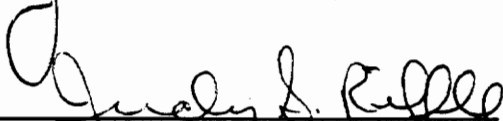
Dissertation submitted to the Faculty of the
Virginia Polytechnic Institute and State University
in partial fulfillment of the requirements for the degree of
Doctor of Philosophy
in
Materials Engineering Science

APPROVED:


Wolfgang G. Glasser, Chairman


James E. McGrath


Kenneth D. Reifsnider


Judy S. Riffle


Garth L. Wilkes

September, 1991

Blacksburg, Virginia

c.2

LD
5655
V856
1991
0448
c.2

Multiphase Star-Like Copolymers Containing Lignin: Synthesis, Properties and Applications.

by

Willer de Oliveira

Wolfgang G. Glasser, Chairman

Materials Engineering Science

(ABSTRACT)

Multiphase star-like copolymers containing lignin have been synthesized and characterized. All copolymers contained hydroxypropyl lignin (HPL) as the central core. Polycaprolactone (PCL), cellulose propionate (CP) or polystyrene (PS), served as radiating blocks attached to the lignin core in star-like manner. These materials were studied in relation to their structure, morphology, effect on crystallization behavior and application in polymer blends.

Three series of semi-crystalline $(PCL)_n$ – HPL have been synthesized with HPL segments of 2,100, 3,500 and 6,400 molecular weight, respectively, and polycaprolactone blocks of varying size. Copolymers were produced by either copolymerizing ϵ -caprolactone or grafting preformed PCL segments onto HPL. The thermal and optical properties of these copolymers were investigated by DSC, DMTA and optical microscopy. The copolymers exhibited variable thermal behavior in relation to composition. The crystallization of PCL blocks was mainly governed by the nature of the HPL phase. PCL block length was another variable that affected crystallinity. The longer the segment, the higher the degree of crystallinity. The compatibility, morphology and mechanical properties of $(PCL)_n$ – HPL copolymers blended with poly(vinyl chloride) were also investigated. Methods used in this study included DSC, DMTA, SEM, TEM and stress-strain testing. The blends were shown to be compatible in all proportions.

Mono-hydroxyl terminated cellulose propionate oligomers were synthesized by degradation with hydrogen bromide of a fully substituted, high molecular weight cellulose propionate molecule. Evidence of strict monofunctionality was demonstrated by H-NMR spectroscopy. Thermal analysis

results indicated that the oligomers were semi-crystalline and their melting points were functions of molecular weight. $(CP)_n$ – HPL copolymers were synthesized by grafting oligomeric CP segments onto HPL via a coupling agent. The thermal and morphological properties of the copolymers were characterized by DMTA, DSC and TEM. Analysis by thermal methods and by electron microscopy showed strong evidence for microphase separation between HPL and CP segments. Cellulose propionate chains crystallize even at a low degree of polymerization, such as DP 5. The copolymer morphologies exhibit a broad variety of features. They vary from dispersed fibrils to spheres like and alternate lamella type patterns according to composition and molecular weights. The interfacial activity of the copolymers in blends of CP and HPL prepared in the melt state was also investigated. The tensile properties of the ternary blends were altered slightly by the presence of the copolymer. Melt blended cellulose propionate and HPL with low degree of propoxylation forms a miscible system with up to 40% HPL component. The incorporation of 5% of the $(CP)_n$ – HPL copolymer reduces the tensile strength by about 10%. Thermal behavior of melt blended cellulose propionate and HPL with high degree of propoxylation indicates the formation of an incompatible system at any composition. Before the addition of the copolymer the blend exhibits higher toughness, elongation up to 160%, and a Young's modulus of 23 ksi. The copolymer-modified blend shows a decrease in toughness and an increase in tensile strength by about 10%.

The synthesis and characterization of $(PS)_n$ – HPL copolymers was accomplished in an analogous manner. When added to blends of PS and HPL, $(PS)_n$ – HPL produced improved mechanical properties of the blends. Scanning electron microscopy of fracture surfaces demonstrated that the addition of copolymer to the PS/HPL blends improved the adhesion of the two phases. The addition of $(PS)_n$ – HPL copolymer to the 90 PS/10 HPL blend system strongly reduced, by about 10 fold, the particle size of the unmodified blend. No significant difference was observed in the morphology of the 80 PS/20 HPL system. The phases exhibited poor adhesion before and after the addition of copolymer.

Acknowledgements

I have many people to thank. I want to express, first of all, my special thanks to my advisor, Dr. Wolfgang G. Glasser, without whose guidance and encouragement I would never have attempted this study and would probably not even have entered this field.

I also want to thank my advisory committee, Drs. J. E. McGrath, K. L. Reifsnider, J. S. Riffle and G. L. Wilkes for their interest, knowledge, expertise, and counseling. I am especially grateful to Dr. J. S. Riffle for her assistance and advice in conducting the polymerization work; and to Dr. Wilkes who has given me many of his valuable hours to help solve the puzzle of many TEM and SEM micrographs.

My appreciation is also extended to my colleagues in the laboratory for their help and support. Grateful acknowledgement goes to Chip Frazier for the time and effort spent on running NMR-spectra. A special thanks goes to everyone who has helped me with the details of conducting my experiments, as well as of making lab life more pleasurable. Estella, Vipul, Ramon, Eberhardt, Khali, Laurence, Raj, Gil, Nancy, Jodi, Tom Pic, Gamini are just a few of the names that I'd particularly like to mention. I extend my thanks to Dr. Geza Ifju for his friendship and support during my graduate research work. And finally, I would like to thank one of the most supportive

and able companions I have ever met; I think here of Klaus Hofmann, a friend whose presence will always remain with me.

I wish to extend deepest gratitude to the many family members and friends whose continuous support, love and encouragement made this project achievable. Many thanks to all of you.

Table of Contents

1.0 INTRODUCTION 1

1.1 REFERENCES 5

2.0 LITERATURE REVIEW 6

2.1 LIGNIN IN SYNTHETIC POLYMERS 7

 2.1.1 Nature and Character of Lignin 7

 2.1.2 Lignin in Structural Networks 12

 2.1.3 Lignin in Thermoplastic Polymers 16

2.2 RESEARCH OBJECTIVES 18

2.3 REFERENCES 24

3.0 SYNTHESIS AND CHARACTERIZATION OF
CAPROLACTONE-HYDROXYPROPYL LIGNIN STAR-LIKE COPOLYMERS 27

3.1 INTRODUCTION 27

3.2 EXPERIMENTAL SECTION 32

 3.2.1 Materials 32

 3.2.2 Synthesis of Mono-Isocyanate Terminated Polycaprolactone 34

3.2.3 Copolymer Synthesis	35
3.2.4 Characterization	39
3.3 RESULTS AND DISCUSSION	42
3.3.1 Effect of Synthesis Parameters on Copolymer Properties	42
3.3.2 Solution Properties	52
3.3.3 Thermal Properties	57
3.3.4 Crystallinity	72
3.4 CONCLUSIONS	76
3.5 REFERENCES	78
 4.0 BINARY BLENDS OF POLYVINYL CHLORIDE AND POLYCAPROLACTONE - HYDROXYPROPYL LIGNIN COPOLYMER	 80
4.1 INTRODUCTION	80
4.2 EXPERIMENTAL SECTION	84
4.2.1 Materials	84
4.2.2 Sample Preparation	84
4.2.3 Characterization	85
4.3 RESULTS AND DISCUSSION	87
4.3.1 Thermal Analysis	87
4.3.2 Tensile Properties	91
4.3.3 Aging studies	92
4.3.4 Crystallinity properties	103
4.3.5 Morphology	108
4.4 CONCLUSIONS	115
4.5 REFERENCES	117
 5.0 SYNTHESIS AND CHARACTERIZATION OF CELLULOSE PROPIONATE SEGMENTS MONO-HYDROXYL TERMINATED	 118

5.1	INTRODUCTION	118
5.2	EXPERIMENTAL SECTION	129
5.2.1	Materials	129
5.2.2	Depolymerization of Cellulose Propionate	129
5.2.3	Hydrolysis of Bromine End Group	130
5.2.4	Determination of Functionality	130
5.2.5	Characterization	131
5.3	RESULTS AND DISCUSSIONS	132
5.3.1	Depolymerization of Cellulose Propionate	132
5.3.2	Determination of Hydroxyl Groups and of Number-Average Functionality of CP Oligomers.	137
5.3.3	Thermal Properties	140
5.4	CONCLUSIONS	150
5.5	REFERENCES	151
6.0	SYNTHESIS AND CHARACTERIZATION OF CELLULOSE PROPIONATE - HYDROXYPROPYL LIGNIN COPOLYMERS	152
6.1	INTRODUCTION	152
6.2	EXPERIMENTAL SECTION	160
6.2.1	Materials	160
6.2.2	Synthesis of Mono-Isocyanate Terminated Cellulose Propionate	161
6.2.3	Copolymer Synthesis	161
6.2.4	Characterization	162
6.3	RESULTS AND DISCUSSION	167
6.3.1	Effect of Synthesis Parameters on Copolymer Properties	167
6.3.2	Solution Properties	171
6.3.3	Thermal Behavior	173
6.3.4	Morphology	182

6.4	CONCLUSIONS	192
6.5	REFERENCES	194
7.0	TERNARY BLENDS OF CELLULOSE PROPIONATE-HYDROXYPROPYL LIGNIN COPOLYMER AND HOMOPOLYMERS	195
7.1	INTRODUCTION	195
7.2	EXPERIMENTAL SECTION	197
7.2.1	Materials	197
7.2.2	Sample Preparation	197
7.2.3	Characterization	198
7.3	RESULTS AND DISCUSSION	199
7.3.1	Dynamic Mechanical Behavior of Blends	199
7.3.2	Tensile behavior	202
7.4	CONCLUSIONS	211
7.5	REFERENCES	212
8.0	POLYSTYRENE-HYDROXYPROPYL LIGNIN COPOLYMERS: SYNTHESIS AND APPLICATION IN TERNARY BLENDS	213
8.1	INTRODUCTION	213
8.2	EXPERIMENTAL SECTION	216
8.2.1	Materials	216
8.2.2	Synthesis of Mono-Isocyanate Terminated Polystyrene	217
8.2.3	Copolymer synthesis	217
8.2.4	Sample Preparation	218
8.2.5	Characterization	218
8.3	RESULTS AND DISCUSSION	220
8.4	CONCLUSIONS	234
8.5	REFERENCES	235

Vita 236

List of Illustrations

Figure 1. Scheme of (a) p-coumaryl, (b) coniferyl, and (c) sinapyl alcohol [5].	8
Figure 2. Simplified representation of lignin's chemical structure [3].	9
Figure 3. Structural scheme of softwood lignin [16]	11
Figure 4. Schematic structure of hydroxyalkyl lignin derivatives [35]	15
Figure 5. HPL structural model	18
Figure 6. Scheme of two types of HPL star-like copolymers [44]	20
Figure 7. FTIR spectra of the qualitative formation of polycaprolactone monoisocyanate	43
Figure 8. Proton-NMR spectra of mono-hydroxyl terminated PCL	44
Figure 9. Molecular weight distribution according to method I and method II	49
Figure 10. Proton-NMR spectrum of PCL-HPL copolymer	51
Figure 11. Relationship between intrinsic viscosity and copolymer arm length	55
Figure 12. DMTA curve of PCL-HPL star-like copolymer	58
Figure 13. DSC curve of copolymer from series A	59
Figure 14. DSC curves of copolymers from series A (see Table 7)	63
Figure 15. DSC curves of copolymers from series B and C (see Table 8)	64
Figure 16. DSC curves of copolymers from series B and C (see Table 8)	65
Figure 17. Melting point vs. PCL-HPL copolymer arm length	67
Figure 18. Optical micrographs of PCL and PCL-HPL copolymers	68
Figure 19. Optical micrographs of PCL and CL-HPL copolymers	70
Figure 20. Optical micrographs of PCL and PCL-HPL copolymers	71
Figure 21. The effect of lignin content on the heat of fusion	73

Figure 22. Degree of crystallinity of the PCL component in the block copolymers as a function of lignin content.	74
Figure 23. Degree of crystallinity vs. copolymer arm length	75
Figure 24. Tg vs.blend composition of PVC/PCL-HPL, experiment vs. Fox model.	89
Figure 25. Temperature dependence on E' and tan δ for PVC/PCL-HPL blends	90
Figure 26. Tensile properties of PVC/PCL-HPL blends	93
Figure 27. Tensile properties of PVC/HPL and PVC/PCL-HPL blends.	95
Figure 28. Loss tangent as a function of temperature for PVC/PCL blends [12]	97
Figure 29. Effect of aging on modulus properties	99
Figure 30. Effect of aging on ultimate strength properties	101
Figure 31. Effect of aging on elongation at break	102
Figure 32. Effect of aging on heat of fusion	103
Figure 33. Effect of aging on degree of crystallinity	105
Figure 34. Degree of crystallinity as a function of composition for PVC/PCL-HPL blends.	106
Figure 35. Melting temperature of copolymer as a function of composition for PVC/PCL-HPL blends	107
Figure 36. The effect of crystallinity on tensile properties	108
Figure 37. SEM micrographs of PVC/PCL-HPL polymer blends	110
Figure 38. SEM micrographs for the PVC/HPL blend system	112
Figure 39. TEM of thin films of PVC/PCL-HPL blends.	113
Figure 40. TEM micrographs of thin films of PVC blended with HPL and PCL-HPL copolymer	114
Figure 41. Structure of cellulose.	119
Figure 42. Cleavage of trimethyl cellulose with hydrogen chloride [9]	123
Figure 43. Scheme of TMC (g-POTM) graft copolymerization [9].	124
Figure 44. POTM-TMC star blocks coupled by poly(4-vinylpyridine) [9].	126
Figure 45. Examples of reducing (1,2) and nonreducing (3) sugars	127
Figure 46. Synthesis route for the preparation of 1-mono-hydroxyl cellulose triesters [12] ..	128
Figure 47. FTIR of cellulose propionate	133
Figure 48. Typical H-NMR spectra of cellulose propionate	134

Figure 49. Degree of polymerization vs. hydrolysis time.	136
Figure 50. Molecular weight distribution of CP	138
Figure 51. Typical H-NMR-spectrum of low-molecular weight CP bromoglucoside	139
Figure 52. Proton-NMR-spectrum of cellulose propionate	141
Figure 53. Intrinsic viscosity of CP segments vs. hydrolysis time	142
Figure 54. MHS constant vs. degree of polymerization	143
Figure 55. Typical DSC thermogram of cellulose propionate	146
Figure 56. DSC thermograms of a series of cellulose propionate segments	147
Figure 57. Melting point vs. molecular weight	148
Figure 58. Relationship between heat of fusion and molecular weight	149
Figure 59. Depolymerization scheme of the CTA molecule [2]	154
Figure 60. Depolymerization scheme for CTA chains [2]	155
Figure 61. Deacetylation of CTA blocks [5]	157
Figure 62. Synthesis route for the preparation of cellulose triester macroinitiator [8]	159
Figure 63. FTIR spectra of cellulose propionate oligomers	168
Figure 64. GPC chromatograms of copolymers from grafting	169
Figure 65. GPC chromatograms of CP-HPL copolymers	170
Figure 66. Intrinsic viscosity as a function of copolymer lignin content	173
Figure 67. Intrinsic viscosity as a function of copolymer arm length	174
Figure 68. Mark-Houwink-Sakurada exponent as a function of copolymer arm length	176
Figure 69. Dynamic mechanical behavior of CP-HPL copolymer	177
Figure 70. A typical thermogram of CP-HPL copolymer	179
Figure 71. Melting temperature vs. arm length	181
Figure 72. Optical micrographs of films isothermally crystallized from the melt	182
Figure 73. Heat of fusion vs. copolymer arm length	184
Figure 74. TEM for cast films of CP-HPL copolymer stained with ruthenium tetroxide ..	185
Figure 75. TEM for cast films of CP-HPL copolymer stained with ruthenium tetroxide ..	186
Figure 76. TEM of cast films of copolymer stained with ruthenium tetroxide	187

Figure 77. TEM of cast films of copolymer stained with ruthenium tetroxide	188
Figure 78. TEM of cast films of copolymer stained with ruthenium tetroxide	189
Figure 79. Dynamic mechanical behavior of CP/HPL(A) blends	203
Figure 80. Glass transition temperature of CP/HPL(A) blends	204
Figure 81. Dynamic mechanical behavior of 80 CP/20 HPL(B) blend	205
Figure 82. Glass transition temperature of CP/HPL(B) blends	206
Figure 83. Typical stress-strain curves of CP/HPL blends	208
Figure 84. Tensile mechanical properties of CP/HPL(A) blends	209
Figure 85. Tensile mechanical properties of CP/HPL(B) blends	210
Figure 86. MWD of a typical PS-NCO and HPL grafting reaction	223
Figure 87. Proton-NMR-spectrum of mono-hydroxyl terminated polystyrene	224
Figure 88. Proton-NMR-spectrum of a typical PS-HPL copolymer	226
Figure 89. Relationship between T _g and PS-HPL copolymer molecular weight	227
Figure 90. Scanning electron micrograph of 80 PS/20 HPL blend	228
Figure 91. Scanning electron micrographs of 95 PS/5 HPL blends	229
Figure 92. Scanning electron micrograph of 90 PS/10 HPL blends	230
Figure 93. Scanning electron micrograph of 80 PS/20 HPL blends.	231
Figure 94. Tensile properties of PS/HPL blends.	233

List of Tables

Table 1.	Lactone Polymerization Systems [1]	28
Table 2.	Experimental Results of Hydroxypropyl Lignin Synthesis	45
Table 3.	Molecular Characterization Data of Polycaprolactone-Hydroxypropyl Lignin Star-Like Copolymers Synthesized According to Method I	47
Table 4.	Molecular Characterization Data of Polycaprolactone-Hydroxypropyl Lignin Star-Like Copolymers Synthesized According to Method II	48
Table 5.	Solution Properties of PCL-HPL Copolymers (Method I)	53
Table 6.	Solution Properties of PCL-HPL Copolymers (Method II)	54
Table 7.	Thermal Data of PCL-HPL Copolymers from Series A	60
Table 8.	Thermal Data of PCL-HPL Copolymers from Series B and C	61
Table 9.	DSC and DMTA Thermal Analysis Data for PVC/PCL-HPL Blends	88
Table 10.	Mechanical Properties of PVC/PCL-HPL Blends	92
Table 11.	Summary of the Aging Effect on Mechanical Properties of PVC/PCL-HPL Blends	98
Table 12.	Molecular Characterization Data of Cellulose Propionate Oligomers as a Function of Hydrolysis Time	135
Table 13.	Thermal Data of CP Oligomers	144
Table 14.	Molecular Characterization Data of CP-HPL Copolymers	171
Table 15.	Summary of Thermal Data of CP-HPL Copolymers	180
Table 16.	Molecular Characteristics and Thermal Data of Pure Blend Components	200
Table 17.	Summary of the Glass Transition Temperatures from DMTA of CP/HPL Blends	201
Table 18.	Molecular Weight and Thermal Properties of HPL's	217
Table 19.	Molecular Characteristics of PS-HPL Copolymers	222

“Though this be madness, yet there is method in it ”

Hamlet

1.0 INTRODUCTION

Since the discovery that block copolymers of appropriate composition and architecture could yield materials having unique and useful properties, extensive research has been carried out to find new polymer combinations that exhibit the same anomalous behavior. The unique characteristic of these block copolymers is the formation of microscopic phase separation systems due to the constraints imposed by the chemical bonding between segments. This approach prevents a gross physical segregation of the two components as often it would occur if they were simply mixed. Such microphase separation of molecular dimensions usually develops a highly organized domain morphology which could lead to materials possessing useful engineering properties [1].

The phenomenon of phase separation of block segments in a certain way should be expected as a result of dissimilarity between block components. As in mixtures of homopolymers that often do not mix at the molecular level, incompatibility between chemically different block segments will be the rule, even if the segments are covalently bonded together. However, in block copolymers, differently from polymer blends, the chemical bonding between segments restricts their segregation into microdomains, i.e., to microphases with dimensions of the order of the molecular size of the blocks. The morphology and nature of these domains will depend on chemical composition, chain structure, molecular weights of the segments, thermodynamic interaction parameters, casting solvent, solidification conditions, and temperature [2].

Perhaps one of the best ways to understand the influence of morphology on polymer physical properties is to study the multiphase system called “thermoplastic elastomer”. Thermoplastic elastomers were commercially introduced by the Shell Company (USA) in 1965 [3]. They represent materials which combine the processing characteristics of thermoplastics with the physical properties of vulcanized rubbers. They have many of the physical properties of rubbers, i.e., softness, flexibility and resilience, but in contrast to conventional rubbers, they are processed as thermoplastics.

Thermoplastic elastomers are multiphase materials of the general structure A-B-A where A is a hard thermoplastic polymer and B is a soft elastomeric polymer. Others have a linear $[A-B]_n$ form where n is very large; or an $(A)_n-B$ star-shaped structure where the A chains are joined together at the center of the star. The selection of monomers or block segments, of block length, and of the weight fractions of A and B is extremely important for meeting the required elastomeric behavior [3]. The soft segments contribute to the flexibility and extensibility of the elastomer, while the glassy or semi-crystalline hard segment domains serve as virtual crosslinks, impeding chain slippage and viscous flow of the polymer.

The unique characteristic of all thermoplastic elastomers is that they are phase-separated systems in which one phase is hard at room temperature, while the other phase is an elastomer [4,5]. In this two-phase system, the middle-block phase constitutes a continuous three-dimensional elastomeric network, and the dispersed end-block phase serves as multijunction point for the ends of the middle blocks. This gives thermoplastic elastomers their strength; otherwise, the elastomer phase would be free to flow under stress. When these hard domains which act as physical crosslinks are melted, softened, or dissolved in a solvent, flow can take place and so the thermoplastic elastomers can be processed. When the material is cooled or the solvent is evaporated, the domains harden and the network regains its original strength. In some ways, this is similar to the network formed by vulcanizing conventional rubbers using sulfur crosslinks. This explanation of the properties can be applied to any block copolymer with either the structure A-B-A, with $[A-B]_n$, or with $(A)_n-B$. Block copolymers having structures such as A-B or B-A-B with A and B defined above, will not

exhibit the tensile behavior characteristic of thermoplastic elastomers since for a continuous network to exist both ends of the elastomer segment must be immobilized in the non-elastomeric domains.

Few examples in the literature have dealt with the use of natural polymers as segments of this class of polymers. Most research with natural polymers is restricted to thermoplastic elastomers containing cellulose [6,7]. The current interest in the development of novel biomass conversion technologies in which the utilization of the polymeric lignin-rich residue is a key feature of the process [8-10], encourages us to investigate the performance of lignin in a star-like block copolymer system. In fact, there exist a number of studies concerning the evaluation of lignin as an active component in various polymer networks [11]. They support the conclusion that lignin, as any polymeric substance, can be analyzed, derivatized and incorporated into material systems by using the same principles of the polymer science methodology applied in other materials. In recent studies [12] lignin has been copolymerized with propylene oxide to produce multifunctional (polyhydroxytelechelic) segments exhibiting glassy or rubbery behavior. This type of lignin-derived telechelic polymer has been used in the synthesis of segmented copolymers and thermosets. Thus in light of the importance of morphological features on block copolymer properties, and considering the success of making lignin-based polytelechelic polymers, it seems worthwhile to explore how to what extent and with what limitations, a multiphase lignin-containing macromolecular system can be realized.

To adequately carry out this investigation, a set of goals was adopted:

1. Synthesis of hydroxytelechelic polymers through chemical modification of lignin: The lignin-derived telechelic polymer was to be evaluated in terms of molecular weight, lignin content, functionality, thermal properties, etc.
2. Synthesis of star-like block copolymers containing lignin, and evaluation of the synthesis variables on the final architecture of the multiphase block copolymers.

3. Evaluation of the effect of the lignin-derived block copolymer on phase morphology and miscibility in polymer blends prepared from them.

1.1 REFERENCES

1. D. J. Meier, "Block Copolymers Morphological and Physical Properties", D. J. Walsh, J. S. Higgins and A. Maconnachie, Ed., **"Polymer Blends and Mixtures."** NATO ASI Series. Series E. no. 89 (1985)
2. S. L. Aggarwal, "Introduction and Overview", M. J. Folkes, Ed., **"Processing, Structure and Properties of Block Copolymers"**, chap. 1, 1985
3. G. Holden, E. T. Bishop, and N. R. Legge, *J. Polym. Sci.: Part C*, **26**, 37 (1969)
4. G. Holden, "Applications of Thermoplastic Elastomers", N. R. Legge, G. Holden, and H. E. Schroeder, Ed., **"Thermoplastic Elastomers: A Comprehensive Review"**, chap. 13, 481-506 (1987)
5. A. Noshay, J. E. McGrath, **"Block Copolymers: Overview and Critical Survey"**, Academic Press, New York, 1977
6. H. W. Steinmann, *ACS Polym. Prep. Am. Chem. Soc. Div. Polym. Chem.*, **11**, 285 (1970)
7. C. Feger and H. -J. Cantow, *Polymer Bulletin*, **3**, 407 (1980)
8. W. G. Glasser, *Forest Products Journal*, **31**(3), 24 (1981)
9. W. G. Glasser, L. C. -F. Wu, and J. -F. Selin, **"Wood and Agricultural Residues - Research on Use for Feed, Fuels and Chemicals"**, E. J. Soltes, Ed., Academic, New York, 149 (1983)
10. P. C. Muller and W. G. Glasser, *Biotechnology and Bioengineering Symp.*, No. 13, 481 (1983)
11. W. G. Glasser and S. S. Kelley, "Lignin" in **"Encyclopedia of Polymer Science and Engineering"**, volume 8, second edition, 795 (1987)
12. S. S. Kelley, W. G. Glasser, and T. C. Ward, *J. Wood Chem. Technol*, **8**(3), 341(1988)

2.0 LITERATURE REVIEW

The following literature review will provide the basic foundation for the dissertation presented here. The review will start with a summary of activities regarding the use of lignin as an active component in synthetic polymers, and it will continue with the concept of “polytelechelic polymers” and its application to the lignin field. The discussion will include the nature and character of lignin, lignin in structural networks, and lignin as star-like polytelechelic polymer for the synthesis of thermoplastic block copolymers. The reason for going into lignin-based polymeric products is to show the diversity of lignin research in the polymer field, which can justify the interest in exploring the lignin potential for the synthesis of multiphase block copolymers.

Once this has been established, a review on multiphase block copolymers containing either ϵ -caprolactone or cellulose derivatives will be explored, with special emphasis on the synthesis and properties of these materials. Polycaprolactone and cellulose propionate were segments selected to be graft or co-polymerized (ϵ -caprolactone) into the lignin derivative polyol in order to create the thermoplastic star-like copolymers. This review is meant to yield a basis for interpretation of the experimental results, as well as a justification for this dissertation.

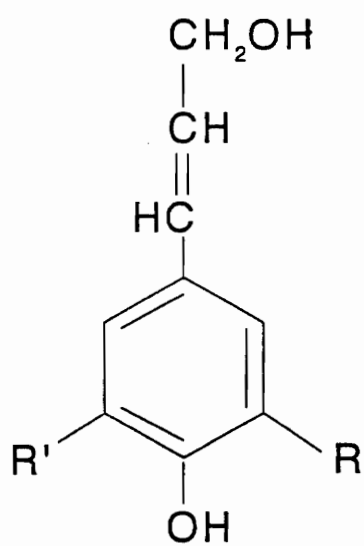
2.1 LIGNIN IN SYNTHETIC POLYMERS

2.1.1 Nature and Character of Lignin

After cellulose, lignin is the second most abundant natural polymer, with an annual biosynthesis rate of ca. 2×10^{10} t [1]. It is recognized as an amorphous three-dimensional, highly branched polymer that binds the cellulose fibers together in wood. As a composite material, lignin plays a major role in controlling stresses to which trees are subjected [2]. Even though about 50×10^6 t of lignin is produced annually from woody plants at pulp mills worldwide [3], lignin continues to be under-utilized as raw material for commercial products. Presently, lignin is used almost exclusively as fuel to power evaporators of the chemical recovery process and liquor concentration system of pulp mills [4].

Chemically lignin is formed in wood by a dehydrogenative(chain growth) polymerization mechanism (see Figure 1) of p-coumaryl(a), coniferyl(b), and sinapyl alcohols(c), all in the trans configuration [5]. Structurally, lignin is a polymer of phenylpropane units. In contrast to cellulose, which consists of polymeric glucose involving only one type of bond, lignin is constituted of phenylpropane (C_6-C_3) substructures, which are linked by a multitude of interunit bonds [3], as seen in Figure 2. The major types of intermonomer linkages are ether(β -O-4, α -O-4, and 4-O-5), accounting for more than two thirds of all intermonomer bonds, and the rest by carbon-to-carbon linkages [5]. Besides these interunit linkages, there are different types of functional groups in lignin which influence its character and properties. The functional groups of major influence on lignin reactivity are phenolic hydroxyl, aliphatic hydroxyl, and carbonyl groups [6].

Biosynthetically, lignin is manufactured from phenylpropanoid precursors by way of an enzymatic dehydrogenation process involving a variety of oxidative coupling reactions between free phenoxy radicals [4]. These processes are probably controlled by thermodynamics rather than enzyme



(a) $R = H, R' = H$

(b) $R = OCH_3, R' = H$

(c) $R = OCH_3, R' = OCH_3$

Figure 1. Scheme of (a) p-coumaryl, (b) coniferyl, and (c) sinapyl alcohol [5].

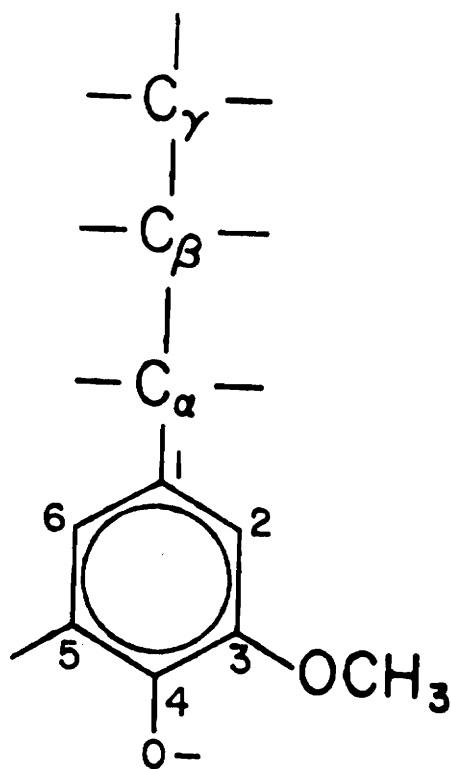


Figure 2. Simplified representation of lignin's chemical structure [3].

kinetics, which explains the statistical nature of the polymer structure [7,8]. In absence of rigorous data, a substantial number of hypothetical lignin structures has been proposed to date. Most are based on the dehydrogenation theory of para-hydroxy cinnamyl alcohols [8-16]. Basically, these hypothetical lignin structures were obtained either by manually composing random polymers of phenylpropane units, or by simulating the process of lignin formation by computer, as exemplified in Figure 3 [16].

There are not many studies about the physical properties of lignin [17]. To obtain its true molecular weight is a problem because, during lignin isolation, it is inevitable that some degradation occurs. This makes molecular weight and polydispersity data unreliable [18]. Molecular weights of isolated lignins, kraft lignin, or lignin sulfonates, have been determined; they range anywhere between 10^3 to more than 10^6 daltons. Glass transition temperatures of softwood lignins were studied by Hatakeyama and co-workers [19]. The T_g estimated from DSC varied from 109 to 124°C, and it was linearly dependent on lignin molecular weight. In a study of mechanical properties of softwood, the lignin- T_g was attributed to the primary relaxation of softwood flakes at temperatures above 160°C [20]. The Young's modulus of lignin was also determined, and its value was approximately 3.3×10^9 Pa [20]. Cousins [21] also determined the Young's and shear moduli of two lignins measured at different moisture content. The Young's modulus of periodate lignin increased linearly from 3.1×10^9 to 6.7×10^9 Pa, and the shear modulus from 1.2×10^9 to 2.1×10^9 Pa, with moisture content decreasing from 12 to 3.6%. The same behavior was reported for Klason lignin, except that moduli were always much lower.

There are many methods available for the isolation and purification of lignin, although only two main methods are commercially important, the sulfite and kraft process. The sulfite process generates a lignin derivative in the form of lignin sulfonate, which is water-soluble over the entire pH-range. Lignin sulfonates are among the most important industrial surfactants, and they are commercially available in various forms. They constitute the major type of lignin produced in the U.S. The lignin from the Kraft process has a variety of functional groups, is soluble in polar hydrogen-bond breaking solvents, and has high thermal stability and a high heat value. Kraft lignin

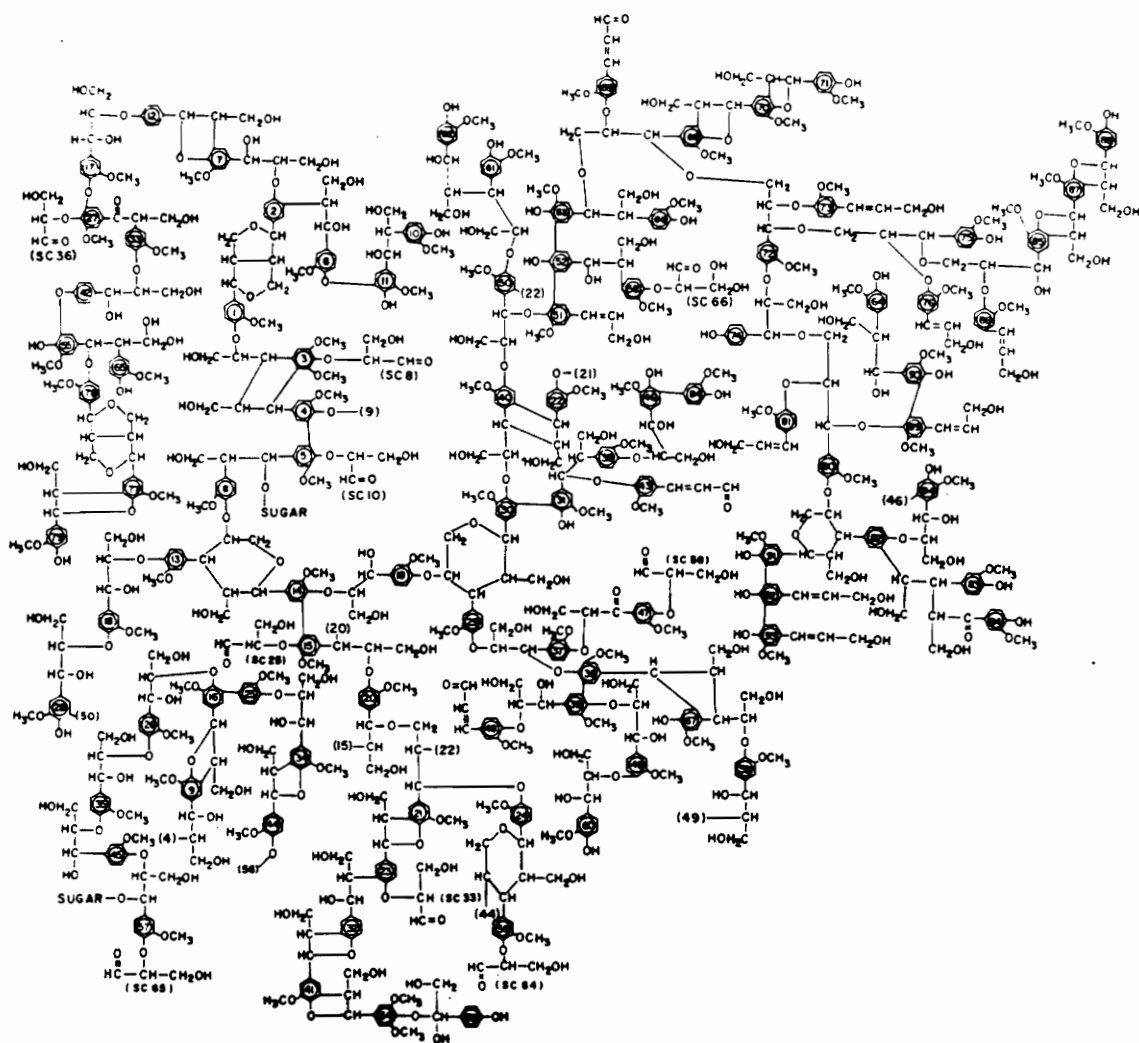


Figure 3. Structural scheme of softwood lignin [16]

is used predominantly as fuel in the Kraft-pulping operation for the recovery of process chemicals. The other methods for lignin production on a scale larger than laboratory, but still not yet on industrial scale, include processes based on the involvement of mineral acid (acid hydrolysis lignin), water and steam at various temperatures and pressures (autohydrolysis and steam explosion lignin), and organic solvent mixtures, such as ethanol and water (organosolv lignin). All these methods of lignin isolation have a significant influence on its structural, chemical and physical properties. Perhaps the least altered lignin by isolation chemistry is that isolated by mechanical ball milling of solvent extracted sawdust, with subsequent extraction and purification. This lignin, so-called milled wood lignin, is presumed to be closely representative of native lignin in wood.

2.1.2 Lignin in Structural Networks

The major drawback to the utilization of lignin in material systems is its structural complexity and chemical variability which makes the control of chemical and physical properties of lignin-derived materials a difficult task. However, many examples in the literature show that these constraints can be overcome [2, 22-27].

Many attempts have been made to copolymerize lignin with phenol-formaldehyde resin (PF). The results, however, have been met with limited success. The incorporation of lignin into PF resin is limited by the availability and reactivity of suitable functional groups. Forss and Fuhrmann's [23,24] investigations have shown that the inferior results are not due to the poor reactivity of lignin, but rather to the presence of low molecular weight lignin fragments generated during the pulping process. They have developed and patented a process for the synthesis of a lignin-based adhesive for plywood, particleboard, and fiberboard. The adhesive was synthesized by the copolymerization of high molecular weight lignin with PF resin. The product, which contained 40 to 70 percent lignin, produced a strong and resistant glueline. On comparing the properties of the boards with other boards made with ordinary commercial PF resins, parity was found. Dolenko and Clark [25]

also reported to have prepared a water-proof resin based on Kraft lignin and PF resin. A lignin dispersion was initially produced via methylation and acidification and then blended with an acid curing PF resin. The resulting product was qualified as a waterproof adhesive for plywood and waferboard. This data also showed that up to 70% of petroleum-based PF resins could be replaced with Kraft lignin on a weight-by-weight basis.

Lignin epoxide resins have been synthesized by the chemical reaction of lignin with epichlorohydrin. A number of publications, as well as patents, has appeared in this area [28-31].

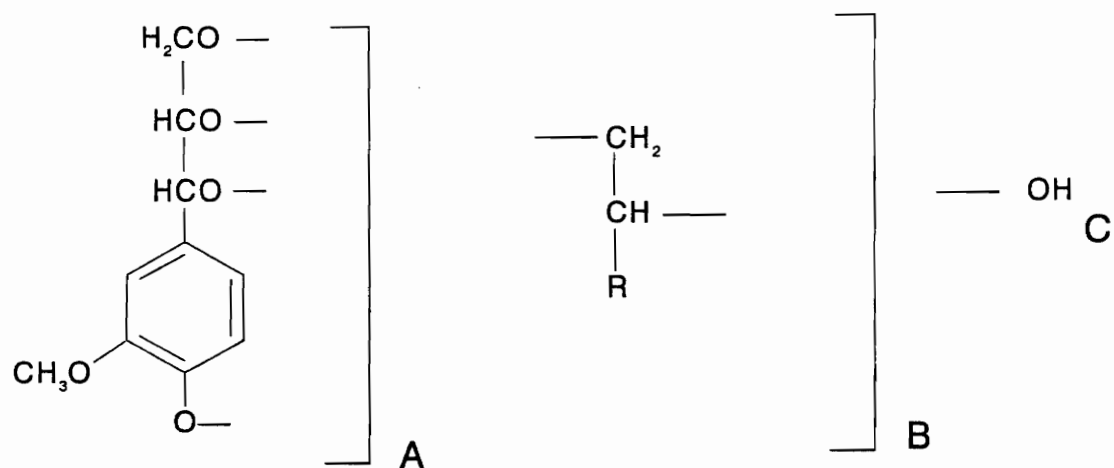
Studies concerning the synthesis and characterization of lignin-based polyurethanes have occupied lignin scientists for a great number of years. Kratzl and co-workers [30] have investigated the reaction of lignin with isocyanates and diisocyanates by means of model compounds. The results showed that lignin has poor reactivity with isocyanates. No acceptable polyurethane could be produced by crosslinking with diisocyanates, supposedly because few reactive groups were present. Improvements in lignin reactivity by means of chemical modification were recognized to be important for the synthesis of lignin-based polyurethanes with better properties. Christian and co-workers [31] reacted lignin with ethylene oxide, propylene oxide, and alkyl sulfide for the preparation of polyoxyalkylene ether polyols. These polyols were reported to have a wide range of molecular weights and viscosities, which were then suitable for the preparation of a variety of flexible to rigid urethane foams after crosslinking with diisocyanates. However, despite the improved lignin reactivity, the polyurethane foams were still brittle, had high water absorption and low strength.

Glasser and Hsu [32] have patented a process of pretreating lignin with maleic anhydride for the purpose of improving polyol properties. The pretreatment involved a reduction of lignin unsaturation by reaction with maleic anhydride; and an activation of the phenolic hydroxyl groups for later oxyalkylation with propylene oxide. The polyols were then used for the preparation of polyurethane foams [33], adhesives, and coatings [34] with acceptable properties. The major advantages of oxyalkylated lignins are their uniform terminal functionality, in terms of aliphatic hydroxyl groups,

and improved solubility in various organic solvents, which make these lignin derivatives useful prepolymers for copolymerization. Figure 4 shows a schematic structure of hydroxyalkyl lignin derivatives, where A, B and C are lignin, alkylene oxide and hydroxyl components, respectively [35]. Studies on the synthesis and characterization of hydroxypropyl lignin (HPL) have shown that the molar substitution, defined as the number of propylene oxide repeat units (component B) attached to a single reaction site on lignin, ranged from 1.0 to 2.6, on average. The lignin content of these derivatives was as high as about 60% [35].

Oxyalkylated lignin-based polyurethanes have been extensively studied in recent years [36-42]. Polyurethane films were synthesized by solution casting from hydroxypropyl lignin derivatives, using either hexamethylene diisocyanate (HDI) or tolylene diisocyanate (TDI) as crosslinking agent [36]. The effect of lignin type, the diisocyanate structure, and the NCO to OH ratio on thermal and mechanical properties was examined. The glass transition temperature was observed to increase with increasing NCO/OH ratio. The study showed no apparent effect on modulus or tensile strength after varying the NCO/OH ratio, but there was significant influence on swelling, and on strain at break. These lignin-based polyurethanes were brittle and had poor elongation properties. The incorporation of a soft segment, such as polyethylene glycol (PEG) [38], or polybutadiene glycol (PBG) [39], into the network before (or during) crosslinking resulted in reduced brittleness and better mechanical properties. No phase separation was observed in polyurethanes containing PEG. However, it seemed that the thermal and mechanical properties of the products were dependent on both PEG content and PEG molecular weight. On the other hand, two-phase network systems were observed for the polyurethanes containing PBG. In general, phase separation was found to affect thermal and mechanical properties of the lignin-based polyurethanes. The films were either tough when PBG was the discrete phase, or rubber-like at low lignin content.

Even though the soft segment resulted in improved strain behavior, the polyurethane properties were restricted by either the PEG content or by PBG phase separation [38,39]. A way to overcome this situation was by combining a lignin derivative, by covalent bonding, with a soft segment [40-42]. The segment of choice to be attached to the lignin molecule was, for practical reasons, a



B - Component:

$\text{R} = \text{H}$ Ethylene Oxide

$= \text{CH}_3$ Propylene Oxide

$= \text{C}_2\text{H}_5$ Butylene Oxide

Figure 4. Schematic structure of hydroxyalkyl lignin derivatives [35]

polyalkylene oxide, since it could be added by chain extension of the preformed alkylene oxide component of the hydroxypropyl lignin. Kelley [41] has synthesized a series of chain extended hydroxypropyl lignin (CEHPL) derivatives. After crosslinking with diisocyanate, the polyurethane films varied from brittle glasses to soft rubbers, according to the length of the propylene oxide chains. A decrease in the glass transition temperature was observed and an increase in modulus of elasticity of the crosslinked polyurethanes (from 1.4 to 10 MPa) as the propylene oxide chain length increased. These results show that the viscoelastic properties of polymeric lignin derivatives can be tailored to specific end uses.

2.1.3 Lignin in Thermoplastic Polymers

Polymers with reactive functional groups have been extensively applied to obtain a great variety of polymeric materials. Many examples can be cited in the literature, especially the use of hydroxyl-terminated low molecular weight aliphatic polyesters or polyethers for the commercial production of thermoplastic polyurethane, polyester, and polyamide elastomers (e.g., Spandex fibers, Hytrel, etc.). These polyols are usually bifunctional linear polymers having reactive OH groups at their extreme positions. They have been termed either *telechelic polymers* or *liquid rubbers* [45].

The concept of telechelic polymers has been used since 1960 to designate low molecular weight oligomers possessing two reactive functional groups situated at both chain ends. The term comes from the Greek words *telos*, far, and *chelos*, claw, and was adapted to describe a molecule that has two reactive groups far away from each other, at the extremities of the chain, which are able to react with another functional group.

Telechelic polymers are macromolecules which have attracted the attention of scientists for a long time. This is primarily due to the fact that such polymers can be used, usually in conjunction with suitable linking agents, to perform important industrial operations. An example is the so-called

“liquid polymer” technology, in which low molecular weight telechelic polymers are used with great advantage, because of their low shrinkage during the reaction. Molds can be easily filled with these liquid polymers, the curing of which results in either a three-dimensional network (RIM process), or in extended linear chains. Telechelic polymers have also played an important role in the synthesis of multiblock copolymers by step-growth processes. By combining telechelic oligomers with different backbones, (poly)block copolymers with multiphase characteristics can be obtained, such as thermoplastic polyurethanes, polyesters, and polyamide elastomers [45,46].

Although the traditional telechelic polymers are usually bifunctional linear polymers, there are also number of telechelic polymers which have functionalities other than two, such as star-like tri- and tetrafunctional telechelic polymers.

Lignin with its macromolecular nature and polyfunctionality fits well with the concept of telechelic polymers. As shown in Figure 3, lignin, with its high molecular weight and its diverse functional groups (such as phenolic and aliphatic hydroxyl groups among others), can be easily classified as a potential natural telechelic polymer. However, the utilization of lignin as a raw material for the synthesis of thermoplastic polymers has some limitations. The major problem concerns its poor solubility in neutral organic solvents, and its diversity in functional groups which leads to an uncontrollable reactivity towards copolymerization.

One way to overcome these limitations is by chemical modification of lignin, as in the case of hydroxypropyl lignin. In HPL, not only is the terminal functionality made uniform with the majority of the functional groups (aliphatic hydroxyl groups), but also is its solubility greatly improved. Figure 5 represents the structure of an HPL molecule with 5 phenylpropane (or C₉) units. With a hydroxyl functionality of about 1.2 OH per phenylpropane repeat unit, an average organosolv hydroxypropyl lignin would possess about 6 functional groups. Since all the segments (side chains) emanate from the lignin core, the copolymer structure will resemble a star-like architecture. Thus, star-like structures result from the copolymerization of a monomer with the hydroxyl groups of HPL, or by the incorporation of segmental components (prepolymers) via a

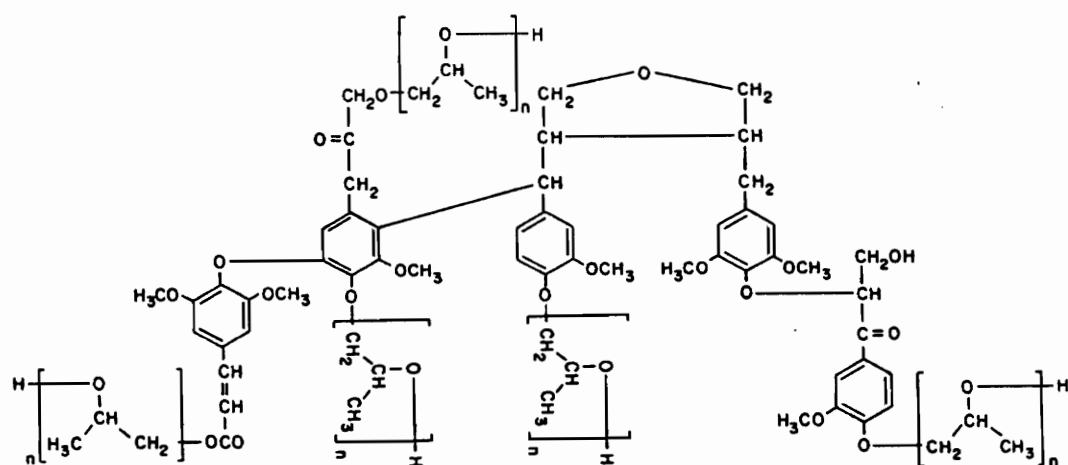


Figure 5. HPL structural model

coupling agent. Both number and length of arms can be tailored in these star-like copolymers. The number of arms can be limited to a target number by capping the functional sites available for chain extension, and the length of arms can be controlled, either by monomer/OH feed ratio in the copolymerization reaction, or by the size of the grafted segment, if a prepolymer route were selected [43,44].

Star-like copolymers were prepared from hydroxypropyl organosolv lignin by reaction with propylene oxide (PO), and they were analyzed by a combination of conventional analysis techniques. The average number of arms was controlled by partial capping of OH with diethylsulfate, and the average length of arms by PO/OH feed ratio [43,44]. Analysis methods included VPO, titration, treatment with hydriodic acid followed by gas chromatography, UV, H-NMR, and thermal analysis. Star-like copolymers were also prepared from HPL with monofunctional isocyanate end-capped cellulose triacetate segments of low degree of polymerization [47]. Copolymer films were obtained by solution casting the uncured mixture, followed by curing. The products were solid materials with distinct crystallinity, even at 20 and 40% HPL content. Figure 6 schematically illustrates the structures of (a) a partially capped (ethylated) HPL followed by copolymerization with propylene oxide, and (b) the grafting of monofunctional cellulose triacetate onto an HPL.

2.2 RESEARCH OBJECTIVES

The focus of the proposed research is the synthesis and characterization of multiphase block copolymers containing lignin. As discussed in the literature review, lignin has been successfully used as a component in engineering plastics, either in the synthesis of thermosets or as a segment for thermoplastic materials. The ability to chemically modify lignin makes lignin a potential raw material for the synthesis of block copolymers. It was seen that through chemical modification, star-like telechelic polyols having rigid aromatic lignin centers and multiple flexible polyether arms,

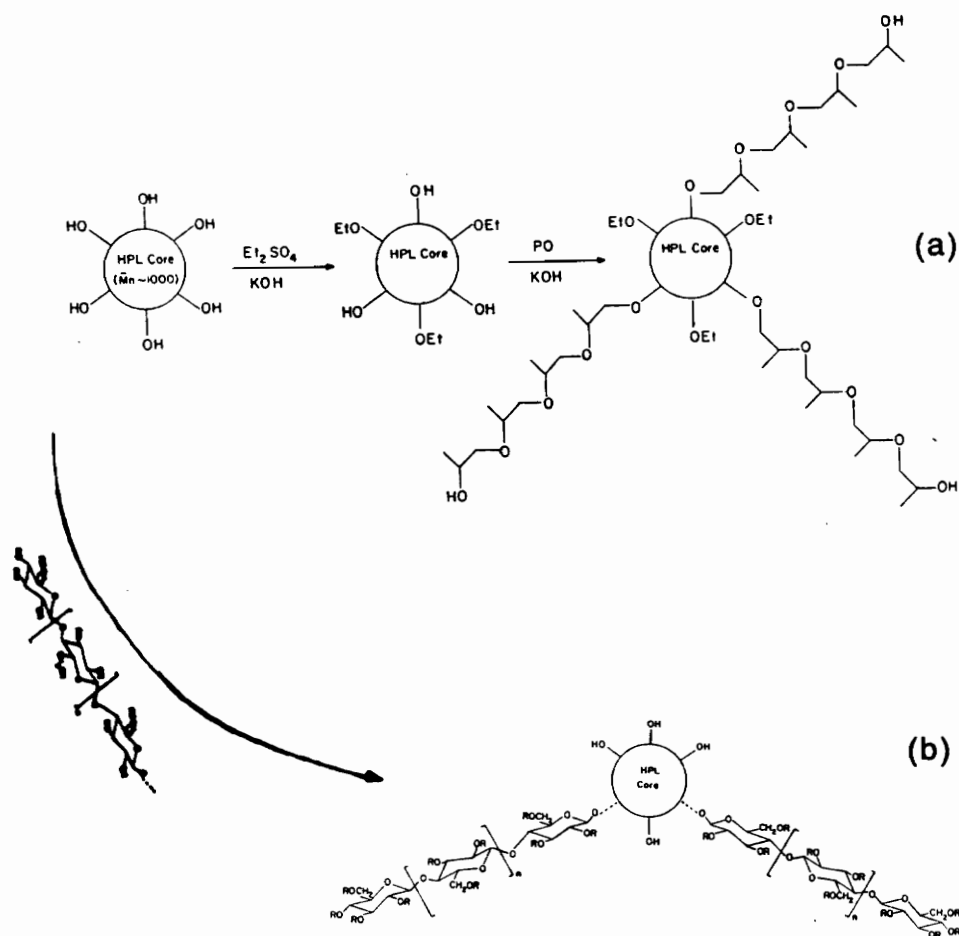


Figure 6. Scheme of two types of HPL star-like copolymers [44]: (a) partially blocked (ethylated) HPL; (b) HPL grafted with monofunctional cellulose triacetate.

could be obtained. Therefore, lignin can be used as a raw material for the synthesis of thermoplastic elastomers. Even though the polyol has lost the high modulus typical of lignin, the rigid aromatic center can regain its “reinforcement” function when coupled with hard segments. It can be expected that the lignin domain in the resulting star-like block copolymer will play a role similar to that of cross-linking agents, such as divinyl benzene (DVB) in polystyrene-polydiene star block copolymers.

In fact, a parallel can be traced between the lignin segment and the polydivinyl benzene microgel at the center of multi-armed stars. According to Bi et al. [48,49], star block copolymers containing up to 10 arms of a styrene-isoprene diblock, with isoprene at the core and DVB of number-average molecular weight about 2,500 daltons as the cross-linking agent, exhibited mechanical behavior far different from the correspondent linear block copolymers. The multi-armed stars yielded higher strengths and smaller extension ratios, and they had a less permanent set than the linear ones. These properties were attributed to the presence of permanent crosslinks due to the DVB in the system which works as a “secondary” filler particle in the multiphase block copolymer. As we recall, lignin also works as a reinforcing component in wood against mechanical stresses, and it behaves like a toughening agent for the high modulus crystalline cellulose fibers. In addition to this potential application, an appropriate selection of segments to be attached to, or copolymerized onto HPL can be expected to promote compatibilization of lignin with otherwise immiscible polymer blend systems, thereby opening new avenues for lignin utilization. Thus, this route appears to hold promise for the creation of multiphase block copolymers, such as thermoplastic elastomers or high impact resistance thermoplastics, based on lignin as a structural segment. Therefore, this study was intended (a) to continue with the evaluation of the effect of chemical modification of lignin with propylene oxide for the synthesis of lignin-based star-like polyols; (b) to synthesize star like block copolymers containing lignin and to evaluate their thermal, optical and morphological properties; and (c) to evaluate miscibility and phase morphology in polymer blends containing lignin-based star-like block copolymers.

To meet these goals, two important variables of the system were studied:

1. Type of Hard Segment

In the synthesis of thermoplastic elastomers (TPE), an essential requirement is to have (at least) one component in liquid phase (above its T_g), and another in solid phase (below its T_g or T_m), at normal operating temperatures. Since the lignin derivative is the soft segment, any hard segment to be incorporated into the telechelic HPL will generate, in principle, a TPE material. Although there is a wide selection of hard segments available, this study concentrates on three different segments representing two kinds of hard blocks, amorphous and crystalline. (The selection was based on the nature of the research program which deals, primarily, with natural polymers). The polymers were polycaprolactone, cellulose propionate and polystyrene. The first two polymers are semi-crystalline with low and high melting point, and the latter one is an amorphous segment. Polycaprolactone was chosen due to its biodegradability, and the remarkable ability to blend with different polymers, especially SAN, ABS, PVC, PE, etc. over wide composition ranges. Since polycaprolactone has a low T_m (60°C), the copolymer service temperature is limited to around room temperature. However, because of the polycaprolactone miscibility, the copolymer may also contribute this property to the lignin application. Lignin (or hydroxyalkyl lignin derivatives) that is immiscible with many polymers, can become miscible, or at least compatible, with a broad range of polymers after copolymerization with caprolactone. The role of polycaprolactone in the block copolymer is to act as a "surfactant", to improve the adhesion of the lignin phase to the other polymer in the blend. Cellulose propionate was chosen because of its carbohydrate nature; its high melting point; and its ability to serve as a model for exploring the re-association of lignin and cellulose in a composite system. It is well known that wood behaves like a fiber-reinforced composite with excellent strength and plasticity. These properties are derived from the lignocellulosic part of the wood, where lignin and cellulose fibers are cemented together as a tough composite. When removed from lignin, cellulose (and cellulose derivatives) still hold outstanding properties, sometimes superior to synthetic polymers. Among them are moisture absorption; the ability to withstand high temperatures; high strength; and high durability. However, cellulosic

fibers have some inherent drawbacks, such as lack of extensibility. By grafting cellulose ester oligomers onto hydroxypropyl lignin, not only will the cellulosic oligomer keep its crystallinity (cellulose is a highly crystalline polymer) and, consequently, its strength, but also will some chain flexibility be gained due to the elastomeric core segment lignin. Because of the high melting point of the cellulose ester derivative, the upper service temperature of the TPE can be as high as 200°C. The third segment to be studied is polystyrene. Polystyrene was chosen because it is the most common hard segment in TPE and because it is widely used in many applications. Since polystyrene is a very brittle material, increased toughness can be expected, after coupling polystyrene segments onto the rubbery telechelic HPL.

2. Segment Size

One important concern of this project is to study phase separation. Therefore, a study on the effect of hard segment molecular weight on determining morphology and domain formation is extremely important. For the system with polycaprolactone, both commercially available (monohydroxy terminated) oligomers of molecular weight 4,400 and 11,300 daltons were used, as well as monomer (ϵ -CL)-extended polytelechelic hydroxypropyl lignin. For the cellulose ester system, blocks of different molecular weights were prepared. For the polystyrene-based copolymers, commercially available oligomeric monohydroxy-terminated polystyrene of M_n 10,200 daltons was used.

2.3 REFERENCES

1. H. Sandermann, D. Scheel and T. Trenck, *Appl. Polym. Symp.*, **37**, 407 (1983)
2. S. I. Falkehag, *Appl. Polym. Symp.*, **28**, 247 (1975)
3. W. G. Glasser, *Forest Products Journal*, **31**(3), 24 (1981)
4. W. G. Glasser, L. C. -F. Wu, and J. -F. Selin, "Wood and Agricultural Residues - Research on Use for Feed, Fuels and Chemicals ", E. J. Soltes, Ed., Academic, New York, 149 (1983)
5. T. E. Timell, "Wood Chemical Composition", in "Enc. Mat. Sci. Eng.", vol. 7, 5402 (1986)
6. E. Sjostrom, "Wood Chemistry: Fundamentals and Applications", Academic Press, New York, 1981
7. W. G. Glasser and S. S. Kelley, "Lignin", in "Enc. Polym. Sci. Eng. ", vol. 8, second edition, 795 (1987)
8. K. V. Sarkanen, "Wood Lignins", B. L. Browning, Ed., " The Chemistry of Wood", New York, 1975, 689p.
9. K. V. Sarkanen and C. H. Ludwig, Ed., **Lignins - Occurrence, Formation, Structure and Reactions**. Wiley-Interscience, N. Y., 1971, 916p.
10. K. Freudenberg and A. C. Neish, "Constitution and Biosynthesis of Lignin", Springer-Verlag, New York, 1968
11. E. Adler, *Wood Sci. Technol.*, **11**, 169 (1977)
12. K. Freudenberg, *Holzforschung*, **18**(1,2), 3 (1964)
13. K. Freudenberg, *Holzforschung*, **18**(6), 166 (1964)
14. J. M. Harkin, *Rec. Adv. Phytochemistry*, **2**, 35 (1969)
15. W. G. Glasser and H. R. Glasser, *Holzforschung*, **28**(1), 5 (1974)
16. W. G. Glasser and H. R. Glasser, *Pap. Puu*, **63**(2), 71 (1985)
17. W. G. Glasser in J. P. Casey Ed., **Pulp and Paper: Chemistry and Chemical Technology**, vol. 3, 3rd., Wiley-Interscience, New York, 39 (1980)

18. E. Sjostrom, "Wood Chemistry: Fundamentals and Applications", Academic Press, New York, 1981
19. H. Hatakeyama, K. Iwashita, G. Meshitsuka, and J. Nakano, *J. Jap. Wood Res. Soc. (Mokuzai Gakkaishu)*, **21**(11), 618 (1975)
20. W. J. Cousins, R. W. Armstrong, and W. H. Robinson, *J. Mat. Sci.*, **10**(10), 1655 (1975)
21. W. J. Cousins, *Wood Sci. Technol.*, **10**(1), 9 (1976)
22. W. G. Glasser, O. H. -H. Hsu, D. L. Reed, R. C. Forte, and L. C. -F. Wu, *ACS Symp. Ser.*, **172**, 311 (1981)
23. K. Forss and A. Fuhrmann, *Paperi ja Puu*, **58**(11), 817 (1976)
24. K. Forss and A. Fuhrmann, *Forest Products J.*, **29**(7), 39 (1979)
25. A. J. Dolenko and M. R. Clark, *Forest Products J.*, **28**, 41 (1978)
26. P. C. Muller, S. S. Kelley, and W. G. Glasser, *J. Adhes.*, **17**, 185 (1984)
27. H. H. Nimz, in A. Pizzi Ed., "Wood Adhesives: Chemistry and Technology", Marcel Dekker, Inc., New York, chap. 5, 247 (1983)
28. D. B. Holsopple, W. W. Kurple, and K. R. Kurple, U. S. Patent 4,265,809 (May 5, 1981)
29. K. Hofmann, "Ph.D. Dissertation", Virginia Polytechnic Institute and State University, Blacksburg, VA, May, 1991
30. K. Kratzl, K. Buchtela, J. Zauner, and O. Ettingshagen, *TAPPI*, **45**(2), 113 (1962)
31. D. T. Christian, M. Look, A. Nobell, and T. S. Armstrong, U. S. Patent 3,546,199 (Dec. 8, 1970)
32. W. G. Glasser and O. H. -H. Hsu, U. S. Patent 4,017,474 (Apr.12, 1977)
33. O. H. -H. Hsu and W. G. Glasser, *Appl. Polym. Symp.*, **28**, 297 (1975)
34. O. H. -H. Hsu and W. G. Glasser, *Wood Sci.*, **9**(2), 97 (1976)
35. W. G. Glasser, C. A. Barnett, T. G. Rials and V. P. Saraf, *J. Appl. Polym. Sci.*, **30**, 2207 (1985)
36. V. P. Saraf and W. G. Glasser, *J. App. Polym. Sci.*, **29**, 1831 (1984)
37. T. G. Rials and W. G. Glasser, *Holzforschung*, **38**, 263 (1984)

38. V. P. Saraf, W. G. Glasser, G. L. Wilkes, and J. E. McGrath, *J. Appl. Polym. Sci.*, **30**, 2207 (1985)
39. V. P. Saraf, W. G. Glasser, and G. L. Wilkes, *J. Appl. Polym. Sci.*, **30**, 3809 (1985)
40. S. S. Kelley, W. G. Glasser, and T. C. Ward, *J. Wood Chem. Technol.*, **8**(3), 341 (1988)
41. S. S. Kelley, "**Ph.D. Dissertation**", Virginia Polytechnic Institute and State University, Blacksburg, VA, Mar., 1986
42. L. C. -F. Wu and W. G. Glasser, *J. Appl. Polym. Sci.*, **29**, 1111 (1984)
43. W. de Oliveira and W. G. Glasser, *J. Appl. Polym. Sci.*, **37**, 3119 (1989)
44. W. de Oliveira and W. G. Glasser, "**Lignin: Properties and Materials**", ACS Symposium Series No. 397, chap. 32, 1989
45. R. Jerome, "Halato-Telechelic Polymers: A New Class of Ionomers", E. J. Goethals, Ed., "**Telechelic Polymers: Synthesis and Applications**", chapt. 11, 1989
46. E. J. Goethals, "Introductory Remarks", E. J. Goethals, Ed., "**Telechelic Polymers: Synthesis and Applications**", chapt. 1, 1989
47. V. Demaret and W. G. Glasser, *J. Appl. Polym. Sci.*, **30**, 570 (1989)
48. L. K. Bi, L. J. Fetters, M. Morton, *Polym. Prep. (Am. Chem. Soc., Div. Polym. Chem.)*, **15**(2), 157 (1974)
49. L. K. Bi, L. J. Fetters, *Macromolecules*, **9**(5), 732 (1976)

3.0 SYNTHESIS AND CHARACTERIZATION OF CAPROLACTONE-HYDROXYPROPYL LIGNIN STAR-LIKE COPOLYMERS

3.1 INTRODUCTION

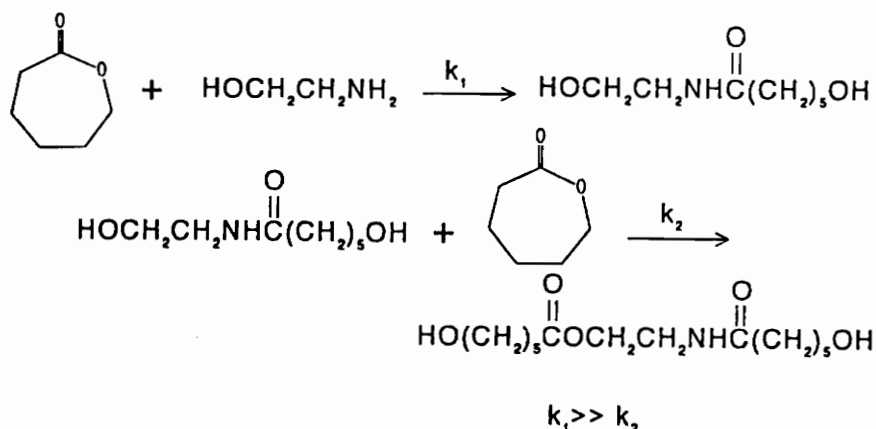
There has been much interest in studying poly(ϵ -caprolactone) (PCL) and its copolymers, mostly because the miscibility characteristics of the homopolymer (PCL) [1,2]. Other attractive features are the biodegradability of PCL, its ability to disperse pigments, and its low-temperature adhesiveness [2]. All this combined makes PCL a segment of choice for copolymerization.

Brode and Koleske [1] have studied in detail methods for lactone polymerization with major emphasis on ϵ -caprolactone. In general there are three types of systems that can initiate the polymerization of lactones (Table 1).

Table 1. Lactone Polymerization Systems [1]

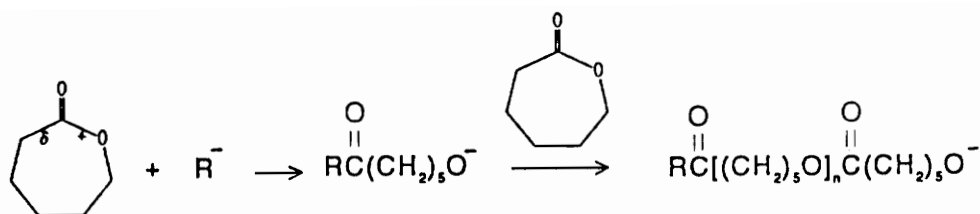
Type	System	Examples
1	Active hydrogen initiator, no catalyst	ROH, RNH ₂ , etc.
2	Nonactive hydrogen initiator, or catalyst only	R ₂ Zn, Sn(OR) _{2,4} , etc.
3	Active hydrogen initiator plus catalyst	ROH + Ti(OR) ₄ , etc.

The copolymerization of lactones with conventional active hydrogen initiators (type 1), such as alcohols, amines and carboxylic acids without the help of a catalyst, usually produces low-molecular weight products. For example, the ethylene glycol-initiated polymerization of ϵ -caprolactone requires a reaction cycle of 35 hours at 190°C for quantitative conversion and for molecular weights of about 5,000 daltons. The cyclic ester monomer will open in the presence of an initiator that contains an active hydrogen atom, as shown in reaction scheme 1.



In the type 2 system, it is possible to reach high-molecular weight polymers by using anionic or cationic catalysts, such as dibutylzinc or stannous octanoate. Organometallic catalysts, such as stannous diacrylate or stannic tetracylate have been used without active hydrogen initiators to obtain PCL of at least 100,000 molecular weight [1]. In general, the shortcoming of this type of polymerization is the poor control over both molecular weight and polymer end groups. This problem can be overcome by using an active hydrogen initiator in conjunction with a catalyst, such as stannous octanoate (type 3). Polyols, polyamides, carboxylic acids, etc., have been used with catalyst systems, such as zinc or lead salts, alkyl titanates, stannous esters, stannic esters, and phosphines to control molecular weight and polymer end groups.

The mechanism of lactone polymerization is generally an anionic type involving acyl-oxygen fission with propagation through an alkoxide anion [3], as seen in reaction scheme 2.



This type of mechanism favors, most often, side reactions, such as intra - and intermolecular transesterification which leads to a mixture of linear and cyclic molecules [4,5]. As a consequence, undesirable results are frequently encountered in the anionic polymerization of lactones. Among the more common consequences are low polymer yield, uncontrollable molecular weight, broad distribution, coupling linkage, and cyclic ester oligomers [6]. Recently more suitable catalytic pathways for the polymerization ϵ -caprolactone have been devised [7-10]. It has been found that less reactive initiators, like aluminum alkoxide, can favor linear chain formation at the expense of macrocycles. PCL has been produced from ϵ -CL through a perfectly living polymerization initiated by bimetallic μ -oxo alkoxides under mild conditions [2]. The usually observed intramolecular transesterification was considerably suppressed with these initiators. Similar observations have been reported by Inoue and co-workers for the polymerization of ϵ -CL initiated with (5,10,15,20-tetraphenylporphinato) aluminum methoxide-methanol mixture [9,10].

In general high-molecular weight PCL is a tough, crystalline polymer with a melting point of about 63°C, and tensile strength of 3,500 psi. It has a high degree of crystallinity (ca. 60%) and it cannot be quenched to a glass due to its high crystallization rate. By studying compatible blends with poly(vinyl chloride), the T_g of amorphous PCL was found to be -71°C at about 1 Hz [11]. For the annealed and crystalline sample, the T_g was about -60°C. At molecular weights lower than 25,000 daltons, the polymer is hard and brittle, and its tensile properties are difficult to measure.

Several studies have been investigating the properties and applications of graft and block copolymers containing PCL. Hsieh [12] has synthesized styrene-butadiene-caprolactone terpolymers of high butadiene content, which behaved much like a thermoplastic elastomer. The polymers varied from rubbers with high strength, to clear, thermoplastic resins. They presented very good ozone resistance. Blends of the terpolymers with styrene-acrylonitrile showed good properties. High tensile strength, fair melt flow, and remarkable Izod impact were reported for the blend 25-50-25 (styrene-butadiene- ϵ -caprolactone) block terpolymer with 75-25 (styrene-acrylonitrile) copolymer. Tensile strength, flexural modulus, and melt flow increased, while impact resistance decreased with decreasing amount of block terpolymer in the polymer blend.

Koleske and co-workers [13] have patented a process to synthesize A-B-A block copolymers in which the A blocks comprise linear lactone units. These block copolymers exhibit thermoplastic elastomeric properties. According to the authors, these copolymers could be used as plasticizers for poly(vinyl chloride) resins; as additives in tape joint compounds with improved drying characteristics; and as surfactants.

Triblock poly(propylene oxide)-polycaprolactone copolymers with elastomeric properties were also synthesized by McGrath and co-workers [14]. The reaction of poly(propylene oxide) directly with aluminum porphyrin as initiator, and bisphenol A as a chain transfer agent, produced a rubbery segment. By this method, poly(propylene oxide) with controlled molecular weight and narrow molecular weight distribution was produced. The hard segments constituted chains of polycaprolactone built up through the copolymerization of the monomer ϵ -caprolactone on both end groups of poly(propylene oxide). Stannous octanoate served as catalyst. Block copolymers with crystalline-rubbery-crystalline properties were produced. The mechanical properties of these copolymers exhibited two-phase behavior characteristic of a thermoplastic elastomer.

The objective of this study was to synthesize and characterize multiphase block copolymers based on poly(ϵ -caprolactone) and hydroxypropyl lignin. Three series of star-like copolymers were pre-

pared covering a wide range of composition. The research included a study of the effect of the PCL block size on the copolymer solution and thermal properties, as well as the effect of the HPL segment on the solid state morphology of the copolymers. This study also evaluated the extent to which the degree of propoxylation of HPL could affect the crystallization behavior of the polyester block.

3.2 EXPERIMENTAL SECTION

3.2.1 Materials

Epsilon-Caprolactone (ϵ -CL): Epsilon-caprolactone used in this study was obtained from Aldrich Chemical Company. Typically, 500 mL of ϵ -CL and ground calcium hydroxide were added to a one liter round bottle flask. The flask was connected to a distillation apparatus, and the mixture was stirred under nitrogen for 24 hours (room temperature). The dried ϵ -CL was then distilled under vacuum, and the distillate stored in a bottle containing molecular sieves.

Polycaprolactone mono-hydroxyl terminated (PCL): Mono-hydroxyl terminated polycaprolactone with number-average molecular weights of 11,300 and 4,400 daltons was purchased from Scientific Polymer Products. Once received, the samples were dried and kept in a desiccator. These compounds were used without further purification.

Stannous octanoate: The catalyst, stannous octanoate, was obtained from Aldrich Chemical Company. It was used as received.

2,4-Tolylene diisocyanate (TDI): TDI was supplied by Aldrich Chemical Company and used without further purification.

Tetrahydrofuran (THF): THF was supplied by Fischer Scientific Chemical Company. The solvent was dried over a mixture of metallic potassium and benzophenone, refluxed and distilled under dried nitrogen. The material was collected in a bottle and stored over molecular sieves.

Hydroxypropyl lignin (HPL): Hydroxypropyl lignins were prepared according to a procedure described elsewhere [15,16]. Typically, 400 g of dried lignin was slurried in 1.5 L of toluene and charged into a 4 L wide-neck resin kettle equipped with condenser and water separation tube. KOH was added as 50% aqueous solution in approximately 7% by weight of lignin. The mixture was stirred and refluxed overnight. After cooling, the toluene suspension was charged into a one gallon pressure reactor. The reactor was heated to 120 to 140°C and propylene oxide (PO) was added stepwise. The PO addition continued until the desired level of propoxylation had been reached. The reactor was then cooled, and the product recovered by drainage through the bottom drain valve. The toluene solution was saturated with CO₂ to neutralize KOH. The solvent was then recovered by evaporation under reduced pressure.

HPL purification: Two methods for removal of propylene glycol, oligomers and poly(propylene oxide) formed during the reaction were used. They consisted of either liquid-liquid extraction with hexane/acetonitrile, or fractional precipitation using hexane and acetone as non-solvent and solvent, respectively.

(a) Liquid-liquid extraction: The solvent-free reaction product was dissolved in acetonitrile and transferred to an apparatus for liquid-liquid extraction. Hexane was used to extract homopolymer and oligomers. After 2 to 14 days of extraction, the acetonitrile-soluble fraction was roto-evaporated, and the solvent-free HPL was dried under vacuum and stored in a desiccator.

(b) Fractionation: An alternative (and faster) procedure to remove poly(propylene oxide) consisted of fractional precipitation. Typically a 10% acetone solution of solvent-free reaction product was prepared. To that solution, a ten fold volume of hexane (non-solvent) was added. After 2 hours the supernatant was removed from the precipitate. The precipitate was then redissolved in acetone to form a 10% solution. Following that, a five fold volume of hexane was added. Again, after 2 hours of precipitation, the supernatant was removed. The final precipitate was roto-evaporated to remove acetone, dried under vacuum and stored in a desiccator.

Gel permeation chromatography was used to monitor homopolymer extraction [16].

Capping of OH groups: Aliphatic OH groups of HPL were partially capped with diethylsulfate in aqueous KOH, at room temperature. The ethylation consisted of dissolving 100 g of HPL in 500 mL of acetone in a three-necked round bottom flask. Potassium hydroxide was added to maintain an alkaline medium throughout the reaction. A target amount of diethylsulfate was then added dropwise into the solution, and the reaction was continued overnight under a constant flow of nitrogen. At the end of the reaction, the pH was adjusted to 2.0 - 3.5 with 5N HCl, the mixture heated to destroy any remaining diethylsulfate, and the product extracted from the solution with chloroform in a separatory funnel. After extraction, the solution was freed from chloroform by evaporation under reduced pressure (rotation evaporation). The resulting syrup was precipitated into a large excess (ca. 10:1) of acidified water. The precipitate was filtered, washed and freeze-dried.

3.2.2 Synthesis of Mono-Isocyanate Terminated Polycaprolactone

Mono-isocyanate terminated polycaprolactone prepolymers were prepared from the reaction of hydroxyl-terminated polycaprolactone (one hydroxyl group per polymeric chain, molecular weights of either 11,300 or 4,400 daltons) with TDI. In a typical reaction, 1 g of PCL along with 0.1% by weight of stannous octanoate, were introduced into a two-necked flask equipped with a magnetic

stir bar, and the flask connected to a vacuum line for further drying. After 4 hours, the reactor was sealed with rubber septa, transferred to an oil-bath on a stir plate, and purged with prepurified and dried nitrogen. Under a constant flow of nitrogen, 10 mL of freshly distilled THF were added into the reaction flask through a hypodermic syringe to dissolve the reactants. The reactor was heated to 50°C, and then 65 μ L of TDI in excess (approximately 5:1 molar ratio of TDI:PCL), was added. The reaction was kept at 50°C and under stirring for 24 hours. After cooling, the product was precipitated into a large excess of petroleum ether to eliminate unreacted TDI, filtered, washed with petroleum ether, and dried under vacuum. The mono-isocyanate capped prepolymer was immediately used for grafting. Infrared spectroscopy was used to monitor the reaction.

3.2.3 Copolymer Synthesis

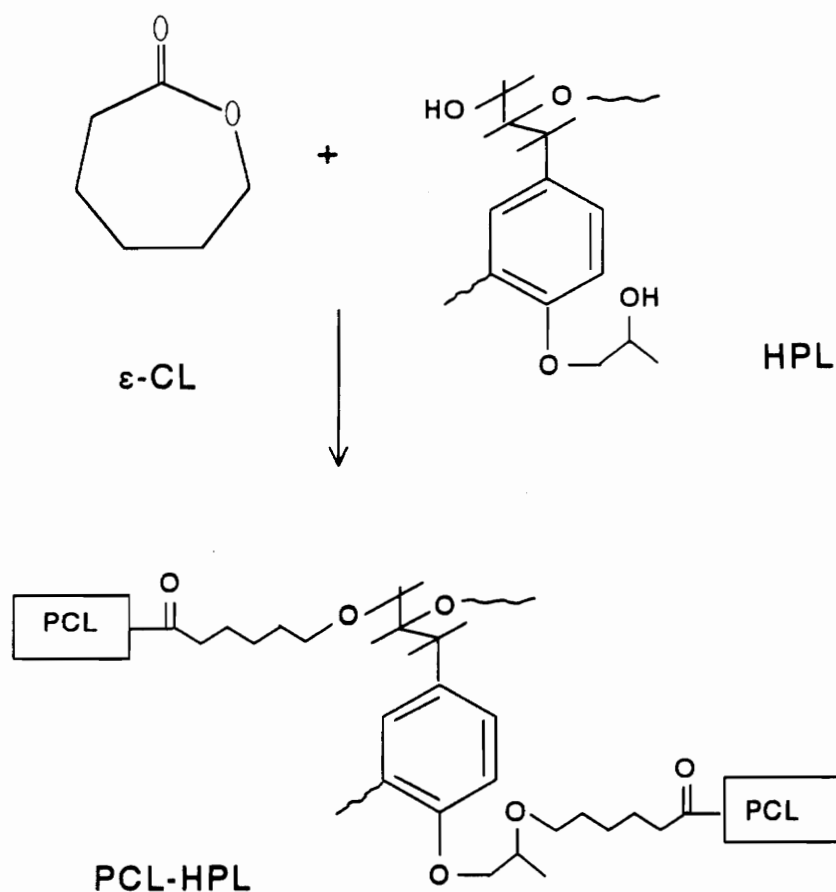
Star-like copolymers of HPL and PCL were prepared by two different methods. The first method (method I) consisted of the initiation and propagation through anionic polymerization of ϵ -caprolactone via hydroxyl end groups of HPL, as seen in reaction scheme 3. The second method (method II) involved the grafting of monofunctional isocyanate terminated polycaprolactone (PCL-NCO) onto HPL, as shown in reaction scheme 4.

Method I: The anionic copolymerization of ϵ -CL with HPL was carried out in a 3-necked round bottom flask fitted with a mechanical stirrer, inert gas inlet and a condenser. In a typical reaction, a calculated amount of HPL and stannous octanoate was charged into the flask, which was hooked to a vacuum line for further drying of HPL and catalyst. Then the flask was immediately connected to the mechanical stirrer and condenser and the reactor was flushed with prepurified and dried nitrogen. A calculated amount of ϵ -CL (previously distilled) was then syringed into the flask, and the mixture was stirred until a homogeneous solution resulted. The reactor flask was submerged into an oil-bath, and the temperature was raised to 100-110°C. After approximately 15 hours of reaction, the oil-bath temperature was raised to 150-160°C and the reaction allowed to proceed for more 5-10

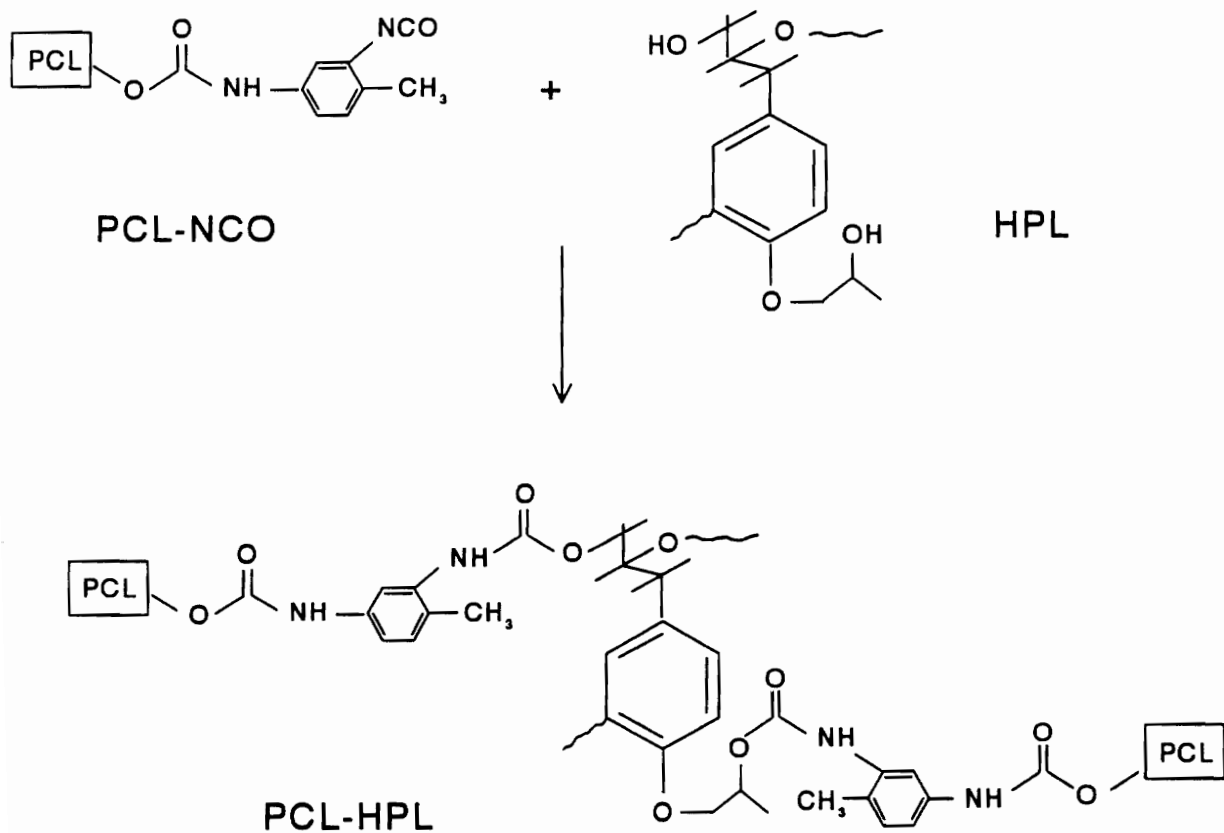
hours in order to produce the desired molecular weight. At the end of the reaction, the product was cooled to room temperature, dissolved in THF and precipitated in a large amount of methanol or aqueous methanol (in case of copolymers with low ϵ -CL content). The copolymer was then filtered, purified in a soxhlet apparatus to extract unreacted HPL and low molecular weight copolymer, and finally dried under vacuum.

Method II: In method II, star-like copolymers of HPL and PCL were prepared by a two-step process. The first step consisted of the synthesis of PCL-NCO, which has been described in section 3.2.2. The second step involved the grafting reaction of PCL-NCO segments onto telechelic HPL. Basically, the grafting reaction was performed in a cleaned, flamed and nitrogen purged 2-necked round bottom flask, equipped with a magnetic stir bar and rubber septa under prepurified dried nitrogen atmosphere. First, a calculated amount of HPL and stannous octanoate dissolved in THF were charged to the reaction flask through a hypodermic syringe. Next, PCL-NCO previously dried and dissolved in THF was syringed into the flask in the desired ratio of PCL-NCO to HPL polyol. The reaction flask was submerged into the oil-bath and heated to 50°C. The grafting reaction was terminated after 24 hours through precipitation into aqueous methanol.

Extraction of unincorporated HPL: Since both PCL and $(PCL)_n$ -HPL copolymers are usually soluble in the same solvents, the extraction of unreacted PCL segments becomes difficult. It is easier, however, to separate PCL from HPL because the latter is soluble in aqueous methanol, while PCL is not. Therefore, it was possible to remove unreacted HPL. That was the reason for precipitating the reaction product into aqueous methanol and further extracting with methanol in a soxhlet apparatus. The reaction product was later characterized by GPC and UV analysis.



Scheme 3. Anionic polymerization of ϵ - caprolactone
via hydroxyl end groups of HPL (Method I)



Scheme 4. Synthesis of PCL-HPL copolymers via grafting of
PCL preformed segment (Method II)

3.2.4 Characterization

Gel Permeation Chromatography (GPC): Gel permeation chromatography was used to measure the molecular weights and molecular weight distributions of HPL and of the copolymers. A GPC with both differential viscosity and refractive index detectors was used for absolute molecular weight determination. The method works by the universal calibration approach, in which the log of intrinsic viscosity times molecular weight is plotted against elution volume. Standards for each polymer are not necessary because the method is universal for all polymers, linear and branched. The analyses were performed on a Waters equipped with Ultrastaygel columns of 10^6 , 10^4 and 10^3 Å, in connection with a refractive index (concentration) and sequential differential viscometry (DV) detectors. Polystyrene standards were used for the construction of the universal calibration curve. The flow rate of a polymer sample dissolved in HPLC grade THF was 1.0 mL per minute.

Fourier Transform Infrared Spectroscopy (FTIR): The progress of the isocyanate capping reaction was monitored by using a Nicolet 55XC FTIR spectrometer. Samples were taken during the course of the reaction, purified and run as KBr pellets. The rate of formation of the PCL-NCO product was observed in the absorption spectra at 3448 cm^{-1} and 2274 cm^{-1} . The absorbance at 2274 cm^{-1} was studied to evaluate the presence of an isocyanate group.

Ultraviolet Spectroscopy (UV): UV spectroscopy was used to determine the molar mass of lignin in the copolymers based on a procedure described elsewhere [17]. The wavelength maximum for lignin was established to be 280 nm. Copolymer solutions of known concentration were made in chloroform. The absorbance of the solutions were then read at 280 nm, on a Varian/Cary-219 UV-VIS spectrophotometer.

Proton-Nuclear Magnetic Resonance Spectroscopy (H-NMR): H-NMR analysis was used to determine the number-average functionality of PCL-OH prepolymer, chemical information of the

copolymer and degree of propoxylation in the HPL samples. The analyses were performed on either a JEOL 270 MHz, or a VARIAN 400 MHz spectrometer. The samples were dissolved in deuterated chloroform and run at room temperature. Tetramethylene silane was used as an internal standard. For HPL samples, acetylation was performed prior H-NMR analysis, according to a procedure described elsewhere [18]. The number-average PCL-OH chain per OH group was estimated by end-group analysis. The procedure consisted of reacting PCL-OH with triethylsilyl chloride in order to replace the hydroxyl group by a triethylsilyl group containing 15 protons. This allowed enhanced sensitivity for the calculation of the concentration (functionality) of OH end-groups.

General Procedure for Silylation: A 0.2 mmol sample of PCL-OH, 4.0 mmol of imidazol, and 2.0 mmol of chlorotriethylsilane were reacted in 10 mL dimethylformamide (DMF). The solution was stirred constantly until the reaction was complete, usually after 2 hours. The reaction product was precipitated into 20 mL of ethanol and stirred for 10 min. Then water was added, the precipitate filtrated and washed with water and petroleum ether. After this workup, the final product was dried under vacuum and stored for H-NMR analysis.

Determination of Functionality: The number-average functionality (F_n) was obtained from the molar concentration of OH groups and the number-average molecular weight (M_n) of the PCL-OH, according to the following equation:

$$F_n = c_{OH} \cdot M_n$$

where c_{OH} is equal to the number of moles of the oligomer per unit weight.

Titration: The total hydroxyl content of HPL was determined by acetylation and back titration of free acetic acid [19]. In general, quadruplicate HPL samples were weighed out in a 5 mL micro re-

action vessel and dissolved in a 3:1 (volume) mixture of pyridine-acetic anhydride. The samples were reacted overnight at 50°C. The micro reaction vessel was then rinsed with acetone into 250 mL beakers following the addition of 100 mL of water. The beakers were covered with paraffin film and allowed to stand for 1 hour. The titration was carried out using a Brinkmann Potentiograph E-576.

Differential Scanning Calorimetry (DSC): DSC thermograms were obtained on a Perkin-Elmer Model DSC-7. The temperature was scanned from -150 to 100°C at a heating rate of 10°C per minute. The scanning procedure consisted of two steps. In the first run, the samples were cooled to -150°C and heated at 10°C/min to 100°C. In the second run, the samples were quenched to -150°C at 200°C/min and reheated at 10°C/min to 100°C. Glass transition temperatures were taken as midpoint of the change in slope of the baseline. The T_m was taken as the temperature corresponding to endothermic peak location. The percent of crystallinity was calculated on the basis of measured heat of fusion per gram of pure 100% crystalline PCL, 32.4 cal/g [20].

Dynamic Mechanical Thermal Analysis (DMTA): The viscoelastic properties of the copolymer were observed by a Polymer Laboratories DMTA instrument, at a frequency of 1 Hz. The injection-molded dogbone sample was rapidly quenched to -100°C, and the measurement was made at a heating rate of 10°C/min until the sample became too soft to be tested.

Optical Microscopy: Optical microscopy was conducted on a Zeiss Axioplan microscope, fitted with a Linkam TMS90 Hot Stage and a Zeiss ML 100 camera. The nucleation and growth behavior were observed on thin films of copolymers between glass plates.

3.3 RESULTS AND DISCUSSION

3.3.1 Effect of Synthesis Parameters on Copolymer Properties

The reaction of mono-hydroxyl terminated PCL with TDI produces a mono-isocyanate terminated PCL segment. The course of this reaction was followed by FTIR in the 2300 cm^{-1} region. Figure 7 shows the spectra of the PCL before reaction, and after 6, 12, and 24 hrs of reaction. After 24 hours of reaction at 50°C , the intensity of the OH absorption peak at 3350 cm^{-1} had decreased, and the NCO absorption peak at 2274 cm^{-1} had appeared. The reaction was practically complete after 24 hours, as seen in curve c of Figure 7.

The concentration of OH groups per PCL-OH chains was estimated by H-NMR Spectroscopy. Since the proton signal of the hydroxyl groups is usually too weak for a direct measurement, OH groups were derivatized in order to improve the measurement. Figure 8 shows the H-NMR spectrum of a mono-hydroxyl terminated PCL (a) before and (b) after incorporation of a triethylsilyl group. By ratioing the integration of the 15 protons of the triethylsilyl present on the end group (0.5-1.0 ppm) to the integration of the methylenic ester protons along the PCL backbone (4.1 ppm), the actual concentration of OH groups could be calculated. Then by taking this concentration value and multiplying it by the number-average molecular weight of the PCL-OH, the number-average functionality of the PCL-OH chains was obtained. The average functionality was about 0.91 OH groups per chain.

Table 2 presents the molecular weights, hydroxyl content, composition and glass transition temperature of the HPL's used in this study. In spite of the fractionation process to remove homopolymer (polypropylene oxide), which also removes low molecular weight lignin derivatives, the HPL's presented, in general, a broad molecular weight distribution. The other important vari-

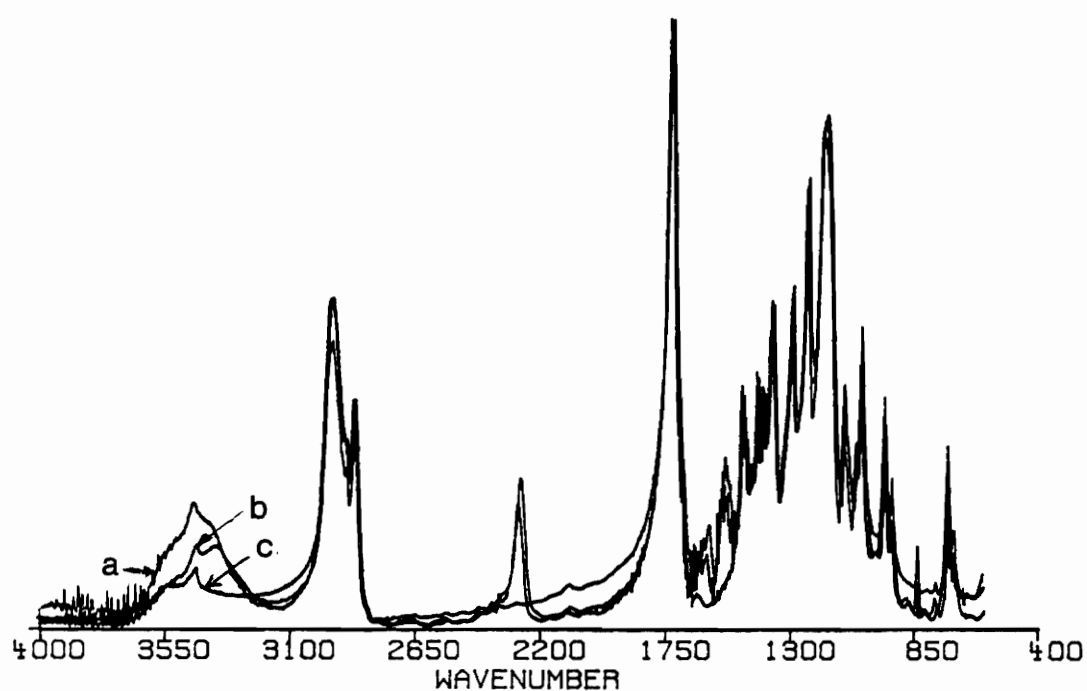


Figure 7. FTIR spectra of the qualitative formation of polycaprolactone monoisocyanate: (a) PCL mono-hydroxyl terminated; (b) the same reacted with TDI (after 12 hrs); (c) the same, reacted with TDI (after 24 hrs)

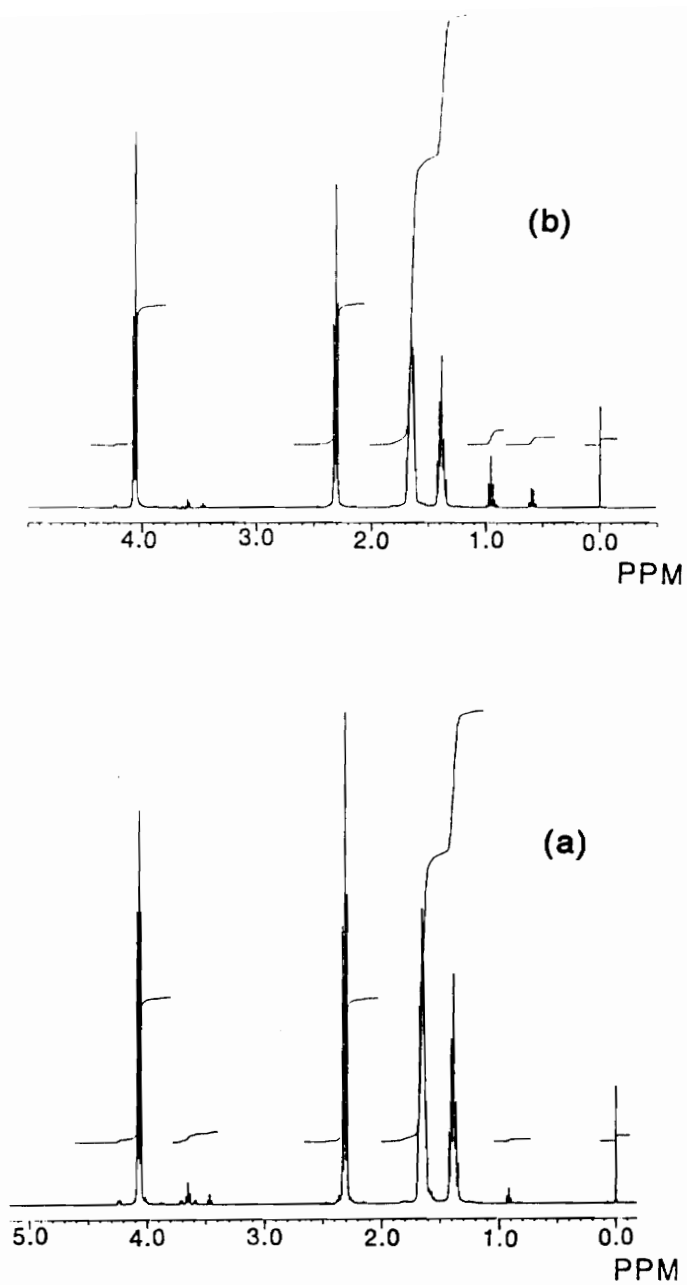


Figure 8. Proton-NMR spectra of mono-hydroxyl terminated PCL: (a) before and (b) after silylation.

Table 2. Experimental Results of Hydroxypropyl Lignin Synthesis

Sample	M_n	M_w	M_w/M_n	OH (%)	OH ^a /mol	T_g (°C)	Lignin (wt%)	PO ^b (wt%)
HPL(A)	2,100	10,000	4.8	5.7	7.0	85	83	17
HPL(B)	6,400	67,900	10.6	1.0	3.5	-7	27	73
HPL(C)	3,500	20,300	5.8	3.0	7.0	1	50	50

a Number of hydroxyl per mol

b Propylene oxide

able in Table 2 is the glass transition temperature. As it will be discussed later in this section, HPL glass transition plays a major role in determining copolymer morphology and crystallization behavior. HPL(A) was a glassy solid with its T_g above room temperature, whereas the other two HPL's (B and C) were low and high viscosity liquids at ambient temperature, respectively.

The physical aspects of the copolymers varied from dark, waxy products (high HPL content) to light brown powders (low HPL content). The copolymers were soluble in various solvents, such as THF, acetone, toluene and chlorinated solvents, but they were insoluble in alcohols and non-polar solvents.

The molecular characteristics of the copolymers synthesized in this study are summarized in Tables 3 and 4. Three series of $(PCL)_n$ -HPL star-like copolymers are presented, based on HPL number-average molecular weight of 2,000; 3,500, and 6,400 daltons, respectively. Series A and B represent copolymers synthesized according to method I (see scheme 3), in which ϵ -CL is copolymerized through the hydroxyl groups of HPL (Table 3). Series C combines the data from method II (see scheme 4) (Table 4). In this case, a preformed functionalized PCL segment was introduced to HPL via graft copolymerization. In both methods the data show that copolymers from HPL and PCL can be prepared at variable composition, with number-average molecular weights ranging from 3,700 to 53,000 daltons.

When both methods are compared in terms of molecular weight distribution, it is seen that method II produces copolymers with much narrower polydispersity, as shown in Figure 9. In method II the preformed PCL segments have a narrow polydispersity from the beginning. After grafting, the copolymer still will present a somewhat narrow molecular weight distribution if the HPL content is low. The MWD starts broadening as the HPL content rises. GPC chromatograms illustrate both cases in Figure 9 (b, c). On the other hand, method I gives in all cases high polydispersity, with values ranging from 1.7 to 11.6, as seen in Figure 9 (a)(and Table 3).

Table 3. Molecular Characterization Data of Polycaprolactone-Hydroxypropyl Lignin Star-Like Copolymers Synthesized According to Method I

Sample	M_n HPL	M_w/M_n HPL	M_n cop. ^c	M_w/M_n cop.	# ^a	M_n arm	Lignin wt%	(PO + PCL) ^b wt%
A1	2100	4.8	3800	11.6	7.0	250	38	52
A2	2,100	4.8	4,400	10.6	7.0	800	28	72
A3	2,100	4.8	6,900	2.5	7.0	700	20	80
A4	2,100	4.8	9,800	2.7	7.0	1,100	20	80
A5	2,100	4.8	14,400	2.4	7.0	1,800	17	83
A6	2,100	4.8	11,100	9.6	7.0	1,300	16	84
A7	2,100	4.8	17,400	2.5	7.0	2,200	12	88
A8	2,100	4.8	52,800	2.0	7.0	7,200	5	95
B1	6,400	10.6	9,400	4.3	3.5	850	18	82
B2	6,400	10.6	9,600	1.7	3.5	900	3	97
B3	6,400	10.6	12,500	3.4	3.5	1,700	21	79
B4	6,400	10.6	11,900	3.9	3.5	1,600	17	83
B5	6,400	10.6	14,000	9.2	3.5	2,200	12	88
B6	6,400	10.6	14,500	4.0	3.5	2,300	6	94
B7	6,400	10.6	23,600	2.1	3.5	4,900	14	86

a Number of arms

b PO = Propylene Oxide, PCL = Polycaprolactone

c copolymer

Table 4. Molecular Characterization Data of Polycaprolactone-Hydroxypropyl Lignin Star-Like Copolymers Synthesized According to Method II

Sample	M_n HPL	M_w/M_n HPL	M_n cop. ^c	M_w/M_n cop.	# ^a	M_n arm	Lignin wt%	(PO + PCL) ^b wt%
C1	6,400	10.6	16,900	1.6	2.4	4,400	6	94
C2	3,500	5.8	18,300	1.9	3.4	4,400	8	92
C3	3,500	5.8	19,900	2.1	3.7	4,400	12	88
C4	3,500	5.8	31,900	1.4	2.5	11,300	13	87
C5	3,500	5.8	21,100	5.1	1.6	11,300	15	85

a Number of arms

b PO = propylene Oxide, PCL = Polycaprolactone

c copolymer

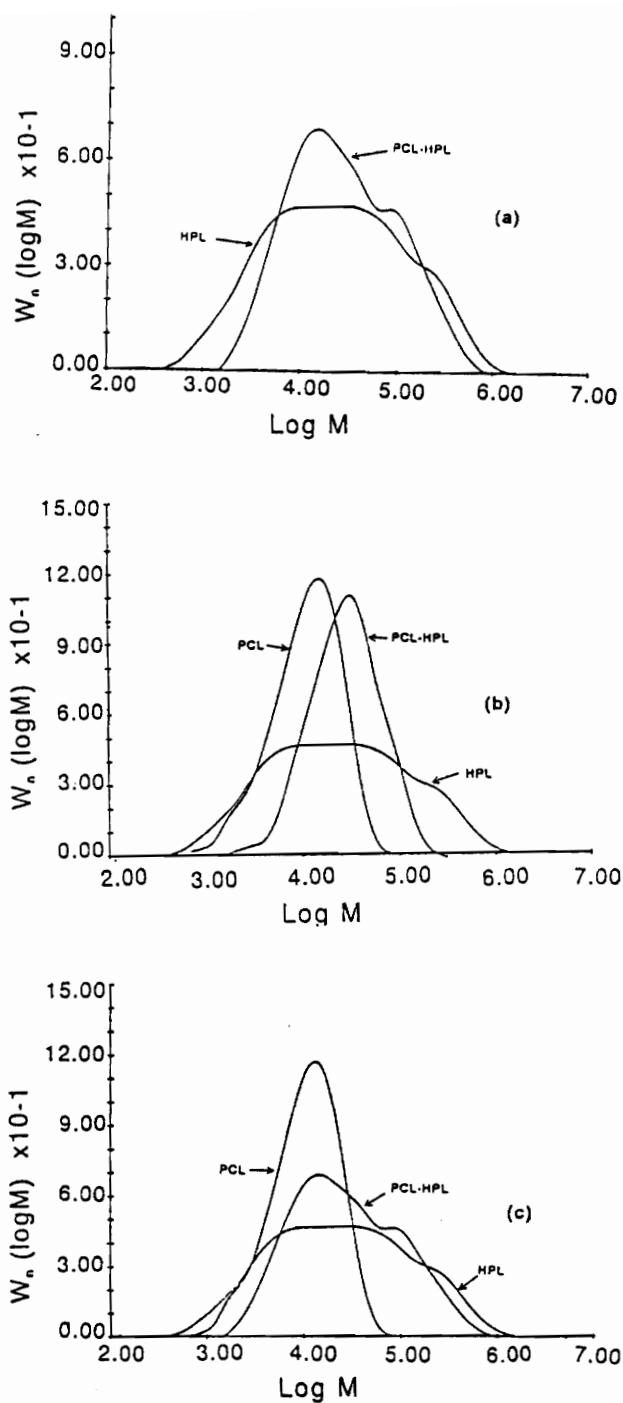


Figure 9. Molecular weight distribution according to method I and method II: (a) method I; (b) method II, low HPL content; (c) method II, high HPL content.

The number of arms of each copolymer was determined on the basis of the functionality of HPL, that is, the number of free hydroxyl groups available for copolymerization (or grafting). The length of the arms will depend on the conversion of ϵ -CL, or the efficiency of PCL grafting and the amount of homopolymer produced. However, no trace of homopolymer or oligomeric species from both methods was detected by GPC. The functionality averages were calculated from the total OH content determined by titration and HPL number-average molecular weights obtained by GPC. The HPL used in method I had on average 7.0 and 3.5 OH groups per molecule, respectively (see Table 2). The latter was the result of 50% capping of the hydroxyls from the original HPL (7.0 OH/mol) with diethylsulfate, according to a procedure described elsewhere [17]. In method II the average functionality of HPL was 7.0 OH/mol. However, the stoichiometry of the synthesis was aimed to form star-like copolymers with 2 (samples C4 and C5) and 4 (samples C1, C2 and C3) arms. The estimation of the number-average molecular weight arm length was calculated from the knowledge of both M_n of HPL and copolymer, and HPL functionality. These are average numbers of broadly polydisperse polymers. Therefore, the results represent means of relatively broad distributions.

Figure 10 presents an H-NMR spectrum of the structure of a typical $(PCL)_n-HPL$ copolymer. The peaks are assigned based on the structure proposed (Figure 10). Resonances at 3.5 ppm (f) were assigned to the methylene and methoxy protons of the HPL component, whereas the signals at 1.1 ppm (e) were due to the methyl protons of the propylene oxide chains. The triplet centered at 4.1 ppm (a) was assigned to the two methylenic ester protons of the PCL component. The methylenic protons on the carbon adjacent to the carbonyl gave rise to a triplet centered at 2.2 ppm (b). The other major peaks at 1.6 and 1.3 ppm were due to methylenic protons (c) and (d) from the PCL segments of the copolymer. Since virtually all unreacted HPL had been removed from the copolymer, the presence of resonance peaks attributed to HPL is an indication of block copolymer formation.

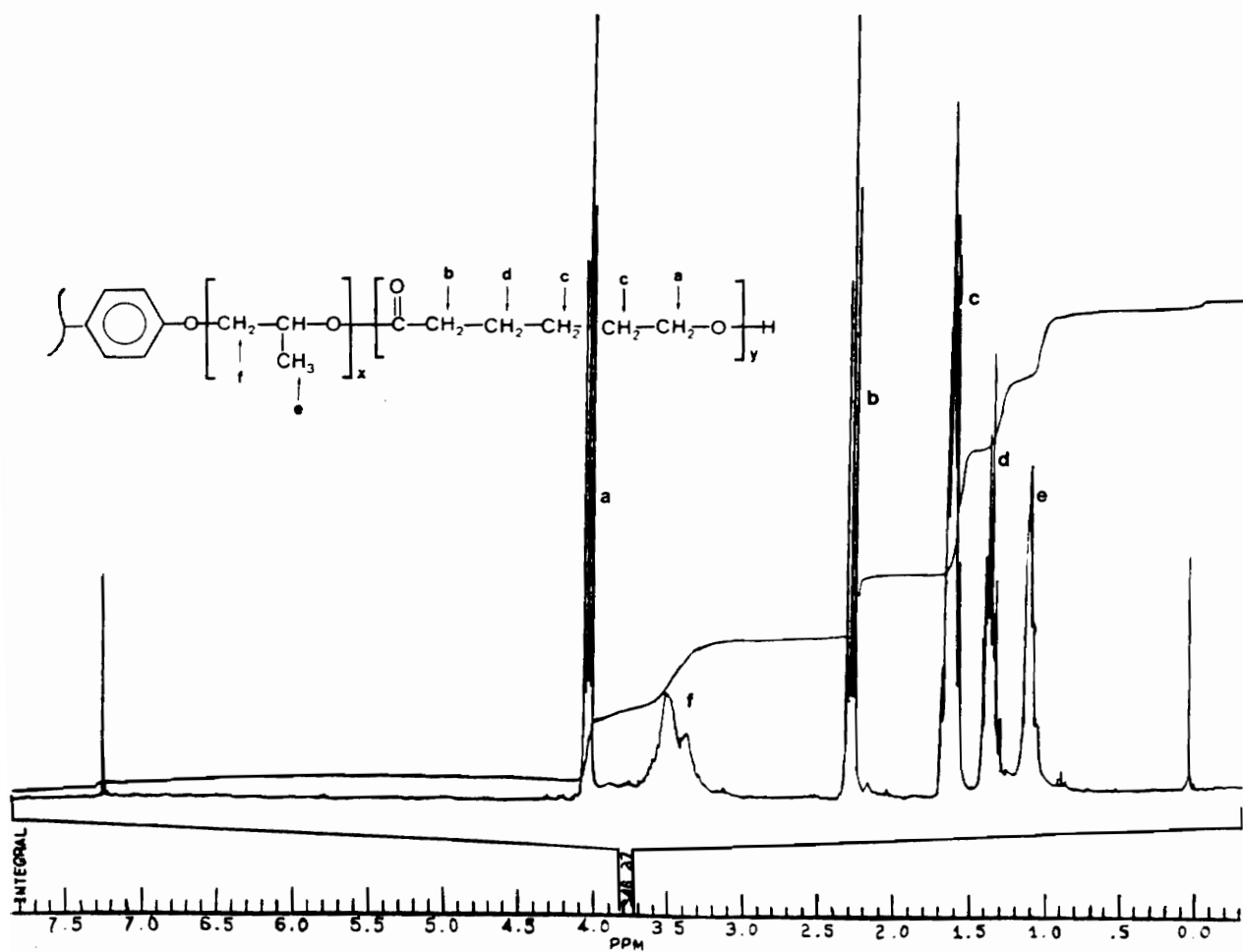


Figure 10. Proton-NMR spectrum of PCL-HPL copolymer

3.3.2 Solution Properties

The intrinsic viscosity and Mark-Houwink-Sakurada (MHS) constant data from gel permeation chromatography analysis are presented in Tables 5 and 6. There was virtually a constant value for the MHS exponent a , which oscillated around 0.66. The occasional values of around 0.2 must be questioned on account of the broad polydispersity observed on those samples. Apparently, the degree of branching, polydispersity, and method of synthesis of the copolymers (series A, B & C) has no effect on the MHS constant. Both copolymer and homopolymer (PCL) had almost identical a -values.

On the other hand, the data in Tables 5 and 6 show that the intrinsic viscosities are dependent upon arm molecular weight but not upon the overall degree of branching. Figure 11 illustrates how the intrinsic viscosity varies with molecular weight when the average arm length is increased (from M_n 250 to M_n 7,200), but the number of arms remains unchanged (series A & B). As the average arm length increases, the intrinsic viscosity becomes greater. The rate of increase is the same in both series. Even when the average arm length is nearly as long as that of the linear polymer, the viscosities of the branched polymers are still below that of the linear polymer of equivalent arm length molecular weight. Thus, the presence of short and intermediate-size arms has the effect of lowering the intrinsic viscosity below the value that should be expected for linear polymer with equivalent molecular weight. For series C in which the number of arms is varied at a fixed arm length, the surprising finding is that the overall increase in intrinsic viscosity is greater than that of the linear PCL segments that gave rise to the star-like copolymers. A possible explanation for this behavior can be attributed to the incorporation of a foreign group at the end of the PCL segments, as result of end-group capping with diisocyanate. It has long been recognized, on the basis of experimental evidence, that terminal polar groups can affect the solution properties of polymers [21]. This has been demonstrated especially for polystyrene where the incorporation of hydroxyl end groups was claimed to produce hydrophilically associated complexes in hydrocarbon solvents (other

Table 5. Solution Properties of PCL-HPL Copolymers (Method I)

Sample	Arm Length (M_n)	IV (dl/g)	MHS ^a
A1	250	0.112	0.627
A2	800	0.125	0.237 *
A3	700	0.141	0.653
A4	1,100	0.173	0.661
A5	1,800	0.202	0.662
A6	1,300	0.305	0.206 *
A7	2,200	0.212	0.662
A8	7,200	0.290	0.665
B1	850	0.173	0.648
B2	900	0.167	0.659
B3	1,700	0.137	0.655
B4	1,600	0.199	0.649
B5	2,200	0.203	0.198 *
B6	2,300	0.394	0.643
B7	4,900	0.199	0.649
PCL ^b	4,400	0.312	0.620
PCL	11,300	0.320	0.635

* Suspected experimental errand

a Mark-Houwink-Sakurada constant

b Polycaprolactone

Table 6. Solution Properties of PCL-HPL Copolymers (Method II)

Sample	Arm Length (M_n)	IV (dl/g)	MHS ^a
C1	4,400	0.408	0.669
C2	4,400	0.407	0.662
C3	4,400	0.458	0.458 *
C4	11,300	0.446	0.592
C5	11,300	0.512	0.172 *

* Suspected experimental errand

^a Mark-Houwink-Sakurada constant

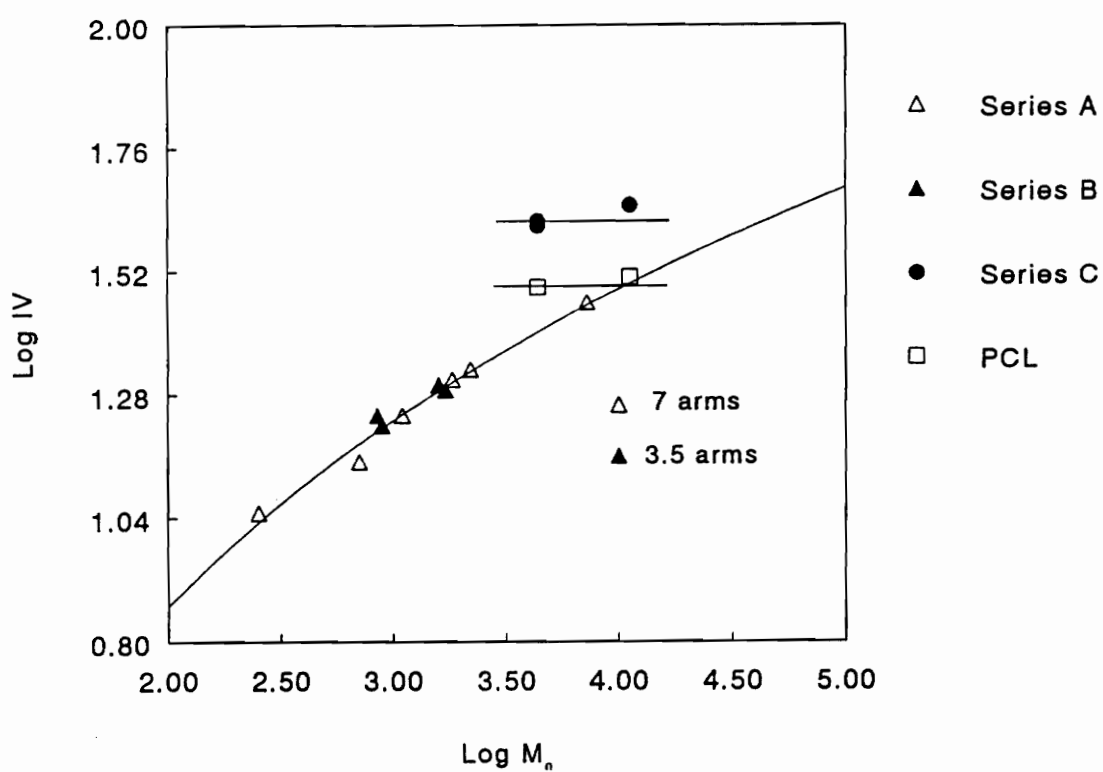


Figure 11. Relationship between intrinsic viscosity and copolymer arm length

factors, such as theta temperature, molecular conformation, etc., may also play a role). The change in solution properties has been attributed primarily to internal chemical differences between groups, which may affect the interaction parameter χ on the local segment concentration of the star polymers. It has been confirmed that the presence of even a very small segment of a comonomer in the polymer chain can alter the solution behavior of the chain [22]. A similar behavior was observed in polystyrene-polydiene star block copolymers. According to Bi and Fetters [23] this type of behavior is not predicted by theory, nor has it been observed for star materials containing homopolymer arms. It seems that these unexpected results are related to the incompatibility of the segments. One model suggests that the conformation of these star block copolymers in dilute solution is spherical in shape, i.e, a "vesicle" of polydiene surrounded by a shell of polystyrene. This explains the observed independence of the intrinsic viscosity on the extent of branching for a series of star block copolymers where the arm molecular weight and composition remain nearly constant. However, detailed experimental verification of this model still remains to be obtained.

In the absence of further experimental evidence, especially that based on concentrated solution viscosity measurements, the unexpected rise in intrinsic viscosity of the star-like copolymers of series C over their linear PCL segments can be attributed to the incorporation of polar urethane-type linkages. In addition, as a consequence of the grafting process, there always exists the possibility of the presence of ungrafted segments with the copolymer. This may possibly generate problems in the separation of ungrafted chains from the reaction mixture. Therefore, it seems reasonable to assume that the differences noted between the intrinsic viscosities of the star-like copolymers produced according to method II (series C) as opposed to method I (series A & B) are believed to be due to the differences in chemistry at the branch points. The difference between these two methods of synthesis suggests that the effect of urethane groups on the intrinsic viscosity in THF may be larger than that of branching.

3.3.3 Thermal Properties

The poor mechanical strength and brittleness characteristics of most of the copolymers prevented measurements of their dynamic mechanical properties. This must be attributed to the low overall molecular weight of the copolymers, and to the HPL composition which is too low to produce elastomeric properties of a TPE material. Figure 12 shows the DMTA spectrum of a high molecular weight $(PCL)_n$ -HPL copolymer. The modulus and $\tan\delta$ curves provide strong evidence for the formation of a multiphase block copolymer. Although the weight fraction of PCL is higher (by approximately 70%) than the HPL fraction, the glass transition temperature of the amorphous phase of PCL (-60°C) could not be detected. The T_g of HPL, on the other hand, is shifted to a lower temperature, -27°C . This particular HPL sample has a high degree of propoxylation and its T_g was about -7°C . Therefore, the migration of the glass transition to a temperature intermediate of the T_g 's of PCL and HPL components suggests miscibility of the two components forced by the covalent bonds. The gradual change of modulus above the T_g of the major amorphous phase is typical of graft and block copolymers that exhibit multiphase behavior. The melting temperature of PCL segments (60°C) is responsible for a substantial final drop in modulus.

Figure 13 shows a typical DSC thermogram for a selected $(PCL)_n$ -HPL block copolymer, obtained in a second heating mode after quenching from the melt. Three major transitions are evident: a first order endothermic transition A at about 50°C which corresponds to the crystalline fusion of the polycaprolactone segment; a second order transition B at -57°C that corresponds to the glass transition of polycaprolactone; and an exothermic peak C at about -25°C which is due to the crystallization of PCL segments. The glass transition of the HPL segment could not be detected by DSC in this particular sample. This is explained with both the low molecular weight of HPL and its high T_g (approximately 85°C) that is too close to the melting point of PCL segments. These two factors combined make the HPL glass transition temperature hard to be detected. The main information derived from DSC measurements is summarized in Tables 7 and 8. These data include

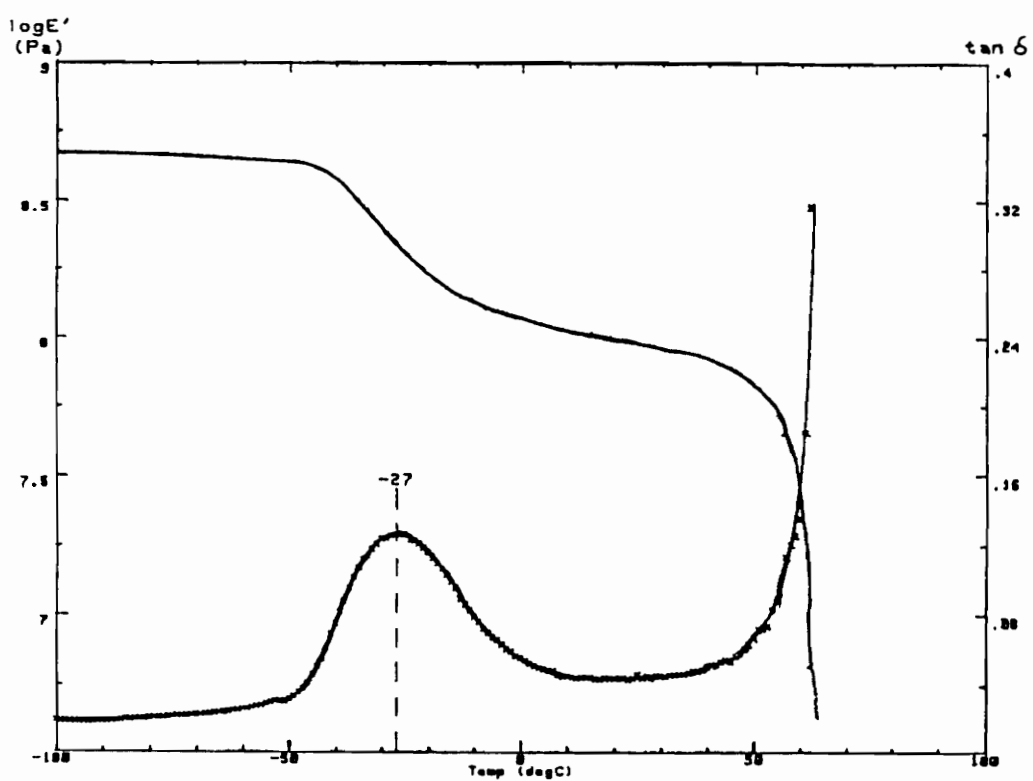


Figure 12. DMTA curve of PCL-HPL star-like copolymer

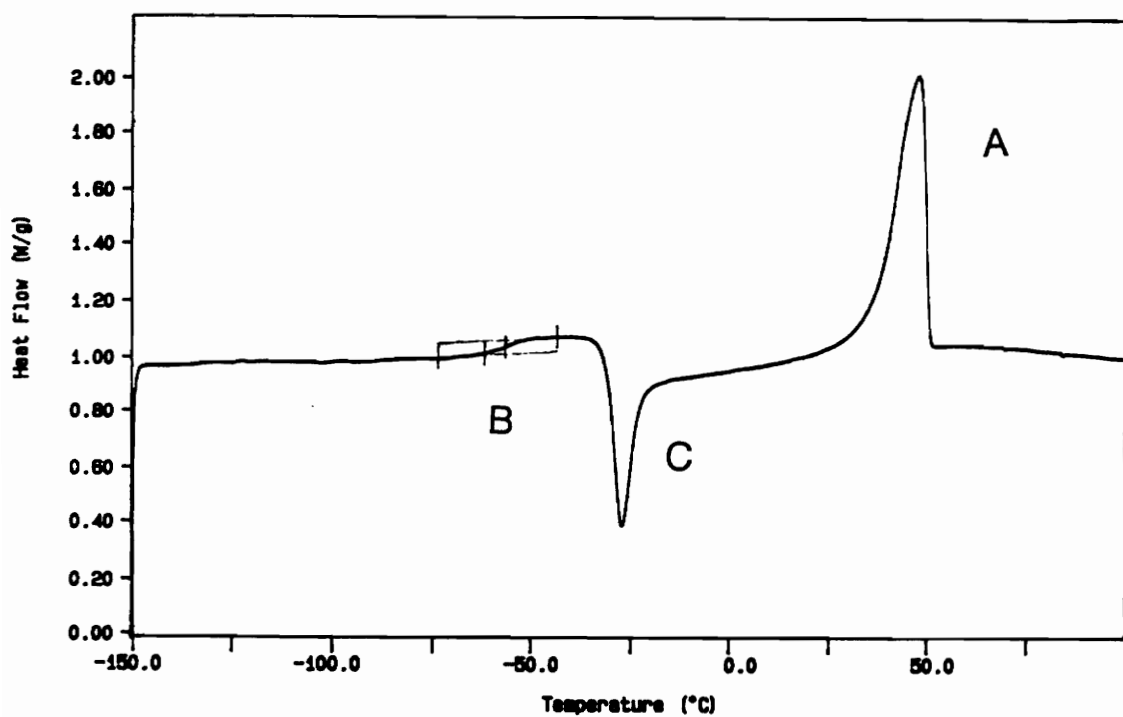


Figure 13. DSC curve of copolymer from series A

Table 7. Thermal Data of PCL-HPL Copolymers from Series A

Sample	$T_g(\text{PCL})$ (°C)	T_m^a (°C)	T_m^b (°C)	ΔH_f^a (J/g)	ΔH_f^b (J/g)	X_c^a (%)	X_c^b (%)
A1	-50	45	27	24	25	5	9
A2	-50	57	46	153	110	34	37
A3	-57	58	47	146	123	33	41
A4	-57	58	48	159	133	36	44
A5	-54	53	43	140	109	32	36
A8	-55	59	46	147	109	33	36

a First heating

b Second heating

X_c Degree of crystallinity

Table 8. Thermal Data of PCL-HPL Copolymers from Series B and C

Sample	T_g (HPL/PCL) °C (range)	T_m^a (°C)	T_m^b (°C)	ΔH_f^a (J/g)	ΔH_f^b (J/g)	X_c^a (%)	X_c^b (%)
B1	-70 to -25	56	39	112	95	25	32
B2	-70 to -25	62	51	163	112	37	38
B3	-70 to -25	52	35	102	99	23	33
B6	-70 to -25	62	55	210	150	48	50
B7	-70 to -25	63	58	173	114	39	38
C2	-70 to -25	63	56	225	140	32	47
C3	-70 to -25	66	58	188	111	43	37
C4	-70 to -25	62	58	233	163	53	54
C5	-70 to -25	65	56	157	113	36	38

a First heating

b Second heating

X_c Degree of crystallinity

the results of samples that have been heated above the melting point of PCL and then quenched rapidly (in the DSC) to -150°C .

The data presented in Tables 7 and 8 show that there is a distinct difference in thermal behavior between the copolymers of series A and those of series B and C. In the entire series A, the T_g of the HPL phase could not be detected based on the reasons given above. Both factors, low molecular weight and T_g close to the PCL melting point, complicate the observation of the glass transition temperature of HPL. Figure 14 shows typical DSC results for selected copolymers of series A. All copolymers exhibit crystallinity as supported by the presence of a melting endotherm, even for sample A1 which contains less than 50% by weight PCL. The T_g of PCL can be seen to range from -49 to -57°C . Upon heating the quenched samples, the PCL segments crystallize and give a crystallization exothermic peak somewhere between -30 and -10°C .

Thermograms of copolymers from series B and C are presented in Figure 15. The HPL used in both series has a higher molecular weight, which translates into a higher degree of propoxylation than reported previously. The glass transition temperature of HPL is below room temperature (Table 2). Like the copolymers of series A, two major transitions are detected. A first order transition at about 60°C accounts for the melting point of PCL; and a very broad, second order transition, in the range of -75 to -20°C , corresponds to the glass transition of both amorphous HPL and PCL phases. Differently from series A, no crystallization exotherm is seen throughout the samples from both series, B and C. This phenomenon will be discussed later. It is important to notice in these two series that the melting point of the PCL crystalline phase is separated into two peaks, about two or three degrees apart. The separation into two peaks only occurs during the second heating. Figure 16 shows the thermogram of a copolymer annealed at room temperature for several months (curve a). The melting transition is seen quite clearly, but the location of the T_g is very questionable. However, very fast cooling of the melted copolymers maintained 3 minutes at 100°C allows, in the second heating (curve b), a very well defined T_g to be revealed. This is located in between the glass transition temperature of the corresponding "homopolymers", HPL and PCL.

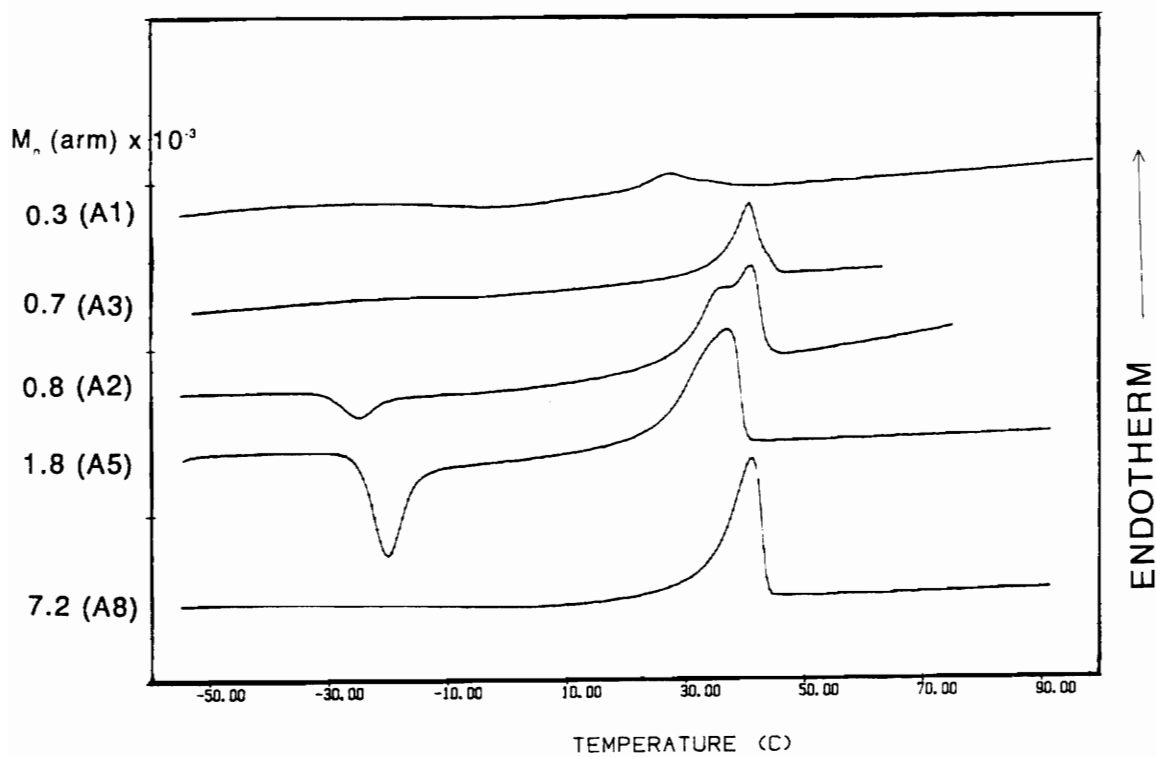


Figure 14. DSC curves of copolymers from series A (see Table 7)

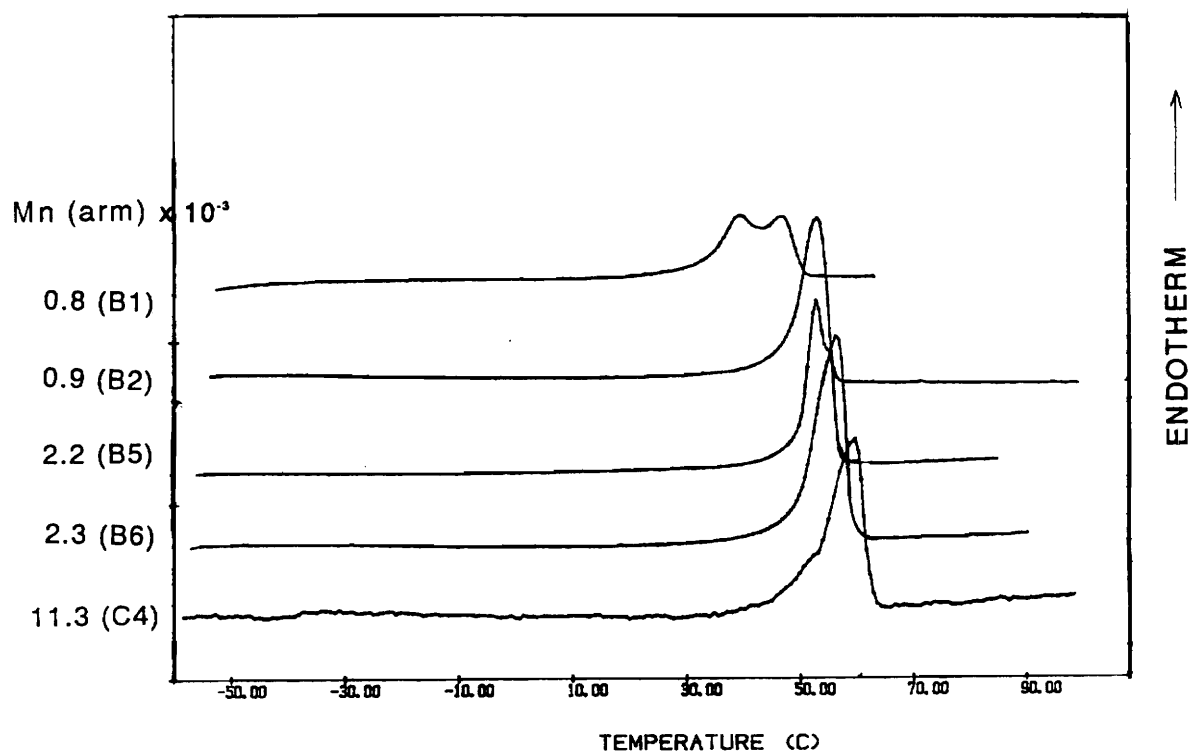


Figure 15. DSC curves of copolymers from series B and C (see Table 8)

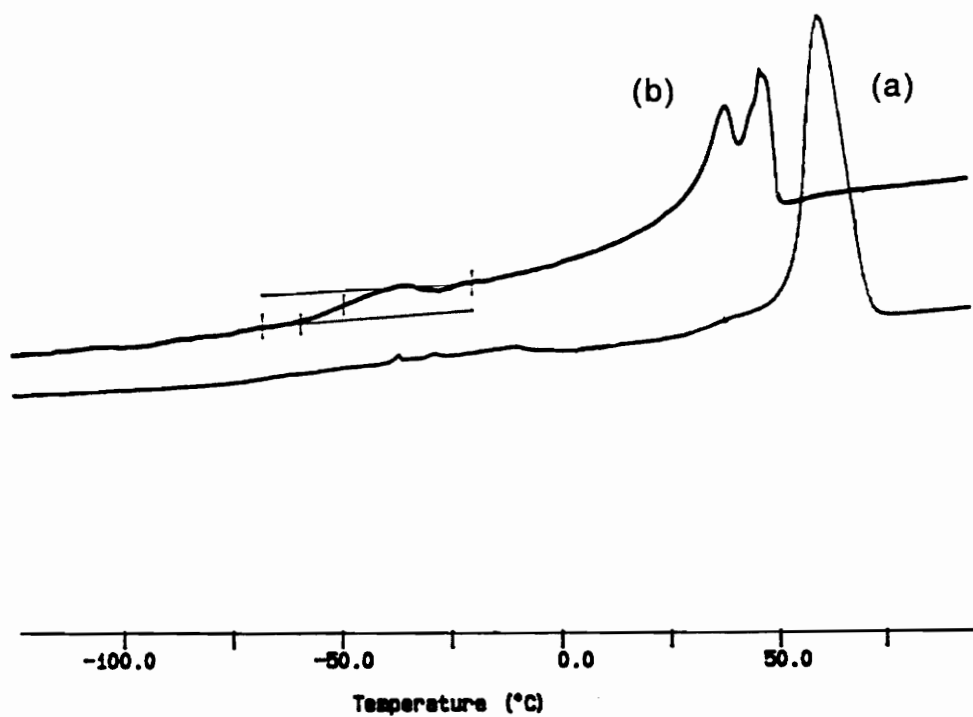


Figure 16. DSC curves of copolymers from series B and C (see Table 8): (a) first heating and (b) second heating quenched from the melt.

The melting point is not only depressed by about 4-16 degrees, but it is also split into two peaks, one observed on first and one on second heating. The presence of two melting points has been reported for several polymer systems [24,25]. It seems that these two peaks are associated with two different crystalline structure not yet in equilibrium. If enough time is given for crystallization to occur, both peaks will eventually merge into one peak, as seen in Figure 16, curve (a), for the aged sample.

From Tables 7 and 8 it is seen that the thermal behavior of the copolymers within each series does not change much with the molecular weight. The melting point is the parameter which varies most with molecular weight. As an illustration, Figure 17 shows the relationship between T_m and copolymer arm length. The melting point approaches a limit of 60°C as the molecular weight of the PCL segments increases. Figure 17 also shows that the highest molecular weight copolymer from series A does not fit the curve. As discussed previously, copolymers from series A require more time to reach a thermal equilibrium, and this affects T_m . As seen in Tables 7 and 8, after aging (T_m of the first heating), the melting points of high molecular weight copolymers migrate to a higher temperature, in accordance with the pattern of Figure 17.

As discussed in the previous section, the crystallization of PCL chains is greatly affected by the T_g of the HPL segment. In order to examine the morphology during the crystallization of PCL chains, thin films were heated while under observation by optical microscopy in polarized light. Figure 18 (A to F) compares optical micrographs of block copolymers from series A with varying PCL content and arm length, isothermally crystallized from the melt. The micrographs show that the samples exhibit spherulitic texture and that the shape of the spherulites changes as the concentration of amorphous HPL in the copolymer increases. The coarseness of the spherulites at high HPL content (ie., 18 E and F) is a consequence of the covalent bonds between amorphous and crystalline blocks. Within the spherulites are both segments, amorphous HPL and crystalline PCL chemically tied together by covalent bonds. Since they cannot macroscopically separate, the PCL chains still

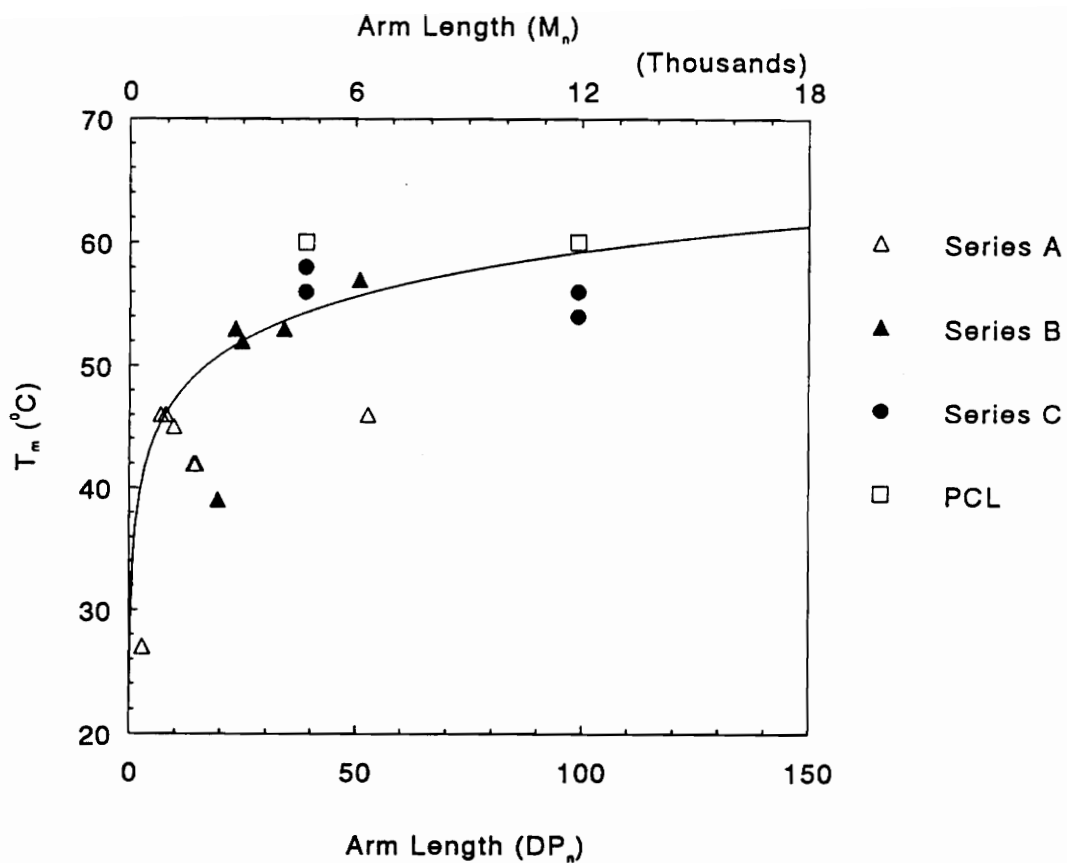


Figure 17. Melting point vs. PCL-HPL copolymer arm length: second heating mode after quenching from the melt

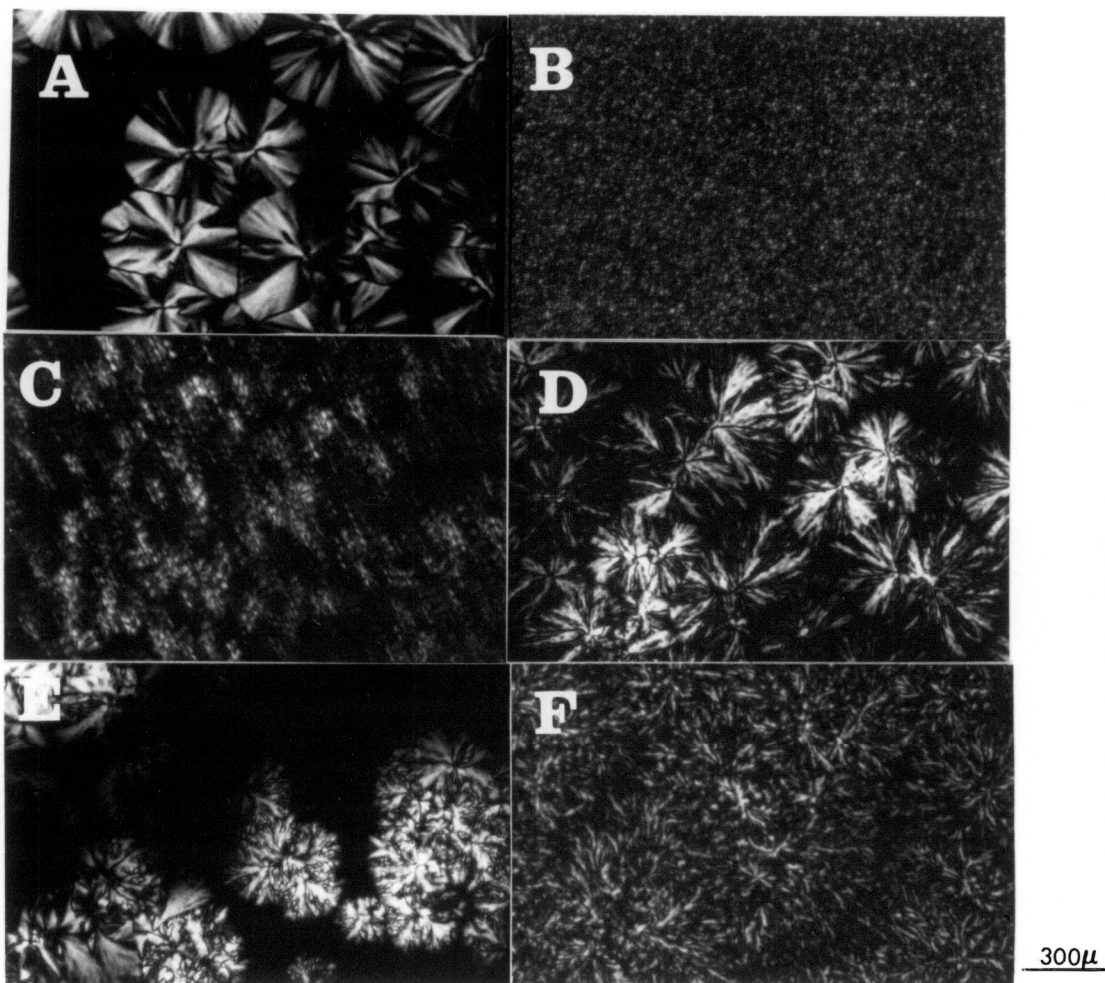


Figure 18. Optical micrographs of PCL and PCL-HPL copolymers: (a) PCL; (b) sample A8 (see Table 3 for sample identification); (c) A7; (d) A5; (e) A4, and (f) A2 (32x)

SYNTHESIS AND CHARACTERIZATION OF CAPROLACTONE-HYDROXYPROPYL LIGNIN STAR-LIKE COPOLYMERS

crystallize, but the shape of the spherulites is perturbed by the presence of amorphous material forced to stay within the spherulite.

Figure 19 combines optical micrographs of copolymers from series B and C with decreasing PCL content. Similarly to what has been observed in series A, the irregularity of the spherulites increases as the copolymer becomes richer in amorphous HPL phase. However, a close inspection of selected micrographs, as illustrated in Figure 20, reveals that those from series A are much more irregular than the copolymers from series B and C. Even though it is true for all three series that the coarseness of the spherulites increases with HPL content, the spherulite shapes in series B and C are almost identical to the homopolymer PCL. The presence of HPL does not prevent a well defined spherulite formation. The reason for that can be explained by the nature of HPL in series B and C. As reported previously, at the crystallization temperature of PCL chains, both HPL and PCL are in the rubbery stage, above their T_g 's. There is no restriction to chain mobility, and that helps both spherulite formation and the definition of contours. Similar observations have been reported in block copolymers of polystyrene-polycaprolactone and polybutadiene-polycaprolactone [26]. In series A, the nature of the HPL component is different. Its T_g is above the melting point of PCL segments, and this restricts the chain movement during crystallization. As the PCL segments crystallize, the glassy phase of HPL tends to counteract the radial growth of crystalline fibrils into spherulites, and this results in much greater coarseness in the texture of the spherulites. It also seems as if the HPL solid phase, along with high molecular weight PCL chains, helps to increase the nucleation density, as seen in the optical micrograph of sample A8 in Figure 18 (B). However, a more detailed crystallization kinetics study would be required to be definitive on this point. These results are consistent with the thermal properties discussed previously.

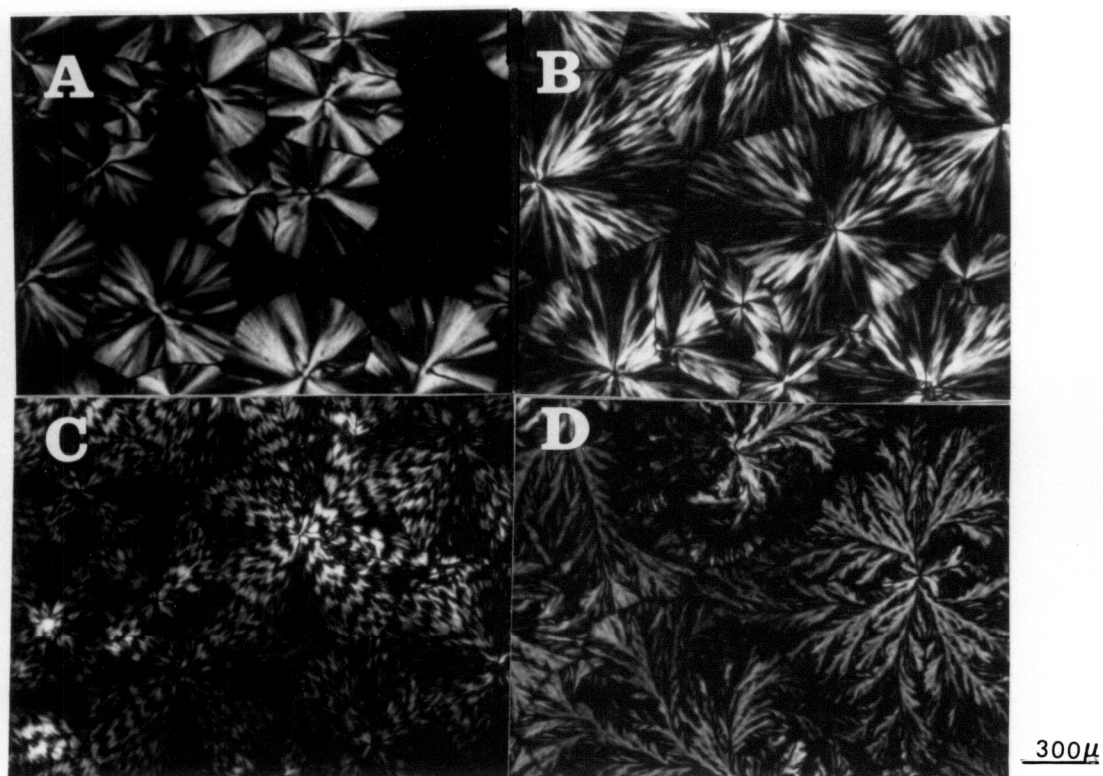


Figure 19. Optical micrographs of PCL and CL-HPL copolymers: (a) PCL; (b) B6 (see Tables 3 and 4 for sample identification); (c) C5; (d) B (32x)

SYNTHESIS AND CHARACTERIZATION OF CAPROLACTONE-HYDROXYPROPYL LIGNIN STAR-LIKE COPOLYMERS

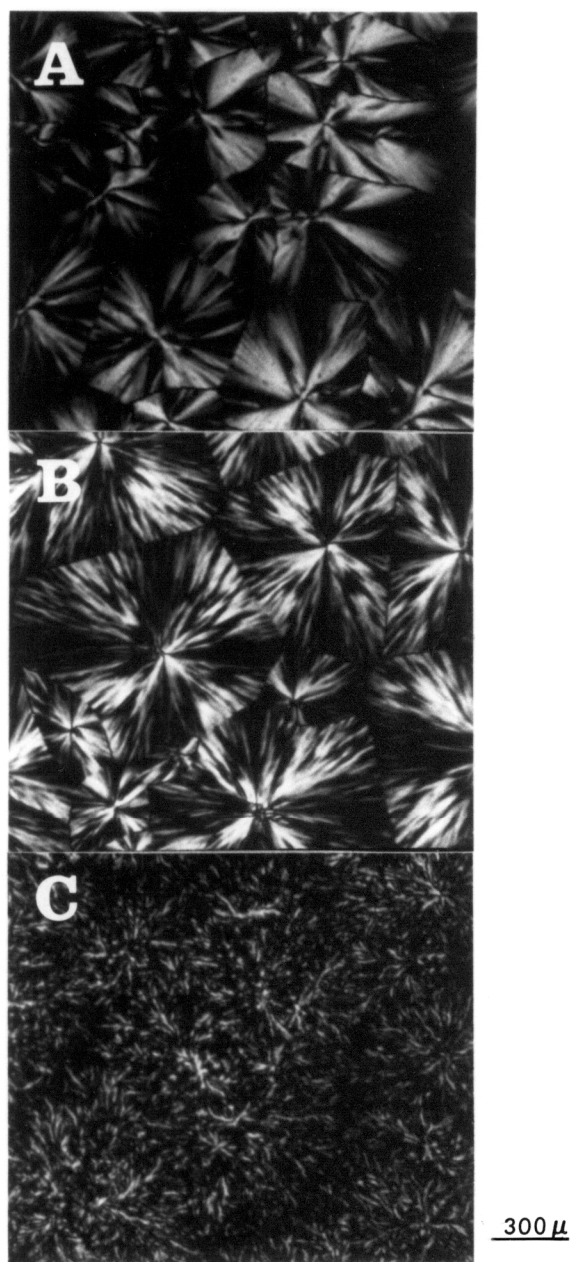


Figure 20. Optical micrographs of PCL and PCL-HIPL copolymers: (a) PCL; (b) B6 (see Tables 3 and 4 for sample identification); (c) A2 (32x)

3.3.4 Crystallinity

Figure 21 presents the heat of fusion data from DSC for PCL and copolymers synthesized in this study. Since the copolymer melts only about 30°C above room temperature, the amount of crystallinity changes with time due to a continuous crystallization process at room temperature. Therefore, the data presented in Figure 21 are from the first heating treatment of samples that have been aged for at least 6 months at ambient temperature in the desiccator. The heat of fusion was plotted against lignin content in the copolymer, since lignin content, and consequently copolymer composition, can be measured by UV in a much more reliable way as compared to GPC. The curve clearly shows that as the concentration of lignin increases, the measured heat of fusion decreases, and so does the degree of crystallinity. Figure 22 illustrates the degree of crystallinity of the copolymer as a function of lignin content. The variation of crystallinity content was also plotted as a function of arm length (Figure 23). The results indicate that the degree of crystallinity is not only related to composition, but also to the length of PCL segments. As the PCL arm lengths increase, their ability to crystallize also increases, and this reaches the level of PCL homopolymer at about DP 100.

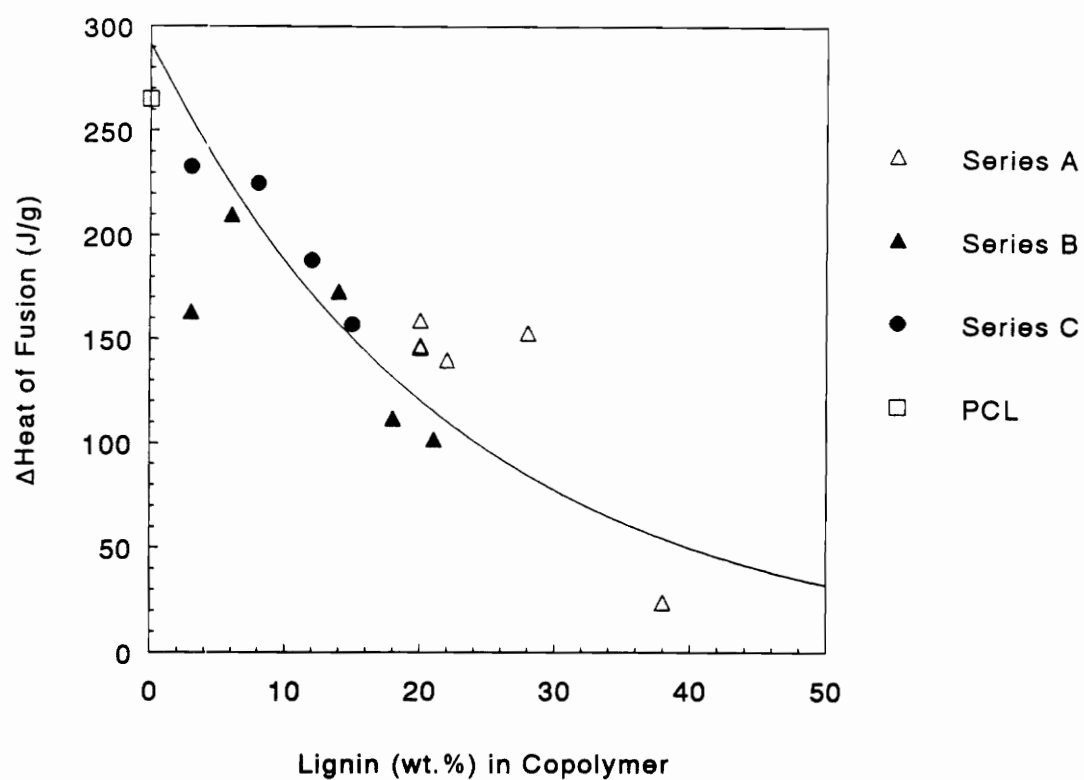


Figure 21. The effect of lignin content on the heat of fusion

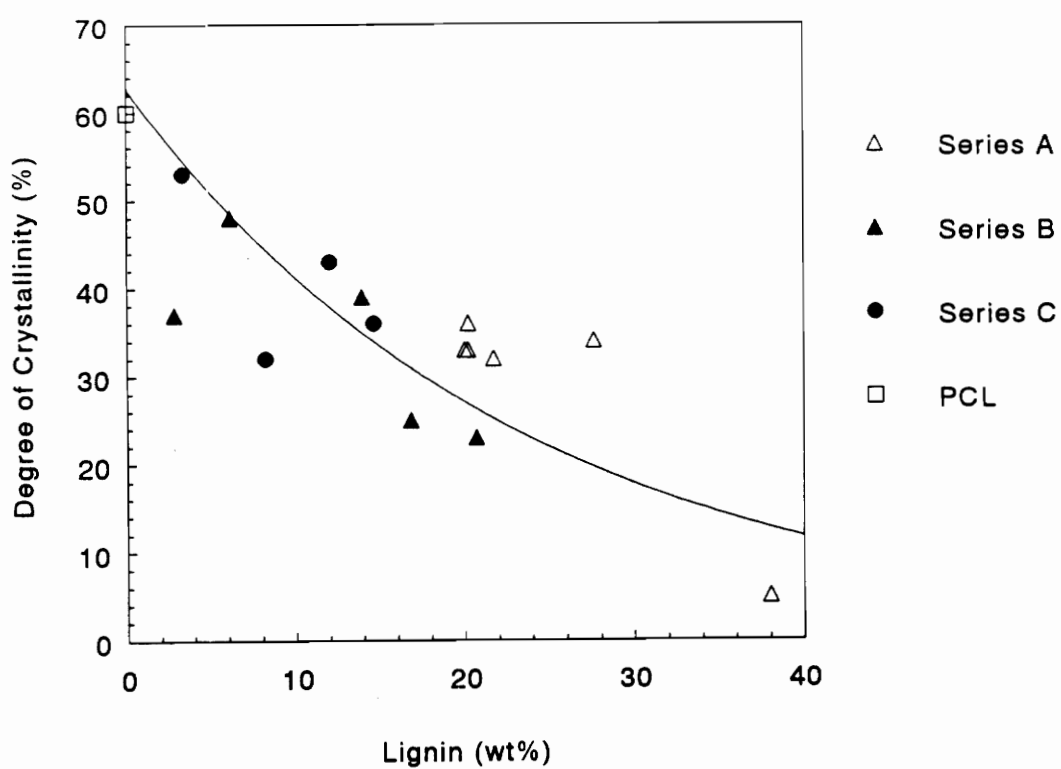


Figure 22. Degree of crystallinity of the PCL component in the block copolymers as a function of lignin content.

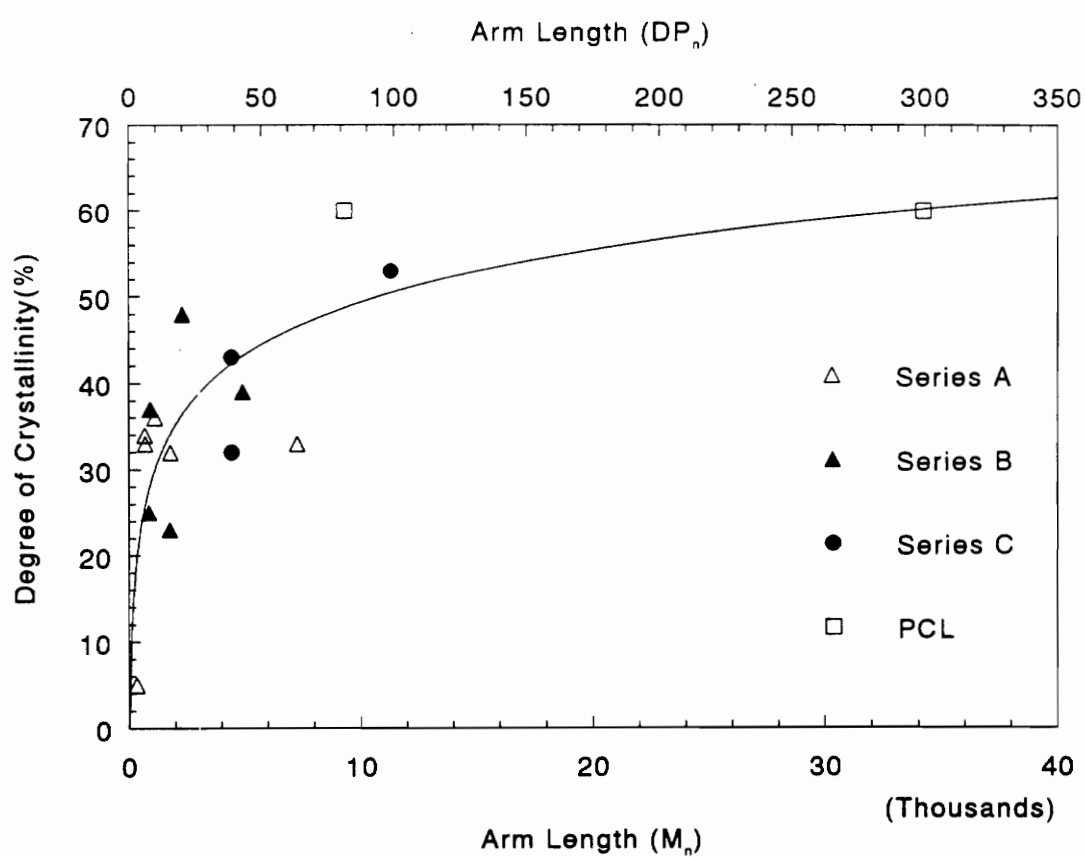


Figure 23. Degree of crystallinity vs. copolymer arm length

3.4 CONCLUSIONS

Three series of star-like copolymers were prepared covering a wide range of compositions. (The synthesis is straight forward, and it has already been scaled-up in a pilot plant to the production of 1 kg batches). Copolymers can be produced by either copolymerizing ϵ -caprolactone or grafting preformed PCL segments onto HPL. Critical variables affecting copolymer properties are molecular weight of the arms, and number of arms. Both variables can be controlled reasonably well during the synthesis.

The grafting of preformed PCL segments onto HPL resulted in materials with more narrow polydispersity. The grafting procedure not only allows a better control of molecular weight distribution, but also has the advantage of selecting desired arm lengths. This plays a major role in determining copolymer properties.

The intrinsic viscosity of the copolymer is a function of the arm length, regardless of the nature of the HPL. However, the synthesis method may have an effect on solution behavior of the copolymers. The grafting of PCL segments into HPL resulted in copolymers with higher intrinsic viscosities than the copolymers produced via anionic polymerization. The introduction of a strong polar group, such as TDI during the grafting process, may account for the higher intrinsic viscosity values.

The thermal behavior of the copolymers is somewhat affected by molecular weight. The copolymer melting point is the parameter that varies most with the length of the PCL segments. It approaches a limiting temperature (around 60°C) as the copolymer arm length increases beyond 10,000 daltons.

The copolymers were found to exhibit variable thermal behavior in relation to composition. The fact that the T_g of PCL is shifted, as well as the T_g of HPL (series B and C), indicates that some

sort of miscibility exists between the amorphous regions of both HPL and PCL. The miscibility is a consequence of the covalent bonds linking both segments. When PCL and HPL are blended in solution, films produced exhibit macrophase separation. This is an indication of incompatibility.

The crystallization of PCL chains is greatly affected by the T_g of HPL segments. Block copolymers derived from HPL with T_g above room temperature require longer time to achieve thermal equilibrium as compared to those copolymers synthesized from HPL with T_g below room temperature. This has a profound effect on the coarseness and shape of the spherulite morphology, which greatly depends on the "softness" of the HPL phase.

As expected, composition of the copolymer plays an important role in controlling crystallization of PCL segments. The degree of crystallinity of the copolymers declines with lignin content. Arm length is another variable which affects crystallinity. The longer the arm length, the higher the degree of crystallinity.

ACKNOWLEDGEMENT

Acknowledgement is made to Mr. Paul S. Vail for his technical assistance in differential scanning calorimetry. The author is very much indebted to Dr. Abaneshwar Prasad for his skilful technical support in optical microscopy. Both works were carried out in the Chemistry Department at VPI&SU.

3.5 REFERENCES

1. G. L. Brode and J. V. Koleske, *J. Macromol. Sci. - Chem.*, **A6**(6), 1109(1972)
2. J. Heuschen, J. Jerome, and Ph. Teyssie, *Macromolecules*, **14**, 242(1981)
3. H. Cherdrón, H. Ohse, and F. Korte, *Macromol. Chem.*, **56**, 179(1962)
4. H. R. Kricheldorf, M. Berl, and N. Scharnag, *Macromolecules*, **21**, 286(1988)
5. K. Ito and Y. Yamashita, *Macromolecules*, **11**, 68(1978)
6. H. L. Hsieh and I. W. Wang, "An Improved Process for ϵ -Caprolactone- Containing Block Copolymers", J. E. McGrath, Ed., "**Ring-Opening Polymerization. Kinetics, Synthesis and Mechanisms**", ACS Symposium Series 286, Washington, D. C., 161(1985)
7. T. Onhadi, C. Stevens, Ph. Teyssie, *Macromol. Chem.*, **Suppl. 1**, 191(1975)
8. R. Jerome and Ph. Teyssie, "**Comprehensive Polymer Science**", G. C. Eastmond, A. Ledwith, S. Russo, P. Sigwalt, Eds., Pergamo Press, vol. 3, Part i, 501(1989)
9. M. Euco, T. Aida, S. Inoue, *Macromolecules*, **20**, 2982(1987)
10. Y. Yasuda, T. Aida, S. Inoue, *Macromolecules*, **17**, 2217(1984)
11. J. V. Koleske and R. D. Lundberg, *J. Polym. Sci.*, Part A-2, **vol. 7**, 795(1969)
12. H. L. Hsieh, *J. Appl. Polym. Sci.*, **22**, 1119(1978)
13. J. V. Koleske, R. M. J. Roberts, and F. P. Gludice, U. S. Patent 3,670,045 (June 13, 1972)
14. J. E. McGrath, A. M. Hellstern, J. M. DeSimone, T. E. Long, C. Cho, Y. Yoo, P. Wood, C. D. DePorter, and J. S. Riffle, *Polym. Prep., Am. Chem. Soc. Polym. Chem. Div.*, **29**(2), 57 (1988); Y. Yoo, "**Ph.D. Dissertation**", VPI&SU, December, 1988; *Multiphase Polymer Systems*; B. M. Culbertson, Ed., 1989
15. L. C. Wu and W. G. Glasser, *J. Appl. Polym. Sci.*, **29**, 1111 (1984)
16. W. G. Glasser, "Modification of Lignin with Propylene Oxide", in "**Fourth Annual Progress Report Industry-University Cooperative Project**", BMC, Dept. Wood Sci. & For. Prod., VPI & SU, 1991

17. W. de Oliveira and W. G. Glasser, *J. Appl. Polym. Sci.*, **37**, 3119(1989)
18. W. G. Glasser, C. A. Barnett, T. G. Rials, and V. P. Saraf, *J. Appl. Polym. Sci.*, **30**, 2207(1985)
19. N. Morohoshi, *Bulletin of the Experiment Forest*, **10**, 183(1973)
20. V. Crescenzi, G. Manzini, G. Calzolari, and C. Borri, *Eur. Polym. J.*, **8**, 449(1972)
21. F. Candau, P. Rempp and H. Benoit, *Macromolecules*, **5**, 627 (1972)
22. M. Bohdanecky and J. Kovar, "Viscosity of Polymer Solutions", A. D. Jenkins, Ed., "**Polymer Science Library 2**", Elsevier Scientific, Amsterdam, 1982
23. L. Bi and L. J. Fetters, *Macromolecules*, **9**(5), 732 (1976)
24. J. M. Huet and E. Marechal, *Eur. Polym. J.*, **10**, 757(1974)
25. B. Jasse, R. Perret and A. Skoulios, *Makromol. Chem.*, **156**, 157(1972)
26. J. Heuschen, R. Jerome and Ph. Teyssie, *J. Polym. Sci.: Part B: Polym. Phys.*, **27**,523(1989)

4.0 BINARY BLENDS OF POLYVINYL CHLORIDE AND POLYCAPROLACTONE - HYDROXYPROPYL LIGNIN COPOLYMER

4.1 INTRODUCTION

Polymer blends have become an important subject for scientific investigations in the past two decades. Many producers of polymeric materials are interested in developing new blended products because the mixing of polymers offers a convenient and inexpensive alternative to developing totally new polymers [1].

The term polymer blend refers to a mixture of two or more different polymers, which are not covalently bonded together. This distinguishes them from block or graft copolymers, in which two or more polymers are chemically linked together through covalent bonds. The ability to produce blends that have better properties than the corresponding polymer components depends on the compatibility of the system. Compatibility implies a blend system which does not exhibit gross

symptoms of macrophase separation. If that is the case, the blend should be considered incompatible [2]. In any event, a compatible polymer blend system can be viewed as a material of potential utility. The incompatibility between polymers leads to phase separation. In blends, macroscale phase separation can lead to a material with very poor mechanical properties due to the presence of large domains which have poor interfacial bonding.

By microscopic inspection, a compatible blend consists of a single phase; it exhibits a high degree of mixing; and its mechanic properties reflect an average between the constituent polymers. For example, plasticized blends of poly(vinyl chloride)/nitrile rubber combine the low-temperature flexibility and ease of processing of nitrile rubber and the high-temperature permanence and flame retardant properties of poly(vinyl chloride) [3]. Another example is the blend of poly(phenylene oxide) with styrene copolymers. These blends have the excellent dimensional stability at high temperatures and good electrical properties of poly(phenylene oxide) combined with the lower melt viscosity, shear sensitivity, and cost of polystyrene [3,4].

A common criterion used to determine compatibility is the existence of a single glass transition temperature, intermediate between the blend components. In incompatible systems, the T_g 's of the pure blend components remain unchanged. Other clues are their opacity and poor mechanical properties relative to the constituent polymers. On the other hand, complete compatibility is not easily demonstrated. The presence of discrete phases or domains can be detected by light or electron microscopy. However, the analysis could also be misleading, since incompatible systems can also present very small domain sizes which result in an optically clear specimen.

Polycaprolactone has been the subject of many polymer blend studies due to its miscibility with a variety of commercial polymers [5,6]. Koleske and co-workers [5] have demonstrated the advantages of blending PCL with a wide range of polymers and the benefits resulting from the blends. An interesting system for study is found in the binary blend of PCL and polyvinyl chloride. These

two polymers form a system compatible over the full range of compositions [7-9], and the blend's T_g could be predicted by both Fox and Gordon Taylor's copolymer equations.

Koleske and Brode have conducted a detailed study on blend properties of PCL with a large variety of commercial polymers [6]. PCL has been blended with polyethylene (PE), polypropylene (PP), polystyrene, PMMA, PVC, nitrocellulose, phenoxy A (a polyhydroxyether), Penton (a chlorinated polyether), styrene-acrylonitrile copolymer, etc. The blend studies were divided into three types of categories. First, there were blends which exhibited a crystalline interaction. This type of interaction was observed in blends of PCL with polyolefins, such as PE and PP. These blends, as in the case of PCL and PE, at certain composition exhibit an unaltered T_g of the polyolefin, which would indicate incompatibility between the polymers. However, the T_m of the PE was affected. The blend has a relaxation maximum that was comparable to that of the polyolefin, but at a higher temperature and larger magnitude. The authors [6] concluded that PCL restricts the motion within the PE crystallites through some form of interaction.

Blends of PCL with poly(vinyl acetate), in spite of exhibiting the glass transitions of the constituent homopolymers and no trace of crystalline interaction, nevertheless showed improved mechanical properties when compared to the homopolymers. Thermodynamically, they are considered incompatible, but their good mechanical properties, as totally unexpected in an incompatible system, classify them as being mechanically compatible. It seems that even though the blend domain sizes are big, there must be sufficient interactions of the polymers between the macrophases, therefore resulting in good mechanical properties. Similar behavior was observed in blends of PCL with PS or PMMA.

The true compatible system was observed in polymer blends of PCL with either PVC, nitrocellulose, or phenoxy A. In each system, the blend exhibited only one T_g , which was intermediate to those of the constituent components. Blends of PCL and PVC gained more attention in the literature [3, 8-11] because the pair constitutes a unique system, in which a true polymer-

polymer solution is formed. The T_g 's varied according to the blend composition and the data fitted both Fox and Gordon-Taylor expressions.

Ong [8] has studied in detail morphology, melting behavior, degree of crystallinity and crystallization kinetics of PCL/PVC blends. His observations with optical and electron microscopy indicate that crystallinity was present in the blends with up to 70% PVC by weight. X-ray studies revealed that the unit cell dimensions of PCL were not changed by the presence of PVC. On the other hand, PVC was found to reduce the degree of crystallinity of PCL, which could not crystallize in blends containing more than 70% PVC. The crystallization rate of PCL was reduced by PVC, reflecting reduction in both spherulite growth and nucleation rate.

The objective of this study was to analyze polymer blends of polycaprolactone-hydroxypropyl lignin ((PCL)_n-HPL) copolymer with polyvinyl chloride. The study focused on the determination of compatibility and the evaluation of the blend's morphology and mechanical properties.

4.2 EXPERIMENTAL SECTION

4.2.1 Materials

Polyvinyl chloride (PVC): PVC was obtained from Aldrich Chemical Company and it was used as received. It had number and weight-average molecular weights of 28,800 and 52,600 daltons, respectively, relative to polystyrene as the GPC calibration standard.

Polycaprolactone-hydroxypropyl lignin copolymer: $(PCL)_n-HPL$ was prepared by the bulk copolymerization of freshly distilled ϵ -caprolactone monomer initiated by the hydroxyl groups of HPL (method I), according to the procedure outlined in chapter 3. The number and weight-average molecular weights of the copolymers were 9,800 and 26,500 daltons, respectively. The melting point of the copolymer was about 60°C, and its glass transition temperature (PCL component) was observed at -57°C. The T_g of the HPL component (85°C) was too close to the melting point of the copolymer, and it could therefore not be detected by DSC.

Tetrahydrofuran (THF): THF was supplied by Fischer Scientific Chemical Company and used as received.

4.2.2 Sample Preparation

All blends were prepared by solvent casting from polymer solution. Approximately three grams of polymer of a particular blend composition were dissolved in 50 mL of tetrahydrofuran and stirred for 2 hours to insure complete solubilization of the polymers. The solution was transferred into an

evaporation Teflon dish covered by perforated aluminum foil, and the solvent was allowed to slowly evaporate at room temperature for 2 days. The films were then transferred to a vacuum desiccator for further drying for at least one week. Dog-bone shaped samples with a gauge length of 10 mm and a gauge width of 3.2 mm were cut from the thin films using a die.

4.2.3 Characterization

Dynamic Mechanical Thermal Analysis (DMTA): The dynamic mechanical properties of the blend systems such as storage modulus, E' and $\tan\delta$, were determined using a Dynamic Mechanical Thermal Analyzer made by Polymer Laboratories Ltd., England. The measurements were conducted at a frequency of 1 Hz over a temperature range from -150°C to a temperature at which the samples became too soft to be tested. The heating rate was set at 10°C per minute.

Tensile tests: Standard tensile stress-strain experiments were done on dog-bone specimens with a MINIMAT testing machine of Polymer Laboratories Ltd., at room temperature. The tensile tests were performed to measure the modulus, ultimate strength, and elongation at break. The samples were clamped between two clamps and elongated at a rate of 5 mm per minute, which is an engineering strain rate of 50% per minute. The results represent averages of five to six individual tests.

Differential Scanning Calorimetry (DSC): Thermal properties, such as glass transition temperature and melting point, of the blends were determined on a Perkin-Elmer Model DSC-7. The temperature was scanned from -100°C to 100°C at a heating rate of $10^{\circ}\text{C}/\text{min}$. For crystallinity and T_m measurements the samples were first cooled to -100°C and then heated at $10^{\circ}\text{C}/\text{min}$. to 100°C . This represents the first scan. In the second scan, the samples were quenched to -100°C at $320^{\circ}\text{C}/\text{min}$. and reheated at $10^{\circ}\text{C}/\text{min}$. to 100°C . The T_m was taken as the temperature corresponding to the endotherm peak location. The percent of crystallinity was calculated on the basis of measured heat

of fusion per gram of pure copolymer in the sample to the heat of fusion per gram of 100% crystalline PCL, 32.4 cal/g [10].

Scanning Electron Microscopy (SEM): SEM was carried out on a Phillips EM-420 STEM operated in SEM mode. In order to obtain micrographs of fractured surfaces, the films were first immersed in liquid nitrogen and then fractured and analyzed at their fractured surface.

Transmission Electron Microscopy (TEM): TEM was also carried out on a Phillips EM-420 STEM operated in the transmission mode at 100 kV. Ultrathin films were microtomed using a Reichert-Jung ULTRACUT System FC-4 at -70°C. The microtomed samples were then mounted on a copper TEM grid and stained with RuO₄ for 15 - 45 min.

4.3 RESULTS AND DISCUSSION

4.3.1 Thermal Analysis

Table 9 summarizes the DSC and DMTA thermal analysis data for the binary blends of PVC and $(PCL)_n-HPL$ copolymer, over a wide composition range (from 10 to 90 wt% copolymer). Figure 24 shows the glass transition temperature plotted as a function of blend composition. Since only one T_g was observed in each blend composition, a copolymer equation (Fox equation) could be applied. Figure 24 shows that the Fox equation fits the experimental data reasonably well. With the exception of blends with 10, 20, 30 and 40% PVC, all the other points agree with the theoretical relationship. The reason for the < 40% PVC blends to present single T_g 's above the predicted line can be explained with partial crystallinity. The thermograms of all blends with copolymer concentration higher than 60% display a melt endotherm. Therefore, the T_g 's for these blends lie above the curve because the crystallinity of PCL reduces the concentration of the amorphous phase of the copolymer. The presence of only one glass transition temperature showing a continuous progression from the T_g of one pure component to the T_g of the other is probably an indication of compatibility between PVC and the block copolymer.

The dynamic mechanical properties of the blends are shown in Figure 25. The DMTA results reveal not only the dynamic moduli but also the $\tan\delta$ transition which is another measure of the glass transition. Usually the T_g 's found by this method are somewhat less precise (ie., frequency-dependent) than those by DSC, but DMTA has the advantage to detect segmental motion on a smaller scale than does DSC [11]. Thus, many kinds of molecular motion, transitions and relaxation processes can be easily detected by DMTA.

Table 9. DSC and DMTA Thermal Analysis Data for PVC/PCL-HPL Blends

PVC wt(%) in blends	T_g (DSC) (°C)	T_g (DMTA) (°C)	T_m (DSC) (°C)	ΔH_f (J/g)	X_c^1 (%)
100	80	90	-	-	-
90	65	67	-	-	-
80	38	65	-	-	-
70	39	57	-	-	-
60	39	31	-	-	-
50	35	27	-	-	-
40	-10	30	50	34	11
30	-33	26	47	60	20
20	-38	16	48	85	28
10	-46	11	51	107	36

¹ Degree of crystallinity

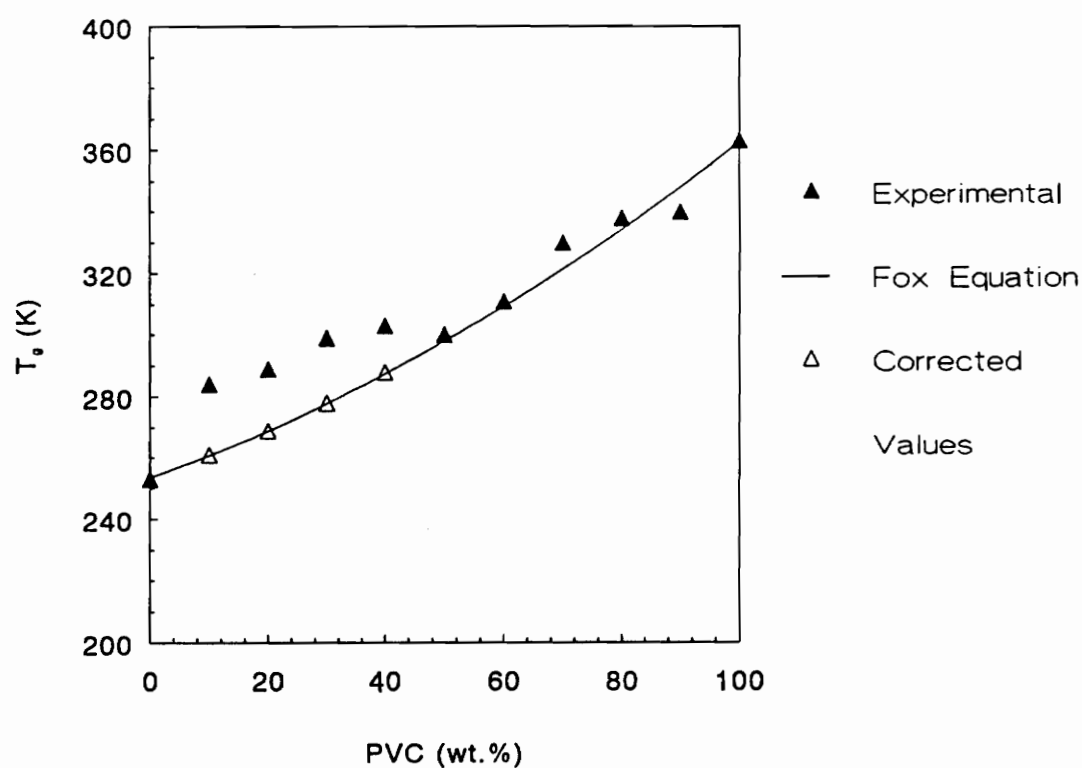


Figure 24. T_g vs. blend composition of PVC/PCL-HPL, experiment vs. Fox model.

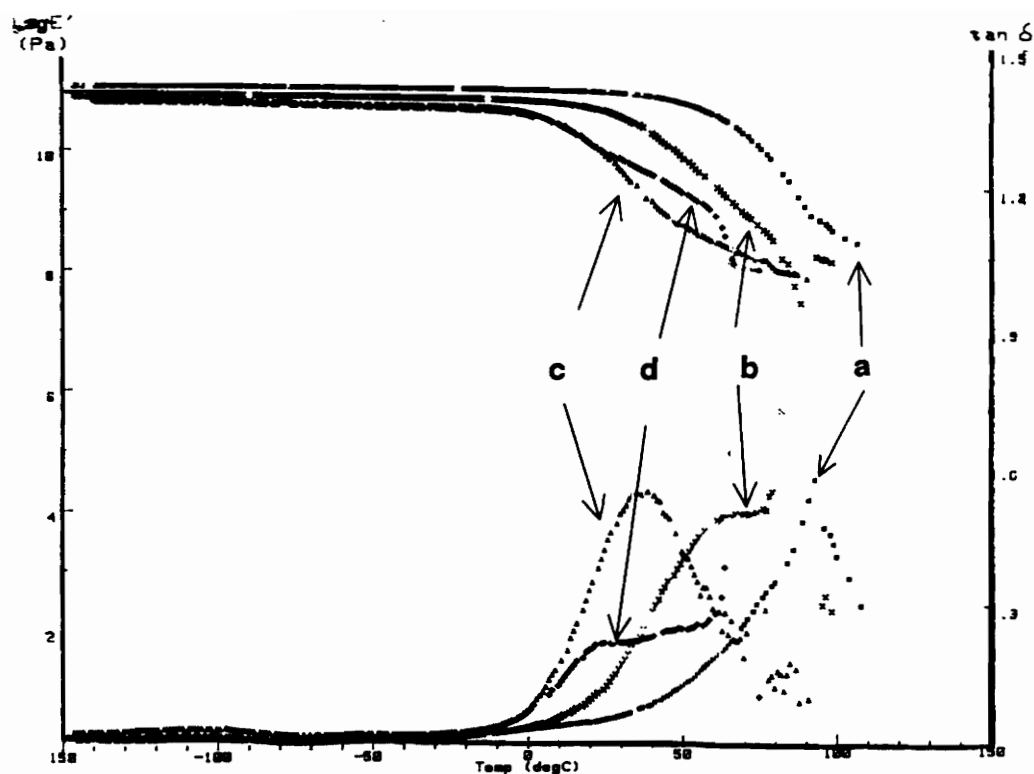


Figure 25. Temperature dependence on E' and $\tan \delta$ for PVC/PCL-HPL blends: (a) 20 %; (b) 40 %; (c) 60 %; (d) 80 % PCL-HPL copolymer

In Figure 25, the dynamic mechanical properties are shown as a function of temperature. There are up to four transition processes in the temperature range investigated. Two lower temperature peaks (-110 and -50°C) that have been attributed to secondary relaxation transitions, the former assigned to PCL [7] and the latter to PVC [12]; the T_g 's of the blends, located between 16 and 67°C, and the melting of the crystalline phase in blends with high copolymer content. Both low temperature relaxation peaks seem not to change with composition, while the blend's T_g systematically shifts to a higher temperature as the PVC concentration in the blend increases. In blends with high copolymer concentration (curves c and d), a first order transition is also observed. Their T_m 's shift to lower temperatures as the amount of PVC increases.

The dynamic mechanical testing results confirm the compatibility of the PVC/PCL-HPL system. At higher concentrations of PVC, the $\tan\delta$ moves progressively to higher temperatures. The secondary relaxation (-110°C) stays the same with blending. As Koleske and Lundberg noted [7] the lower-temperature PCL relaxation at -110°C on the $\tan\delta$ curve can be attributed to movement associated with the 5-(CH)₂ methylene sequence in the PCL backbone.

4.3.2 Tensile Properties

Typical stress-strain behavior of the blends are shown on Figure 26. The results are summarized in Table 10. Each data point averages 5-6 tests for stress at break, initial (Young's) modulus, and elongation at break. Stresses are calculated on the basis of the initial cross-sectional area. As seen in Figure 26, the ability to "elongate" or plastically deform rises quickly with increasing concentration of copolymer, up to about 50% PVC. Simultaneously, the modulus and ultimate strength drop rapidly from 100 to 60% PVC. At higher concentration of (PCL)_n-HPL in the blend, the copolymer crystallizes and an increase in modulus is observed. There is no crystallization in blends containing less than 60% copolymer. In other words, the blends up to 50% copolymer are completely amorphous. Since the polymer constituents are fully miscible, the T_g of the blends is inter-

Table 10. Mechanical Properties of PVC/PCL-HPL Blends

PVC wt(%) in blends	Elongation(%)		Stress at Break(MPa)		Young's Modulus(MPa)	
	mean	range	mean	range	mean	range
100	164	+ /- 62	12	+ /- 5	206	+ /- 77
90	225	+ /- 45	17	+ /- 3	222	+ /- 44
80	287	+ /- 104	20	+ /- 3	140	+ /- 83
70	452	+ /- 31	19	+ /- 0	90	+ /- 29
60	591	+ /- 52	12	+ /- 1	13	+ /- 2
50	513	+ /- 15	6	+ /- 1	2	+ /- 0
40	359	+ /- 56	5	+ /- 1	5	+ /- 1
30	174	+ /- 19	6	+ /- 0	24	+ /- 0
20	80	+ /- 8	7	+ /- 1	51	+ /- 6
10	20	+ /- 4	5	+ /- 1	63	+ /- 10
0	8	+ /- 6	1	+ /- 1	66	+ /- 23

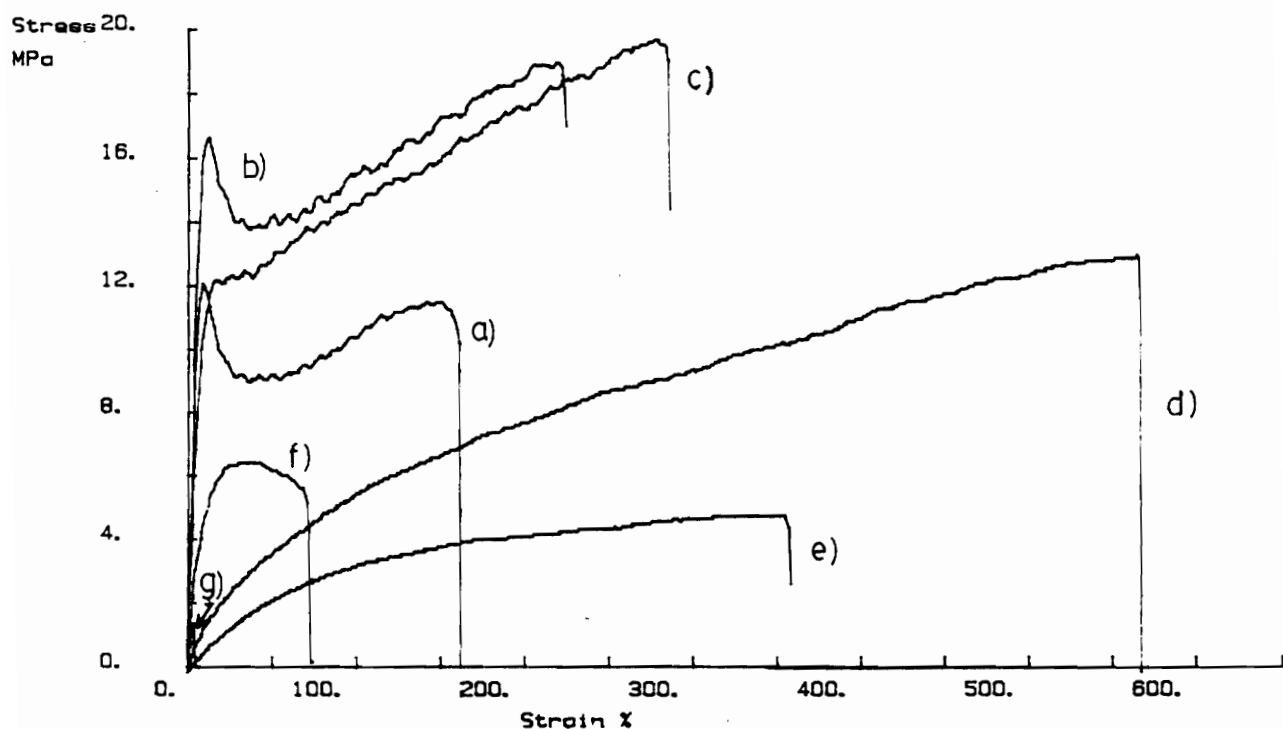


Figure 26. Tensile properties of PVC/PCL-HPL blends: (a) 0 %; (b) 10 %; (c) 20 %; (d) 40 %; (e) 60 %; (f) 80 %; (g) 100 % PCL-HPL copolymer

mediate to those of the individual polymers (for most of the blends below room temperature). Therefore, the plasticization of PVC is responsible for the reduction in strength and modulus, and for the increase in elongation at break as the copolymer content increases in the blend. At copolymer contents greater than 60%, $(PCL)_n$ -HPL crystallizes, and this is responsible for an increase in modulus with a consequent reduction in elongation.

Blends of PVC and HPL rather than $(PCL)_n$ -HPL copolymers (the "control" experiment) were also made in order to examine whether HPL alone is also compatible with PVC. Solvent cast films could only be obtained with blends containing < 40% HPL. Above 40%, immediate macrophase separation was observed without magnification. Tensile tests (Figure 27) provide conclusive evidence that the PVC/HPL system has poor mechanical strength. The samples were brittle and had poor elongation properties.

4.3.3 Aging studies

It is well known that the properties of semi-crystalline polymers are largely dependent on the form and extent of crystallinity. When two polymers are compatible and one of them is semi-crystalline, after blended, the resulting matrix will consist of the entire amorphous polymer in addition to the amorphous part of the crystallizable component. Polycaprolactone, and consequently its copolymers, will develop crystallinity when the polymer is annealed for appropriate periods of time, at temperatures intermediate between melting point and glass transition temperature. In the case of blends of $(PCL)_n$ -HPL and PVC, the crystallization process proceeds slowly at room temperature. Therefore, it is of interest to determine to what extent the blend crystallinity will be affected by aging. The following paragraphs discuss the mechanical behavior of blends containing $(PCL)_n$ -HPL and PVC annealed at room temperature for up to about 6 months.

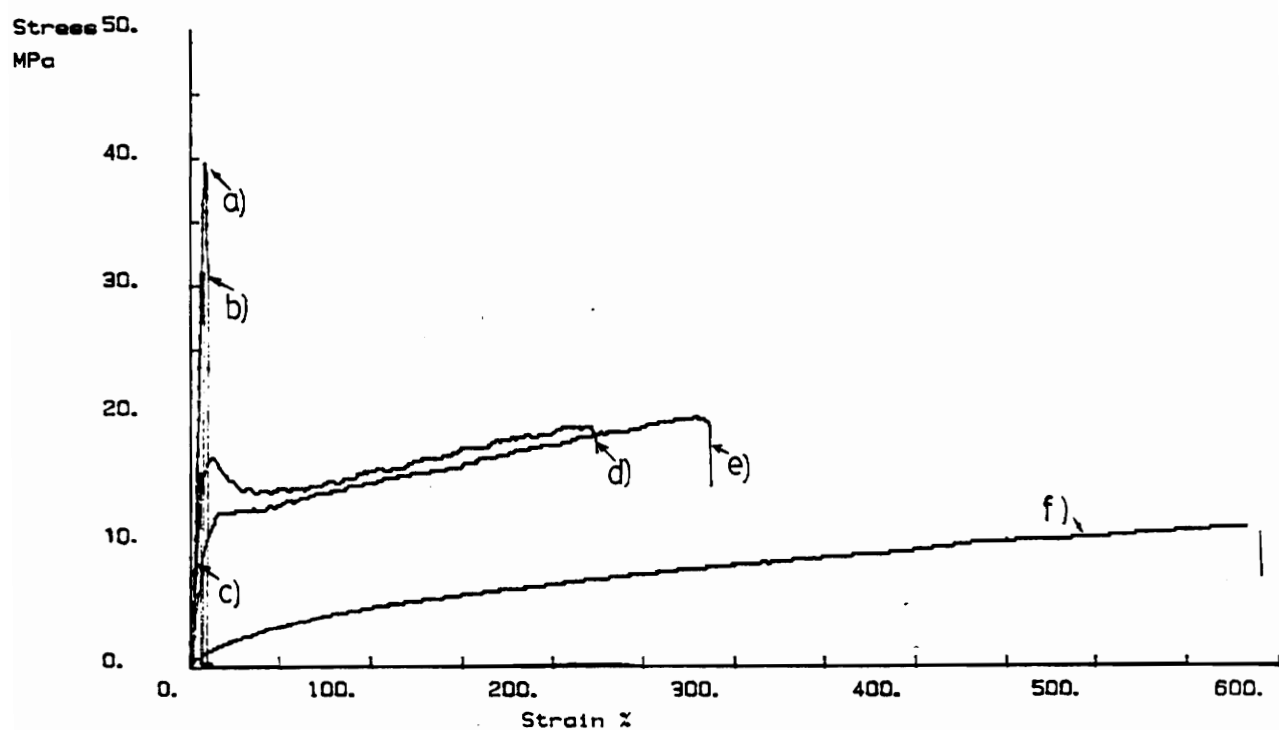


Figure 27. Tensile properties of PVC/HPL and PVC/PCL-HPL blends.: (a) 10 %; (b) 20 %; (c) 40 % HPL, and (d) 10 %; (e) 20 %; (f) 40 % PCL-HPL copolymer

As seen previously, the addition of copolymer into the PVC matrix has caused a decrease in modulus and tensile strength, and an increase in elongation. This is typically an effect of plasticization. When the exact opposite occurs, the phenomenon is called anti-plasticization. It results when relatively small amounts of a plasticizer are used. Several factors are involved, and many theories have been proposed to explain this phenomenon. Among the most popular is the so-called "hindered molecular motion theory" [12]. It is well known that the secondary transitions, particularly the β -transition, are associated with ductility and good impact strength. If such transition does not occur, the resin is brittle at room temperature. Small amounts of anti-plasticizers in PVC reduce and even eliminate its β -transition, as shown in the work of Sundgren and co-workers with PVC (anti)plasticized with polycaprolactone (Figure 28) [12]. Impact energies of these PVC compositions decreased with PCL content rising to about 12% and then improved or rose with further increase in plasticizer content.

The reasons for this β -transition, and why it is inhibited by small amounts of plasticizer, are still debated. An old explanation of PVC anti-plasticization was proposed by Ghersa [13]. According to him, plasticizer molecules become attached to PVC through their polar groups, and at low concentrations they act as crosslinks through increased steric hindrance. This causes an increase in cohesion so that the polymer chains are harder to separate.

Table 11 presents the mechanical and thermal data of the aging study on blends of PVC and $(PCL)_n-HPL$ copolymer. Figure 29 shows the change in modulus with the aging time for three different blend compositions. For the blend rich in PVC, there is a dramatic increase in modulus with time. The opposite happens in those blends where the copolymer content is high. Low and relatively constant moduli are seen during the six-month period. Therefore, the increase in modulus in samples with low copolymer content can be explained by the anti-plasticization "theory" of Sundgren et al. [14]. The small percent of copolymer in the blend causes immobilization of the PVC chains through a type of polar crosslinking mechanism. The loss of this freedom of motion causes the PVC matrix to become brittle. On the other hand, in high copolymer containing blend

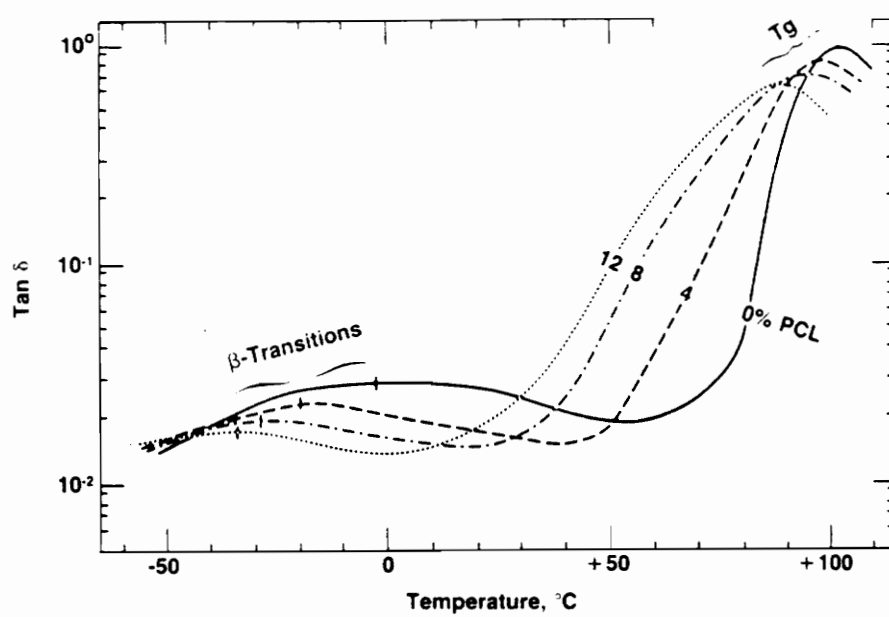


Figure 28. Loss tangent as a function of temperature for PVC/PCL blends [12]

Table 11. Summary of the Aging Effect on Mechanical Properties of PVC/PCL-HPL Blends

Time (days)	T_m (°C)	ΔH_f (J/g)	X_c (%)	Modulus (MPa)	Elongation (%)	Stress (MPa)
<i>10%(PCL)_n -HPL/90%PVC</i>						
3	-	-	-	32	450	12
10	-	-	-	65	310	11
18	-	-	-	140	212	15
30	-	-	-	140	211	15
55	-	-	-	140	234	16
90	-	-	-	360	74	26
180	-	-	-	280	20	20
<i>40%(PCL)_n -HPL/60%PVC</i>						
3	-	-	-	3	600	5
10	-	-	-	3	500	5
18	-	-	-	5	421	6
30	-	-	-	7	380	8
55	-	-	-	7	427	7
90	-	-	-	9	412	7
180	-	-	-	9	400	7
<i>60%(PCL)_n -HPL/40%PVC</i>						
3	49	36	12	6	210	3
10	49	38	13	6	207	2
18	51	38	13	14	191	3
30	53	43	14	16	232	5
55	53	46	15	16	188	4
90	54	43	14	16	160	6
180	54	43	14	16	180	6

X_c = Degree of crystallinity

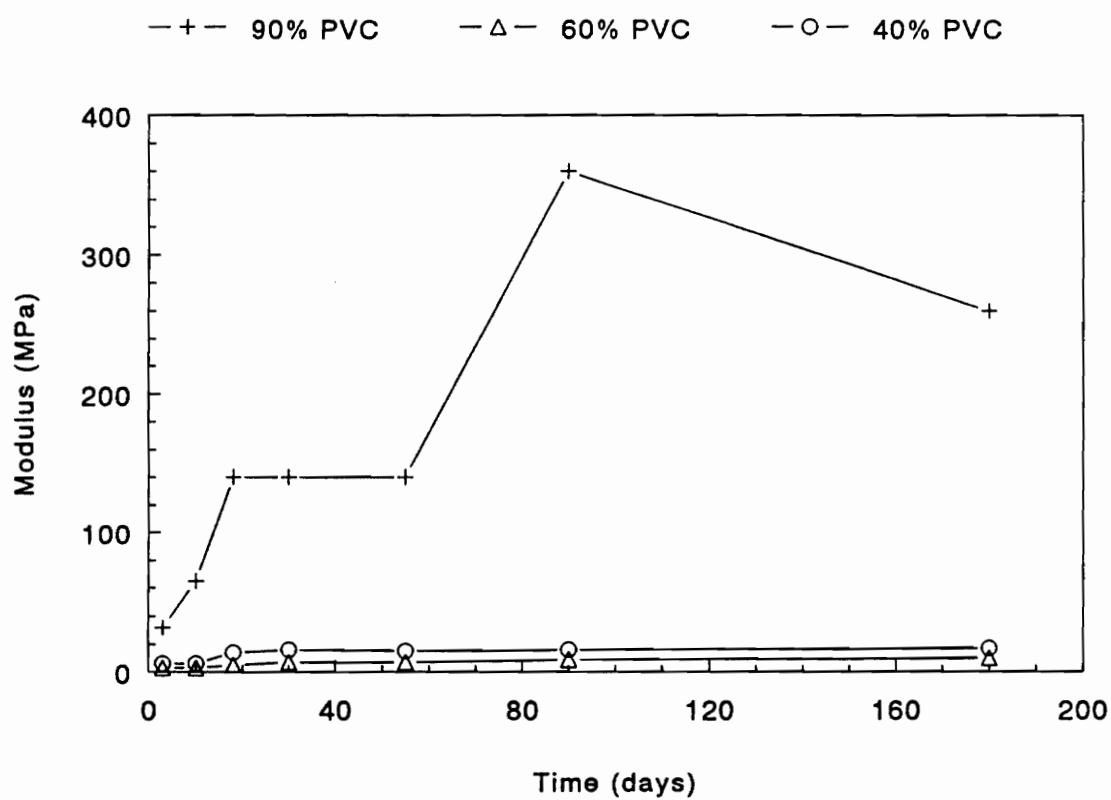


Figure 29. Effect of aging on modulus properties

systems, there are enough PCL segments to be dispersed and therefore dissolved in the PVC, which then produces a flexible and elastomeric material. When the copolymer is the matrix (60% copolymer) there is a slight gain in modulus owing to the crystallization of the copolymer, as detected by DSC.

Figure 30 presents the ultimate strength of the same set of blends studied previously. In all three blends there is an increase in ultimate strength with time of aging. The increase is more significant in the sample rich in PVC due to the anti-plasticization effect. The ultimate strength increases more than two-fold. The samples rich in copolymer show no significant improvement in ultimate strength throughout the six month aging period. Indeed, the sample with higher copolymer concentration presented the lowest ultimate strength, even though it revealed a gain in modulus as compared to the 40% copolymer sample. The decline in ultimate strength is probably due to embrittlement caused by crystallization.

The results of elongation at break are presented in Figure 31. The rather large elongation of the 60% PVC sample is definitely related to improved interfacial adhesion between the copolymer and PVC. The highest elongation that can be achieved is dependent on blend composition. Ideally it should be around 50 percent, when the properties of both polymers are balanced. At low copolymer content, the crystallization rate of $(PCL)_n-HPL$ is suppressed, and consequently the blend is completely amorphous. Since the T_g of $(PCL)_n-HPL$ (PCL component) is much lower than that of PVC, the copolymer reduces the blend T_g and plasticizes the PVC component. As seen previously, this reduces strength and modulus, and increases elongation at break with initial increase in copolymer content. Continued addition of copolymer beyond 60% causes strength to increase and ductility to decrease, as the crystalline portion of the PCL-HPL becomes the principal component.

Heat of fusion data from the DSC studies on the blends are shown in Figure 32. Only the blend with 60% copolymer exhibited an endothermic peak throughout the aging time. There is indeed an increase in the measured heat of fusion during the time period. Translating the heat of fusion

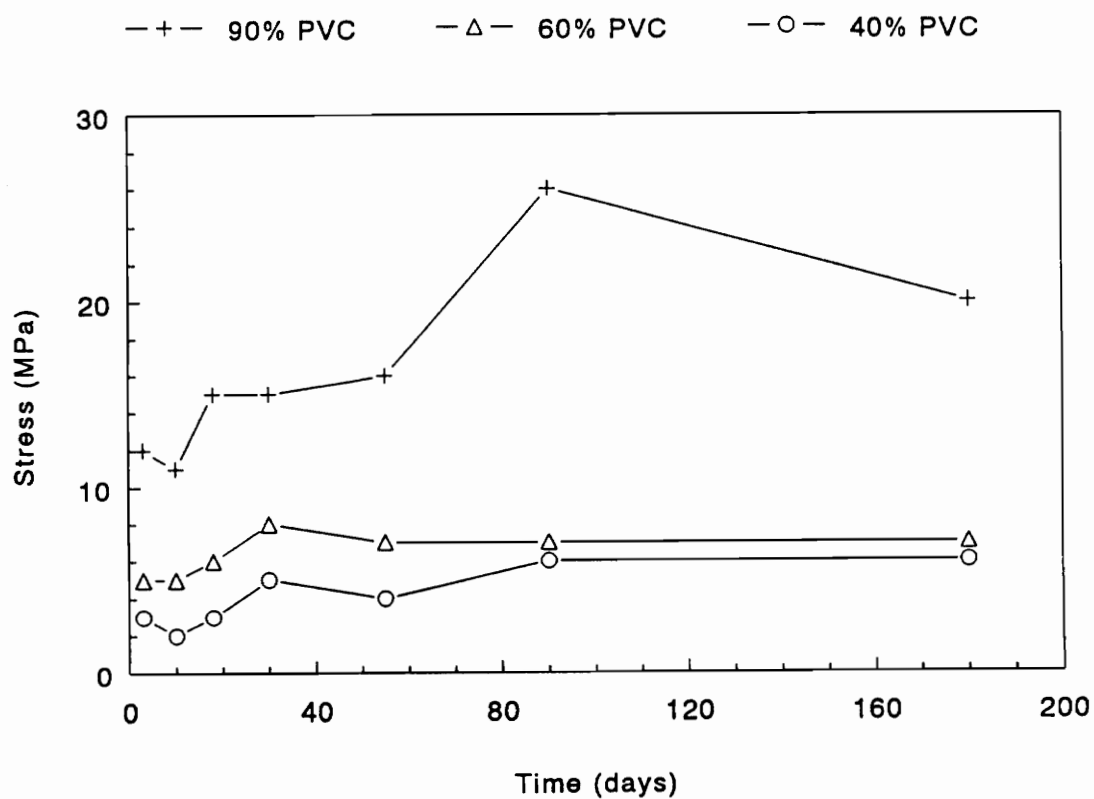


Figure 30. Effect of aging on ultimate strength properties

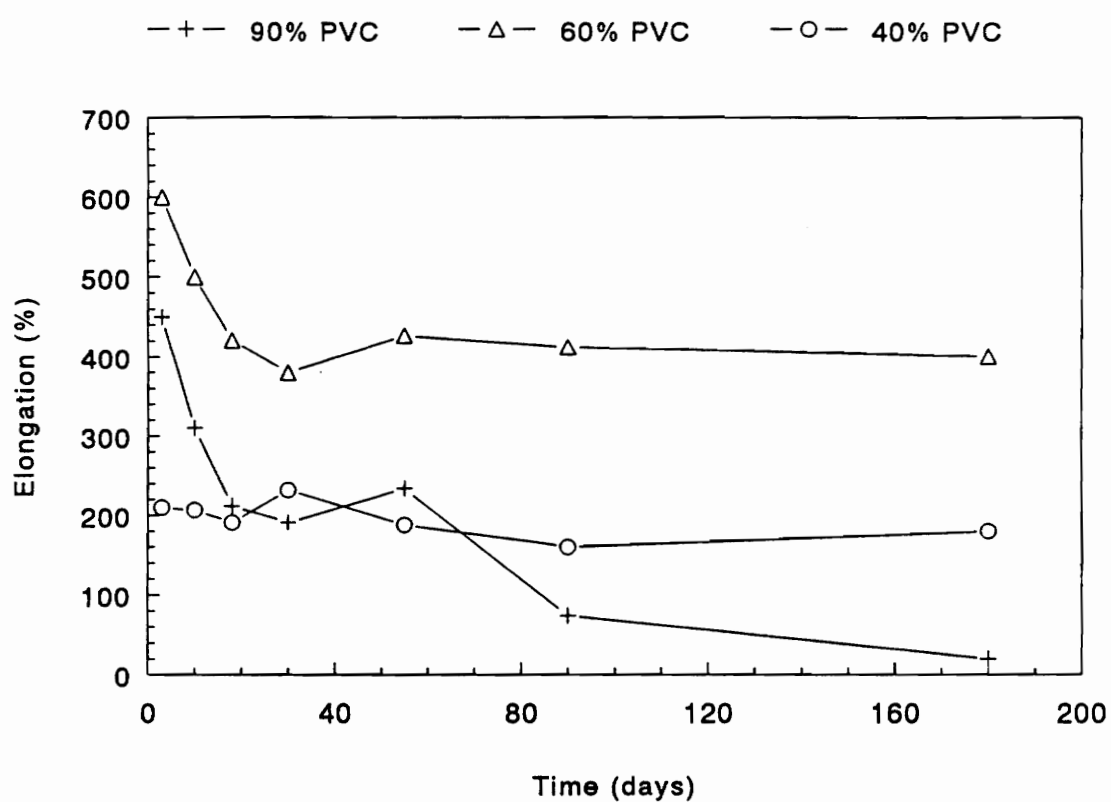


Figure 31. Effect of aging on elongation at break

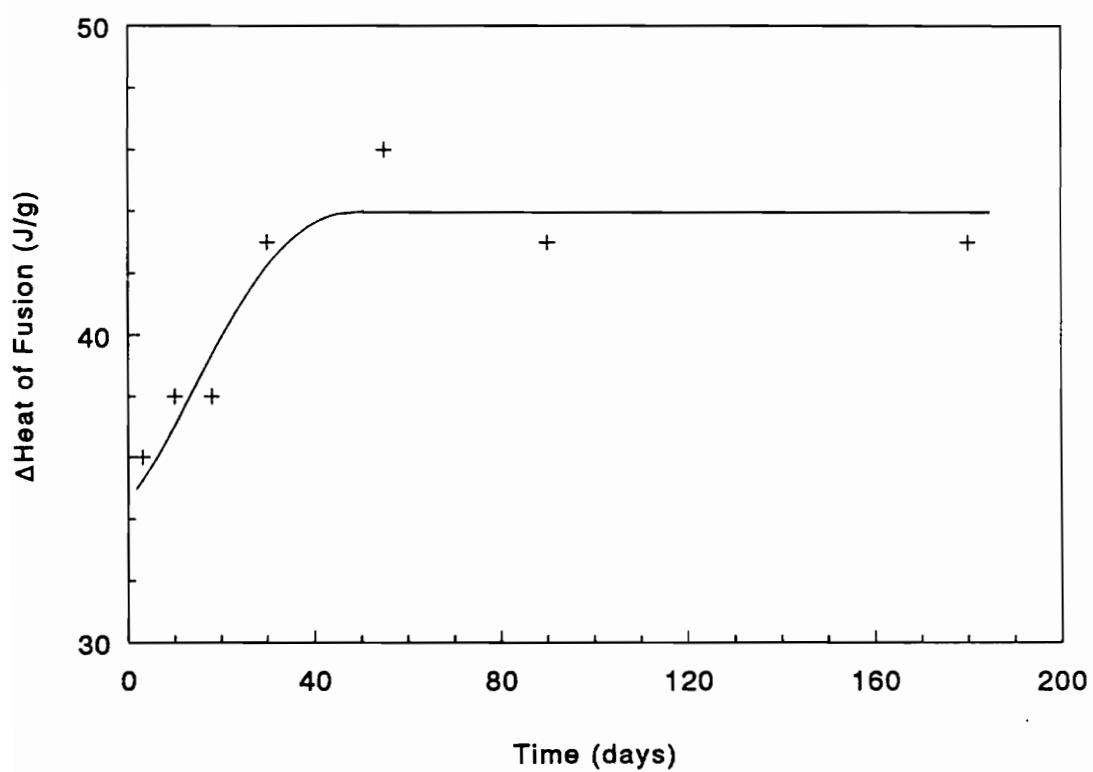


Figure 32. Effect of aging on heat of fusion

into degree of crystallinity, it is seen in Figure 33 that the gain in crystallinity with aging is not significant, demonstrating once more that it is not crystallinity that affects the embrittlement of the matrix, but rather a lack of enough PCL segments to promote plasticization of PVC.

4.3.4 Crystallinity properties

Figure 34 displays the degree of crystallinity as a function of blend composition of aged (> 6 months) samples. The degree of crystallinity is calculated from the area under the heat of fusion peak in the DSC thermograms. Since the copolymer crystallizes at room temperature, the amount of crystallinity present increases with time. Therefore, data presented here were obtained using samples annealed for at least 6 months at room temperature in a desiccator. The results show a decrease in degree of crystallinity as the copolymer is diluted by PVC. At concentrations below 60% copolymer there is no more crystallization of PCL segments. This can be attributed to the dilution of PVC chains within the blend, and this restricts the rearrangement of PCL segments to induce crystallization.

The melting points of the PCL-HPL crystalline phase are shown in Figure 35 as a function of weight percent of copolymer in the blend. There is a decrease in melting point temperature as the blend is enriched with PVC. The decrease in T_m was also reported by Ong [8] in his studies on PCL/PVC blends. According to Ong, wide-angle x-ray results show that only one PCL crystalline form is present in all crystalline PCL/PVC blends. Thus, he concludes that PVC exerts a considerable influence on the melting behavior of PCL. As the PVC content increases, the melting peak is shifted toward lower temperature. Ong's observations indicated that increasing PVC lowers the crystalline order and reduces the crystallite size.

The effect of crystallinity on the tensile properties of the blends is shown in Figure 36, where Young's modulus as determined by the initial slope of the stress-strain curves has been plotted

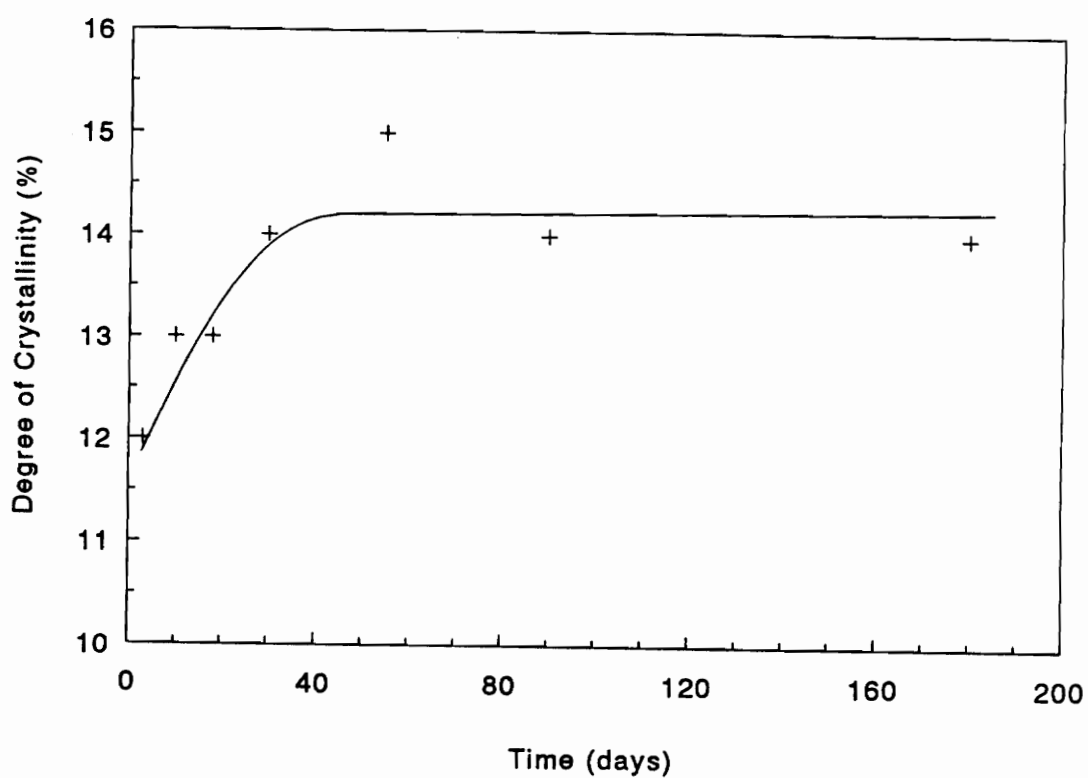


Figure 33. Effect of aging on degree of crystallinity

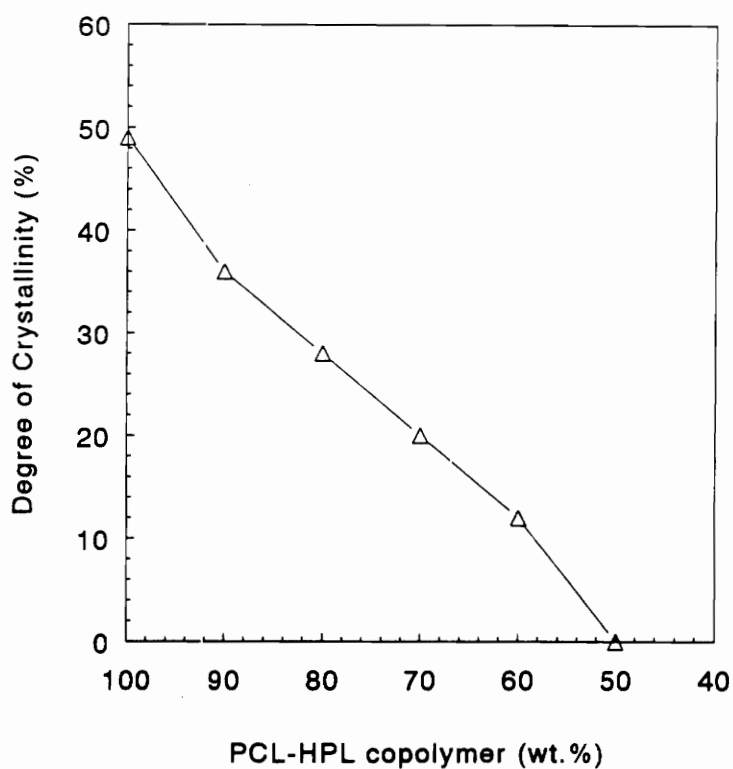


Figure 34. Degree of crystallinity as a function of composition for PVC/PCL-HPL blends.

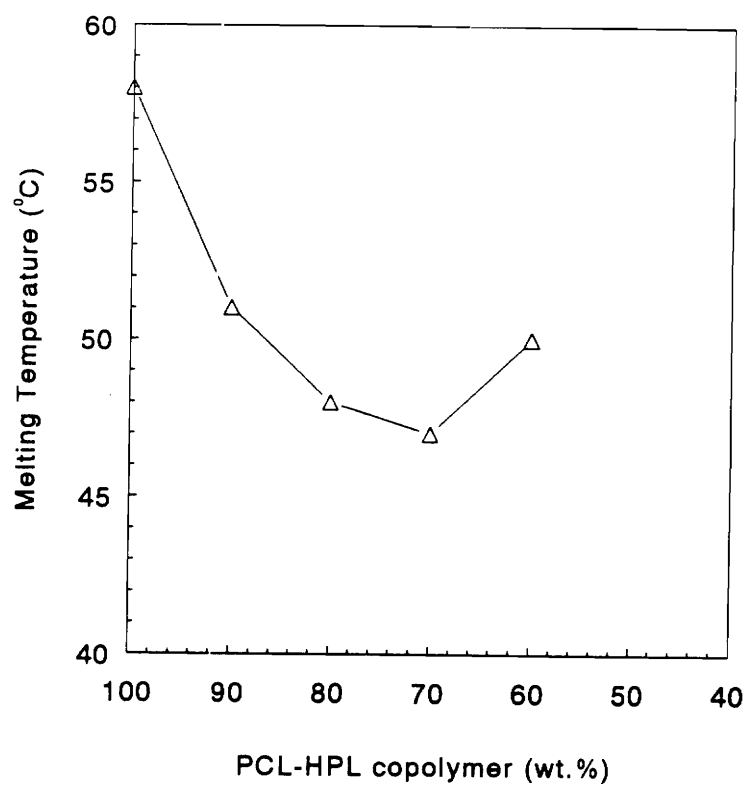


Figure 35. Melting temperature of copolymer as a function of composition for PVC/PCL-HPL blends

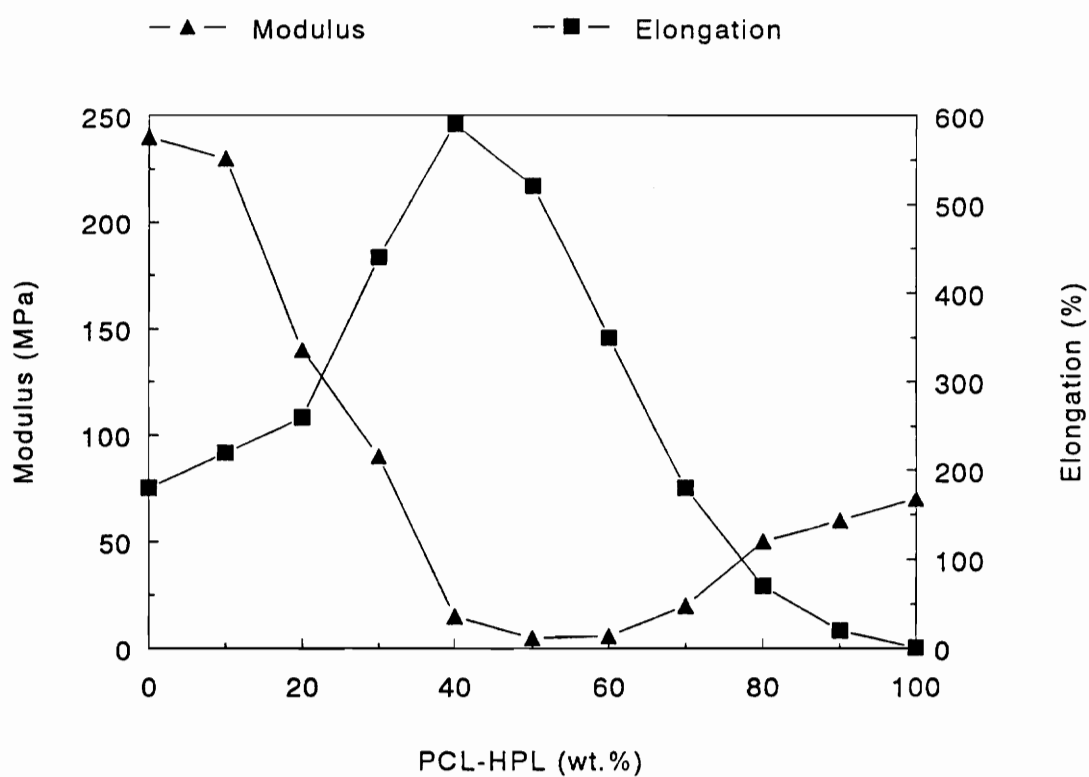


Figure 36. The effect of crystallinity on tensile properties

versus copolymer content. At 50% blend composition, a modulus minimum and elongation maximum is achieved, and the blends are totally amorphous based on DSC measurements. With copolymer concentrations higher than 60%, the copolymer crystallizes, and this results in a strengthened matrix and reduced elongation.

4.3.5 Morphology

Transmission and scanning electron microscopy have become essential tools for investigating the morphology of multiphase polymer systems. Unlike metallic alloys, polymer blends are characterized by a small level of contrast between phases and a high sensitivity toward the electron beam. Recently, staining by ruthenium tetroxide was found to be effective for many saturated and aromatic polymers. RuO_4 can react with polymers containing ether, alcohol, aromatic, amine, etc. functional groups. The darkening of the stained regions arises from the local precipitation of RuO_2 produced by the oxidation of the polymer. Both TEM and SEM were used to study the morphology of PVC and $(\text{PCL})_n\text{-HPL}$ blends. RuO_4 was used for TEM analysis.

The changes in morphology of polymer blend samples versus composition are illustrated in SEM micrographs of fractured surfaces (Figures 37). They cover the range 10% $(\text{PCL})_n\text{-HPL}$ /90%PVC to 60% $(\text{PCL})_n\text{-HPL}$ /40%PVC. The structures range from a continuous PVC phase for compositions above 60% PVC to a continuous $(\text{PCL})_n\text{-HPL}$ phase for compositions below that limit. Basically, only single-phase structures can be seen from these micrographs, in which both PVC and $(\text{PCL})_n\text{-HPL}$ exist as a continuous phase. The SEM micrographs reveal that it is almost impossible to detect phase separation, since the copolymer particles were very small in size, and they were evenly distributed in the PVC matrix. This type of morphology can be described as a coarse structure with a fine dispersion of phases, which can be interpreted as a blend of two miscible polymers.

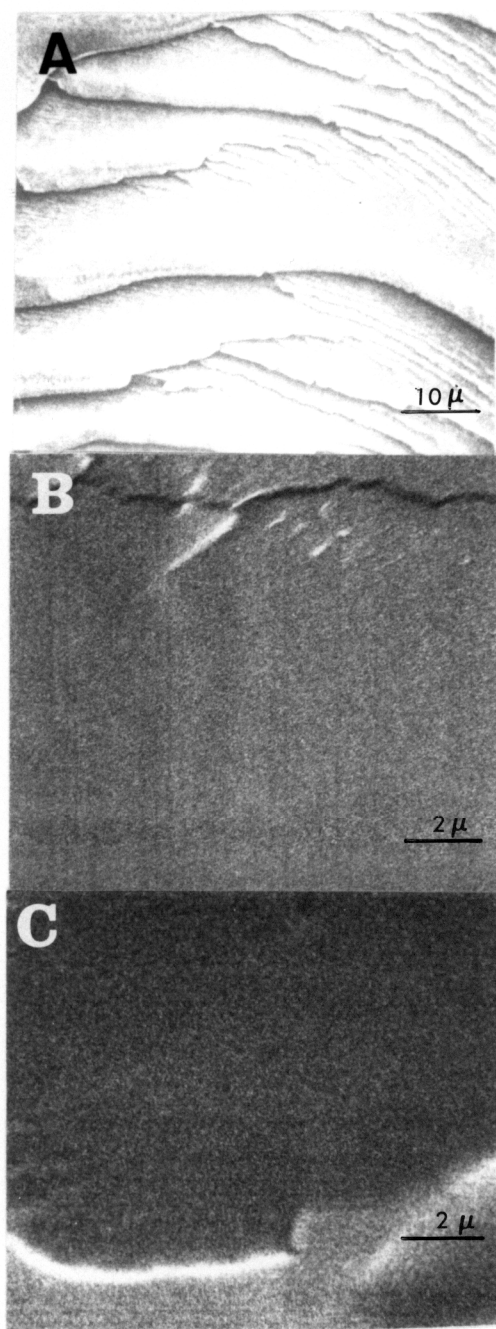


Figure 37. SEM micrographs of PVC/PCL-HPL polymer blends: (a) 10% (1000x), (b) 20%, (5000x), (c) 60% PCL-HPL copolymer (5000x).

BINARY BLENDS OF POLYVINYL CHLORIDE AND POLYCAPROLACTONE -
HYDROXYPROPYL LIGNIN COPOLYMER

Although solution blending provides mixing of the two components at the molecular level, phase separation is evident for the PVC/HPL system. Figure 38 illustrates SEM micrographs for the 10, 20 and 40% HPL blends with PVC. Besides the two-phase structure and the type of distribution of one phase in the other, there is an increase in the HPL particle size as the HPL content in the blend increases. There is clear evidence of macrophase separation, and this agrees with the tensile test results. The way in which the samples fractured is another indication of poor adhesion between the components. The PVC/HPL system seems to fail in a macroscopically brittle fashion, while the PVC/PCL-HPL system fails ductilely as evidenced by the smooth fracture surface seen in the micrographs of Figure 37.

Figure 39 shows TEM's of thin films of PVC/PCL-HPL blends cast from dilute solution. PCL-HPL domains were preferentially stained with RuO_4 . These domains range in size from 10 to 30 nm. The matrix is formed by the major component, and there is a transition at about 50% composition. Phases are small, but clearly visible, with defined boundaries at high copolymer content. The small size distribution observed in all compositions is another indication for significant miscibility between the polymers.

Transmission electron microscopy was also applied to the PVC/HPL system. Figure 40 compares TEM micrographs of the 10, 20 and 40% HPL specimens with those containing 10, 20 and 40% copolymer. Two-phase and macrophase-separated systems are revealed by the blends of PVC and HPL. Stained HPL particles are irregular in shape and vary within a wide size range (0.1-1.0 μm). They are unevenly distributed. On the other hand, in the $\text{PVC}/(\text{PCL})_n\text{-HPL}$ system, TEM micrographs show that the compatibility of $(\text{PCL})_n\text{-HPL}$ with PVC is far superior to that of HPL. The copolymer particle sizes are very small and evenly distributed in the PVC, forming an almost single phase system.

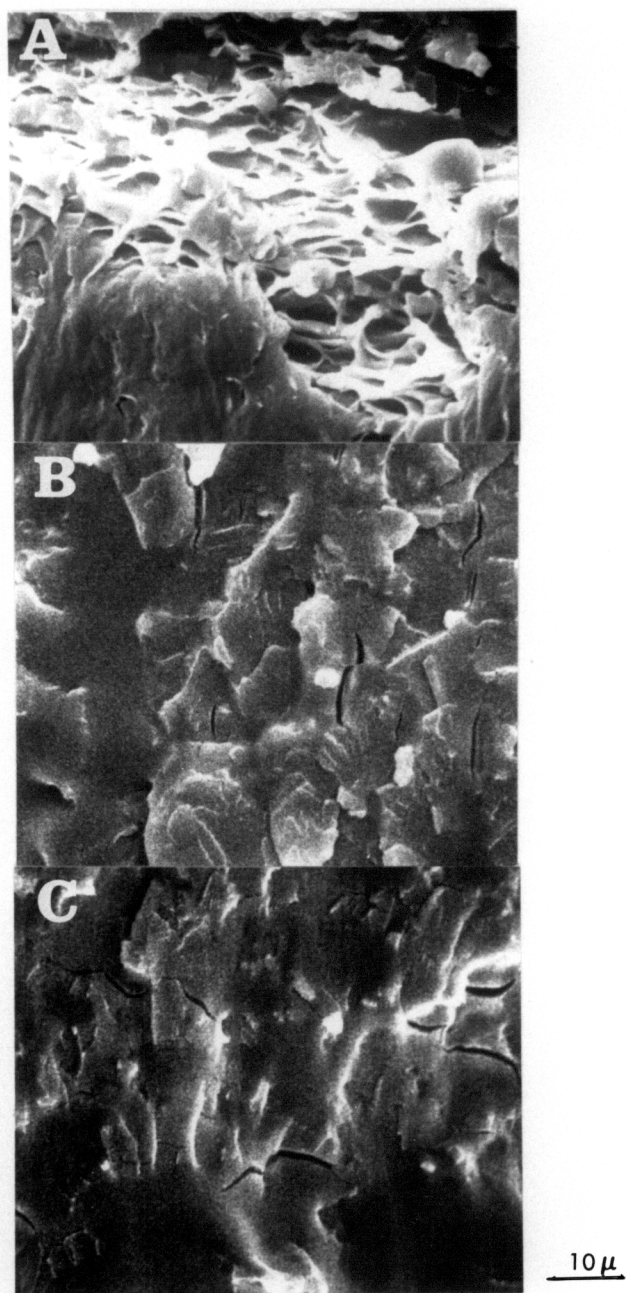


Figure 38. SEM micrographs for PVC/HPL blend system: (a) 10%; (b) 20%, and (c) 40% HPL (1000x)

BINARY BLENDS OF POLYVINYL CHLORIDE AND POLYCAPROLACTONE -
HYDROXYPROPYL LIGNIN COPOLYMER

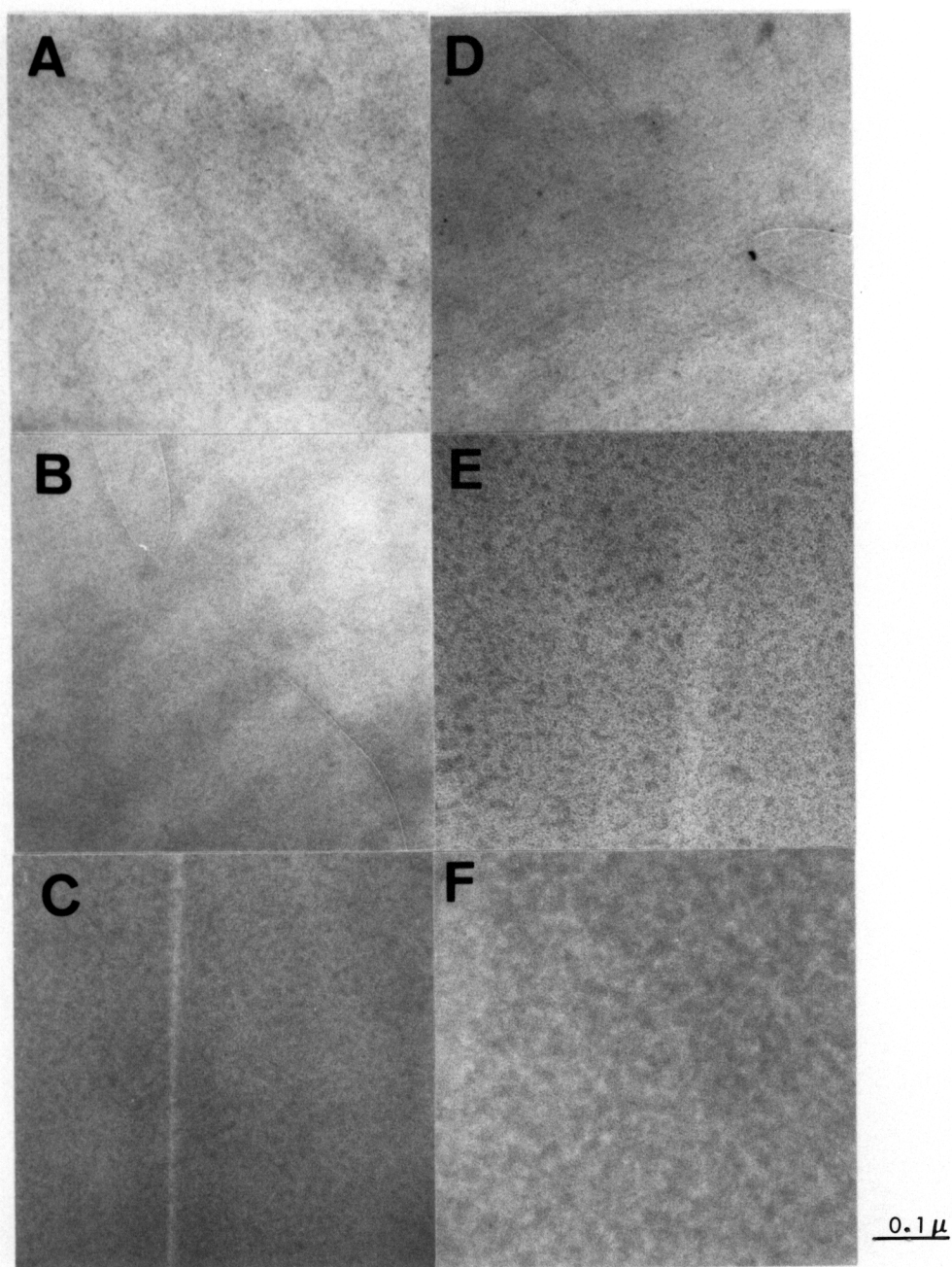


Figure 39. TEM of thin films of PVC/PCL-HPL blends.: (a) 5%; (b) 10%; (c) 20%; (d) 40%; (e) 60%; (f) 80% copolymer (105000x)

BINARY BLENDS OF POLYVINYL CHLORIDE AND POLYCAPROLACTONE -
HYDROXYPROPYL LIGNIN COPOLYMER

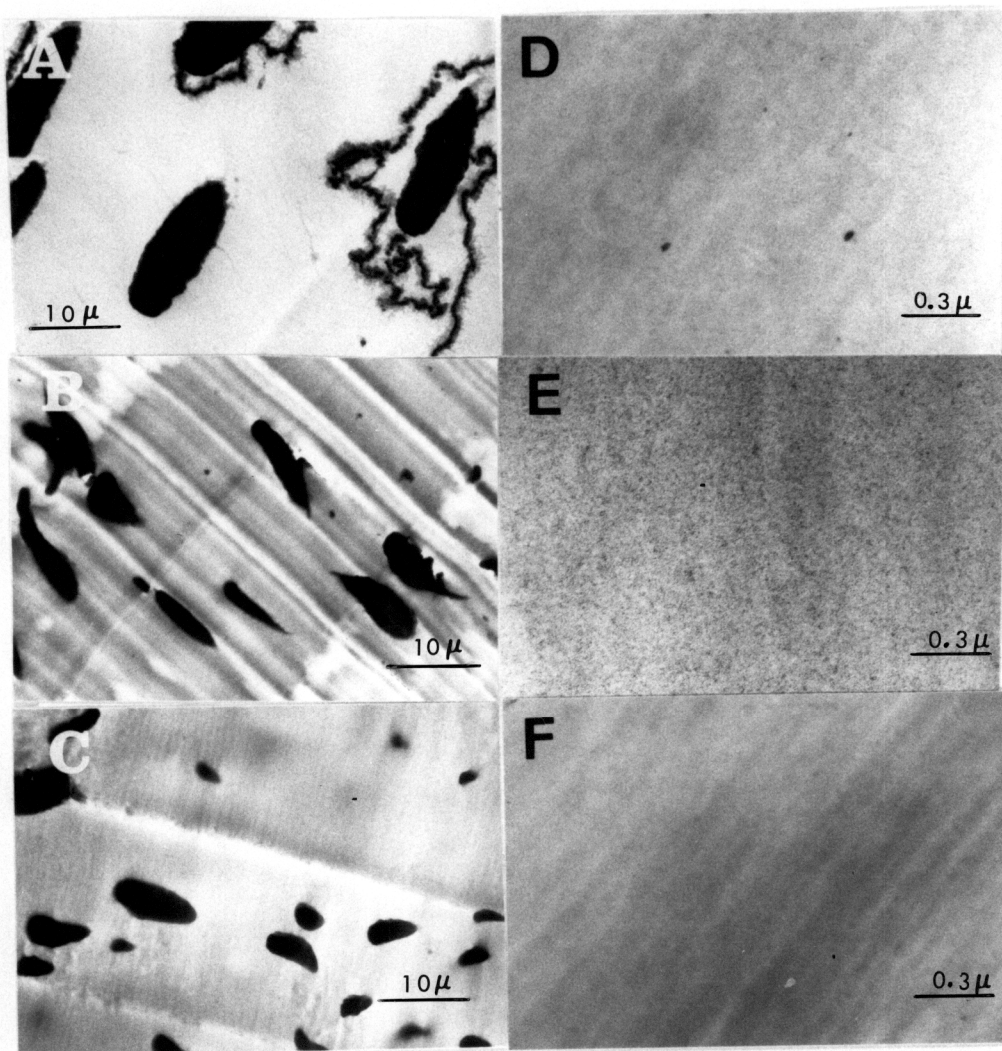


Figure 40. TEM micrographs of thin films of PVC blended with: (a) 10%; (b) 20%; (c) 40% HPL (6000x); (d) 10%; (e) 20%; (f) 40% PCL-HPL copolymer (37500x)

BINARY BLENDS OF POLYVINYL CHLORIDE AND POLYCAPROLACTONE -
HYDROXYPROPYL LIGNIN COPOLYMER

4.4 CONCLUSIONS

Blends of PCL-HPL with poly(vinyl chloride) were prepared by solvent casting from solution. The blends were shown to exhibit only one glass transition temperature intermediate between those of the blend components. With exceptions of the blends with high copolymer concentration (above 60%), the blend's T_g followed reasonably well the Fox equation.

The morphology of the blends was investigated by DSC and electron microscopy. The presence of PVC plays a major role in depressing the T_m of the PCL segments present in the blends. Copolymer crystallinity was found to exist with PVC concentrations ranging between 0 and 40%. The degree of crystallinity of the blend decreases with increasing PVC content up to about 40% PVC content. Above that, no crystallinity is detected.

The dynamic mechanical properties, as determined by DMTA, show that for the polyblends there are up to four transition processes in the temperature range investigated. Both low-temperature relaxation peaks seem not to change with composition. However, the blend's T_g systematically shifts to a higher temperature as the PVC concentration in the blend increases. A first order endothermic transition is also observed in blends with high copolymer concentration (60 to 90%). Their T_m 's shift to lower temperatures as the amount of PVC increases. Crystallinity shows a considerable influence on T_g because the crystallites restrict the motion of the amorphous sequence. This requires more energy for the transition to occur, and it consequently increases the T_g .

Stress-strain properties showed a decrease in modulus and increased ductility as the PVC was diluted with copolymer. This trend, caused by increasing PVC plasticization by the copolymer, is reversed at higher copolymer contents where, due to crystallization, an increase in modulus and reduction in elongation is observed.

The mechanical properties of the blends are affected by the aging process, especially the 10% copolymer composition, due to its anti-plasticization effect. Modulus and tensile strength increase, and elongation decreases with time. Blends rich in copolymer are slightly affected by the aging process. The copolymer acts as a true anti-plasticizer. High copolymer containing blends exhibit lower modulus and tensile strength and increased elongation without significant change with time.

Electron microscopy reveals a significant miscibility between PVC and $(PCL)_n-HPL$ copolymers, over a wide composition range (from 10% to 90% copolymer). TEM illustrates a two-phase structure that is microscopically phase separated with domain sizes ranging from 10 to 30 nm, approximately.

4.5 REFERENCES

1. A. Rudin, *J. Macromol. Sci.-Rev. Macromol. Chem.*, **C19**(2), 267(1980)
2. D. R. Paul, "Interfacial Agents (Compatibilizers) for Polymer Blends", D. R. Paul and S. Newman, Ed., "**Polymer Blends**", vol. 2, chap. 12, 35(1978)
3. D. S. Hubbel and S. L. Cooper, *J. Appl. Polym. Sci.*, **21**, 3035(1977)
4. R. L. Jalbert, in "**Modern Plastics Encyclopedia, 1975-1976**", J. Agranoff, Ed., McGraw-Hill, New York, 1975, p.107
5. J. V. Koleske, C. J. Whitworth, Jr., and R. D. Lundberg, "**U. S. Patent 3,892,821 (July 1, 1975)**"
6. G. L. Brode and J. V. Koleske, *J. Macromol. Sci.-Chem.* **A6**,1109(1972)
7. J. V. Koleske and R. D. Lundberg, *J. Polym. Sci. A-2*, **7**, 795(1969)
8. C. Ong, "**Ph.D Thesis**", University of Massachusetts, 1973; O. Olabisi, L. M. Robenson, M. T. Shaw, "Polymer-Polymer Miscibility", Academic Press, New York, NY, 1979
9. F. B. Khambatta, F. Warner, T. Russel, and R. S. Stein, *J. Polym. Sci.: Polym. Phys. Ed.*, **14**, 1391 (1976)
10. V. Crescenzi, G. Manzini, G. Calzolari, and C. Borri, *Eur. Polym. J.*, **8**, 449(1972)
11. W. J. MacKnight, J. Stoelting, and F. E. Karasz, *ACS Adv. Chem. Ser.*, **99**, 29(1971)
12. T. F. Schatzki, *J. Polym. Sci.*, **57**, 496(1962).
13. P. Ghera, *Mod. Plast.*, **36**(2), 135 (1958)
14. N. Sundgren, G. Bergman and Y. J. Shur, *J. Polym. Sci.*, **22**, 1255 (1978)

5.0 SYNTHESIS AND CHARACTERIZATION OF CELLULOSE PROPIONATE SEGMENTS MONO-HYDROXYL TERMINATED

5.1 INTRODUCTION

Cellulose is the most abundant organic polymer on earth, comprising the principal component of plants. Over 10^{11} t is synthesized and degraded annually [1].

Natural cellulose occurs morphologically as fibers, such as cotton or wood fiber [2]. Chemically, cellulose is a long-chain polymer of β -D-glucose in the pyranose form linked together by 1,4' glucosidic bonds to form cellobiose residues, considered the repeat units in the cellulose chains (Figure 41). Values for degree of polymerization (DP) range from 500 for regenerated cellulose to 3,000-5,000, for (wood) pulp fibers, and to as high as 15,000 for cotton fibers.

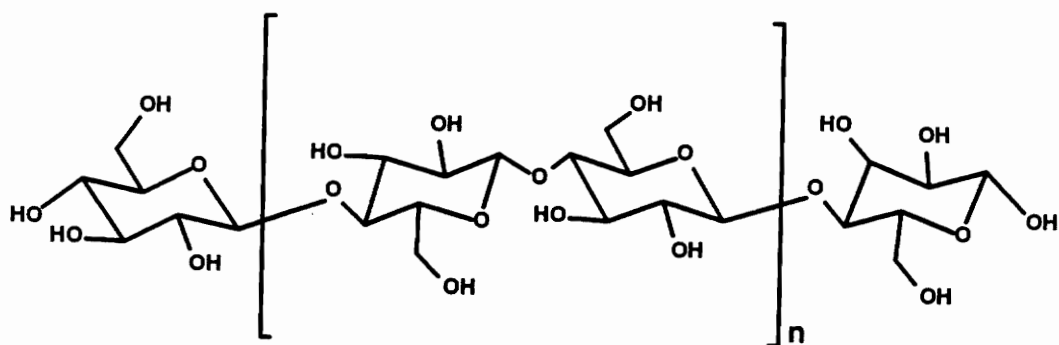


Figure 41. Structure of cellulose.

Cellulose molecules are completely linear and have a strong tendency to form intra- and intermolecular hydrogen bonds. Bundles of cellulose molecules are aggregated together forming microfibrils in which highly ordered (crystalline) regions alternate with less ordered (amorphous) regions [3]. These different regions do not have clearly defined boundaries, but rather blend into each other. Since cellulose crystallizes into different polymorphic forms, it is classified according to lattice type. Cellulose lattice type **I** is found in cotton fibers, among other sources, and it consists of about 70-80 percent crystalline regions as recorded by X-ray analysis. Cellulose lattice type **II** is found whenever the lattice of cellulose **I** is destroyed, for example, on swelling with strong alkali or on dissolution of cellulose. It is found in isolated wood pulp fibers, and it consists of about 60 percent highly ordered or crystalline regions. Since the strongly hydrogen bonded cellulose **II** is thermodynamically more stable than cellulose **I**, it cannot be reconverted into the latter. All naturally occurring cellulose has the structure of cellulose **I**. Other polymorphic forms have been reported as cellulose **III**, **IV**, etc.. However, the current opinion is that these are not true polymorphic forms, but are rather disordered versions or mixtures of cellulose **I** and **II** [3,4].

Despite cellulose being a polymer consisting of β -anhydro glucose, it has remarkable insolubility in water. Hydrogen bonding between cellulose chains is so intense that water cannot disrupt it by complexing with the hydroxyl groups. Low molecular weight fractions, however, can be solubilized by concentrated acids and bases, concentrated salt solutions and metal complexes.

The problems of cellulose insolubility can be overcome by converting cellulosic hydroxyls into derivatives which force the chains apart and decrease the interchain attraction. This results in the formation of substituted celluloses which are soluble, fusible, or both; and that are thus much easier to process although they no longer possess many of the desirable properties of cellulose.

Cellulose derivatization is not a simple matter. The interchain hydrogen bonding in the crystalline regions is often strong enough to greatly inhibit the reagent's access to the hydroxyl groups. Thus, unless care is taken, only the hydroxyls of the cellulose amorphous regions are completely

derivatized, while those in the crystalline regions remain unreacted. Such block copolymers rarely have the melt or solution properties required for ready processing.

Most of the applications of cellulosic materials are in the form of cotton, paper and wood. To increase the range of properties and usefulness of cellulosic fibers, products have been made that are (1) blends of cellulosic fibers and fibers derived principally from petroleum; (2) composites of cellulosic fibers; (3) chemically modified cellulosic fibers; and (4) macromolecularly modified cellulosic fibers such as cellulose graft copolymers.

The first steps toward the synthesis of thermoplastic elastomers containing cellulose were taken by Steinmann [5] who synthesized segmented multiblock copolymers with elastomeric properties by coupling hydroxyl terminated cellulose triacetate with diisocyanates. The cellulose triacetate (CTA) blocks were prepared by depolymerizing a fully substituted cellulose triacetate either by solubilizing it in acetic acid containing small amounts of water and acid catalysts, or in ethylene chloride in the presence of dioxolane and boron trifluoride-etherate as catalyst. The polyester blocks containing hydroxyl end groups were condensation products of adipic acid and diethylene glycol. The segmented multiblock copolymers were prepared by first reacting the polyester blocks with methylene di(p-phenylene) diisocyanate (MDI) to chain extend and chain terminate with isocyanate groups. Then the isocyanate capped polyester was reacted with the CTA blocks in methylene chloride solution using triethylamine as catalyst. Films cast from the reaction mixture were crystal clear and elastic. Fibers spun from the reaction mixture were bright and elastomeric.

Kim and co-workers [6] have also synthesized polyurethane block copolymers of cellulose triacetate and, by removal of the hydroxyl-blocking acetyl groups, prepared a polyurethane block copolymer having cellulose oligomer segments. This approach led them to the preparation of biodegradable polymers.

Block copolymers of cellobiose, diisocyanate and polyester having hydroxyl end groups have been reported by Pohjola and co-workers [7,8]. Films produced were clear, elastic and had good tensile

strength and elongation [7]. The results showed that elongation increases as the molecular weight of the polyester increases. They also prepared polyurethane block copolymers from diisocyanate, hydroxyl terminated poly(diethyleneglycoladipate) and low molecular weight cellulose triacetate segments [8]. The polyurethane block copolymer was synthesized by a prepolymer route, and low molecular weight CTA segments were coupled with the isocyanate polyester prepolymer.

The properties of polyurethane block copolymers could be modified by varying the size of the soft polyester block and the molecular weight of the stiff CTA segment, or by varying the molar ratio of the components, which influence both the molecular weight of the block copolymer and the probability of crosslinking. They reported that the tensile strength of the CTA-based polyurethane block copolymers prepared by Steinmann [5] was somewhat higher than the tensile strength of polymers prepared by Pohjola and Eklund [8], but the elongation remained quite high, from 600% to 1,100%.

The common characteristics of these films were the relatively poor mechanical properties caused by insufficient length of the hard blocks, which resulted in poor phase segregation [9]. In order to improve the mechanical properties of cellulose containing block copolymers, Feger and Cantow [9] developed a method to synthesize block copolymers with block molecular weights of more than 10,000 g/mol. The new approach involved first forming a cellulose block with a reactive end-group that was used to initiate the polymerization of a second block. Both chain-growth condensation and chain-growth addition polymerization have been used for the preparation of the second block. They described a synthetic route to trimethylcellulose-poly(oxytetramethylene) block copolymers via acidolytic cleavage of high molecular trimethyl cellulose (TMC) with water-free hydrogen chloride (Figure 42) and treatment of the resulting chlorine terminated TMC prepolymers with silverhexafluoroantimonate (AgSbF_6) in THF. Monofunctional termination of the initiated living THF block polymerization leads to TMC-poly(oxytetramethylene)(POTM) two block copolymers as shown in Figure 43.

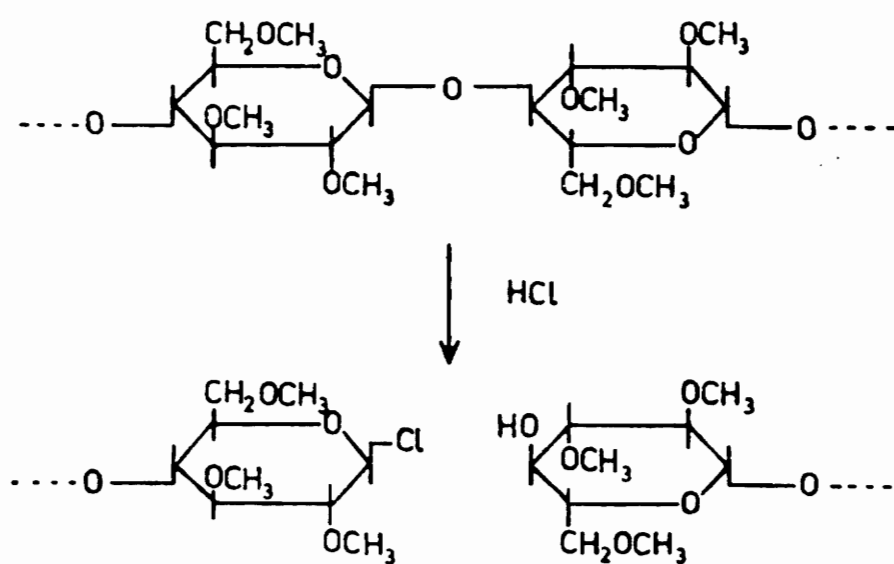


Figure 42. Cleavage of trimethyl cellulose with hydrogen chloride [9]

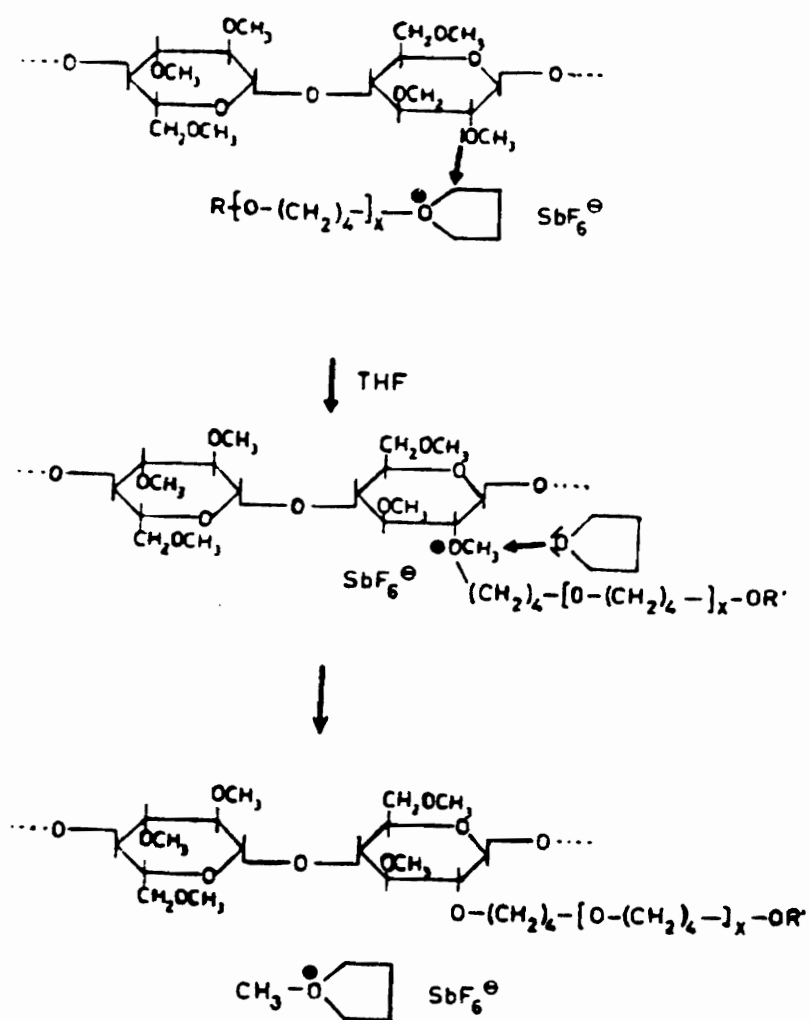


Figure 43. Scheme of TMC (g-POTM) graft copolymerization [9].

Low molecular weight poly(4-vinylpyridine) as terminating agent yielded star-shaped block copolymers, where POTM formed the center blocks as illustrated in Figure 44.

In order to synthesize mono-hydroxyl cellulose ester blocks of higher molecular weight, Mezger and Cantow [10,12] developed an alternative method of HBr cleavage, which is similar to those applied in mono- and oligosaccharide chemistry for the preparation of 1-bromo peracetyl sugars [11]. According to carbohydrate chemistry, disaccharides are called *reducing* or *nonreducing*, depending on whether one or both reducing groups are involved in the formation of the glycosidic linkage. Cellobiose and maltose obtained by partial hydrolysis of cellulose and starch, respectively, are reducing disaccharides, while sucrose, another important disaccharide, is an example of a nonreducing type molecule. Figure 45 illustrates the three disaccharides.

In the degradation of cellulose ester chains by hydrogen halide under esterification conditions, one end of the oligomer chain (the nonreducing end) will exhibit an ester group, while the other chain end (the reducing end) will have a halogen in the α -position at the reducing carbon. A schematic illustration of the cleavage reaction is shown in Figure 46.

The objective of this study was to explore Mezger and Cantow's hydrolysis technique for the synthesis of mono-hydroxyl terminated cellulose propionate oligomers with different molecular weights. The method consisted of the synthesis of a fully substituted, high molecular weight cellulose propionate molecule, followed then by partial hydrolysis of the polymer to produce cellulose propionate segments containing only one OH group per chain end.

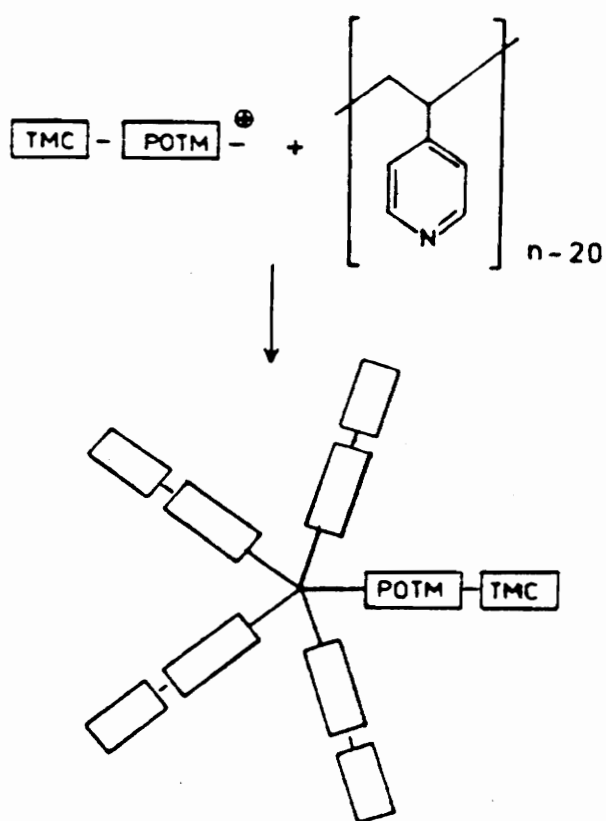


Figure 44. POTM-TMC star blocks coupled by poly(4-vinylpyridine) [9].

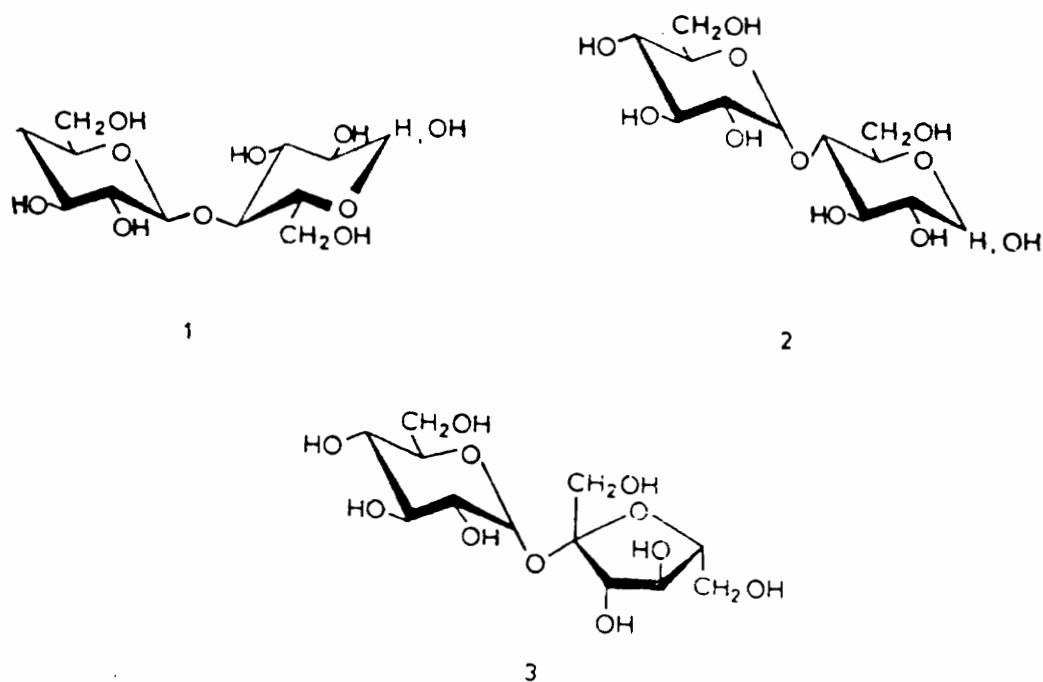


Figure 45. Examples of reducing (1,2) and nonreducing (3) sugars: (1) cellobiose; (2) maltose, and (3) sucrose

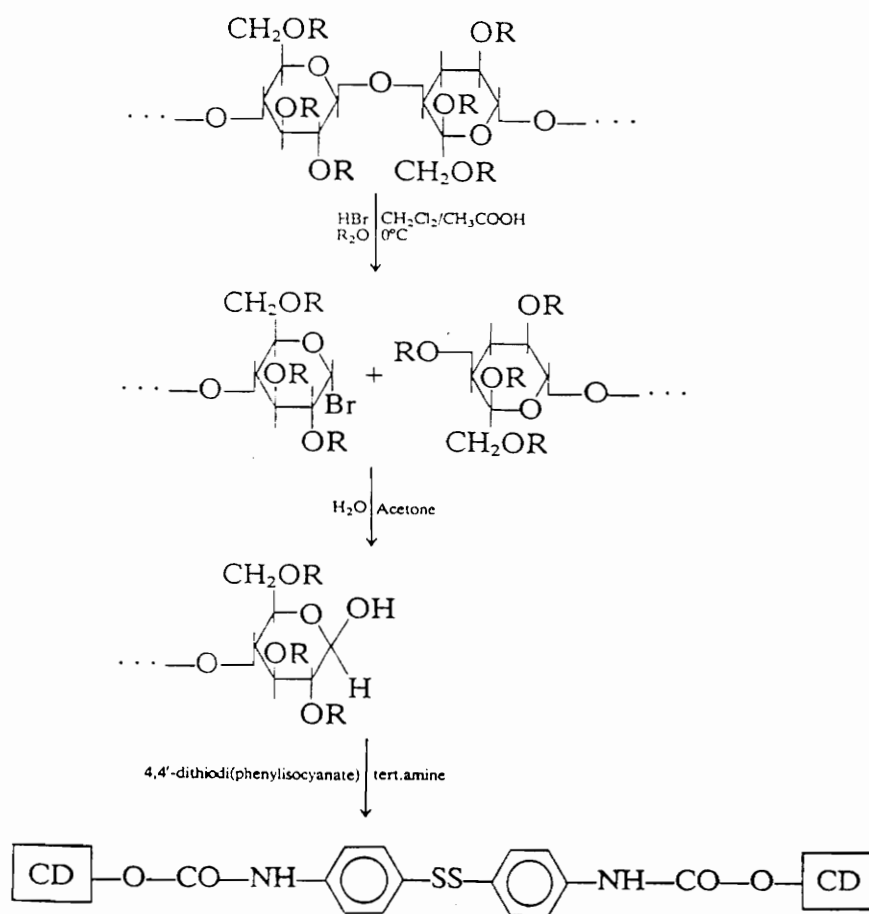


Figure 46. Synthesis route for the preparation of 1-mono-hydroxyl cellulose triesters [12]: R = acyl (propionyl, acetyl or butyryl) group.

5.2 EXPERIMENTAL SECTION

5.2.1 Materials

Cellulose Propionate: Cellulose propionate (CP) was purchased from Aldrich Chemical Company and used without further purification.

Hydrogen Bromide: Hydrogen bromide (33% solution in acetic acid) was obtained from Aldrich Chemical Company and used as received.

Propionic Anhydride: Propionic anhydride was obtained from Aldrich Chemical Company.

Solvents: Solvents, such as dichloromethane and chloroform, were supplied by Fischer Scientific Chemical as commercial grade.

5.2.2 Depolymerization of Cellulose Propionate

Typically in a 500 mL two-necked flask fitted with a mechanical stirrer and a dropping funnel, 10 g of CP ($M_n = 120,000$) were dissolved in 100 mL dichloromethane and cooled to 0°C. Propionic anhydride (20 mL) and 50 mL hydrogen bromide, 33% solution in acetic acid, were added to the solution and allowed to react for a specific time (usually from 6 to 24 hrs.), based on a target desired molecular weight of the oligomer. The purpose of adding anhydride was to prevent hydroxyl group formation during the isolation procedure. The hydrolysis reaction was quenched by adding the mixture to a vigorously stirred solution of sodium hydrogen carbonate in ice water. The organic

layer was extracted with chloroform, and washed several times with water in a separatory funnel. The product was then evaporated and dried under vacuum.

5.2.3 Hydrolysis of Bromine End Group

A common procedure to hydrolyze bromine end groups consists of preparing a 1% solution of brominated cellulose propionate in acetone and heating the solution to 40°C under agitation [10]. Water is then added till the solution becomes cloudy. At this point, more acetone is added, or the temperature is raised again to 40°C to redissolve the precipitate. After that, the solution is cooled slowly to room temperature, and the precipitate filtered, washed and freeze-dried.

5.2.4 Determination of Functionality

The number-average functionality, (F_n), was obtained from the molar concentration of OH groups, c_{OH} , and the number-average molecular weight of the oligomer M_n ,

$$F_n = c_{OH} \cdot M_n$$

where c_{OH} is equal to the number of moles of the oligomer per unit weight.

5.2.5 Characterization

Gel Permeation Chromatography (GPC): Gel permeation chromatography was used to measure the molecular weights and molecular weight distribution of the oligomers, according to the procedure described in chapter 3.

Proton-Nuclear Magnetic Resonance Spectroscopy (H-NMR): H-NMR analysis was used to determine the degree of substitution in commercial cellulose propionate and the number-average functionality of the oligomer based on the procedure described in chapter 3.

Fourier Transform Infrared Spectroscopy (FTIR): FTIR was used to observe qualitatively the degree of substitution in commercial cellulose propionate. The absorbance at 1700 cm^{-1} was studied to evaluate the presence of a carbonyl group.

Differential Scanning Calorimetry (DSC): DSC thermograms were obtained using a Perkin-Elmer Model DSC-4. The temperature was scanned from -60 to 300°C at a heating rate of 10°C per minute. The scanning procedure consisted of two steps. In the first run, the samples were cooled to -60°C and heated at $10^{\circ}\text{C}/\text{min}$ to 300°C . In the second run, the samples were quenched to -60°C at $200^{\circ}\text{C}/\text{min}$ and reheated at $10^{\circ}\text{C}/\text{min}$ to 300°C . Glass transition temperatures were taken as midpoint of the change in slope of the baseline. The T_m was taken as the temperature corresponding to endothermic peak location.

5.3 RESULTS AND DISCUSSIONS

5.3.1 Depolymerization of Cellulose Propionate

The commercial cellulose propionate used in this study had an incomplete degree of substitution (less than three propionate groups per anhydroglucose unit) as detected by FTIR. The ratio of the carbonyl absorption peak at 1700 cm^{-1} over the OH band at around 3460 cm^{-1} was too high. Therefore, a propionation reaction on the remaining OH groups was performed. FTIR results before and after re-propionation are presented in Figure 47.

The degree of substitution was determined by H-NMR. Figure 48 illustrates the peak assignment for a cellulose propionate molecule. The degree of substitution is calculated by ratioing the integration of the H_3 peak (at 5.1 ppm) over the methyl protons (1.4 - 0.9 ppm). On average, a commercial cellulose propionate has approximately 2.8 propionyl groups per anhydroglucose unit. The same procedure was applied to samples after re-propionation. The results indicate a degree of substitution of 3.1 which suggests complete substitution of OH groups.

The method used to depolymerize cellulose propionate was based on a partial degradation of the cellulose propionate chains with hydrogen bromide, under esterification conditions, according to Mezger and Cantow [10]. By controlling the hydrolysis time, a fully esterified cellulose segment of sensible chain length with a bromine at the reducing chain end was obtained. Table 12 presents the molecular characteristics of the depolymerization reaction products as a function of hydrolysis time. The measurements of DP indicate that after treatment of CP with HBr, significant degradation of the CP macromolecule took place. This is best illustrated by the data of Figure 49. Under the particular reaction conditions, after 15 hours of hydrolysis time, a minimum DP of ca. 5-10 was reached.

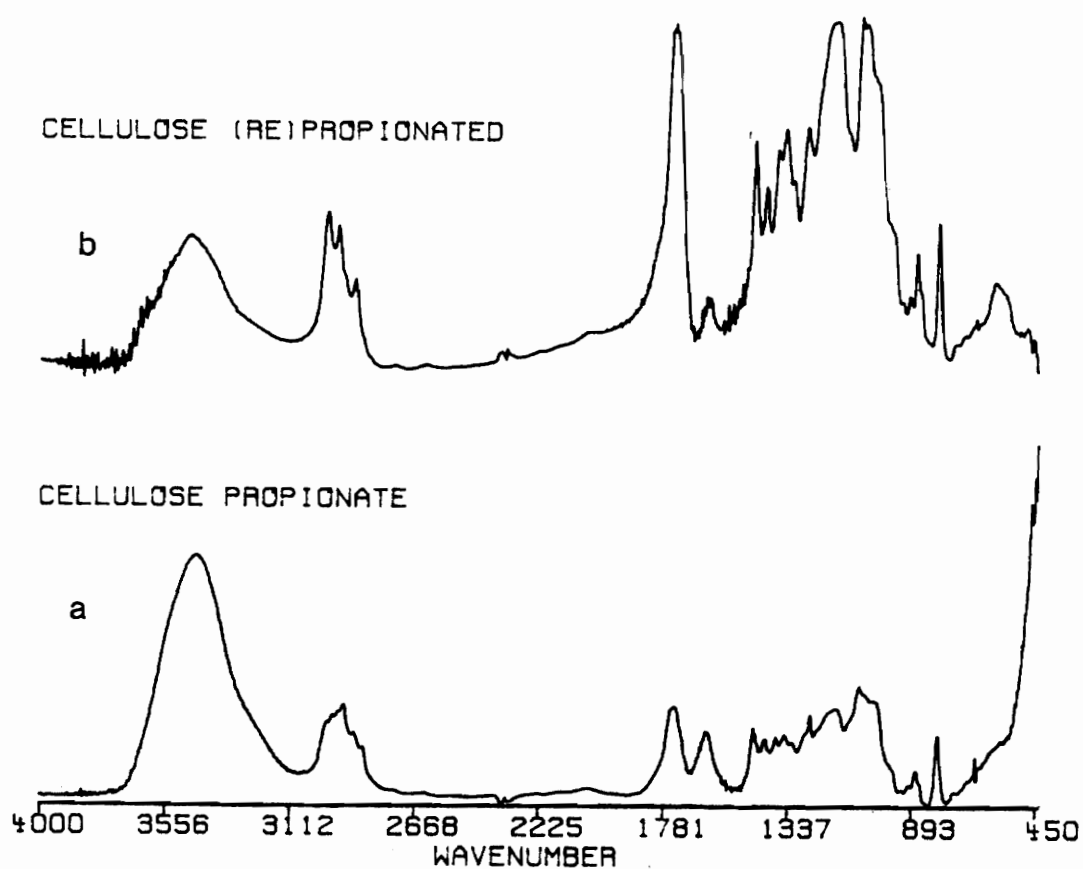


Figure 47. FTIR of cellulose propionate: (a) before, (b) after propionation

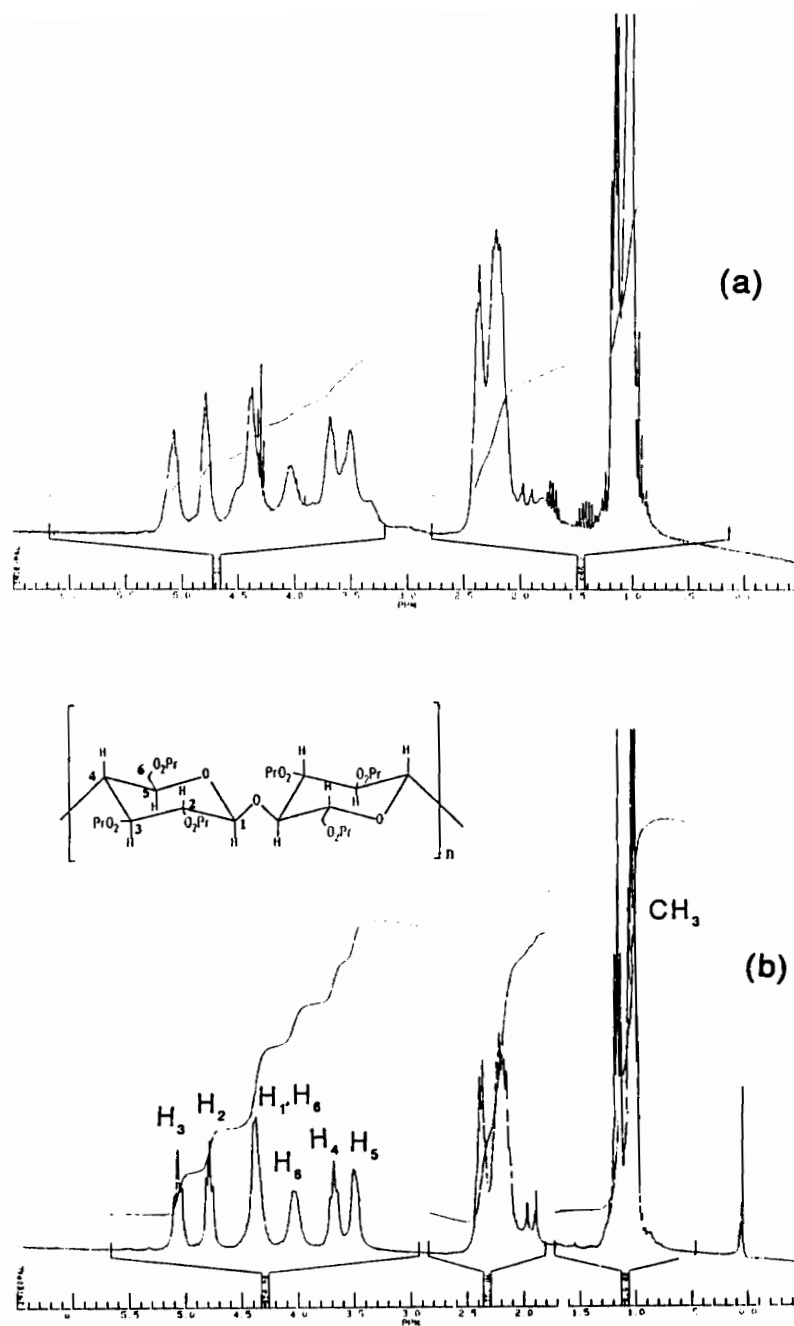


Figure 48. Typical ^1H -NMR spectra of cellulose propionate: (a) before, (b) after propionation

Table 12. Molecular Characterization Data of Cellulose Propionate Oligomers as a Function of Hydrolysis Time

Sample	Hydrolysis time (h)	M_n	DP_n	M_w/M_n	a^*	IV (dl/g)
E1	0.0	115,700	351	1.6	0.803	1.802
E2	0.5	68,400	207	1.6	0.928	1.121
E3	1.0	57,600	175	1.7	0.938	0.781
E4	2.0	29,800	90	1.8	0.924	0.495
E5	3.0	30,900	94	1.6	0.946	0.377
E6	4.0	16,100	49	1.8	0.890	0.312
E7	5.0	15,900	48	1.9	0.877	0.243
E8	6.0	11,200	34	1.6	0.872	0.212
E9	7.0	8,500	26	1.7	0.846	0.179
E10	11.0	6,400	19	1.4	0.829	0.100
E11	23.0	2,300	7	1.2	0.614	0.042
E12	28.0	3,300	10	1.3	0.470	0.028

* Mark-Houwink-Sakurada constant

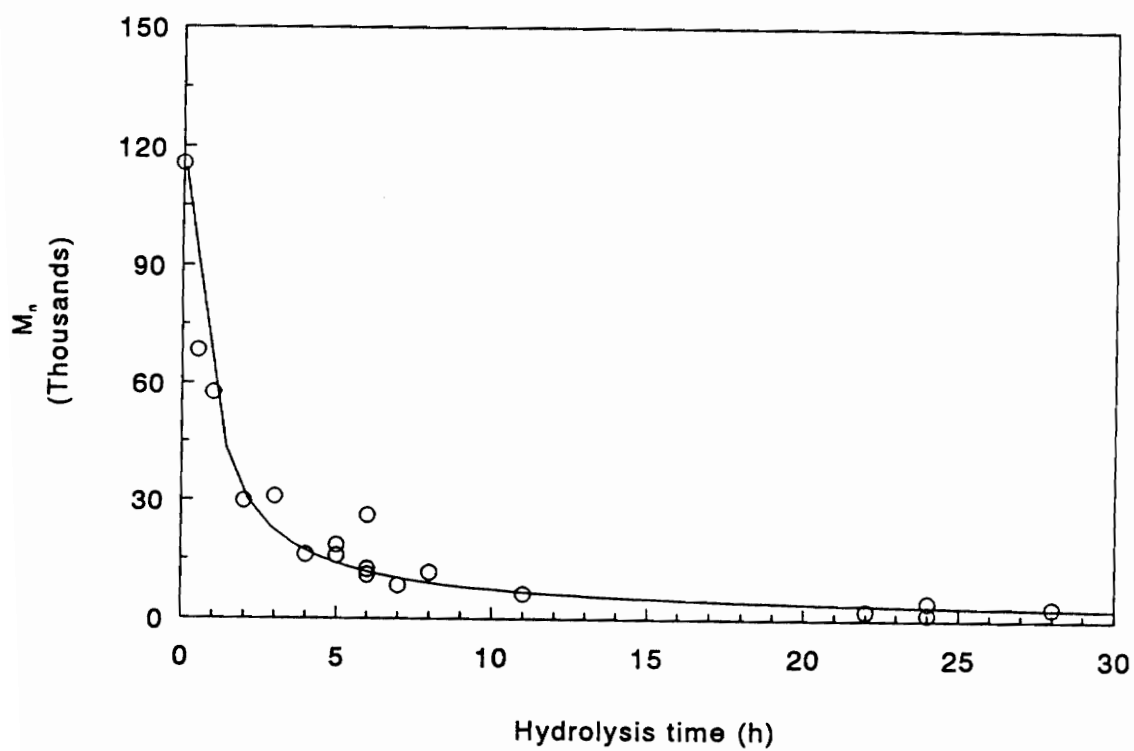


Figure 49. Degree of polymerization vs. hydrolysis time.

For all samples, the molecular weight distribution was consistently below 2.0, which is an indication of the homogeneity of the hydrolysis. Figure 50 compares the molecular weight distribution of the starting material with that of the oligomer after 23 hours of hydrolysis. The oligomer has a narrower polydispersity as compared to the starting material.

5.3.2 Determination of Hydroxyl Groups and of Number-Average Functionality of CP Oligomers.

The concentration of hydroxyl groups (determined by H-NMR), combined with the molecular weights, were used to calculate the number-average functionality of the cellulose propionate oligomers.

H-NMR allows the indirect determination of OH groups because of the proportionality between recorded signals and the number of corresponding protons in the sample. In the case of cellulose propionate with a bromine at the reducing chain end, H-NMR is appropriate for calculating the bromine concentration in the sample. In low molecular weight CP, the proton neighboring the bromine atom gives a very strong signal downfield, at 5.5 and 6.5 ppm for β and α substitution, respectively. These signals are far apart and distinguished from the multitude of proton signals from methyl, methylene and glucopyranose groups. Therefore, they can easily be integrated and used for the measurement of bromine concentration.

Figure 51 represents a typical H-NMR spectrum of a cellulose propionate bromoglucoside of low molecular weight ($M_n = 2,300$) obtained on a 400 MHz instrument. The presence of Br at the chain end generates the resonances between 5.6 and 6.5 ppm. These signals, along with the integration of total methyl and methylene protons, were used for the calculation of the molar concentration of bromine groups.

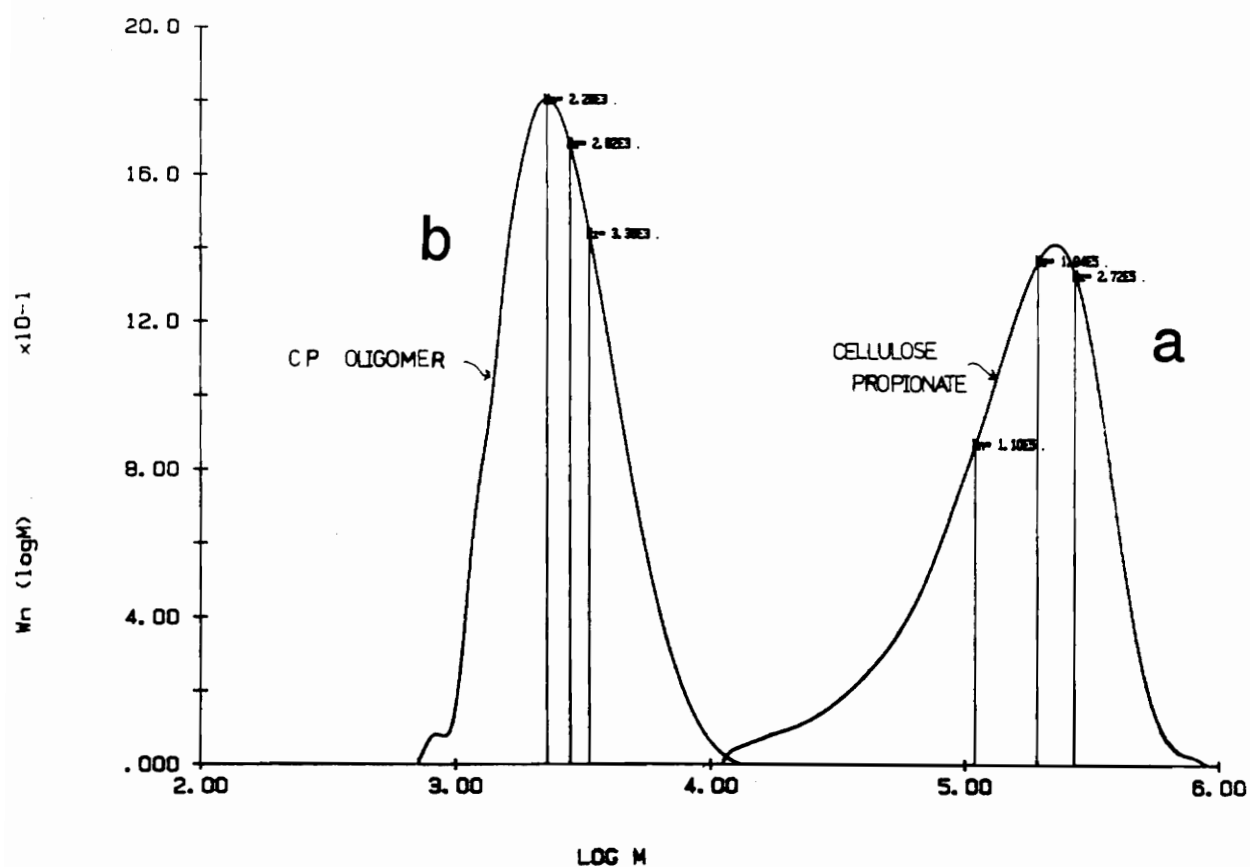


Figure 50. Molecular weight distribution of CP: (a) before hydrolysis and (b) after hydrolysis

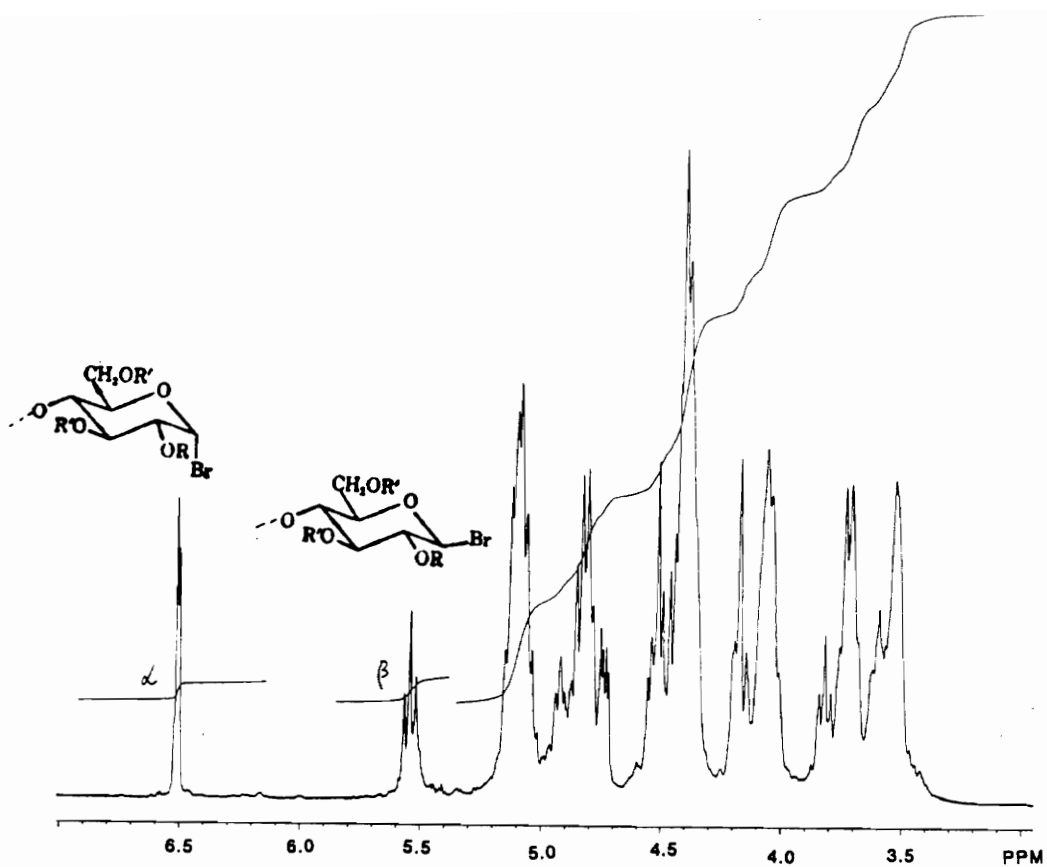


Figure 51. Typical H-NMR-spectrum of low-molecular weight CP bromoglucoside

As the molecular weight of CP segments increases, the signals at 5.6-6.5 ppm decrease in intensity, and it becomes more difficult to use them for quantitative information. In this case, the bromine content is better calculated by elemental analysis, which, combined with GPC, gives an estimation of the molar concentration of Br groups per segment.

The concentration of OH groups was also estimated by H-NMR spectroscopy, after the hydrolysis of bromine end groups. Since the proton signal of hydroxyl groups is usually too weak for direct measurements, the OH groups were derivatized in order to enhance their detectability. By reacting CP with triethylsilyl chloride, each proton from the hydroxyl group is replaced by 15 protons that are easily identified by H-NMR. Figure 52 shows the H-NMR spectrum of a mono-hydroxyl terminated CP (a) before and (b) after incorporation of a triethylsilyl group. By integrating the easily quantified signals at 0.55 ppm, the concentration of OH groups in CP segments could be calculated. Then, by taking these concentration values, and by multiplying them with the number-average molecular weight of the respective sample, the number-average functionality of the oligomers could be determined. In general, the average functionality was about 0.95 OH groups per chain.

From Table 12 it is also apparent that the intrinsic viscosity varies dramatically with hydrolysis time. After treatment of the cellulose propionate with hydrogen bromide, the intrinsic viscosity decreased 64 times compared with the untreated sample (Figure 53). On the other hand, the Mark-Houwink-Sakurada constant does not change much with the size of the oligomer. It stays reasonably constant, between 0.8 and 0.9 (typical of rod-like molecules) for most of the samples. Its value declines to almost half when the DP approaches 10 (Figure 54).

5.3.3 Thermal Properties

Table 13 summarizes the thermal data of the cellulose propionate oligomers synthesized in this study. These data include the results of a first heating mode in samples that have been annealed for

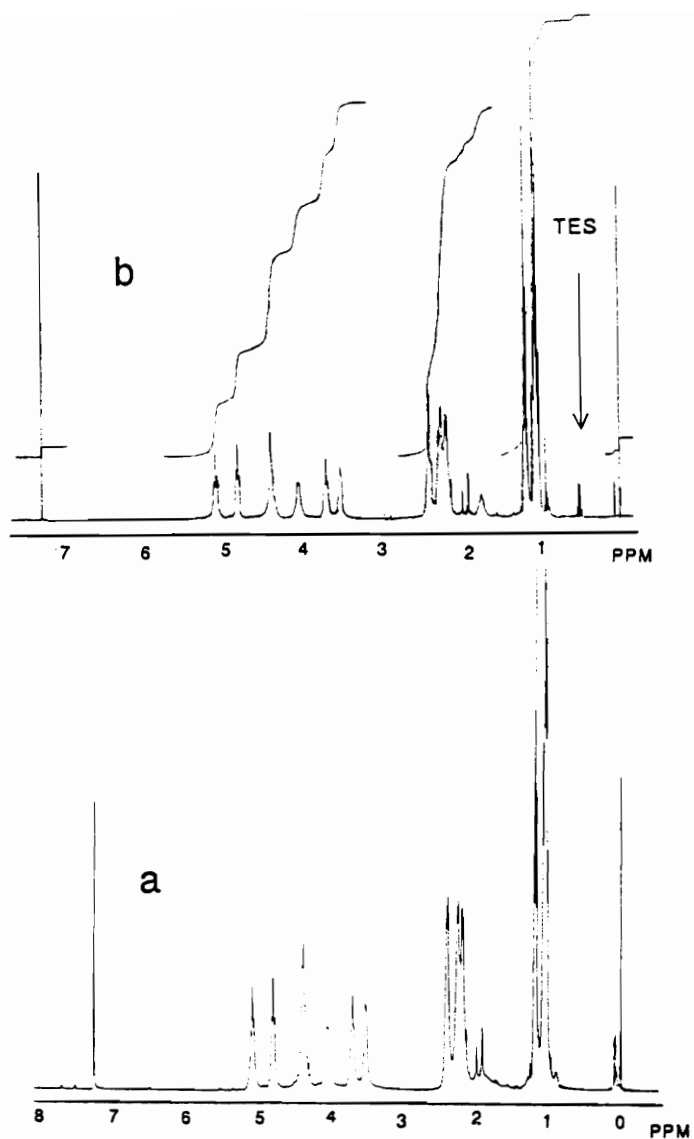


Figure 52. Proton-NMR-spectrum of cellulose propionate: (a) mono-hydroxyl terminated, and (b) triethylsilyl terminated. Note: Triethylsilyl substituent at 0.55 ppm represents hydroxyl groups in CP oligomers.

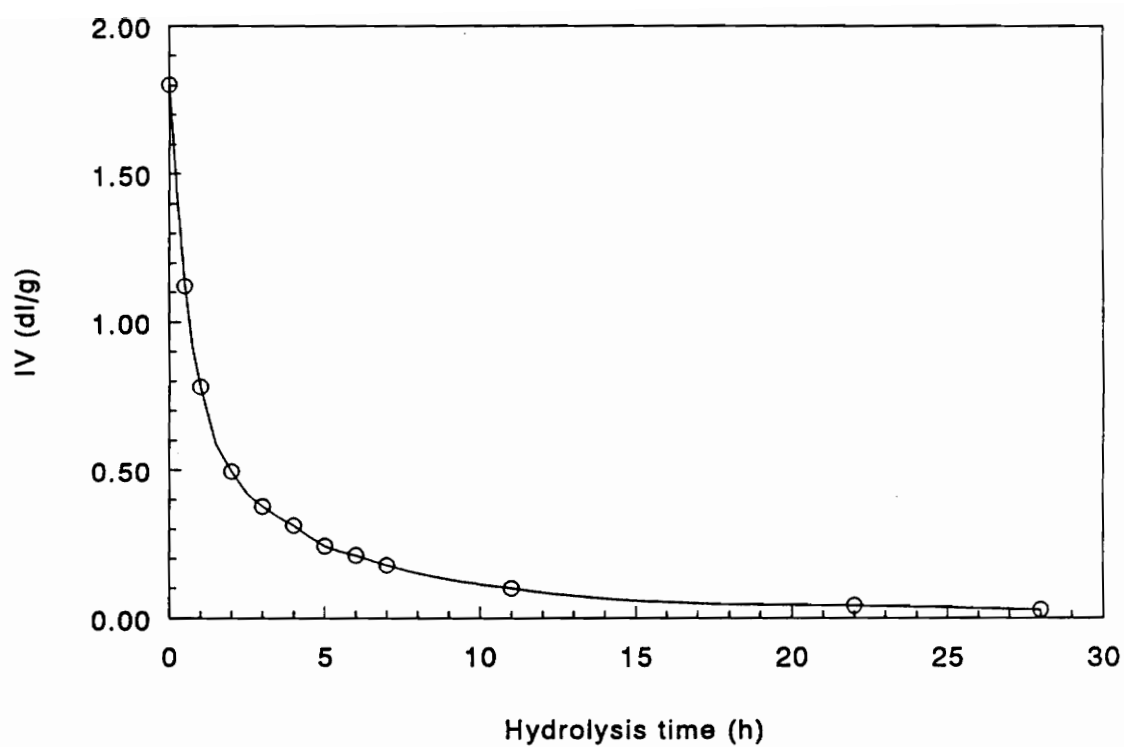


Figure 53. Intrinsic viscosity of CP segments vs. hydrolysis time

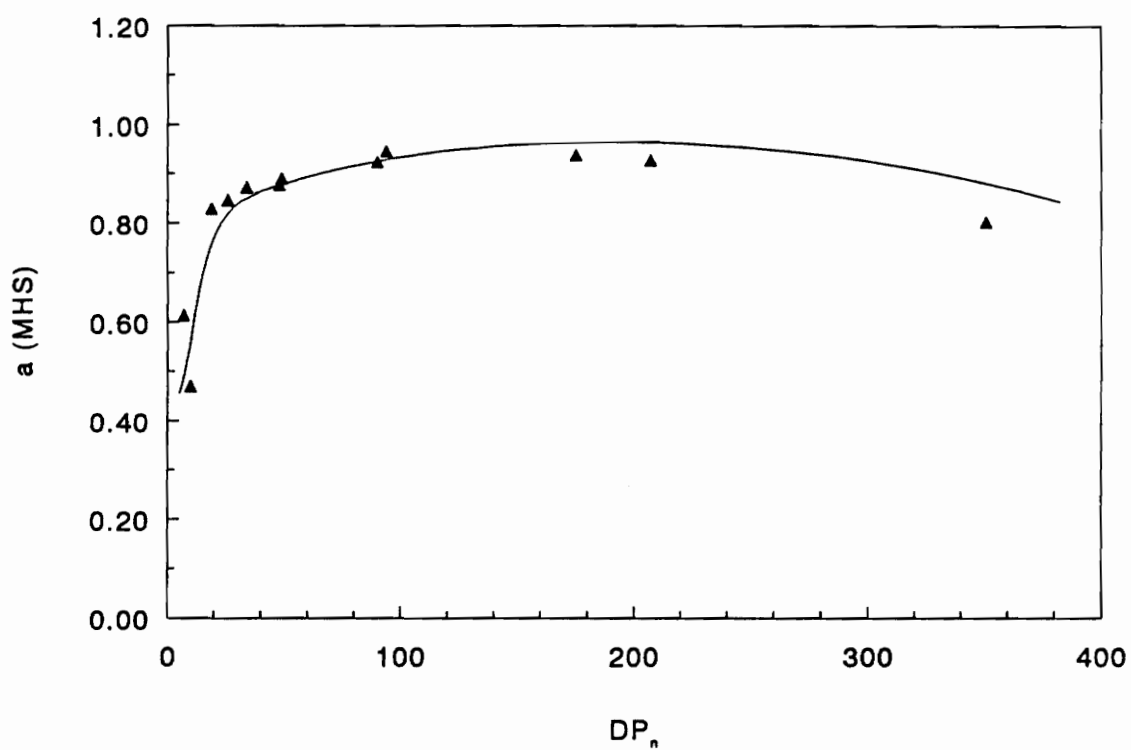


Figure 54. MHS constant vs. degree of polymerization

Table 13. Thermal Data of CP Oligomers

Sample	M_n	DP_n	ΔH_f (J/g)	T_m (°C)
E1	115,700	351	40	233
E2	68,400	207	55	242
E3	57,600	175	52	241
E5	30,900	94	49	232
E6	16,100	49	66	232
E7	15,900	48	63	232
E8	11,200	34	79	222
E9	8,500	26	34	217
E10	7,200	22	34	205
E11	6,400	19	34	186
E12	2,300	7	-	-
E13	3,300	10	-	-

several weeks at room temperature. A typical DSC thermogram of cellulose propionate (DS = 3.0) obtained in a second heating mode quenched from the melt is presented in Figure 55. Three major transitions are evident: a first order endothermic transition (A) at about 235°C, which corresponds to the fusion of crystalline domains of cellulose propionate; an exothermic peak (B) at about 160°C is due to crystallization of CP chains; and a second order transition (C) at 130°C corresponds to the glass transition of the amorphous phase.

The melting point is clearly a function of molecular weight, as seen in a series of DSC thermograms in Figure 56. T_m varies from 242 to 186°C, the latter for cellulose propionate with DP 20. No endotherms were observed at DP below 20.

Figure 57 presents the plot of the melting point versus molecular weight of CP segments. The curve asymptotically approaches a constant temperature level of about 240°C for cellulose propionate with DP greater than 100. The data show that as the number-average molecular weight of CP oligomers increases, the major melt endotherm peak shifts to increasingly higher temperatures.

The degree of crystallinity of the oligomers could not be calculated by DSC measurements due to the unavailability of data in the literature concerning the specific heat of fusion of fully crystalline cellulose propionate polymer. However, by observing the heat of fusion, it is possible to gain a semi-quantitative estimate of the crystallinity variation with molecular weight of the segments. Figure 58 shows the relationship between heat of fusion and molecular weight of the oligomers. The highest heat of fusion is observed in samples with DP between 30-50, which is an indication that the highest degree of crystallinity is achieved in samples with DP within that range.

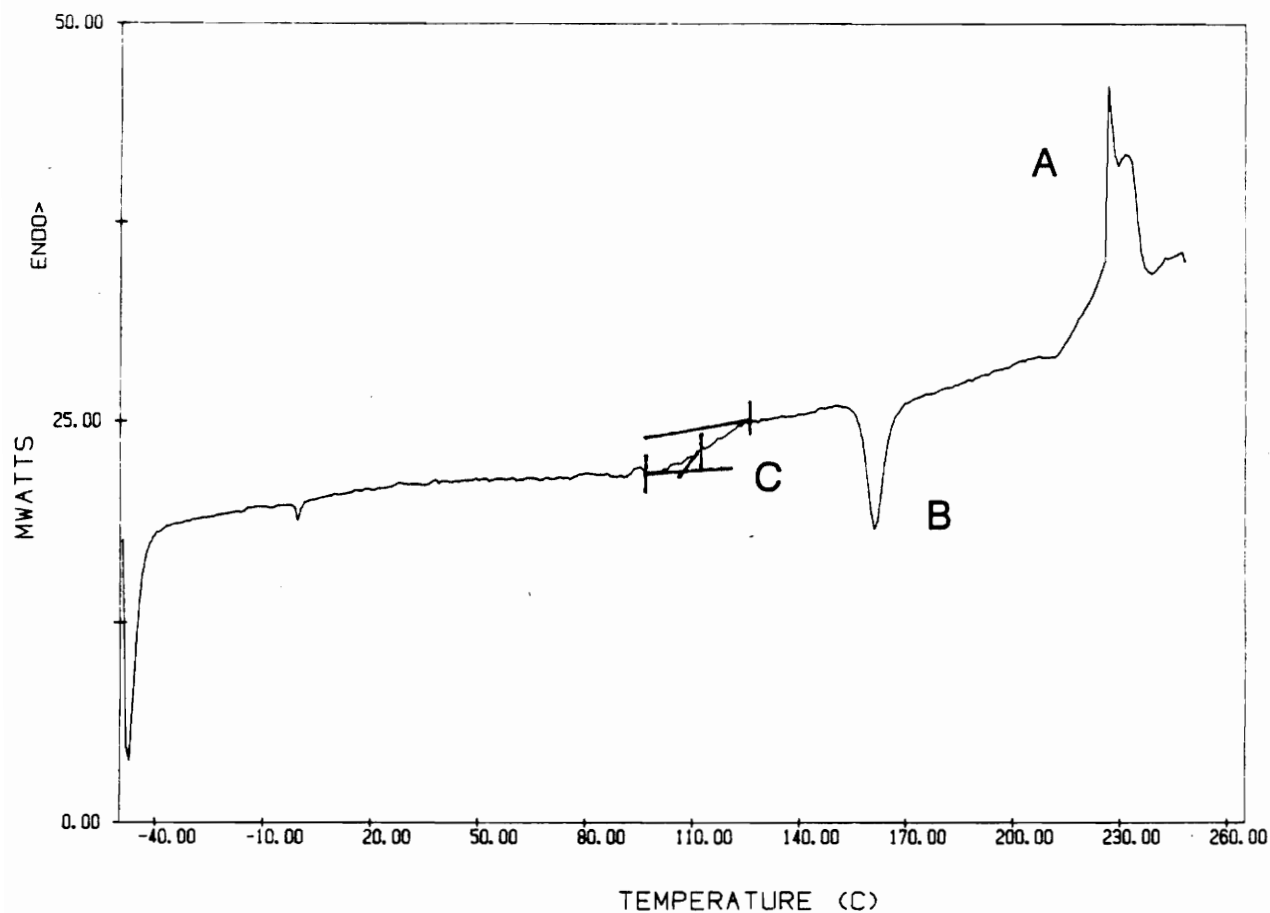


Figure 55. Typical DSC thermogram of cellulose propionate

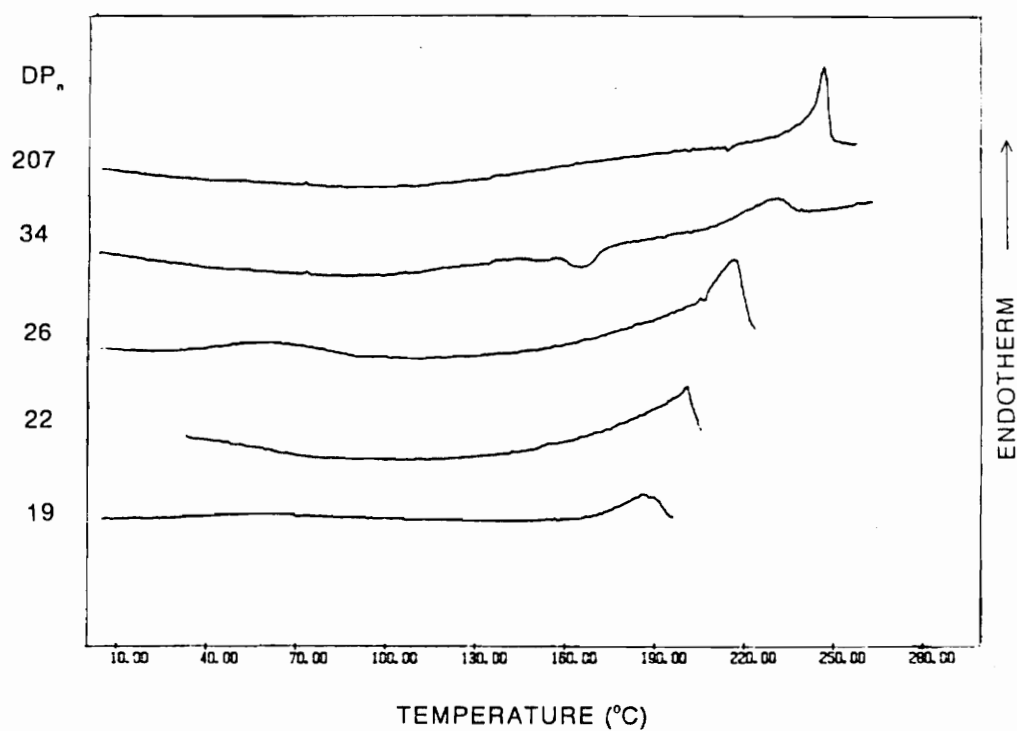


Figure 56. DSC thermograms of a series of cellulose propionate segments

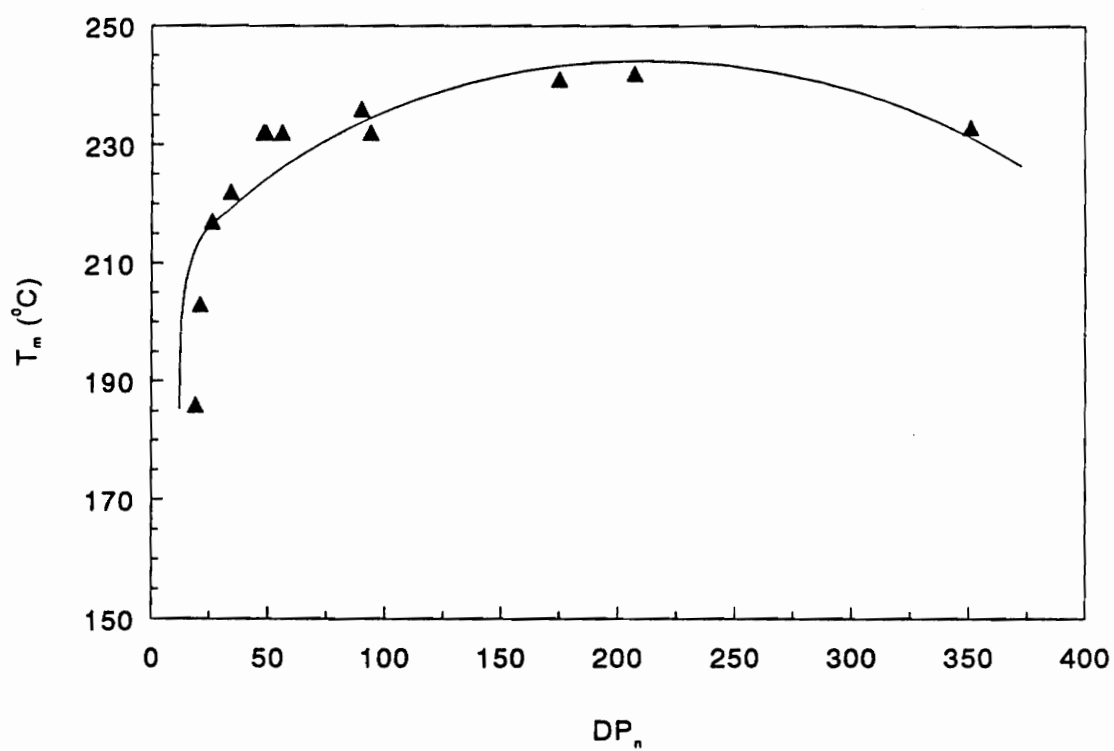


Figure 57. Melting point vs. molecular weight

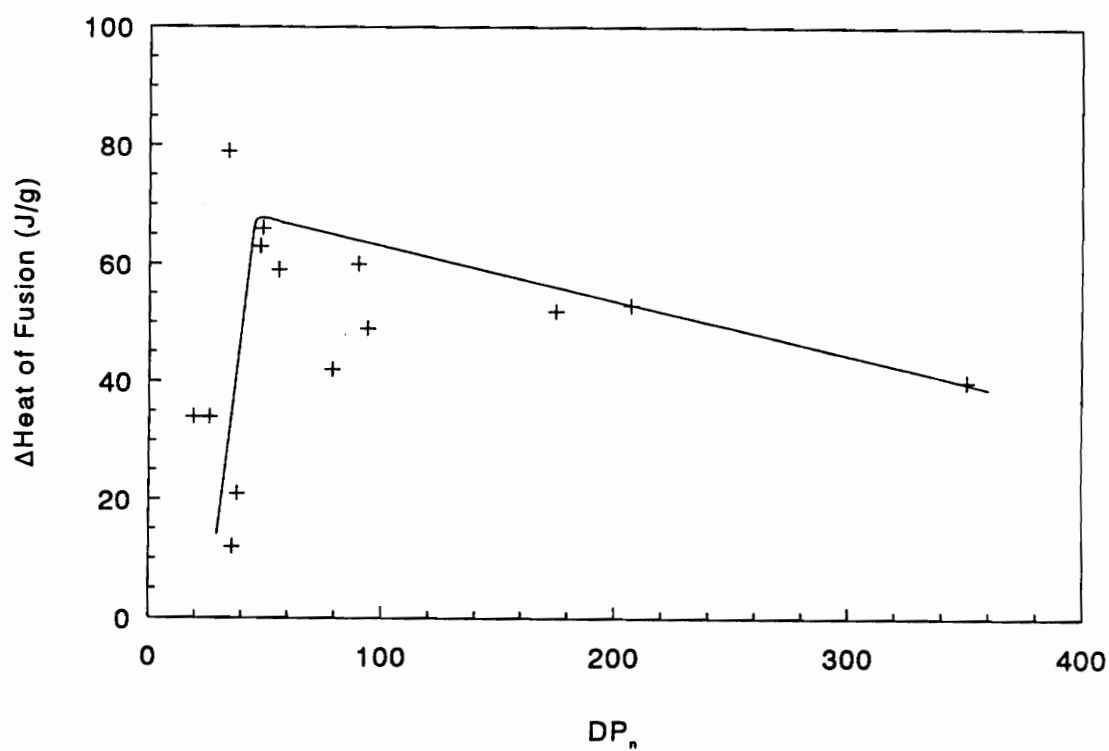


Figure 58. Relationship between heat of fusion and molecular weight

5.4 CONCLUSIONS

Mono-hydroxyl terminated cellulose propionate oligomers can be produced by degradation with hydrogen bromide of a fully substituted, high molecular weight cellulose propionate molecule.

By controlling hydrolysis time, cellulose propionate segments with a target molecular weight and narrow polydispersity can be synthesized.

The number-average functionality of the oligomers can be determined by H-NMR spectroscopy and GPC analysis.

Thermal analysis results indicate that the oligomers are semi-crystalline, and their melting points are a function of molecular weight. No crystallinity could be detected by DSC in oligomers with DP below 20. The highest degree of crystallinity, based on heat of fusion, was observed in segments having DP values between 30 and 50.

5.5 REFERENCES

1. J. R. Colvin, "Cellulose, Biosynthesis", in *Enc. Polym. Sci. Eng.*, vol. 3, 1987, p.60
2. J. C. Arthur, Jr., "Free-Radical Initiated Graft Polymerization of Vinyl Monomers onto Cellulose", D. N. -S. Hon, Ed., *Graft Copolymerization of Lignocellulosic Fibers*, ACS Symposium Series 187, 20 (1982)
3. E. Sjostrom, "**Wood Chemistry: Fundamentals and Applications**", Academic Press, New York, 1981
4. I. S. Goldstein, "Cellulose: Nature and Applications", in *Mat. Sci. and Eng.*, vol. 1, 563(1986)
5. H. W. Steinmann, *Polym. Prep. Am. Chem. Soc. Div. Polym. Chem.*, 11, 285(1970)
6. S. Kim, V. T. Stannett, and R. D. Gilbert, *J. Polym. Sci., Polym. Lett. Ed.*, 11, 731(1973)
7. L. Pohjola, O. Harva, and J. Karvinen, *Finn. Chem. Lett.*, 6, 221(1974)
8. L. Pohjola and V. Eklund, *Paperi ja Puu*, No. 3, 117(1977)
9. C. Feger and H. -J. Cantow, *Polymer Bulletin*, 3, 407(1980)
10. T. Mezger and H. -J. Cantow, *Die Angewandte Makromolekulare Chemie*, 116, 17(1983)
11. M. Barcai-Martos, F. Korosy, *Nature*, 165, 369 (1950)
12. T. Mezger and H. -J. Cantow, *Polymer Photochemistry*, 5, 49(1984)

6.0 SYNTHESIS AND CHARACTERIZATION OF CELLULOSE PROPIONATE - HYDROXYPROPYL LIGNIN COPOLYMERS

6.1 INTRODUCTION

The synthesis of multiphase block copolymers which exhibit rubber elasticity and thermoplastic processability has been the subject of extensive research. Most of this research, however, has focused on synthetic polymers. Cellulose and cellulose derivatives have long been recognized as excellent fiber formers, with outstanding properties sometimes far superior to synthetic polymers. However, only a few successful approaches have been reported on the synthesis of cellulose-containing block copolymers [1,2].

The first attempts to produce block copolymers containing cellulose used the technique of mastication of high molecular weight cellulose esters in the presence of vinyl monomers [1]. The method was based on the fact that polymers in a viscoelastic state, when subjected to mechanical

work, such as mastication, extrusion or milling, undergo main-chain scission to form polymeric free radicals. When mastication is carried out in the presence of a polymerizable monomer, the primary reaction of the polymeric free radical is the initiation of block copolymerization [1]. Methyl cellulose-acrylonitrile copolymers were produced by the mastication of a high molecular weight methyl cellulose polymer in the presence of acrylonitrile monomer. The composition of the block copolymer fraction was 69.6% methyl cellulose and 30.4% polyacrylonitrile. The same procedure was applied to the synthesis of ethyl cellulose-methyl methacrylate and benzyl cellulose-styrene copolymers. The problem with this procedure, since the copolymerization is a statistical process, is the formation of graft and homopolymer mixed with the linear block copolymer.

A different approach to the synthesis of cellulose containing block copolymers was performed by Steinmann et al. [2]. They prepared elastomeric films and fibers using oligomeric cellulose triacetate (CTA) species having hydroxyl end groups. Difunctional CTA blocks were produced by depolymerization of a fully substituted cellulose triacetate, based on two different systems. One method consisted of hydrolyzing the CTA in acetic acid containing small percentages of water and an acid catalyst. Figure 59 shows the depolymerization scheme of the CTA molecule. The critical variables were temperature, catalyst, water and reaction time. However, hydrolysis of the acetate groups was the major problem, and that affected the yields of truly difunctional CTA blocks.

The second method investigated by Steinmann consisted of dissolving CTA in ethylene chloride and depolymerizing it in the presence of dioxolane and boron trifluoride-etherate catalyst. Both BF_3 or BF_3 -dioxolane complex were able to hydrolyze CTA chains. Several end groups could possibly result, such as hydroxyl, hydroxymethyl and hydroxyethyl groups. Figure 60 shows the depolymerization equation. The problems with this system were the diversity of equilibrium reactions that could exist. Therefore, the synthesis of perfect dihydroxy-terminated CTA blocks was highly unlikely. The perfect block would have a hydroxyl group on each end and acetate groups on positions 2, 3 and 6 of the anhydroglucose units. Nevertheless, the blocks produced by either method were reacted with low molecular weight polyesters or polyethers, capped with isocyanate

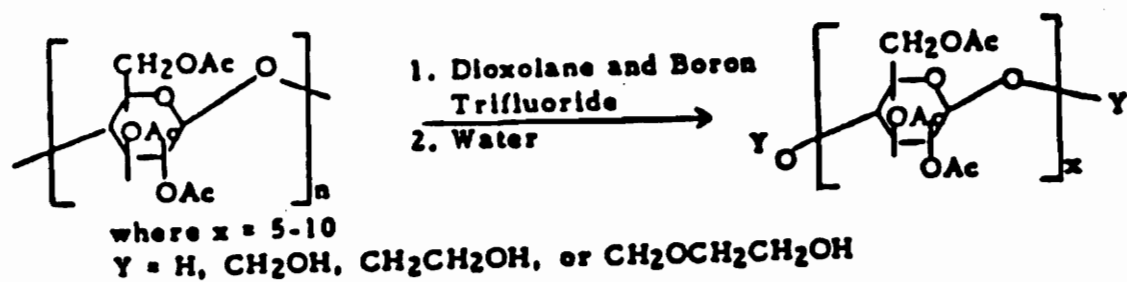


Figure 59. Depolymerization scheme of the CTA molecule [2]

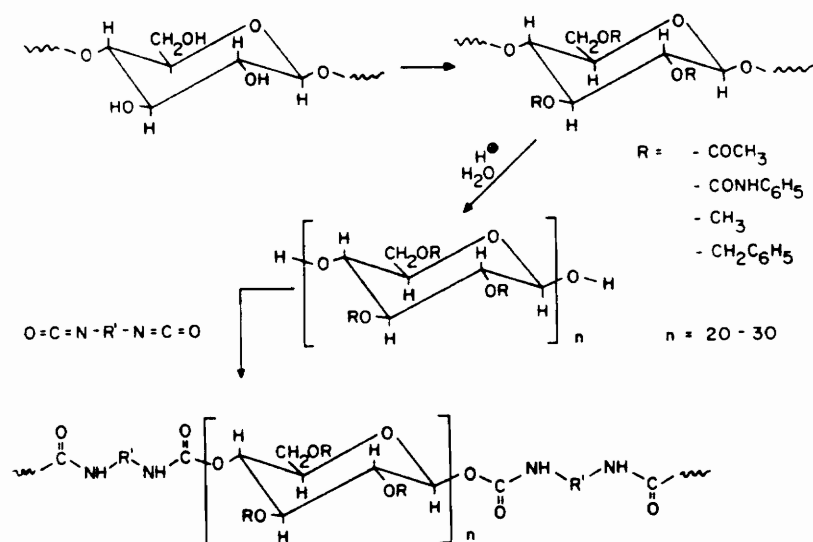


Figure 60. Depolymerization scheme for CTA chains [2]

groups, for the synthesis of segmented multiblock copolymers. Considerable chain branching and crosslinking could not be avoided.

Stannett and Gilbert [3-5] advanced the synthesis of difunctional CTA blocks for the purpose of producing a new class of biodegradable polymers. Their goals were to remove the hydroxyl-blocking acetyl groups on the cellulose triacetate blocks to give rise to another kind of block copolymer, with biodegradable properties. It is suggested that the introduction of "vulnerable units" in the polymer chain, such as a biodegradable polymer-like cellulose, would lead to the synthesis of biodegradable polymers. The synthetic approach for the preparation of block copolymers containing cellulose is outlined in Figure 61. The removal of the hydroxyl blocking groups produces a different block copolymer with properties probably depending upon the composition of the blocks. In order to restore the original OH groups on the cellulose molecule, hydrolysis of the acetyl groups was performed. The deacetylation was realized with sodium methoxide, and the copolymer was subjected to enzymatic hydrolysis in order to test its biodegradability. The results show that copolymers were biodegradable and degraded more rapidly than cellulose itself.

The problem facing all these syntheses is the formation of undesired side reactions that lead to grafting or crosslinking. Therefore, the synthesis of a monofunctional cellulose derivative was required. By using an old concept in carbohydrate chemistry [6], Feger and Cantow [7] realized that the acidolytic cleavage of a fully substituted cellulose derivative would produce monofunctionalized cellulose derivative oligomers, which could be used as prepolymers for the synthesis of block copolymers. Star-like block copolymers of trimethylcellulose-(b-poly(oxytetramethylene)) with the trimethylcellulose blocks being the arms of the star were produced, as described in chapter 5 of this dissertation.

Mezger and Cantow [8] tried an alternative synthesis route for the synthesis of block copolymers containing cellulose. Their approach involved radical polymerization of the soft block, and use of

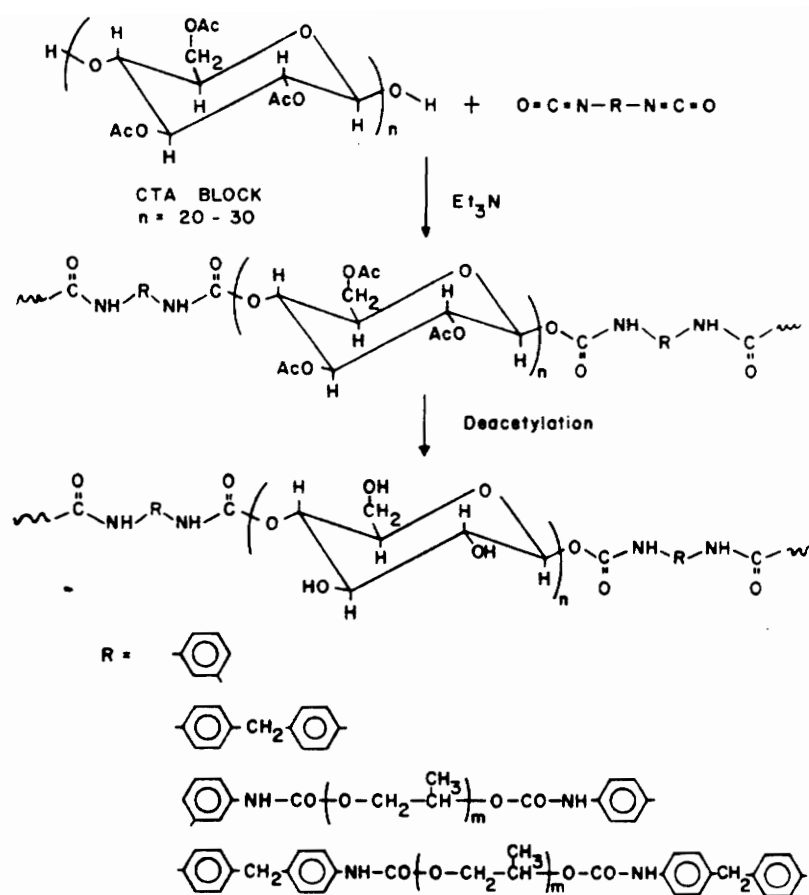


Figure 61. Deacetylation of CTA blocks [5]

the cellulose esters as hard block components. Instead of α -halogen terminated segments, they used mono-hydroxyl terminated cellulose derivatives, which were obtained through hydrolysis of the terminal halide function at mild conditions. The macromer was then coupled with 4,4'-dithiodi-(phenylisocyanate) and then used as a macrophotoinitiator for radical three block copolymer synthesis. Figure 62 shows the synthesis route for the preparation of cellulose triester macroinitiator. Polymerizations were performed at low temperatures by irradiating solutions of the macroinitiators in mixtures of the monomers styrene, chloroprene and methylacrylate. The products were of defined structure. They were obtained in high yield. The copolymers exhibited rubber-like elasticity in connection with thermoplastic processibility, because the central blocks had a low glass transition temperature.

In the preceeding chapter, preparation and properties of monofunctional cellulose propionate segments have been described. It has also been described that HPL can be synthesized with variable thermal properties, with either glassy or elastomeric behavior. Highly propoxylated HPL is a viscous polyol with interesting properties that can be used for synthesis of block copolymers with elastomeric characteristics. The purpose of this work was to synthesize multiphase star-like copolymers by the chemical combination of low molecular weight HPL of inherently rubbery properties with semi-crystalline CP. The main aim was to analyze the influence of CP segment size and HPL molecular weight on the solution, thermal and morphological behavior of $(CP)_n-HPL$ copolymers.

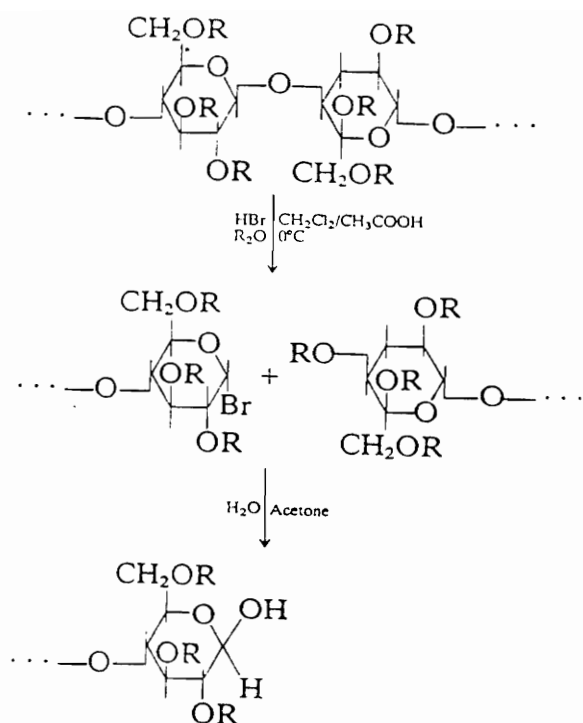


Figure 62. Synthesis route for the preparation of cellulose triester macroinitiator [8]

6.2 *EXPERIMENTAL SECTION*

6.2.1 Materials

Cellulose propionate mono-hydroxyl terminated (CP): Mono-hydroxyl terminated cellulose propionate was prepared according to the method described in chapter 5.

Stannous octanoate: The catalyst, stannous octanoate, was obtained from Aldrich Chemical Company and used as received.

2,4-Tolylene diisocyanate (TDI): TDI was supplied by Aldrich Chemical Company and used without further purification.

Tetrahydrofuran (THF): THF was supplied by Fischer Scientific Chemical Company. The solvent was dried over metallic potassium and benzophenone mixture, refluxed and distilled under dried nitrogen. The material was collected in a bottle and stored over molecular sieves.

Hydroxypropyl lignin (HPL): Typical examples of synthesis and purification of HPL is described in chapter 3 of this work. Hydroxypropyl lignin with variable molecular weights were used. The common characteristic of these HPL's was their "rubbery" nature (T_g below room temperature).

6.2.2 Synthesis of Mono-Isocyanate Terminated Cellulose Propionate

In a typical synthesis of mono-isocyanate terminated cellulose propionate segments (CP-NCO), 1 g of CP and 0.1 % by weight of stannous octanoate, were introduced into a two-necked flask equipped with a magnetic stir bar. The flask was connected to a vacuum line for further drying. After six hours, the reactor was sealed with rubber septa, transferred to an oil-bath on a stir plate and purged with prepurified and dried nitrogen. Under a constant flow of nitrogen, 10 mL of freshly distilled THF were added into the reaction flask through a hypodermic syringe to dissolve the reactants. The reactor was heated to 50 °C and then TDI was added in an approximately 5:1 molar ratio. The reaction was kept at 50 °C under stirring for 24 hours. After cooling, the product was precipitated into a large excess of petroleum ether to eliminate the unreacted TDI, filtered, washed with petroleum ether, and dried under vacuum. The mono-isocyanate-capped prepolymer was immediately used for grafting. Infrared spectroscopy was used to monitor the reaction.

6.2.3 Copolymer Synthesis

A series of ABA star block copolymers has been synthesized and subsequently characterized via gel permeation chromatography. These materials contain hydroxypropyl lignin as the elastomeric center block (B), while the end blocks (A) are cellulose propionate. The synthesis of these materials involved a two-steps process. The first step consisted of the synthesis of CP-NCO, which has been described previously. The second step involved the grafting of CP-NCO segments into HPL polyol. Since the main goal was to synthesize copolymers with elastomeric properties, and being HPL of low molecular weight, the stoichiometric molar ratio of CP/HPL was kept at a minimum (2/1) in order to favour a higher balance of the rubbery phase over the semi-crystalline domains. Thus, star-like copolymers with an average of 2 arms have been synthesized. Basically, the grafting reaction was performed in a clean, flamed and nitrogen-purged 2-necked round bottom flask,

equipped with a magnetic stir bar and rubber septa under prepurified dried nitrogen atmosphere. First, a calculated amount of HPL and stannous octanoate dissolved in THF were charged to the reaction flask through a hypodermic syringe. Next, CP-NCO previously dried and dissolved in THF was syringed into the flask at the ratio 2:1 of CP-NCO to HPL. The reaction flask was submerged into the oil-bath and heated to 50 °C. The grafting reaction was terminated after 24 to 30 hours through precipitation into aqueous methanol. This synthesis scheme is outlined below: scheme 5 shows the copolymer synthesis using CP segments of molecular weights smaller or equivalent of the HPL molecular weight. Since CP has a smaller size than HPL, the final architecture of the star will be predominantly determined by the the branched nature of HPL. As the CP segments increase in length (scheme 6), the spherical architecture of the star will change to a rod-like conformation, in which the branched nature of HPL is no longer the major parameter in determining the architecture of the copolymer, but rather the stiff chains of cellulose propionate.

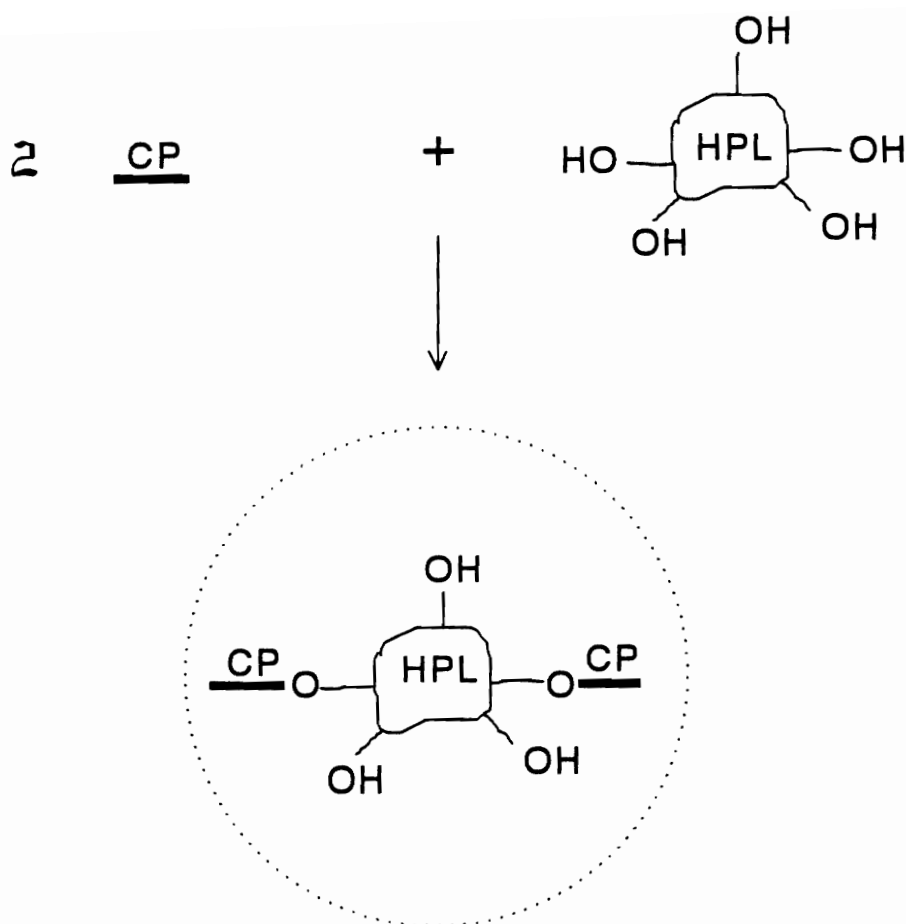
Extraction of unincorporated HPL: Soxhlet extraction with methanol was used to remove unreacted HPL. The reaction product was later characterized by GPC and UV analysis.

6.2.4 Characterization

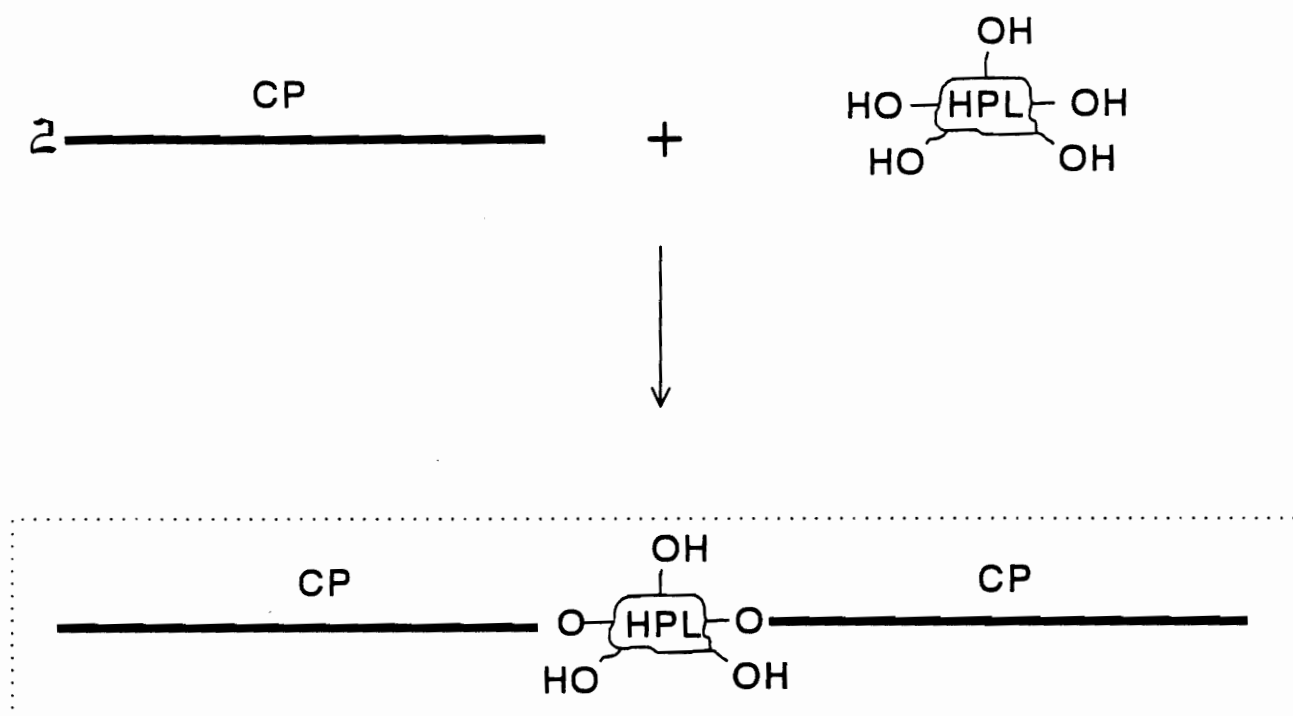
Gel Permeation Chromatography (GPC): Gel permeation chromatography was used to measure the molecular weights and molecular weight distributions of HPL and of the copolymers, according to the procedure described in chapter 3.

Fourier Transform Infrared Spectroscopy (FTIR): The progress of the isocyanate capping reaction was monitored by using a Nicolet spectrometer, as described in chapter 3

Ultraviolet Spectroscopy (UV): UV spectroscopy was used to determine the molar mass of HPL in the copolymers based on a procedure described elsewhere [9]. The wavelength maximum for HPL



Scheme 5: Synthesis scheme of CP-HPL copolymers with CP segments (M_n) < M_n of HPL



**Scheme 6: Synthesis scheme of CP-HPL copolymers
with CP segments (M_n) > M_n of HPL**

was established to be 280 nm. Copolymer solutions of known concentrations were made in chloroform. The absorbance of the solution was then read at 280 nm, in a Varian/Cary-219 UV-VIS spectrophotometer.

Proton-Nuclear Magnetic Resonance Spectroscopy (H-NMR): H-NMR analysis were used to determine chemical information of the copolymer, based on the procedure described in chapter 3.

Titration: The total hydroxyl content of HPL was determined by acetylation and back titration of free acetic acid, as described in chapter 3.

Dynamic Mechanical Thermal Analysis (DMTA): The viscoelastic properties of the copolymer were observed using a Polymer Laboratories Ltd. DMTA, at a frequency of 1 Hz. The injection-molded dogbone sample was rapidly quenched to -50°C, and the measurement was made at a heating rate of 10 °C/min until the sample became too soft to be tested.

Differential Scanning Calorimetry (DSC): DSC thermograms were obtained on a Perkin-Elmer Model DSC-4. Temperature was scanned from -60 to 300 °C at a heating rate of 10 °C per minute. The scanning procedure consisted of two steps. In the first run, the samples were cooled to -60 °C and heated at 10 °C/min to 300 °C. In the second run, the samples were quenched to -60 °C at 200 °C/min and reheated at 10 °C/min to 300 °C. Glass transition temperatures were taken as midpoint of the change in slope of the baseline. The T_m was taken as the temperature corresponding to the location of the endothermic peak.

Optical Microscopy: Optical microscopy was conducted on a Zeiss Axioplan microscope, fitted with a Linkam TMS90 Hot Stage and a Zeiss ML 100 camera. The nucleation and growth behavior were observed on thin films of copolymers between glass plates.

Transmission Electron Microscopy (TEM): TEM was carried out on a Phillips EM-420 STEM operated in the transmission mode at 100 kV. Ultrathin films were microtomed using a Reichert-Jung ULTRACUT System FC-4 at -70°C. The microtomed samples were then mounted on a copper TEM grid and stained with RuO₄ for 15 - 45 min.

6.3 RESULTS AND DISCUSSION

6.3.1 Effect of Synthesis Parameters on Copolymer Properties

The reaction of mono-hydroxyl terminated CP oligomers with TDI produces a mono-isocyanate terminated CP segment. The course of this reaction was followed by FTIR in the 2300 cm^{-1} region. Figure 63 shows the spectra of the CP oligomer before reaction, and after 24 hrs of reaction. Similar to PCL-OH segments (chapter 3), after 24 hours of reaction at 50°C , the intensity of the OH absorption peak at 3350 cm^{-1} had decreased, and the NCO absorption peak at 2274 cm^{-1} had appeared (Figure 63).

The star-like copolymers were characterized by gel permeation chromatography. Figure 64 shows the GPC results of the reaction products of monoisocyanate capped cellulose propionate (CP-NCO) and hydroxypropyl lignin (HPL). The effectiveness of the reaction is established through the formation of higher molecular weight polymers, as compared to the starting material. The coupling of cellulose propionate chains with HPL was found to proceed to completion in pyridine or THF, in approximately 24 hours. Figure 65(a) is a representative GPC chromatogram of a star-like copolymer with high cellulose propionate (CP) content. The molecular weight distribution of the copolymer has approximately the same narrow distribution as the CP oligomers. Figure 65(b) shows the GPC chromatogram of a star-like copolymer with high HPL content. The molecular weight distribution of the $(\text{CP})_n\text{-HPL}$ copolymer is broader than case (a) because of the polydispersity of HPL.

Table 14 contains the molecular characteristics of copolymers synthesized in this work. Due to the broad molecular weight distribution of the copolymers, their composition was better characterized by UV spectroscopy than by GPC. Basically, the copolymer structure is formed by three major

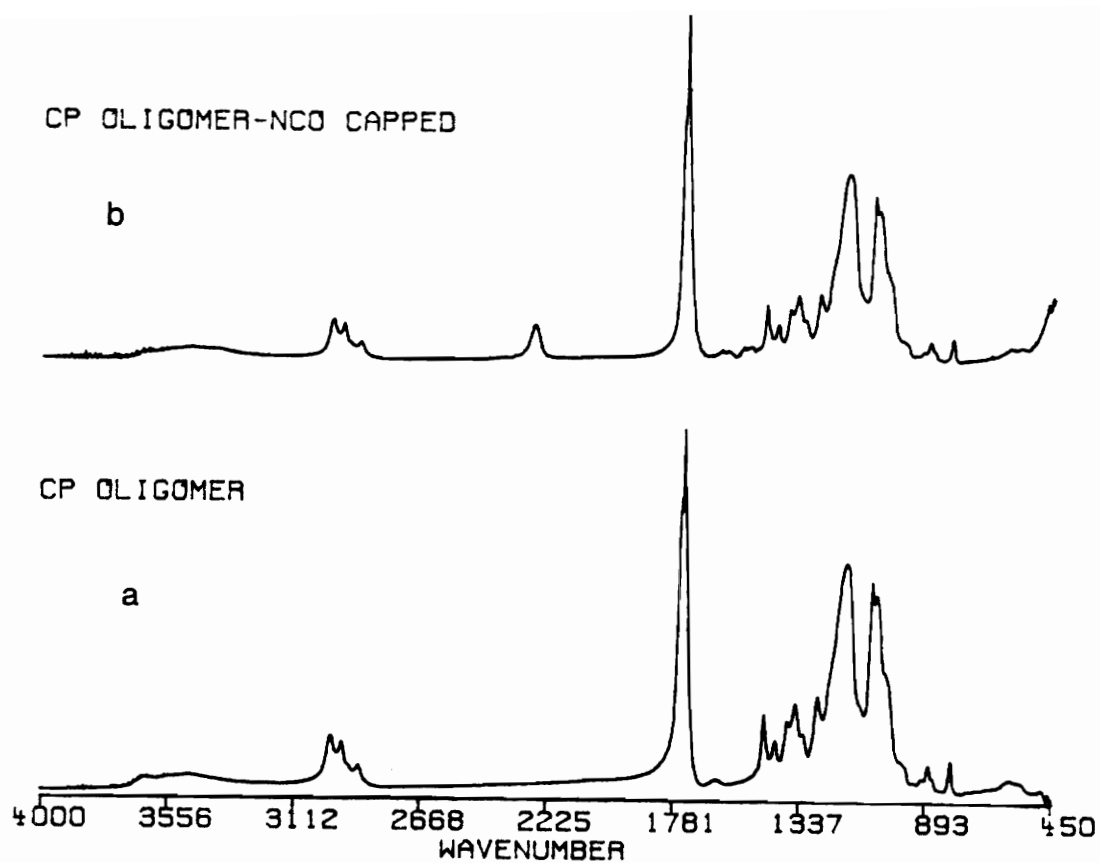


Figure 63. FTIR spectra of cellulose propionate oligomers: (a) before, and (b) after NCO capping

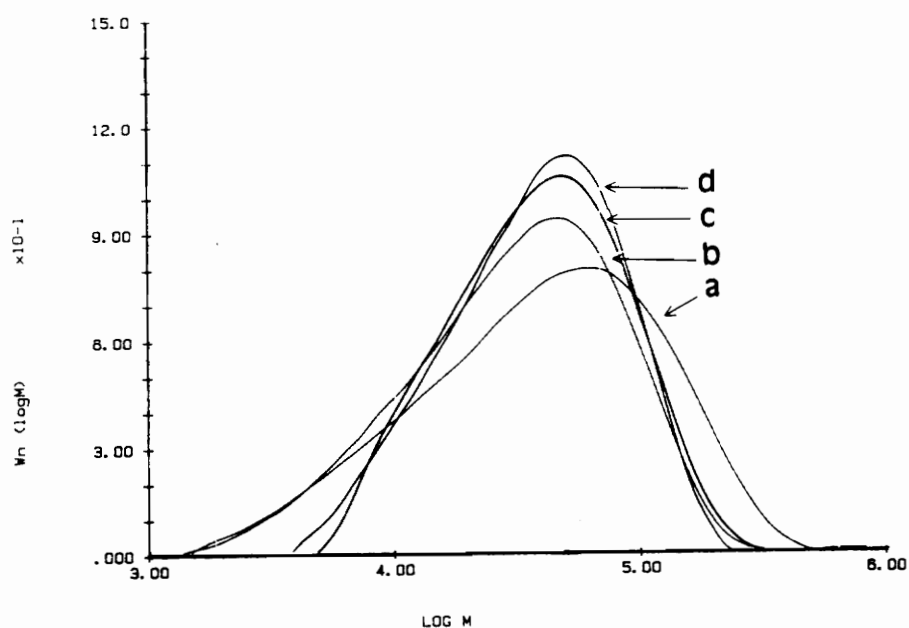


Figure 64. GPC chromatograms of copolymers from grafting: after(a) 0; (b) 6; (c) 24 and (d) 26 hrs.

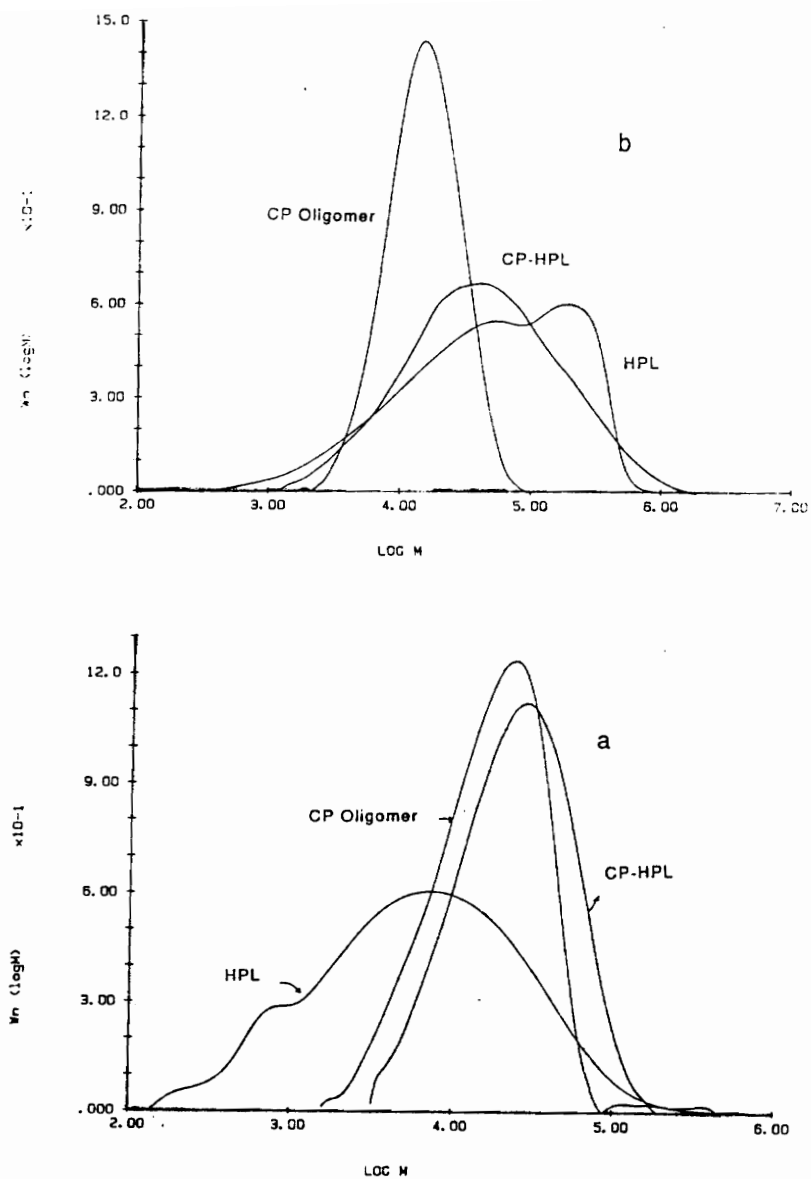


Figure 65. GPC chromatograms of CP-HPL copolymers: (a) high CP content; (b) high HPL content

Table 14. Molecular Characterization Data of CP-HPL Copolymers

Sample	M_n	M_w/M_n	M_n	M_w/M_n	M_n	M_w/M_n	MHS ^a	IV	a_{280}^b
	CP	CP	HPL	HPL	cop. ^c	cop.		(dl/g)	(L/g.cm)
F1	1,600	1.2	3,000	5.1	4,100	3.5	0.227	0.058	9.92
F2	3,900	1.4	1,800	10.5	4,800	2.1	0.464	0.083	4.2
F3	5,000	1.6	2,100	7.5	8,200	1.3	0.544	0.176	5.2
F4	11,800	1.5	2,100	7.5	19,300	1.8	0.873	0.093	1.6
F5	12,600	1.4	6,900	8.9	18,900	6.2	0.864	0.322	3.3
F6	18,500	1.8	1,800	10.5	28,400	1.7	0.793	0.451	1.1
F7	18,500	1.8	1,800	10.5	27,000	1.8	0.911	0.337	1.3
F8	18,500	1.8	1,800	10.5	24,600	2.1	0.596	0.451	0.5

a Mark-Houwink-Sakurada constant

b absorptivity coefficient at 280 nm wave length

c copolymer

components: lignin, propylene oxide and cellulose propionate. Among them, lignin is the only UV absorbing component. Therefore, the copolymer composition could be characterized in terms of UV absorbing mass (lignin segment) and non-UV absorbing mass (propylene oxide and cellulose propionate segments). From Table 14 it is seen that copolymers were synthesized with CP molecular weights (arm length) varying from 1,600 to 18,500 daltons. Their lignin content ranged from 5 to 45%. In general, good incorporation of CP chains into HPL was achieved, as indicated by the GPC results. However, higher molecular weight copolymers could never be obtained as a result of increasing the stoichiometric ratio of CP equivalents per HPL equivalent (samples F7 and F8). It seems that CP segments at higher concentration tend to incorporate to a lesser extent into HPL, probably due to different reasons, such as high degree of phase separation during copolymerization, limited chain mobility (rod-like chain), or lack of functionality.

6.3.2 Solution Properties

The relationship between intrinsic viscosity, as calculated by GPC, and copolymer composition (lignin content) is presented in Figure 66. The viscosity follows the expected trend of branched molecules. Branched molecule, being spherical in nature, have a much lower viscosity than their linear counterparts. This is evident in the case of $(CP)_n$ -HPL copolymers. In Figure 66, at high lignin content, the branched nature of lignin predominates, and the intrinsic viscosity is low. As the lignin content decreases, the size of the CP segments becomes the overriding factor over branching, thereby causing an increase in viscosity. The transition from the point where the effect of branching gives way to the increasing length of CP is apparently abrupt, as indicated by the shape of the curve in Figure 67(A), where the intrinsic viscosity is plotted against copolymer arm length. The viscosity curve rises sharply at about M_n 6,000 daltons. It is interesting to note that this is approximately the size of HPL of highest molecular weight. When the arms become bigger than the central HPL core, the intrinsic viscosity rises abruptly which suggests a change in copolymer conformation. (As dis-

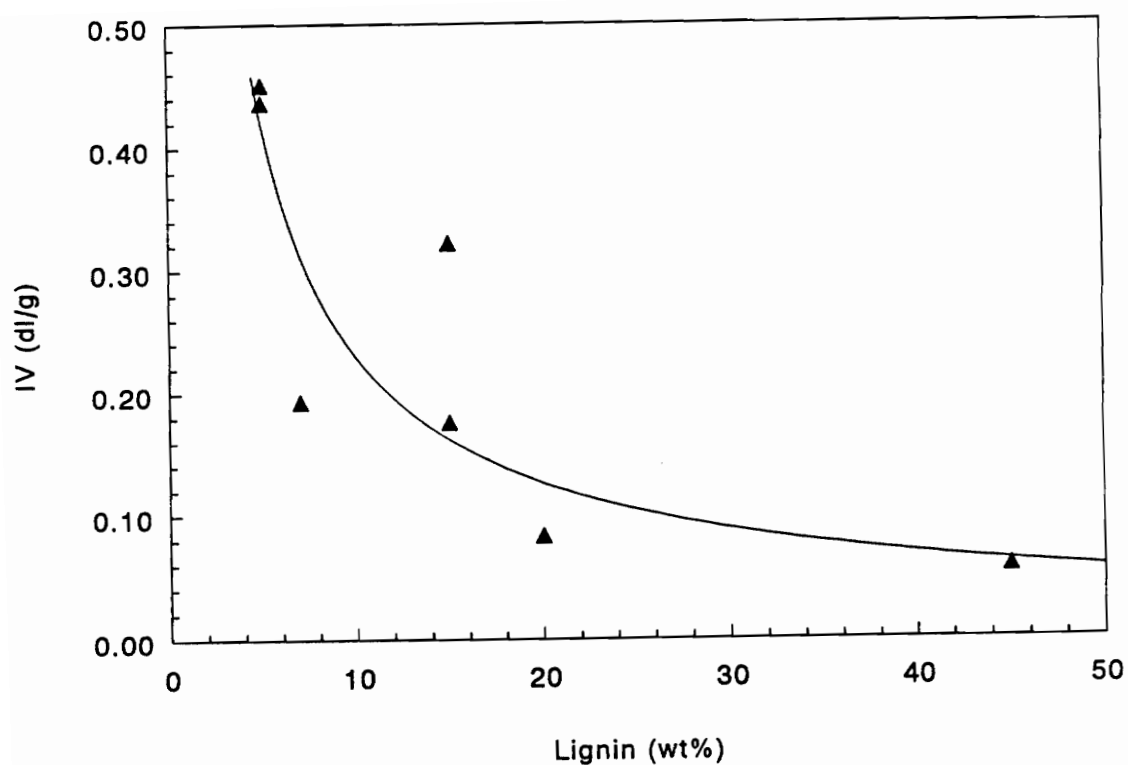


Figure 66. Intrinsic viscosity as a function of copolymer lignin content

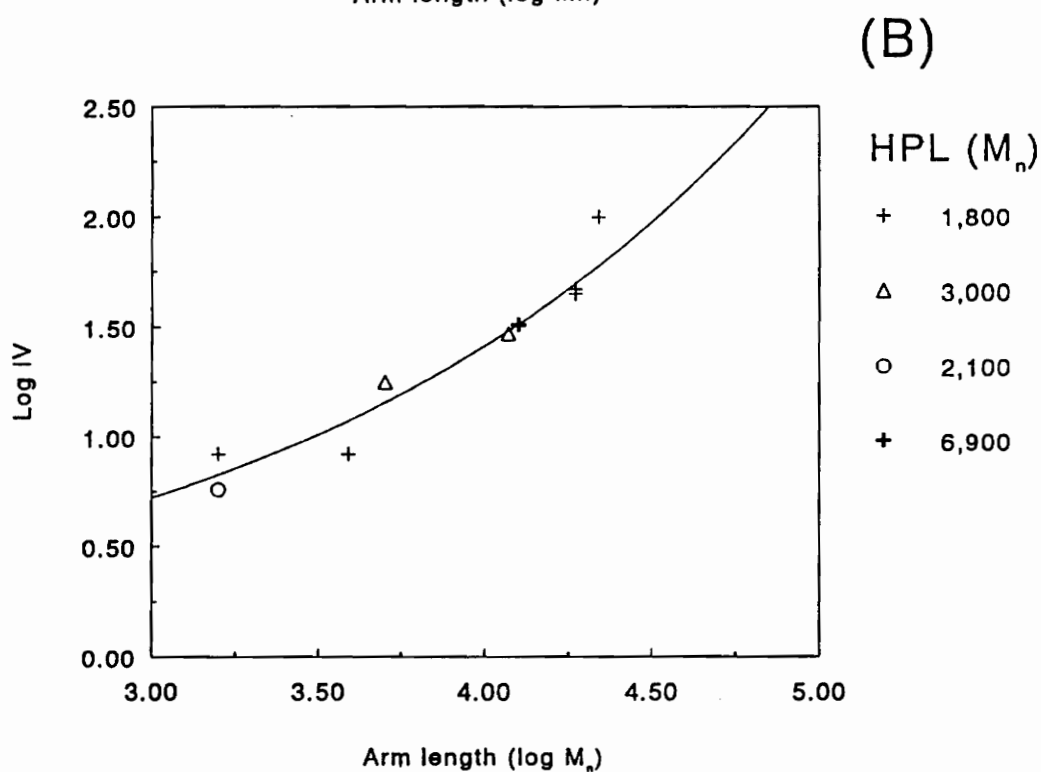
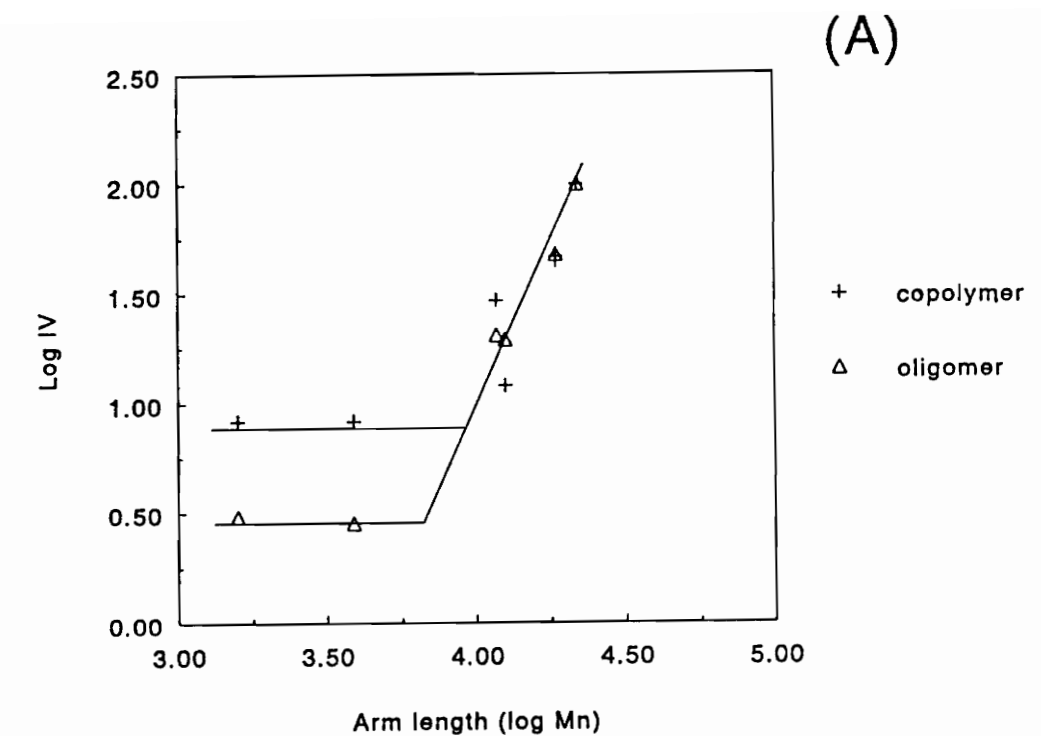


Figure 67. Intrinsic viscosity as a function of copolymer arm length: (A) copolymer (from HPL of M_n 1,800 g/mol) and oligomer; (B) copolymers synthesized from HPL of different molecular weights.

cussed later, the Mark-Houwink-Sakurada constants of these copolymers indicate a change from the spherical to rod-like conformation at about M_n 6,000-10,000 daltons). Contrary to the expected, the intrinsic viscosities of the copolymers with short arm length were higher than the linear CP oligomers of equivalent molecular weight. A similar phenomenon was observed in the case of $(PCL)_n-HPL$, series C. As discussed earlier (section 3.3.2), the rise in intrinsic viscosity may be related to an increase in incompatibility between the segments, as a result of the incorporation of urethane groups introduced during the TDI end capping of cellulose propionate oligomers. As the arm length increases beyond the HPL molecular weight, the difference in intrinsic viscosity between copolymer and its homo-oligomer disappears. Both copolymer and oligomer behave as a rod-like molecule in solution. Figure 67(B) shows the intrinsic viscosity versus arm length for copolymers synthesized from HPL with different molecular weights. It can be concluded that the intrinsic viscosity is a function of the component sizes. When HPL molecular weight predominates in the copolymer composition, the intrinsic viscosity is low, with typical values of a branched polymer, whereas in copolymers where CP molecular weight is greater than HPL, the intrinsic viscosity has the value of the corresponding linear CP oligomer.

The plot of the Mark-Houwink-Sakurada exponent, a , as a function of arm molecular weight is shown in Figure 68. There is an increase in a -value with increasing arm molecular weight. The MHS exponent ranges from numbers typical of flexible chains ($a=0.5$), to a -values common to inherently stiff molecules ($0.5 < a < 0.7$). In other words, copolymers with short arm length behave in solution like flexible polymer molecules, whereas high molecular weight copolymers (long arms) assume a rod-like conformation in solution.

6.3.3 Thermal Behavior

Figure 69 shows the DMTA spectrum of a high molecular weight $(CP)_n-HPL$ copolymer. Three major thermal events are recorded, and these are a T_g of HPL at around 0°C; a T_g of the cellulose

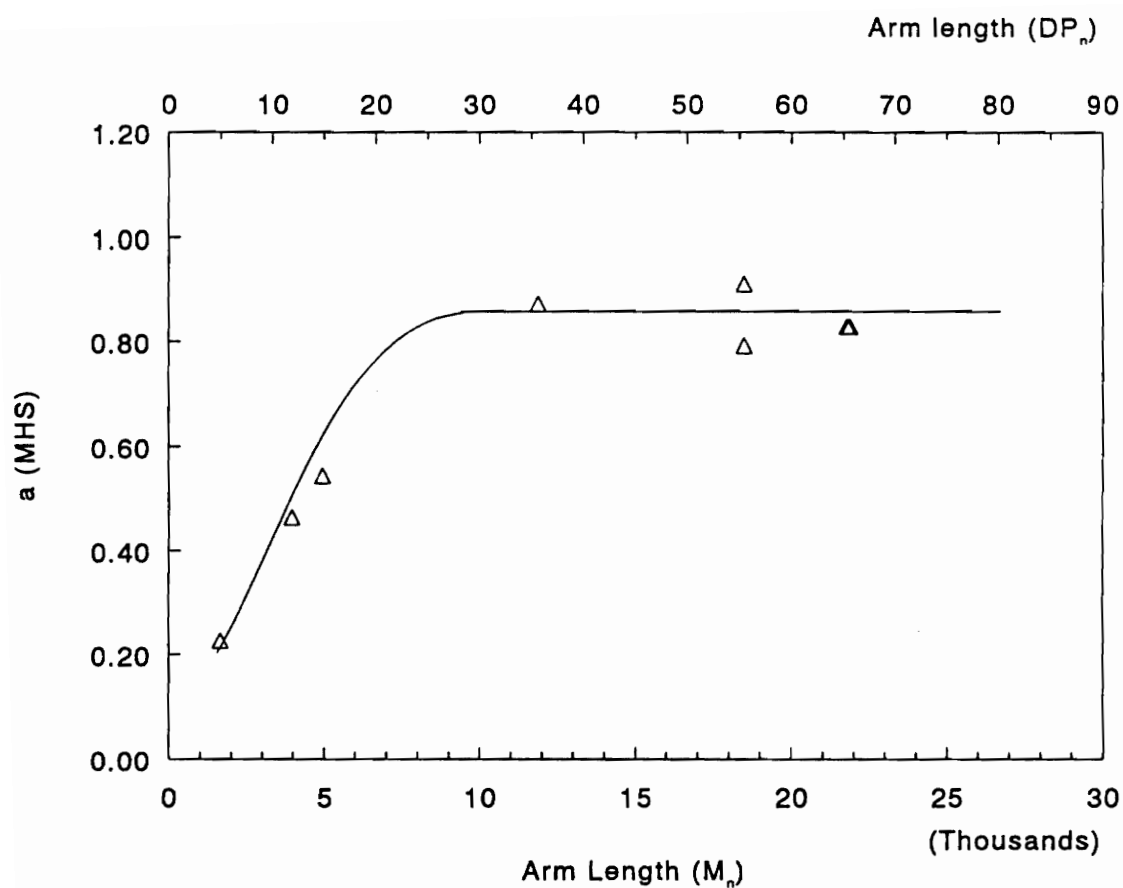


Figure 68. Mark-Houwink-Sakurada exponent as a function of copolymer arm length: molecular weight of HPL segments ranging from 1,800 to 6,900 daltons

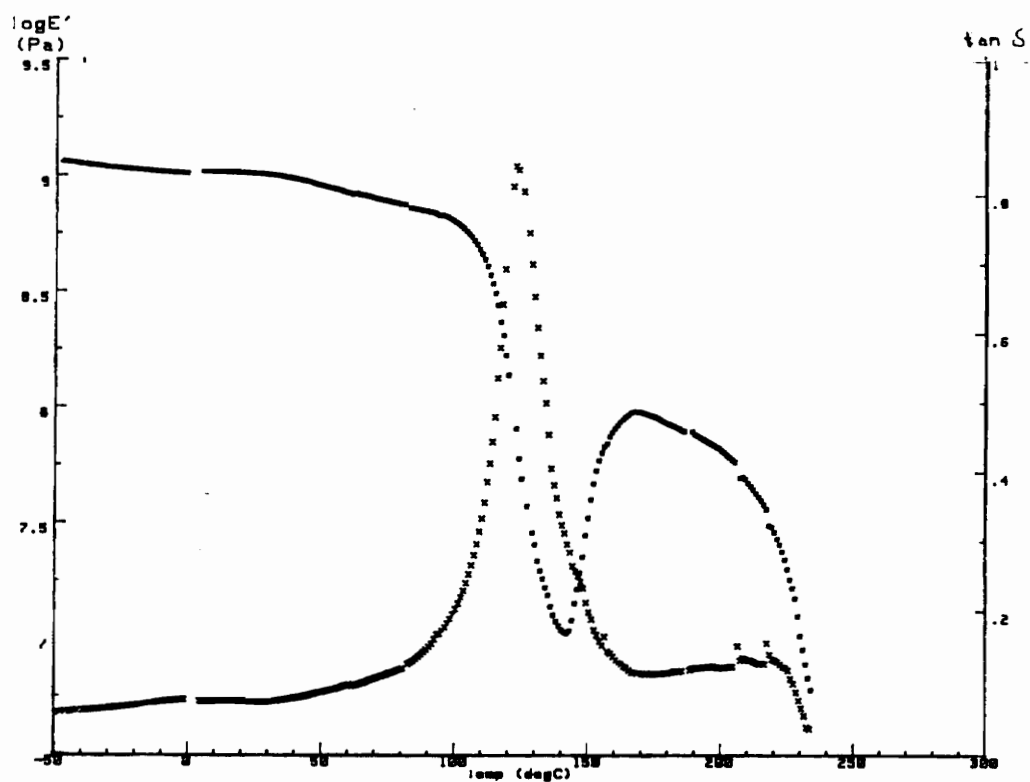


Figure 69. Dynamic mechanical behavior of CP-HPL copolymer

propionate component (124°C); and a CP-melting point at about 230°C. Upon passing through the T_g of the cellulose propionate hard segment, a striking rise in storage modulus is recorded, which signifies a thermally induced organization of the amorphous cellulose derivative chains into a new ordered (crystalline) morphology.

A typical DSC thermogram of $(CP)_n-HPL$ is seen in Figure 70. It shows a sharp melting peak for the CP chains at 230 - 240°C, two glass transition temperatures for the amorphous phases of HPL and cellulose propionate located between -10 and 10°C and at 130°C, respectively, and a crystallization temperature at 160°C. The thermogram provides strong evidence for phase separation of HPL from the cellulose propionate hard segments. Table 15 summarizes the thermal data of $(CP)_n-HPL$ star-like copolymers on the basis of their arm length. Even at DP 5, it is possible to detect the formation of an small endotherm peak at 190°C, which is an indication of the crystallization of cellulose propionate chains. As the molecular weights of the cellulose propionate arm segments increase, the major melt endotherm peak is observed at increasingly higher temperatures, leveling off at a DP of approximately 50, when the crystallites melt at about 240°C. Although not prominent on the second scan, the majority of the copolymers presented in this work reveal glass transition temperatures for HPL and CP during the initial DSC scans.

The relationship between melting temperature and arm length is shown in Figure 71. It shows that as the copolymer arm length increases, the melting temperature asymptotically approaches a constant temperature level of about 240°C. Thus, it can be concluded that as the arm length increases, a higher degree of phase separation between HPL and CP is achieved, and more perfect crystallites are produced, as suggested by the higher melting points.

Optical micrographs of films isothermally crystallized from the melt at 200°C are shown in Figure 72. The micrographs reveal that the crystallized films are spherulitic in texture, but with different sizes. Both copolymers have the same HPL molecular weight. What differs is the arm length of cellulose propionate segment, which have number-average molecular weights of 5,000 and 11,900

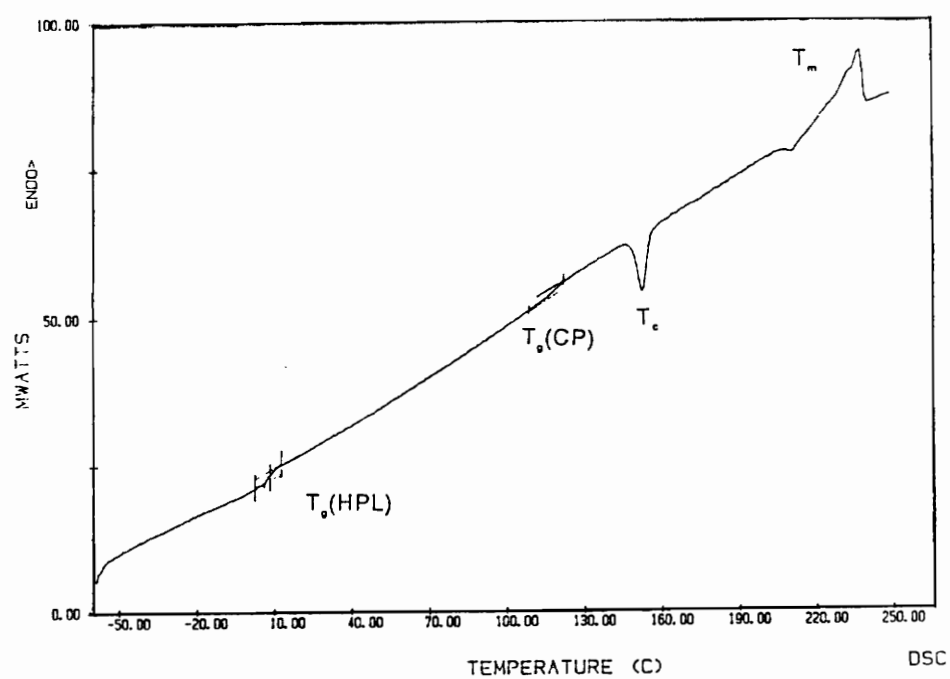


Figure 70. A typical thermogram of CP-HPL copolymer

Table 15. Summary of Thermal Data of CP-HPL Copolymers

Sample	M_n/arm	$T_g(\text{HPL})$ (°C)	$T_g(\text{CP})$ (°C)	$T_m(\text{CP})$ (°C)	ΔH_f (J/g)
F1	1,600	-32	110	190	-
F2	3,900	-19	117	205	2
F3	5,000	-23	125	226	31
F4	11,800	-25	130	224	31
F5	12,600	-15	120	223	35
F6	18,500	-20	118	239	54
F7	18,500	-28	121	237	63
F8	18,500	-30	130	238	72

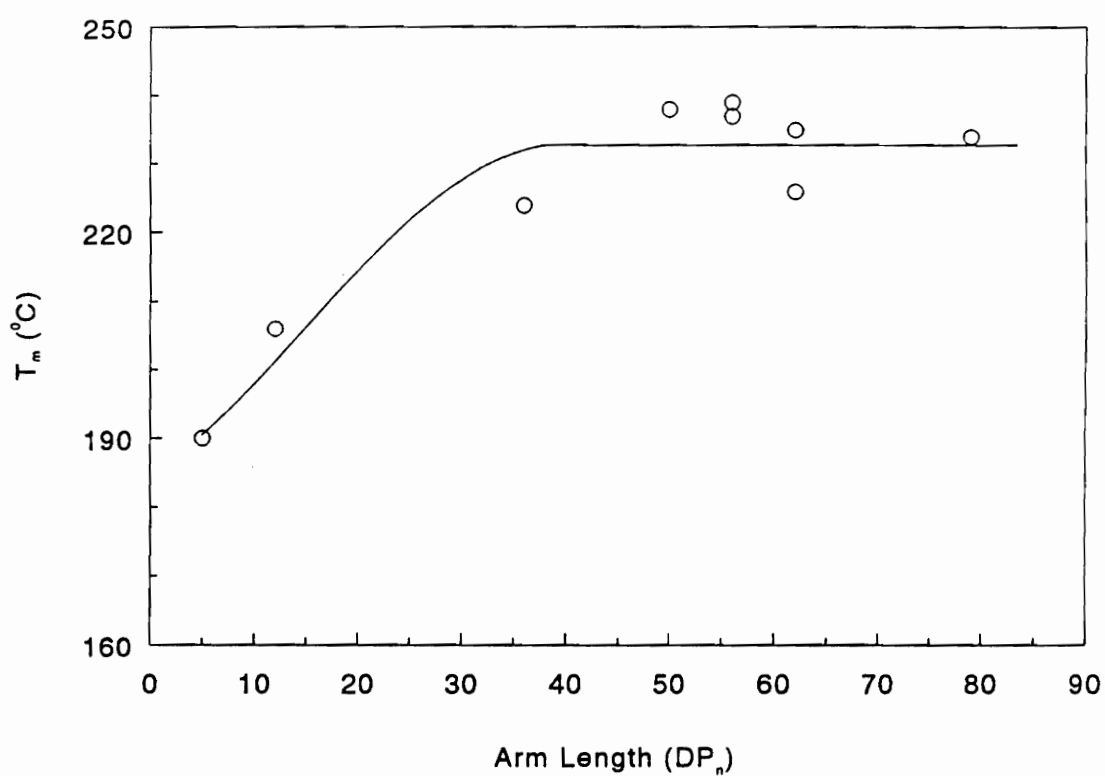


Figure 71. Melting temperature vs. arm length

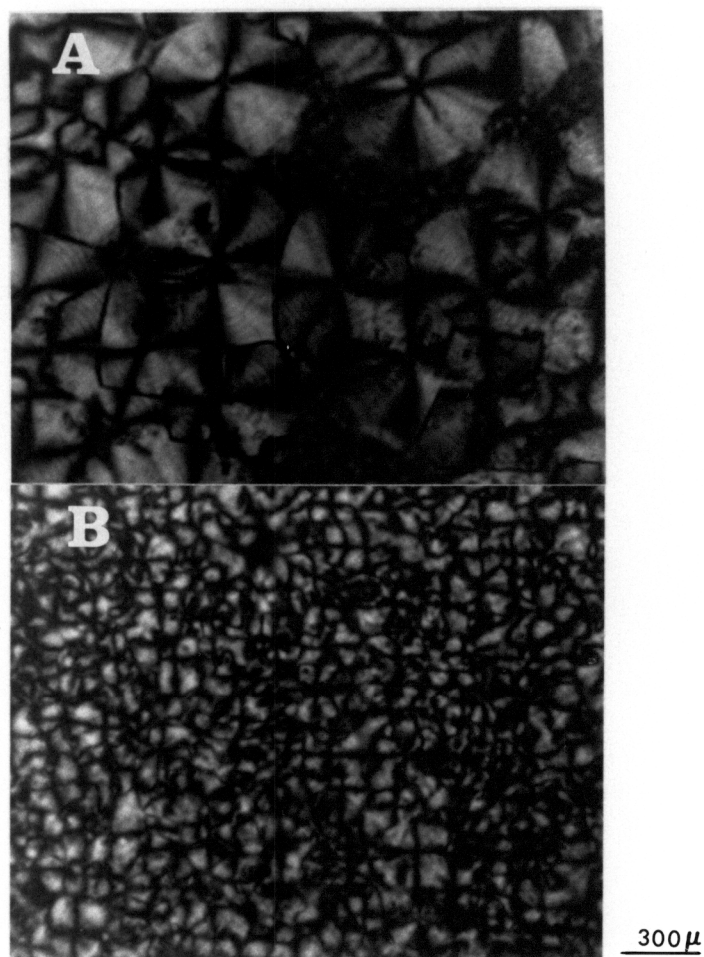


Figure 72. Optical micrographs of films isothermally crystallized from the melt: (a) sample F3; (b) sample F4 (see Table 14) (32x)

**SYNTHESIS AND CHARACTERIZATION OF CELLULOSE PROPIONATE -
HYDROXYPROPYL LIGNIN COPOLYMERS**

daltons. Very small and homogeneous spherulites are produced under isothermal conditions (200°C, 1hr) in the sample with the shorter arm length (Figure 72A). The average spherulite size is about 50 μm . As the cellulose propionate segment molecular weight increases, the size of the spherulites decreases by more than an order of magnitude (Figure 72B).

Figure 73 shows the relationship between heat of fusion and copolymer arm length. As the cellulose propionate chain length increases, the heat of fusion increases, and so does the crystallinity content. At DP 30, the heat of fusion remains approximately constant, which is an indication that the highest degree of crystallinity is achieved at an arm length of around 5-10 thousand daltons.

6.3.4 Morphology

Electron micrographs of thin films of $(CP)_n$ -HPL cast from dilute solution in THF are shown in Figures 74 through 78. The dark regions are the HPL segments selectively stained with ruthenium tetroxide. A broad variety of features is observed. They vary from dispersed fibrils in copolymers with short arm length (Figure 74) to alternate lamellae-type of arrangements (Figure 76) in copolymers in which both cellulose propionate and hydroxypropyl lignin have high molecular weights. Each figure is composed of a set of micrographs of different magnification for a particular block copolymer (see Table 14 for sample identification).

Figure 74 displays the electron micrographs of sample F3. The cellulose propionate number-average molecular weight is 5,000 daltons, which corresponds to a DP of about 15 repeat units. Its composition is made up of approximately 25% HPL and 75% CP. Figures 74 (A, B, C) correspond to pictures taken from different magnifications of a certain portion of the sample. They show structural organization composed of fine dispersed fibrils. The average filament length varies from 1,000 to 2,000 Å, and the width is approximately 100 Å. This type of morphology is not uncommon for cellulose derivatives. Buleon and Chanzy [10] have prepared cellulose II crystals through

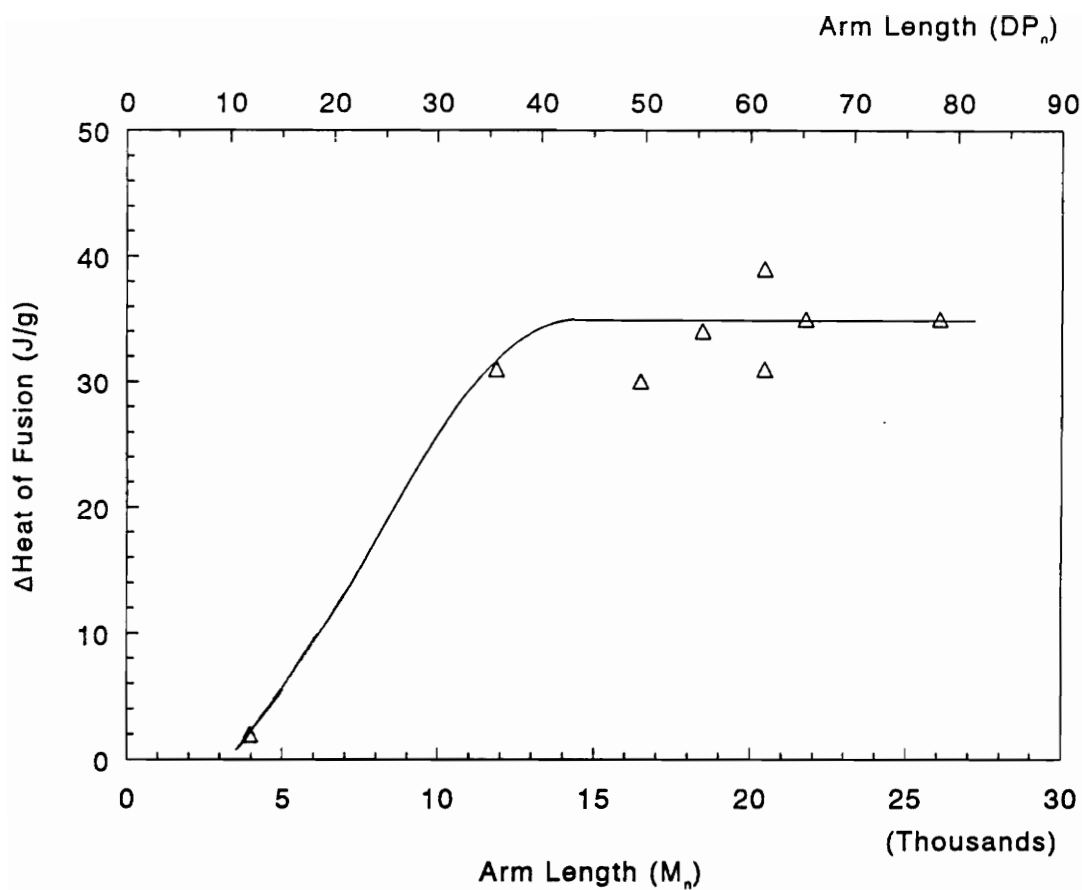


Figure 73. Heat of fusion vs. copolymer arm length

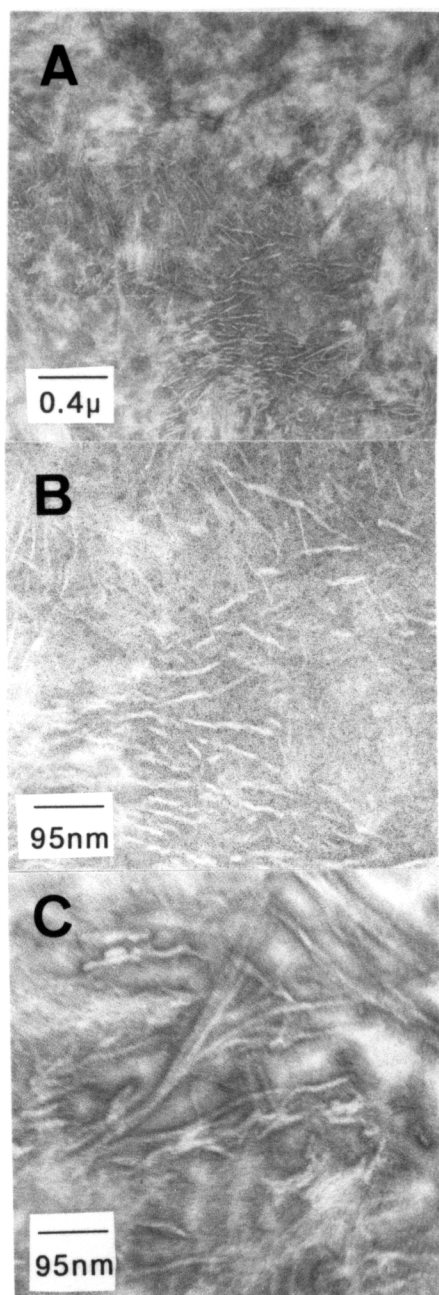


Figure 74. TEM for cast films of CP-HPL copolymer stained with ruthenium tetroxide: Sample F3, CP(M_n = 5000) (see Table 14) (a) Mag. 37500, (b) Mag. 105000, (c) Mag. 105000

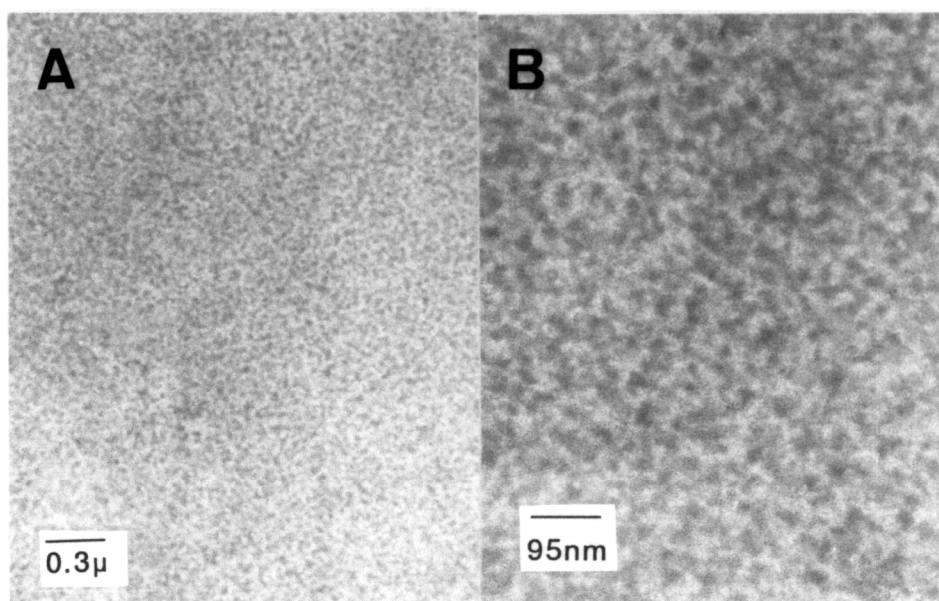


Figure 75. TEM for cast films of CP-HPL copolymer stained with ruthenium tetroxide: Sample F4, CP(M_n = 11800) (see Table 14) (a) Mag. 37500, (b) Mag. 105000

SYNTHESIS AND CHARACTERIZATION OF CELLULOSE PROPIONATE - HYDROXYPROPYL LIGNIN COPOLYMERS

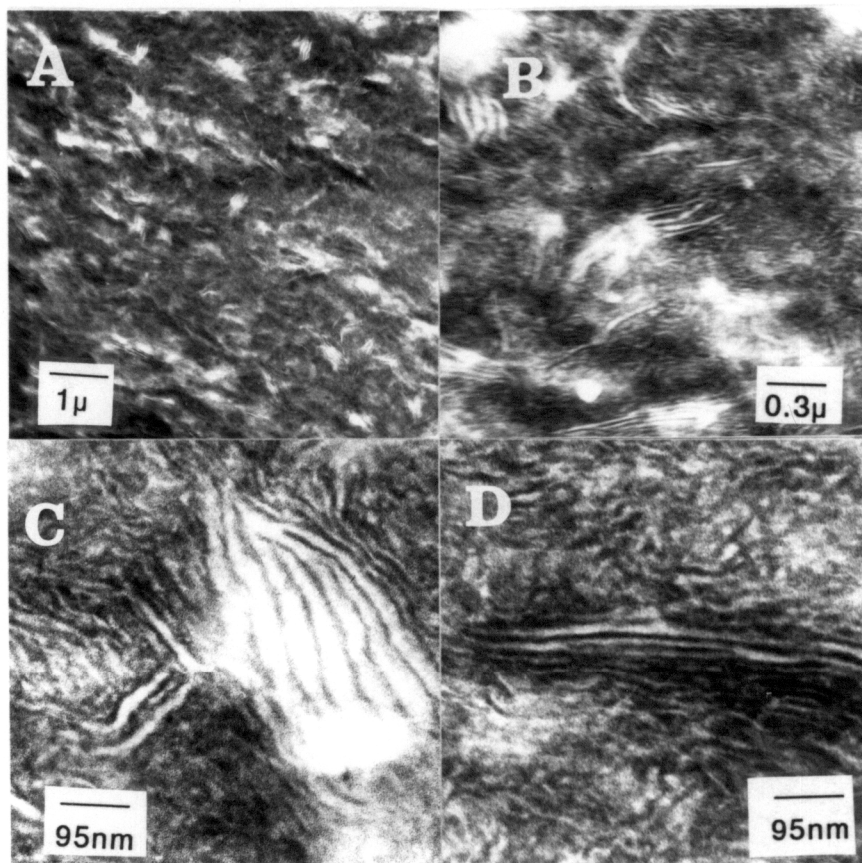


Figure 76. TEM of casting films of copolymer stained with ruthenium tetroxide: Sample F5, CP($M_n=12600$) (see Table 14) (a) Mag. 8200, (b) Mag. 37500, (c) Mag. 105000, (d) Mag. 105000

SYNTHESIS AND CHARACTERIZATION OF CELLULOSE PROPIONATE - HYDROXYPROPYL LIGNIN COPOLYMERS

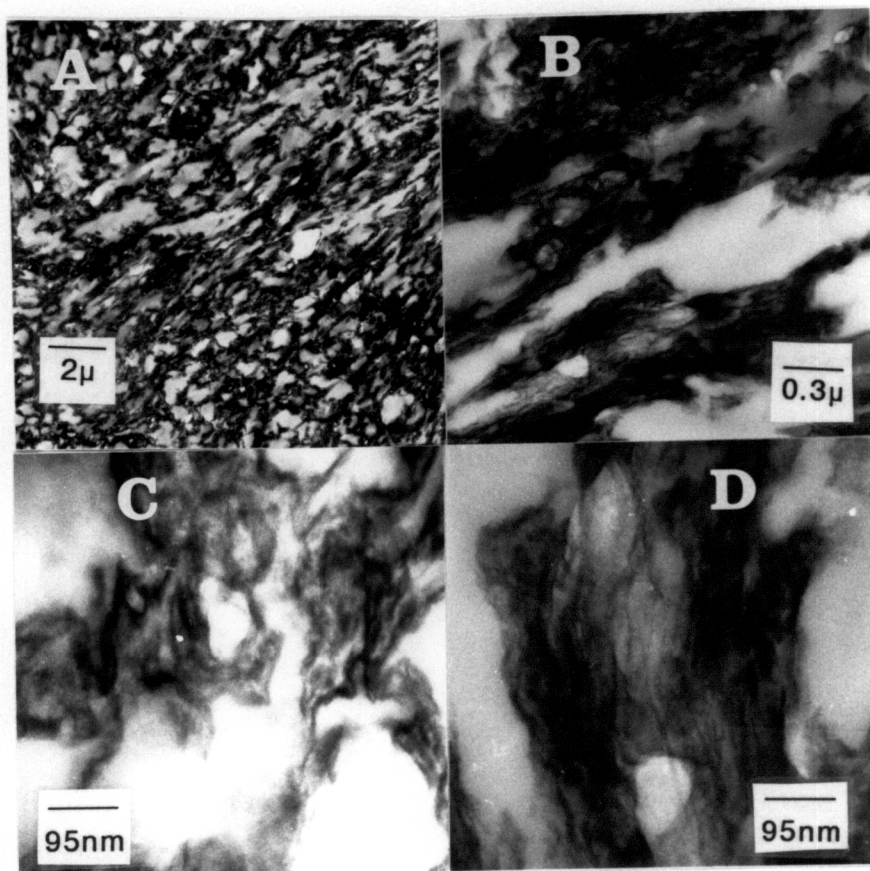


Figure 77. TEM of casting films of copolymer stained with ruthenium tetroxide: Sample F6, CP ($M_n = 18500$) (see Table 14) (a) Mag. 4900, (b) Mag. 37500, (c) Mag. 105000, (d) Mag. 105000

SYNTHESIS AND CHARACTERIZATION OF CELLULOSE PROPIONATE - HYDROXYPROPYL LIGNIN COPOLYMERS

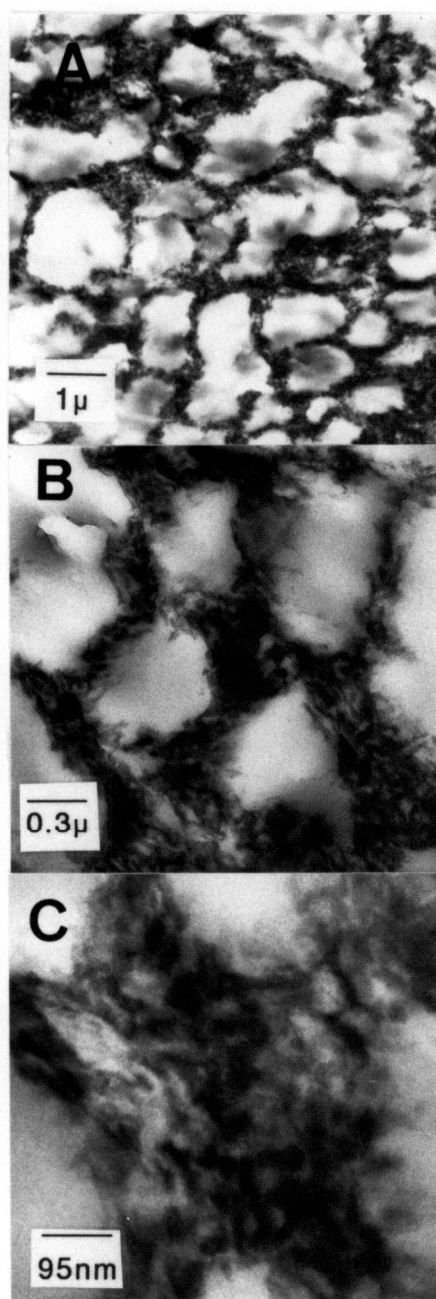


Figure 78. TEM of casting films of copolymer stained with ruthenium tetroxide: Sample F7, CP ($M_n = 18500$) (see Table 14) (a) Mag. 8200, (b) Mag. 37000, (c) Mag. 105000

SYNTHESIS AND CHARACTERIZATION OF CELLULOSE PROPIONATE -
HYDROXYPROPYL LIGNIN COPOLYMERS

homogeneous deacetylation of cellulose triacetate of DP 15 from dilute aqueous solution. Ribbon-like lamellar single crystals were formed with a length between 1 and 2 μm , width of approximately 1,000 Å, and with a thickness of around 80 Å. They were characterized by TEM and electron diffraction. They support the opinion that the cellulose molecular axes are perpendicular to the ribbon length. The chain-folding mechanism during crystallization could not be questioned since only low-molecular weight cellulose samples were used. The filament widths presented here vary from 100 to 300 Å, which are much smaller than the widths of the needle-like structures reported by Buleon and Chanzy. Even though no electron diffraction has been used to further characterize these crystals, it seems that the cellulose propionate chains crystallize in their fully extended form.

Figure 75 (A, B) presents the electron micrographs of sample F4 (ie., arm length of 11,800 M_n and HPL size of 6,100 M_n). It is evident that almost spherical HPL particles (stained black) are dispersed evenly in the CP matrix. The dimensions of the particles vary from 200 to 300 Å, and they are not always separated from each other.

The micrographs of Figure 76 (A, B, C, D) show very different configurations from the previous samples. Differently from Figure 75, the features do not show spherical domains. The copolymer segregates into two phases, mostly in the form of alternate layered structures of hydroxypropyl lignin and cellulose propionate. Roughly, the dimensions of the cellulose propionate layers vary between 100 and 500 Å in width and 2,000 to 7,000 Å in lamella length. The spacing measurements were obtained by averaging the values across several sets of lines in the micrograph. It is interesting to note that the width of the cellulose propionate layers is equivalent to approximately twice that of a fully extended cellulose propionate chain.

Figure 77 (A, B, C, D) represents a sequence of electron micrographs from sample F6 (ie., arm length of 18,500 M_n and HPL size of 2,000 M_n). The cellulose propionate domains, which look like "cobble stones", have a wide variety of sizes. By considering these domains as spheres, the distrib-

ution of sizes will range from 0.3 to 2 μm . However, at DP 56, the average dimension of each chain is about 300 Å or 0.03 μm . Therefore, the domain sizes are much greater than those expected on the basis of molecular weight. One explanation for that is the possible contamination of the copolymer with ungrafted (unfunctionalized) CP segments. This would cause, along with the copolymer microphase separation, a macrophase separation of the loose CP chains in their own domains, as indicated by the wide variety of sizes, 3 to 5 order of magnitude greater than the CP length.

The same type of pattern is seen in Figure 78 (A, B, C) for sample F7, which has the same composition as sample F6. The domain sizes are 3 to 5 orders of magnitude greater than the block lengths of CP and HPL. Besides the cobble-stone-like features, these micrographs show a much more distinct phase interconnectivity. Based on molecular weight considerations this type of structure could not be expected at low phase volume ratios of HPL over CP.

6.4 CONCLUSIONS

Cellulose propionate - hydroxypropyl lignin copolymers have been synthesized by grafting oligomeric CP segments onto HPL via a coupling agent. Arm length seems to be the most critical variable that affects copolymer properties, such as intrinsic viscosity, Mark-Houwink-Sakurada constant, crystallinity and melting point.

The dilute solution properties of the copolymers suggests that these materials behave either like a sphere or like a rod-type molecule. The conformation is dictated by the major component in the copolymer. At high HPL content, the copolymer will behave like a spherical molecule, whereas copolymers with high CP content will form solutions typical of rod-like molecules.

Thermal analysis shows strong evidence for microphase separation between HPL and CP segments. Cellulose propionate chains are able to crystallize, even at a low degree of polymerization such as DP 5, which surprisingly was not seen for pure oligomeric CP segments of equivalent size.

The degree of crystallinity of the copolymer, as indicated by the heat of fusion, remains approximately constant after CP chains reach a minimum DP value of 15.

The copolymer morphologies exhibit a broad variety of features. They vary from dispersed fibrils, to spheres- and alternate lamellae-type patterns, according to composition and molecular weights.

ACKNOWLEDGEMENT

Acknowledgement is made to Dr. Abaneshwar Prasad from the Chemistry Department at VPI&SU for his technical assistance in optical microscopy. The author wants also to thank Mr. Stephen

McCartney from the Department of Materials Engineering at VPI&SU for his skilful technical support in electron microscopy.

6.5 REFERENCES

1. R. J. Ceresa, *Polymer* **2**, 213(1961)
2. H. W. Steinmann, *Polym. Prep. Am. Chem. Soc. Div. Polym. Lett. Ed.*, **11**, 285(1970)
3. S. Kim, V. T. Stannett and R. D. Gilbert, *J. Polym. Sci. Polym. Lett. Ed.*, **11**, 731(1973)
4. S. Kim, V. T. Stannett and R. D. Gilbert, *J. Macromol. Sci. Chem.*, **A(10)(4)**, 671(1976)
5. K. S. Lee, V. T. Stannett, and R. D. Gilbert, *J. Polym. Sci. Polym. Chem. Ed.*, **20**, 997(1982)
6. L. F. McBurney, "Degradation of Cellulose", in *Cellulose*, Ed. Ott, E., Spurlin, H. M. and Grafflin, M. W. High Polymers vol. V, Part I, Interscience, New York, p.99(1954)
7. C. Feger and H. -J. Cantow, *Polymer Bulletin* **3**, 407(1980)
8. T. Mezger and H.-J. Cantow, *Die. Ang. Makromol. Chem.*, **116**, 13(1983)
9. W. de Oliveira and W. G. Glasser, *J. Appl. Polym. Sci.*, **37**, 3119 (1989)
10. A. Buleon and H. Chanzy, *J. Polym. Sci.: Polym. Phys. Ed.*, **16**, 383 (1978)

7.0 TERNARY BLENDS OF CELLULOSE PROPIONATE-HYDROXYPROPYL LIGNIN COPOLYMER AND HOMOPOLYMERS

7.1 INTRODUCTION

There has been considerable research in the area of polymer blends with a view to obtain new polymeric materials with enhanced physical properties when compared to the individual polymer components [1]. The commercial development of polymer blends arises from the advantage of combining existing polymers to produce useful products. Blends become attractive when one of the components is much less expensive than the other, since the final product will have a lower cost as compared to that of the more expensive ingredient [1].

One of the problems usually encountered in polymer blends is the incompatibility of the two polymers, which precludes a truly homogeneous mixture. This generally leads to high interfacial tension and poor adhesion between the two polymers. It has been recognized that the addition of

suitably tailored block or graft copolymers in an immiscible blend can alleviate to some degree the interfacial shortcomings. Due to their role in improving interfacial adhesion and blend properties, these block or graft copolymers are often referred to as “compatibilizers” [2].

The objective of this study is to examine the properties of melt-blended cellulose propionate / hydroxypropyl lignin materials before and after the addition of a $(CP)_n-HPL$ star-like copolymer as a blend compatibilizer.

7.2 EXPERIMENTAL SECTION

7.2.1 Materials

Cellulose propionate (CP): Commercial cellulose propionate was purchased from Aldrich Chemical Company and used as received.

Hydroxypropyl lignin (HPL): Two types of hydroxypropyl lignin were used in this study. These differed in degree of propoxylation and thermal properties. The lesser propoxylated lignin, HPL(A) had its T_g above room temperature (84°C), and was obtained from a commercial kraft lignin (Indulin AT, Westvaco Corp.) in accordance with the procedure described in chapter 3. The more extensively propoxylated lignin, HPL(B) had its T_g below room temperature (-7°C). It was prepared by reaction of organosolv (aqueous ethanol) lignin from aspen and propylene oxide, as described in chapter 3.

Cellulose propionate-hydroxypropyl lignin copolymer: $(CP)_n-HPL$ copolymer was prepared in accordance with the procedure described in chapter 6.

7.2.2 Sample Preparation

The CP/HPL blends were prepared in a Custom Scientific Instrument (CSI) melt extruder and the extrudate was chopped and injection-molded into dogbone test specimens. The extrusion temperature was 200°C and the residence time was no longer than 2 minutes. Blends with more than 40% HPL(A) or 20% HPL(B) could not be prepared by melt extrusion due to viscosity incompatibility.

At the extrusion temperature, HPL had an exceedingly low viscosity as compared to cellulose propionate. This condition resulted in a macroscopic component separation in which HPL simply coated the injector barrel, lubricating the surface of the barrel to the extent that no melt mixture could pass through the orifice into the mold.

7.2.3 Characterization

Dynamic Mechanical Thermal Analysis (DMTA): Dynamic mechanical properties were determined using a DMTA made by Polymer Lab. The measurements were conducted at a constant frequency of 1 Hz with a temperature range from -50 to 250°C, at a scan rate of 10°C per minute. The T_g was determined at the temperature at which the loss modulus E'' is a maximum.

Tensile tests: All mechanical testing of dogbone specimens was performed on a floor model Instron, at a crosshead speed of 0.25 in/min. Each value was the average of 4-7 tests.

7.3 RESULTS AND DISCUSSION

7.3.1 Dynamic Mechanical Behavior of Blends

Blend of CP and HPL(A): The molecular characteristics and thermal data of the individual blend components are presented in Table 16. A common method for determining whether a blend system is miscible is to examine its glass transition behavior. Miscible blends show a single, composition-dependent glass transition; whereas immiscible blends show two T_g 's characteristic of each phase. It is well known now that the properties of immiscible mixtures can be improved by incorporating an interfacially active block or graft copolymer as compatibilizer into the melt mixture. Basically, the compatibilizer has block or graft segments that are chemically identical to those of the respective phases. The compatibilizer improves interfacial adhesion and blend properties, permits a finer dispersion during mixing, and provides a measure of stability against gross segregation. Diblocks are more efficient interfacial agents than triblock copolymers or grafts. Usually as little as 0.5-2.0 wt.% of a diblock copolymer is sufficient to achieve a homogeneous and stable phase dispersion [1].

The glass transition temperatures determined by dynamic mechanical analysis are summarized in Table 17 for all of the blend preparations. In general, a slight decrease in T_g with increasing HPL component is observed. This is particularly true for the CP/HPL(A) blend system, where the T_g is composition-dependent. Different behavior is seen in the CP/HPL(B) system, in which the glass transition temperature is not affected by composition. As a rule, the addition of 5 wt.% copolymer into the blend, regardless of the type of HPL used, does not change the thermal behavior of the blend.

Table 16. Molecular Characteristics and Thermal Data of Pure Blend Components

Polymer	M_n	M_w/M_n	T_g (°C)	T_m (°C)
CP	120,000	1.6	142	240
CP-HPL	26,100	1.4	124	230
HPL(A)	1,900	6.3	84	
HPL(B)	10,000	5.2	-7	

Table 17. Summary of the Glass Transition Temperatures from DMTA of CP/HPL Blends

Composition, wt. %	T_g (°C)	T_g^* (°C)
100 CP	142	-
95 CP/5 HPL(A)	135	135
90 CP/10 HPL(A)	131	131
80 CP/20 HPL(A)	126	126
60 CP/40 HPL(A)	124	119
100 HPL(A)	84	-
95 CP/5 HPL(B)	135	133
90 CP/10 HPL(B)	134	133
80 CP/20 HPL(B)	134	133
100 HPL(B)	-7	-

* T_g of 5 wt. % (CP)_n-HPL copolymer modified blend

The dynamic mechanical behavior of binary blends containing, 95, 90, 80 and 60 wt.% CP is shown in Figure 79. Each blend presented a single T_g . A shift of the T_g peak toward lower temperatures with increasing amounts of HPL is observed. The existence of a single glass transition in these blends and its location between the T_g 's of constituent polymers is a good indication of compatibility between CP and HPL. The addition of 5 wt.% $(CP)_n$ -HPL copolymer to the blends, as a compatibilizer does not result in any significant difference in terms of glass transition, as shown in Figure 80.

Blend of CP and HPL(B): The dynamic mechanical behavior of a binary blend of CP and 80 wt.% HPL(B) is illustrated in Figure 81. Differently from HPL(A), it was not possible to melt extrude blend compositions higher than 20 wt.% HPL(B) due to viscosity incompatibility. The blend- T_g remains constant at about 134°C, independently of blend composition, as illustrated in Figure 82. This is not an indication of miscibility since the glass transition of the system is not a function of the blend composition. The addition of 5 wt.% copolymer apparently provides no benefit to the compatibilization of the system. Somehow the glass transition temperature of HPL could not be detected. The blend seems to be incompatible, and no compatibilization was achieved by adding copolymer. This suggests CP and HPL become increasingly incompatible with rising PO content (of the HPL): lignin has the compatible chemistry for blending with cellulose derivative as observed by Kelley [3,4], Rials [5], Dave [6] et al.

7.3.2 Tensile behavior

Figure 83 shows typical stress-strain curves of 90 CP/10 HPL blends. Curve (a) and (b) represent the tensile strain response of CP/HPL(A) before and after addition of 5 wt.% $(CP)_n$ -HPL copolymer as compatibilizer. It is seen that the incorporation of the copolymer in the blend actually reduces the tensile stress by about 10%. A possible explanation is that by adding a semi-crystalline

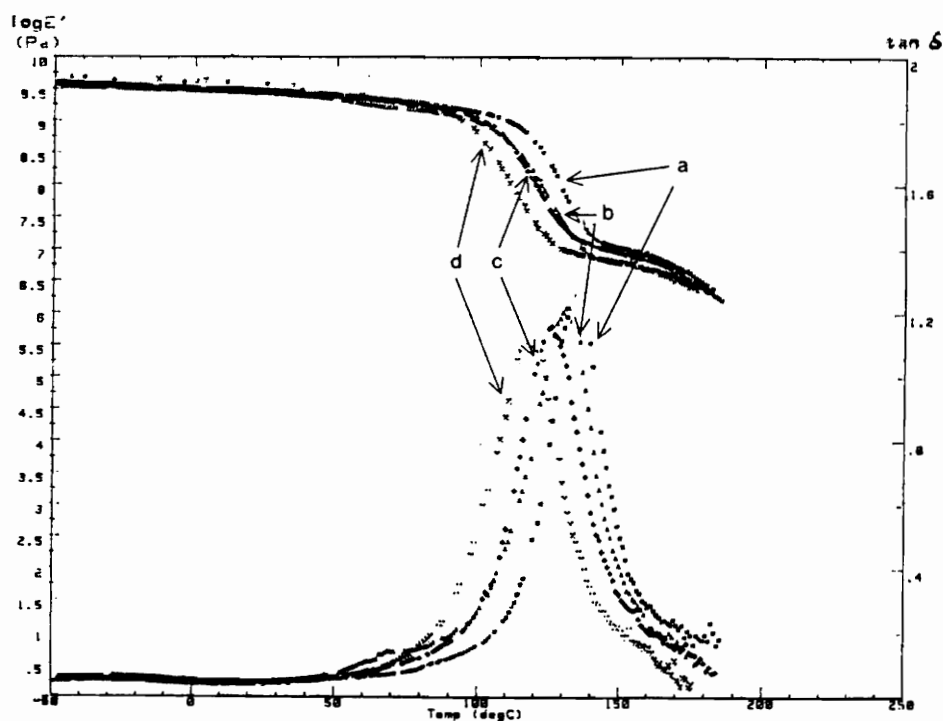


Figure 79. Dynamic mechanical behavior of CP/HPL(A) blends: (a) 95 %; (b) 90 %; (c) 80 %, and (d) 60 % CP

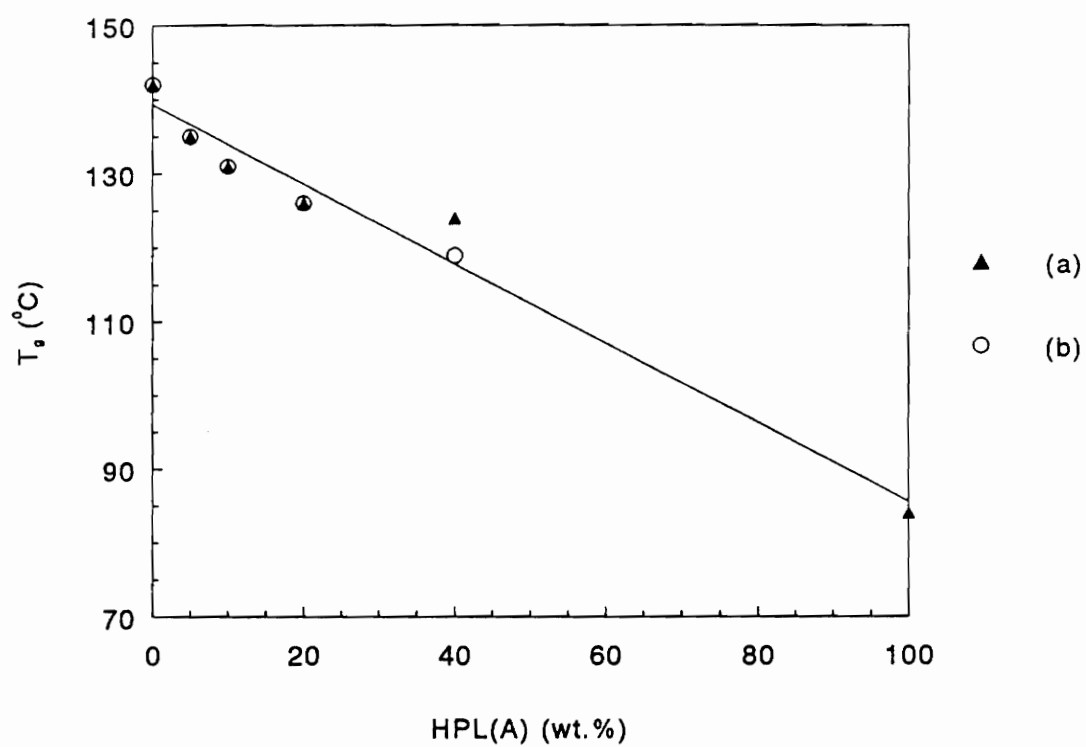


Figure 80. Glass transition temperature of CP/HPL(A) blends: (a) without copolymer; (b) with 5 wt.% CP-HPL copolymer added

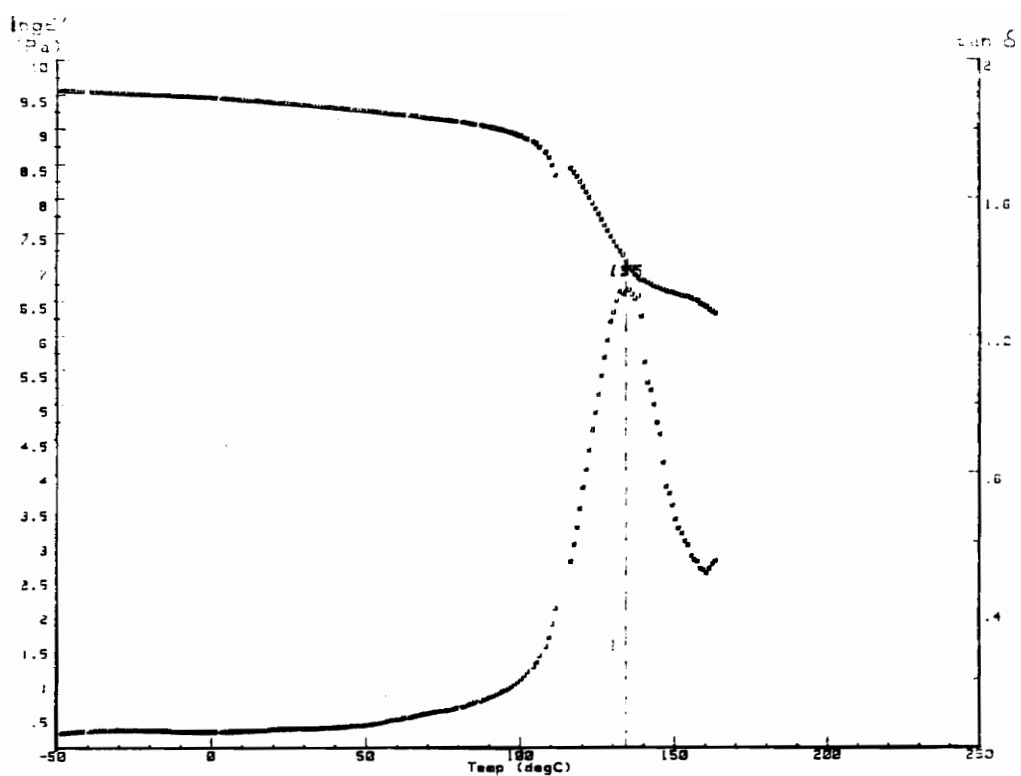


Figure 81. Dynamic mechanical behavior of 80 CP/20 HPL(B) blend

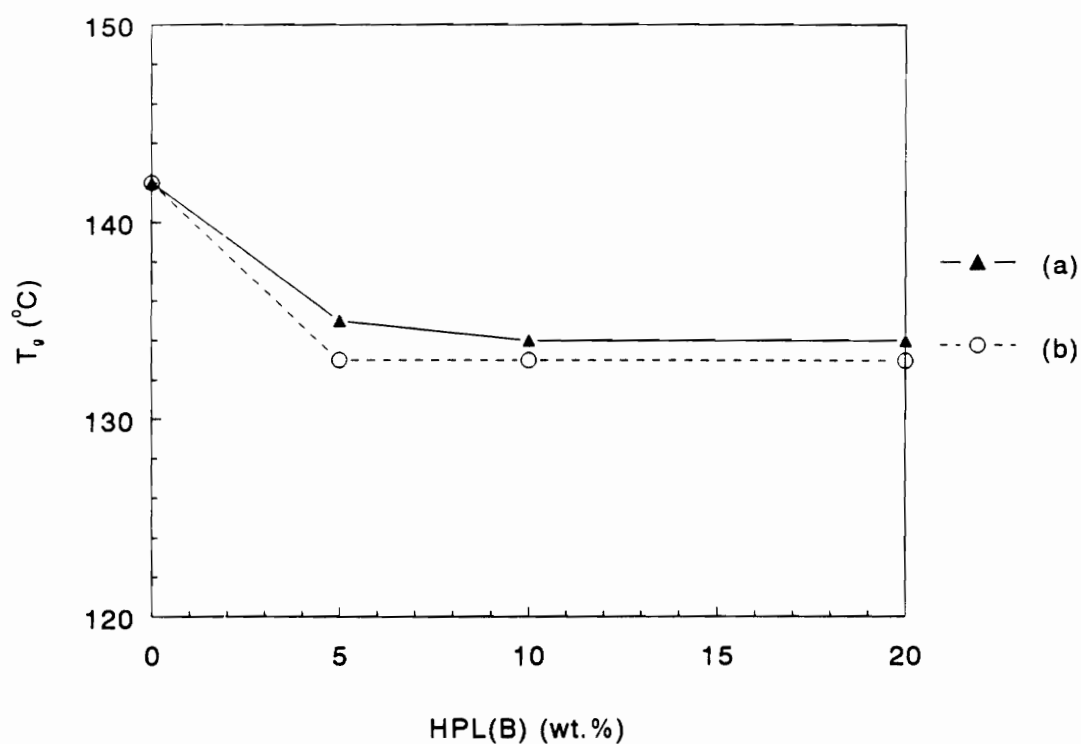


Figure 82. Glass transition temperature of CP/HPL(B) blends: (a) without copolymer; (b) 5 wt.% CP-HPL copolymer added

component, such as $(CP)_n-HPL$ copolymer, this hard component acts as a reinforcing material in a matrix which is already glassy, therefore increasing its brittleness. Curves c and d represent responses of CP/HPL(B) blends to tensile strain. Before the addition of the copolymer (curve c), the blend exhibits greater toughness (ie., elongation up to 160%) and a Young's modulus of 23 ksi. The copolymer modified blend (d) shows a remarkable decrease in toughness and an increase in tensile strength by about 10%. The reason why the blends with HPL(B) are tougher than those of HPL(A) may be attributed to the nature of HPL(B). This material is rubbery at room temperature, and therefore, incorporation of rubber particles into the matrix of brittle cellulose propionate tends to improve the impact resistance of the system. When the blend is modified by the addition of 5 wt.% copolymer, the microcrystalline $(CP)_n-HPL$ domains serve as particulate reinforcements; they strengthen the matrix, and for this reason cause a significant increase in tensile strength.

Tensile properties of CP/HPL(A) blends are presented in Figure 84. In general the addition of the copolymer into the blends has a negative effect on their mechanical properties. By adding 5 wt.% copolymer, a slight improvement in stress at break is seen, as well as a reduction in elongation. However the samples remain rather brittle, as much so as the unmodified blends. Again, this behavior must be attributed to the nature of the glassy blend components. A reduction in mechanical properties was also observed in the copolymer-modified CP/HPL(B) blend system (Figure 85). The copolymer-free blends were, in general, tougher materials; they exhibited lower stress at break, lower Young's modulus, and a much higher elongation at any blend composition. The copolymer-modified blends give rise to higher stress at break, higher Young's modulus, and a reduction in elongation. Therefore, no improvement in ductility was achieved by adding the copolymer as compatibilizer.

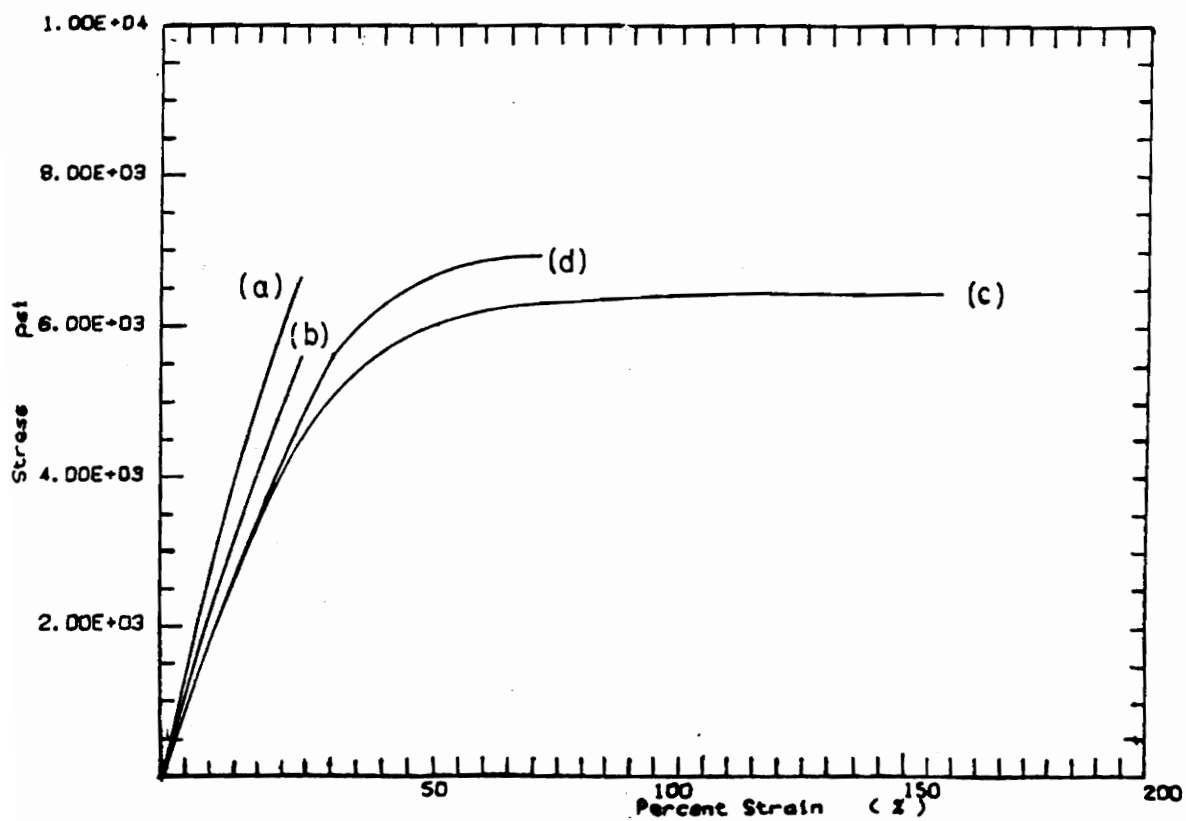


Figure 83. Typical stress-strain curves of CP/HPL blends: (a) 90 CP/10 HPL(A); (b) 85 CP/10 HPL(A) blended with 5 wt.% CP-HPL copolymer; (c) 90 CP/10 HPL(B); (d) 85 CP/10 HPL(B) blended with 5 wt.% CP-HPL copolymer.

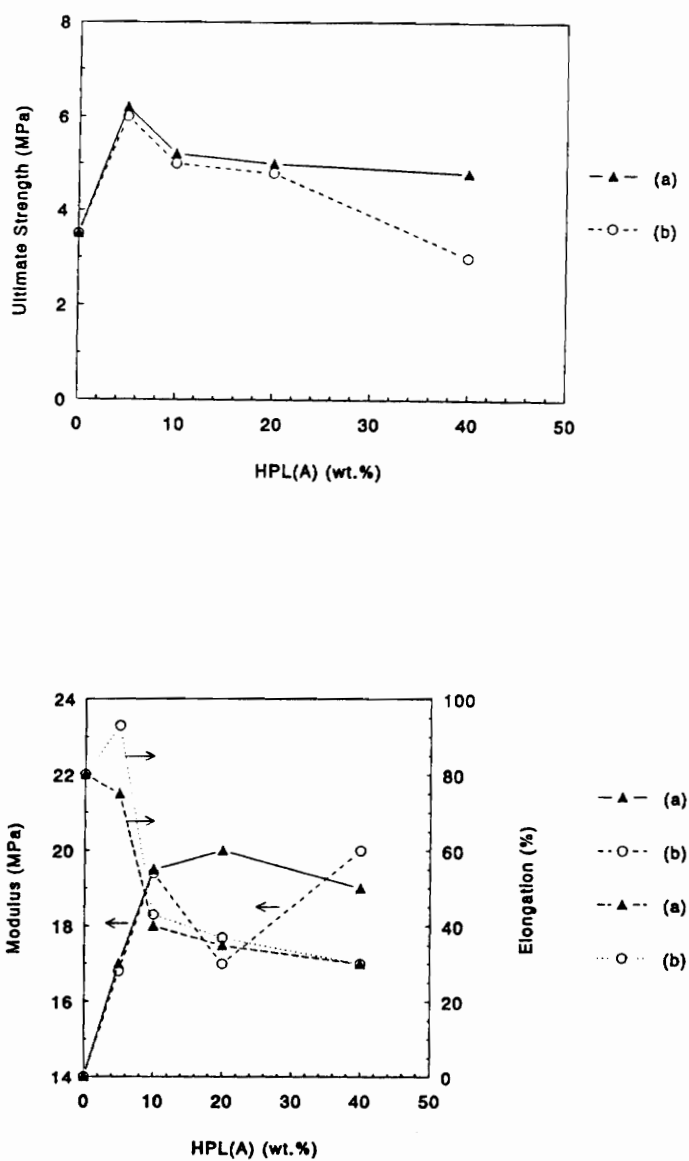


Figure 84. Tensile mechanical properties of CP/HPL(A) blends: (a) without copolymer; (b) with 5 wt.% CP-HPL copolymer added

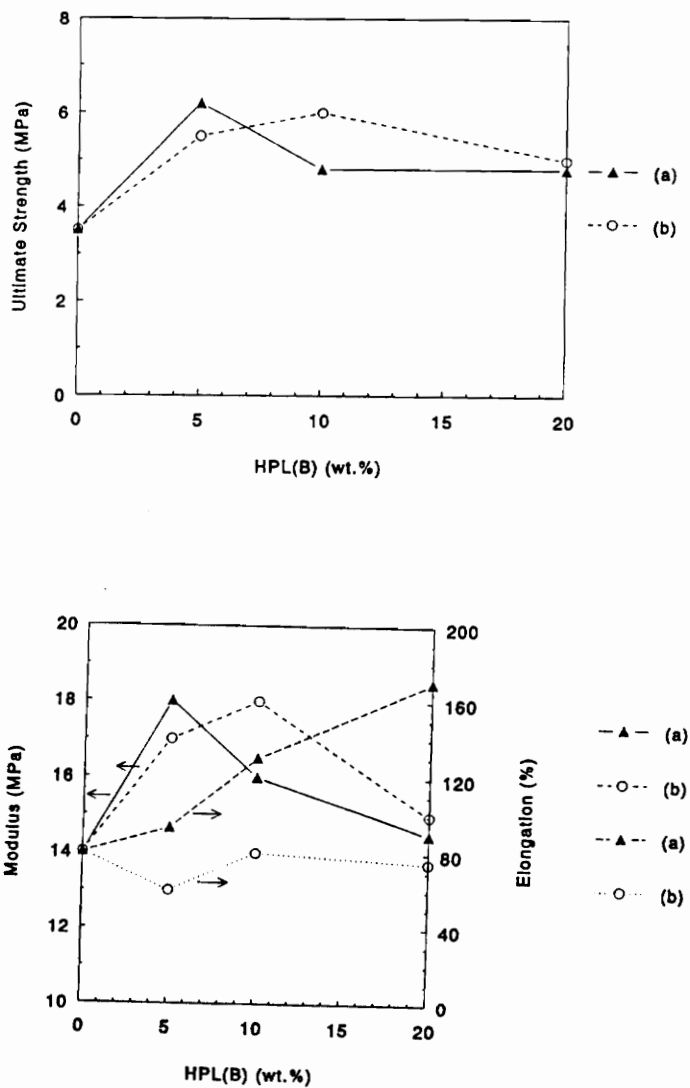


Figure 85. Tensile mechanical properties of CP/HPL(B) blends: (a) without copolymer; (b) with 5 wt.% CP-HPL copolymer added

7.4 CONCLUSIONS

Melt blended cellulose propionate with an HPL having high lignin content and lower degree of propoxylation, HPL(A), showed a single glass transition by dynamic mechanical measurements. While it cannot definitively be concluded that HPL(A) forms a truly miscible system with cellulose propionate at this point, it seems that partial miscibility was achieved with up to 40% HPL(A) component. On the other hand, the thermal behavior of the CP/HPL(B) blends indicated that HPL(B) forms an incompatible system with cellulose propionate (although mechanically compatible) in the range investigated. The addition of moderate amounts of copolymer (5 wt%) into the blends does not have any significant effect on T_g .

The tensile properties of the blends were slightly altered by the presence of the copolymer. The expected "compatibilizer" effect of the copolymer was not achieved, since no improvement in toughness was detected by adding it to the blends. In fact, there was a deterioration in mechanical properties as a result of the addition of copolymer.

7.5 REFERENCES

1. D. R. Paul, J. W. Barlow and H. Keskkula, "Polymer Blends", "Enc. Polym. Sci. Eng.", J. I. Kroschwitz, Ed., Wiley, New York, vol. 12, 399-461 , 1987
2. D. R. Paul, in D. R. Paul and S. Newman, Eds., "Polymer Blends", vol. I, Academic Press, Inc., New York, 1978
3. S. S. Kelley, T. C. Ward, and W. G. Glasser, *J. Appl. Polym. Sci.*, **41**, 2813 (1990)
4. S. S. Kelley, W. G. Glasser, and T. C. Ward, *Polymer*, **30**(12), 2265 (1989)
5. T. G. Rials, and W. G. Glasser, *Wood and Fiber Science*, **21**(1), 80 (1989)
6. V. Dave, and W. G. Glasser. Unpublished results

8.0 POLYSTYRENE-HYDROXYPROPYL LIGNIN COPOLYMERS: SYNTHESIS AND APPLICATION IN TERNARY BLENDS

8.1 *INTRODUCTION*

Much attention has been devoted over the last several years to the synthesis of multiphase polymeric systems, such as block or graft copolymers, composites, polymer blends and interpenetrating networks [1]. The reason is that heterophase systems represent a very attractive way to obtain new and tailor-made materials. Blending polymers is the most popular method for engineering new materials because it is based on the mixing of two or more polymers to obtain products with desirable combinations of characteristics. Although there are several “miscible” polymer blends, most polymers are immiscible with each other, thus leading to heterophase polymer systems [2].

The incompatibility in polymer blends usually leads to a high interfacial tension and poor adhesion between the polymers. Interfacial tension is responsible for a low degree of dispersion of the mix-

ture, and this contributes to gross phase separation. On the other hand, poor adhesion leads to weakness and to brittle mechanical behavior, properties most often undesirable in engineering materials.

It is well known that the adhesion between polymers can be improved by the addition of block or graft copolymers that represent the combination of the chemistries of the two polymers to be mixed. The copolymer usually consists of chain segments chemically identical or similar to the homopolymers to be mixed. The copolymers are generally called "compatibilizers" and their function is to act at the interface between the phases, due to the capability of their individual chain segments to penetrate into the phases to which they are chemically identical or similar [3].

Paul and Barlow [4] have reported that when an AB block or graft copolymer is added to an A/B binary blend, three major effects can be observed: (i) higher degree of dispersion; (ii) better adhesion between phases; and (iii) stabilization of microphases with regard to coalescence phenomena. The combination of these effects can provide indirect evidence of the influence of the addition of copolymers as the third blend component.

A higher degree of dispersion has been observed in the case of 75%PS/25%PE blends having small amounts (0-7%) of added graft copolymer [5]. The dimensions of the PE domains decreased with increasing copolymer concentrations. Similar results were also obtained for other systems, such as PS/polydiene, PVC/PE and polyamide/polyolefin [1,6].

Better adhesion between phases is the second benefit of adding a block or graft copolymer as compatibilizer. Direct morphological evidence that block and graft copolymers promote interfacial interactions between phases has been presented for some PS/LDPE blends [5]. The addition of 1% graft copolymer to PS/LDPE binary blends greatly improved the blend performance, as demonstrated by fractographic analysis. Surface irregularities were developed which were attributed to PS/PE connections being broken during the fracture process.

The third effect is the stabilization of fine dispersions. Block and graft copolymers work as emulsifiers delaying phase separation in immiscible polymers. Several papers have dealt with the emulsifying effect of copolymers for the system PS/polydiene [7]. The behavior observed with this blend after modification with copolymer has provided considerable evidence for the role of copolymers as interfacial agents.

It has been shown that the emulsifying effect of block and graft copolymers is strongly dependent on molecular weight and molecular architecture. If the molecular weights of the homopolymers are about the same or smaller than the corresponding copolymers, the homopolymers will be solubilized into the respective domains, i.e., the domains of the respective homopolymers, and a third domain will result from the copolymer with its inherent microdomain structure. Consequently, in the design of an interfacial agent, a balance between chemistry and size of the copolymer segments must be found.

Polystyrene and lignin are known to be immiscible; and so are polystyrene and hydroxypropyl lignin (HPL). In this research, star-like block copolymers of PS-HPL were synthesized and characterized. The performance of the copolymers was then evaluated with regard to their compatibilization activity for the PS/HPL blend system.

8.2 *EXPERIMENTAL SECTION*

8.2.1 Materials

Polystyrene (PS): Polystyrene ($M_n = 250,000$) and mono-hydroxyl terminated polystyrene having a number-average molecular weight of 10,400 were purchased from Scientific Polymer Products. Once received, the samples were used without further purification.

Stannous octanoate: Stannous octanoate was obtained from Aldrich Chemical Company and used as received.

2,4-Tolyene diisocyanate (TDI): TDI was purchased from Aldrich Chemical Company and used without further purification.

Tetrahydrofuran (THF): THF was supplied by Fischer Scientific Chemical Company. The solvent was dried over a mixture of metallic potassium and benzophenone refluxed and distilled under dried nitrogen. The material was stored over molecular sieves.

Hydroxypropyl lignin (HPL): HPL was synthesized and purified according to a procedure described in chapter 3. Table 18 presents the molecular characteristics and T_g 's of the HPL's used in this study. The common characteristic of these samples was their "rubbery" nature (their T_g 's were below room temperature).

Table 18. Molecular Weight and Thermal Properties of HPL's

HPL	M_n	M_w/M_n	T_g (°C)
1	1,800	10.3	-36
2	2,600	16.4	-17
3	3,000	5.2	-7
4	9,600	5.9	1

8.2.2 Synthesis of Mono-Isocyanate Terminated Polystyrene

Typically, 1 g of PS and 0.1% by weight of stannous octanoate were introduced into a two-necked flask equipped with a magnetic stir bar. The flask was connected to a vacuum line for further drying. After six hours, the reactor was sealed with rubber septa, transferred to an oil-bath on a stir plate, and purged with prepurified and dried nitrogen. Under a constant flow of nitrogen, 10 mL of freshly distilled THF were added into the reaction flask through a hypodermic syringe to dissolve the reactants. The reactor was heated to 50°C and TDI was added in an approximate 5:1 molar ratio. The reaction was kept at 50°C under stirring for 24 hours. After cooling, the product was precipitated into a large excess of petroleum ether to eliminate the excess of TDI. The mixture was filtered, washed with petroleum ether, and dried under vacuum. The mono-isocyanate capped prepolymer was used immediately for grafting. Infrared spectroscopy was used to monitor the reaction.

8.2.3 Copolymer synthesis

Star-like copolymers of HPL and PS were prepared by a two-step process. The first step consisted of the synthesis of PS-NCO (see section 8.2.2). The second step (the grafting reaction) was performed in a clean, flamed and nitrogen- purged 2-necked round bottom flask, equipped with a magnetic stir bar and rubber septa under prepurified dried nitrogen atmosphere. First, a calculated amount of HPL and stannous octanoate dissolved in THF were charged to the reaction flask through a hypodermic syringe. Next PS-NCO, previously dried and dissolved in THF, was syringed into the flask at the desired ratio of PS-NCO to HPL polyol. The reaction flask was submerged into the oil-bath and heated to 50°C. The grafting reaction was terminated after 24 to 30 hours through precipitation into aqueous methanol. Soxhlet extraction with methanol was used to remove unreacted HPL. The reaction product was characterized by gel permeation chromatography.

8.2.4 Sample Preparation

All blends were prepared by solvent casting from polymer solution, according to the procedure described in chapter 4.

8.2.5 Characterization

Gel Permeation Chromatography (GPC): GPC was used to measure the molecular weights and molecular weight distributions of HPL and of the copolymers, according to the procedure described in chapter 3.

Fourier Transform Infrared Spectroscopy (FTIR): The progress of the isocyanate capping reaction was monitored by using a Nicolet spectrometer, as described in chapter 3.

Proton-Nuclear Magnetic Resonance Spectroscopy (H-NMR): H-NMR analysis was used to determine number-average functionality of mono-hydroxyl terminated PS and chemical information of the copolymer, based on the procedure described in chapter 3.

Differential Scanning Calorimetry (DSC): DSC thermograms were obtained on a Perkin-Elmer Model DSC-4. The temperature was scanned from -60 to 150°C at a heating rate of 10°C per minute. The scanning procedure consisted of two steps. In the first run, the samples were cooled to -60°C and heated at 10°C/min to 150°C. In the second run, the samples were quenched to -60°C at 200°C/min. and reheated at 10°C/min. to 150°C. Glass transition temperatures were taken as midpoint of the change in slope of the baseline of the second run.

Tensile tests: Standard tensile stress-strain experiments were performed on dog-bone shaped specimens with a MINIMAT testing machine, at room temperature. The tensile tests were performed to measure the modulus, ultimate strength, and elongation at break. The samples were clamped between two clamps and elongated at a rate of 1 mm per minute; this corresponds to an engineering strain rate of 10% per minute. The results reported represent an average of five to six runs.

Scanning Electron Microscopy (SEM): SEM was carried out on a Phillips EM-420 STEM operated in SEM mode. In order to obtain micrographs of fractured surfaces, the films were first immersed in liquid nitrogen and then fractured and analyzed at their fractured surfaces.

8.3 RESULTS AND DISCUSSION

The copolymers were characterized by gel permeation chromatography, and their molecular characteristics are presented in Table 19. Figure 86 shows the molecular weight distribution of a typical grafting reaction between PS-NCO and HPL. The effectiveness of the reaction is illustrated through the formation of higher molecular weight polymers as compared to the corresponding starting materials. The copolymer molecular weight distribution is highly unsymmetrical, similar to the polydisperse HPL. When superimposing the molecular weight distribution of the starting material on the copolymer, it is seen that the large peak at 10,000 daltons of the copolymer has the same shape and polydispersity as that of the PS homopolymer. The same distribution persists after 60 hours of reaction, and it is observed in all samples of this series. This result can be explained by considering that the initial PS mono-hydroxyl terminated prepolymer was in fact not totally mono-hydroxyl functionalized. Therefore, after capping with TDI, the unfunctionalized PS was carried along with the PS-NCO segments to the reaction medium, and it failed to be grafted onto HPL. Since both PS homopolymer and PS-HPL copolymer have similar solubility properties, the separation of the homopolymer from the copolymer can only be achieved by fastidious fractionation procedures. This was not attempted in this work.

Proton-NMR spectroscopy was applied to the determination of number-average functionalities of PS-OH. As previously applied to PCL and CP segments, the capping with SiEt₃ improved the quantification of OH end groups. Unfortunately, the method could not be applied successfully to PS since there is a multitude of signals below 1 ppm which overlap with the signals due to protons from SiEt₃. The concentration of OH groups, therefore, could not be determined with accuracy. Figure 87 illustrates the H-NMR spectra of PS-OH and of PS-SiEt₃.

Proton-NMR spectroscopy was also used to characterize the copolymers. Even though PS homopolymer could not be extracted from the copolymer, unreacted HPL was easily removed with

Table 19. Molecular Characteristics of PS-HPL Copolymers

Sample	M_n HPL	M_w/M_n HPL	M_n PS	M_w/M_n PS	M_n cop. ^b	M_w/M_n cop.	MHS ^a	IV (dl/g)
G1	3,000	5.2	10,200	1.06	21,100	2.5	0.309	0.236
G2	2,600	16.4	10,200	1.06	25,400	3.8	0.191	0.204
G3	9,600	5.9	10,200	1.06	25,400	4.2	0.159	0.215
G4	2,600	16.4	10,200	1.06	33,400	7.4	0.196	0.221
G5	1,800	10.3	10,200	1.06	44,900	4.1	0.135	0.194

a Mark-Houwink-Sakurada constant

b copolymer

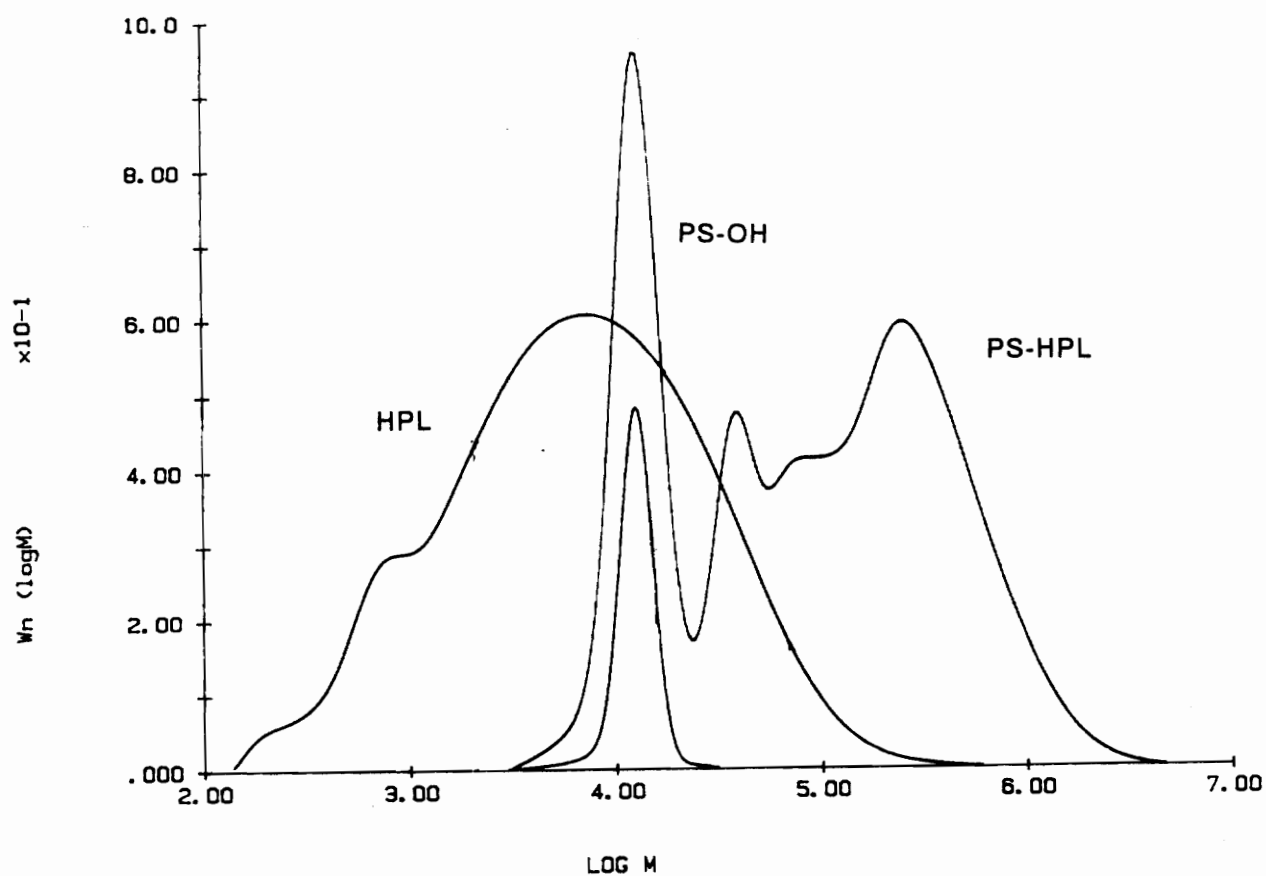
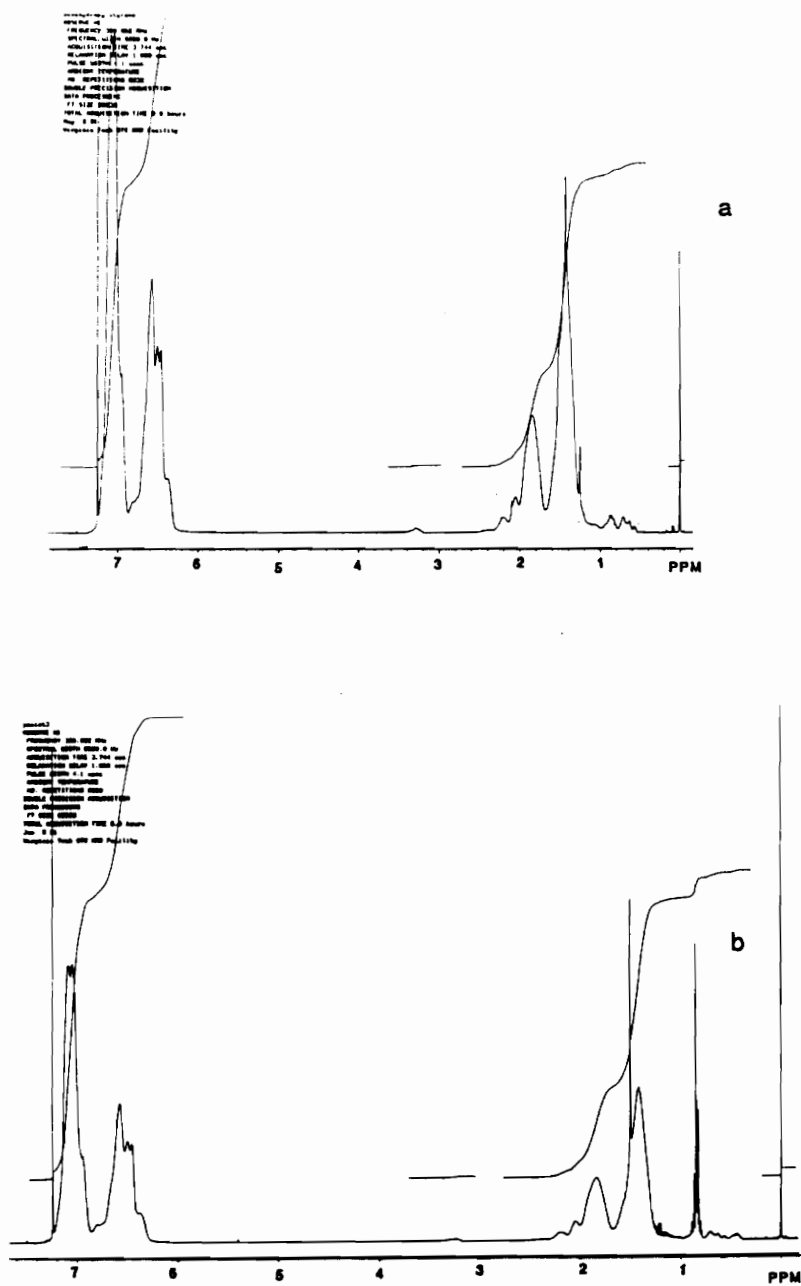


Figure 86. MWD of a typical PS-NCO and HPL grafting reaction



aqueous methanol in a soxhlet apparatus. The resonance peaks at 3.7 ppm can, therefore, only be attributed to the HPL component of the copolymer since PS does not absorb in that region of the spectrum (Figure 88).

The multiphase nature of the PS-HPL copolymers is revealed by DSC. The T_g of the HPL component is observed in the range between -8 and -20°C, whereas the PS glass transition temperature varied from 80 to 107°C. As seen in Table 18, the T_g of the HPL phase does not change much with the copolymer molecular weight, whereas the T_g of the PS component increases with the copolymer weight-average molecular weight, as seen in Figure 89.

The next paragraphs will present the results of the use of PS-HPL copolymer as compatibilizer in PS/HPL polymer blends. As already mentioned, PS and HPL form a highly incompatible mixture which undergoes macrophase separation (Figure 90).

Figures 91-93 present scanning electron micrographs of cryogenic fracture surfaces at 1,000x magnification of copolymer-modified blends of PS/HPL. The binary 95 PS/5 HPL blend (Figure 91 A) presents the morphology of a "cheesy" type material with cavities of about 5-7 μm formed by the rubbery particles of HPL being pulled out during the fracture. This separation of surfaces creates the clean and smooth holes at the fracture surface. The addition of 5 and 10% copolymer (Figures 91 B, 91 C) leads to improved adhesion, as indicated by the reduced number of cavities. This implies that more HPL particles are "anchored" to the PS matrix. By adding copolymer, cavities of smaller and more uniform size are obtained (about 1-3 μm).

The micrograph (at 5,000x magnification) for 90 PS/10 HPL copolymer modified blends reveals interfacial adhesion due to the presence of copolymer (Figure 92). The addition of 10 wt.% copolymer significantly reduces the particle size, as seen by the smaller cavities in the PS matrix (Figure 92 C). The increased copolymer content produces a finer dispersion with particles smaller than 1 μm . This is 10 times smaller than that of the unmodified blend. No significant difference is observed in the morphology of the 80 PS/20 HPL system, before or after copolymer addition

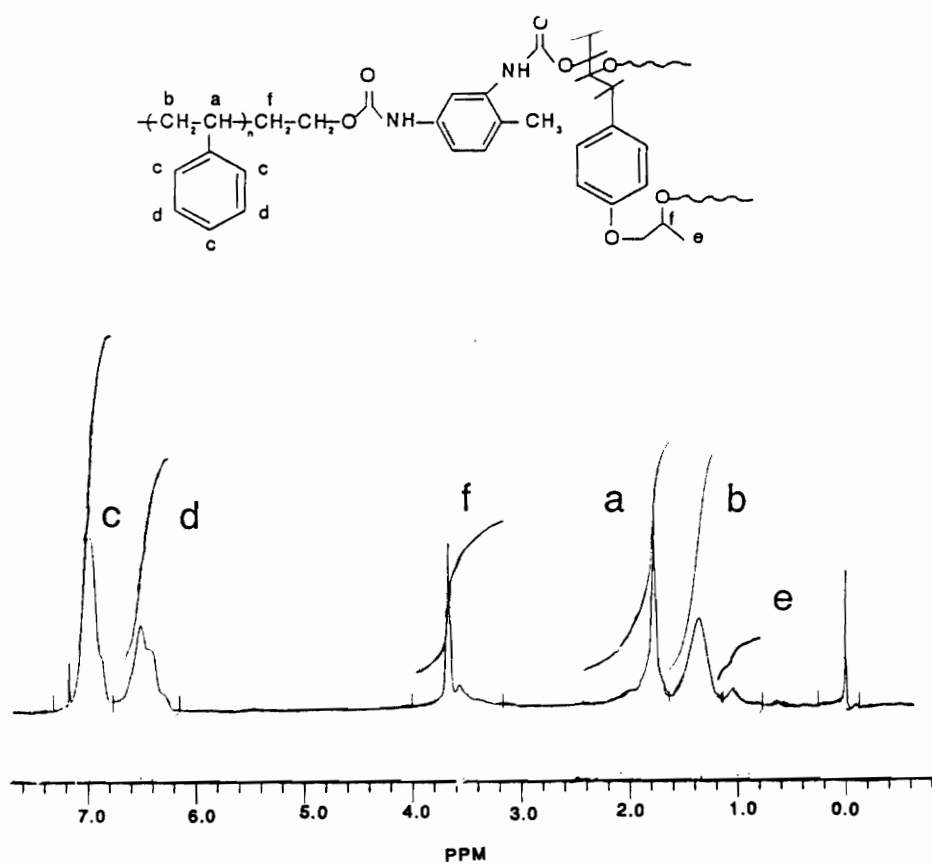


Figure 88. Proton-NMR of a typical PS-HPL copolymer

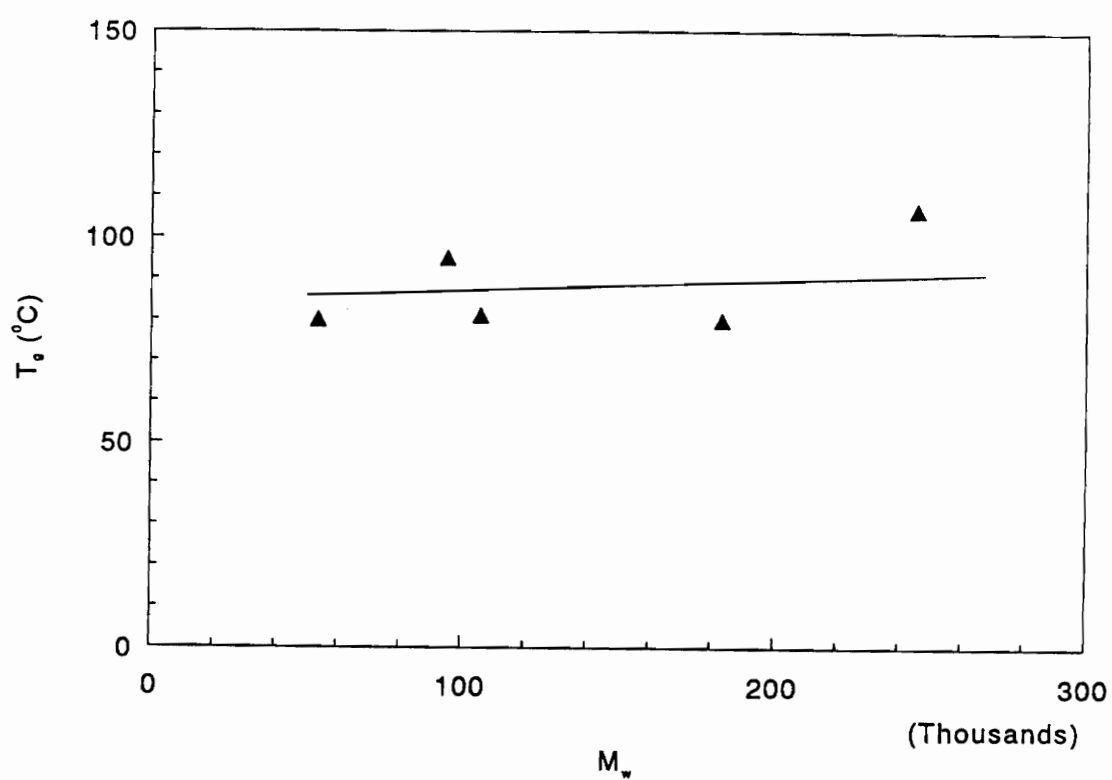


Figure 89. Relationship between T_g and PS-HPL copolymer molecular weight

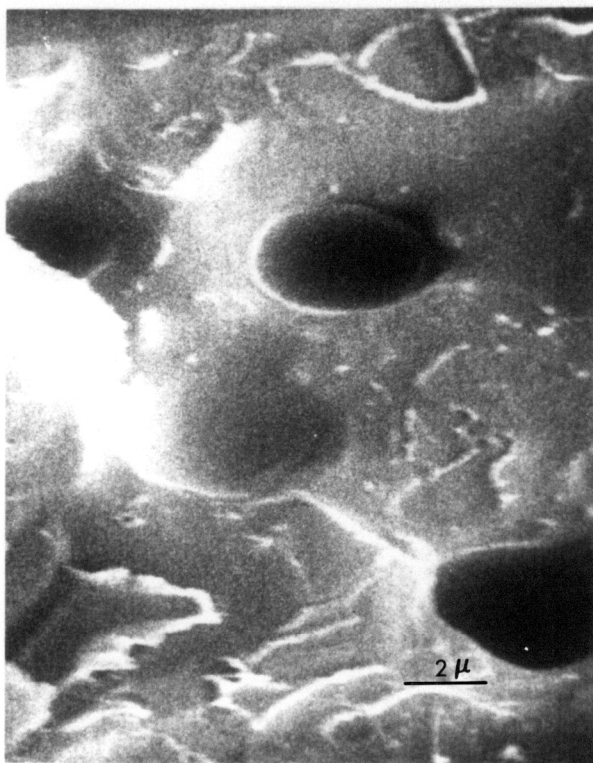


Figure 90. Scanning electron micrograph of 80 PS/20 HPL blend (5000x).

POLYSTYRENE-HYDROXYPROPYL LIGNIN COPOLYMERS: SYNTHESIS AND
APPLICATION IN TERNARY BLENDS

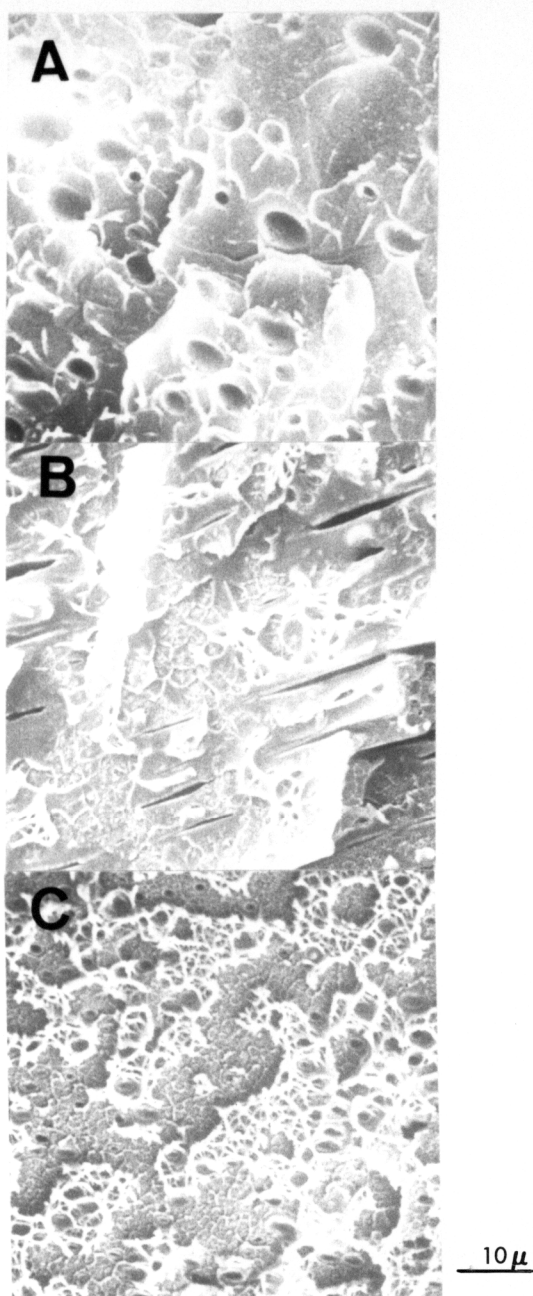


Figure 91. Scanning electron micrographs of 95 PS/5 HPL blends: (a) without copolymer; (b) 5 wt. % PS-HPL; (c) 10 wt. % PS-HPL copolymer added (1000x).

POLYSTYRENE-HYDROXYPROPYL LIGNIN COPOLYMERS: SYNTHESIS AND APPLICATION IN TERNARY BLENDS

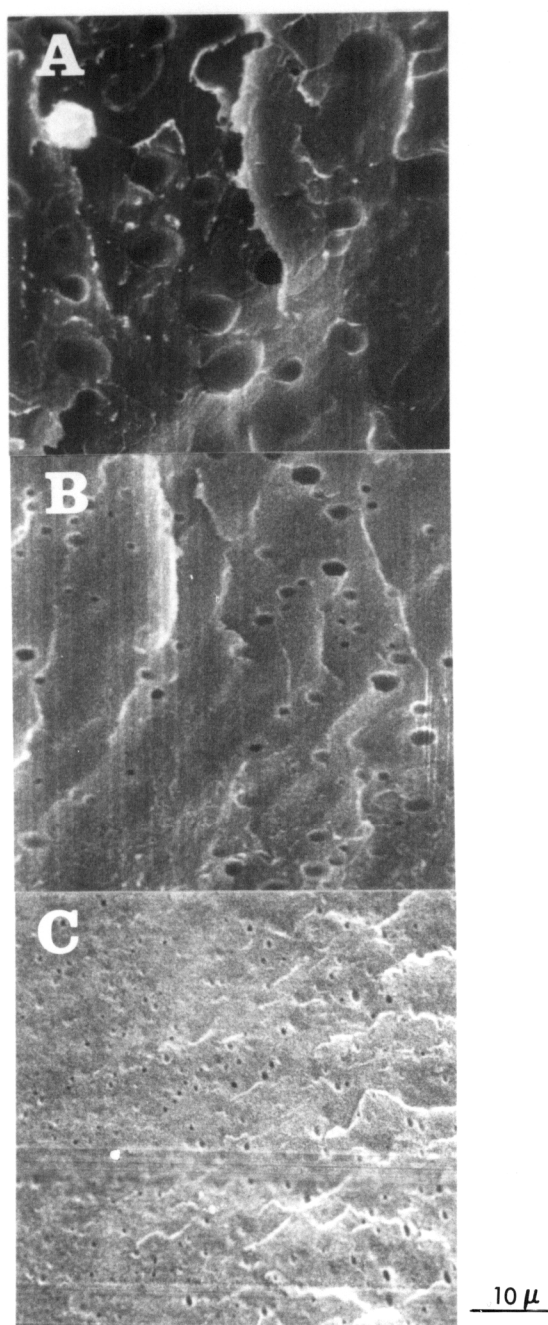


Figure 92. Scanning electron microscopy of 90 PS/10 HPL blends: (a) without copolymer; (b) 5 wt. % PS-HPL; (c) 10 wt. % PS-HPL copolymer added (1000x)

POLYSTYRENE-HYDROXYPROPYL LIGNIN COPOLYMERS: SYNTHESIS AND APPLICATION IN TERNARY BLENDS

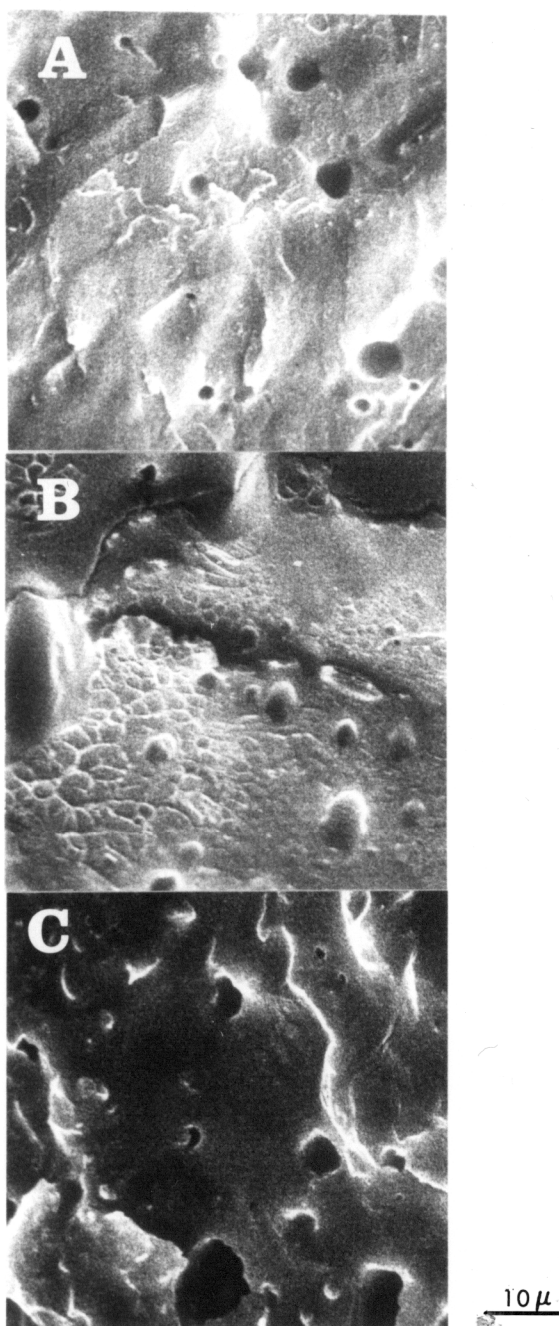


Figure 93. Scanning electron microscopy of 80 PS/20 HPL blends.: (a) without copolymer; (b) 5 wt.% PS-HPL; (c) 10 wt.% PS-HPL copolymer added (1000x)

POLYSTYRENE-HYDROXYPROPYL LIGNIN COPOLYMERS: SYNTHESIS AND APPLICATION IN TERNARY BLENDS

(Figure 93). The phases exhibit poor adhesion as seen by the cheesy structure, with cavities of about 5-10 μm which persist (constant size and distribution) after the addition of the copolymer.

The tensile properties of PS/HPL blends reveal a slight improvement in the adhesion between the phases as a result of adding copolymer into the blends. That effect is observed at every composition. However, HPL could not be blended into PS in amounts greater than 20%, even with the addition of copolymer. Tensile mechanical properties of the blends are presented in Figure 94. A decrease in modulus and ultimate strength with increasing HPL content is observed. However, the addition of copolymer seems to have some effect on the mechanical properties of the blends. The addition of copolymer further reduces the modulus and, as is expected, also decreases the ultimate strength values. For all the mixtures examined, the samples remain rather brittle, as much so as the pure blends, as seen by the insignificant gain in elongation illustrated in Figure 94.

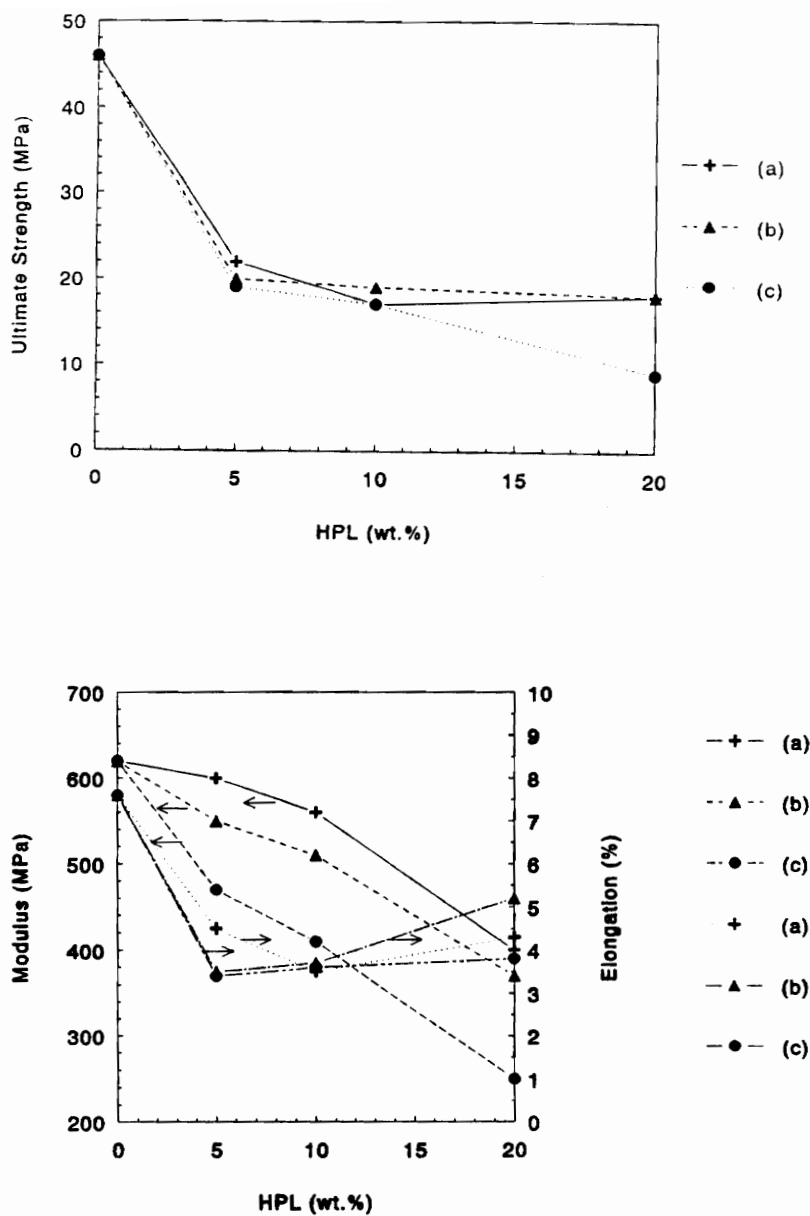


Figure 94. Tensile properties of PS/HPL blends.: (a) without copolymer; (b) with 5 wt.% PS-HPL; (c) with 10 wt.% PS-HPL copolymer added

8.4 CONCLUSIONS

The results of this study show that it is possible to graft polystyrene to hydroxypropyl lignin with a relatively high content of grafted chains.

DSC studies reveal that the HPL glass transition was basically unaltered by grafting. On the other hand, the T_g of PS is shifted to higher temperature with increasing copolymer molecular weight.

The incorporation of copolymer produces a slight enhancement in the miscibility of PS with HPL. Although the results are preliminary, it is possible to conclude that the addition of a moderate (5-10%) amount of PS-HPL copolymer influences the morphology of binary PS/HPL blends. This is supported by electron microscopic analysis.

The tensile mechanical properties of PS/HPL blends are also improved as a result of better adhesion of the two phases following the incorporation of the copolymer into the mixture. Nevertheless, additional studies are needed to fully explain the interfacial effect of the copolymer and to correlate them with the mechanical response of the blends.

8.5 REFERENCES

1. G. Maglio and R. Palumbo, "The Role of Interfacial Agents in Polymer Blends", in M. Kryszeński, A. Galeski and E. Martuscelli, Eds., "**Polymer Blends: Processing, Morphology and Properties**", vol. 2, Plenum Press, New York and London
2. O. Olabisi, L. M. Robeson, M. T. Shaw, "**Polymer-Polymer Miscibility**", Academic Press, 1979
3. D. R. Paul and S. Newman Eds., "**Polymer Blends**", vol. I, II, Academic Press, New York, 1978
4. D. R. Paul and J. W. Barlow, *J. Macromol. Sci., Rev. Macromol. Chem.*, **C-18**, 109 (1980)
5. D. Heikens, N. Hoen, W. M. Barentsen, P. Piet and H. Landan, *J. Polym. Sci., Polymer Symposium*, **62**, 309 (1978)
6. C. E. Locke and D. R. Paul, *J. Appl. Polym. Sci.*, **17**, 2791 (1973)
7. T. Inoue, T. Soen, T. Hashimoto and H. Kawai, *Macromolecules*, **3**, 87 (1970)

Vita

Willer de Oliveira was born as first son to Mr. and Mrs. João Durval de Oliveira on March 9, 1954, in Rio de Janeiro, Brazil. He received a Bachelor of Science degree from Rio de Janeiro Federal University in December of 1976. While working as a Research Chemist at the Foundation for Industrial Technology (FIT) he completed a B. S. degree in Chemical Engineering at Rio de Janeiro State University in December, 1980. His work experience includes eight years as a Research chemist at FIT. In this institution he has been conducting research on lignin utilization, sugar cane bagasse and biomass residues.

In September 1985 he received a scholarship for graduate studies at Virginia Polytechnic Institute and State University (VPI&SU) from the Brazilian Government (CNPq). In January 1987 he earned a M. S. degree in Forest Product. He then entered the Materials Engineering Science Program at VPI&SU as a doctoral student with major emphasis on Polymer Science. After completing his Ph. D. degree in September 1991, he joined the Biobased Materials Center at VPI&SU as a Research Associate.

Willer de Oliveira